GROUNDWATER DEFLUORIDATION IN BATCH SYSTEMS USING ACTIVATED CARBON DERIVED FROM RAFFIA PALM (*RAPHIA HOOKERI* G. MANN & H. WENDL) SHELLS

BY

RAPHAEL TERUNGWA IWAR

B.Eng. Agric. & Environmental Engineering (Makurdi), M.Sc.Environmental Engineering (Ibadan)

A Thesis in the

Department of Agricultural and Environmental Engineering,

Submitted to the Faculty of Technology in partial fulfillment of the requirements for the Degree of

DOCTOR OF PHILOSOPHY

of the

UNIVERSITY OF IBADAN

NOVEMBER 2022

CERTIFICATION

I certify that this work was carried out by Engr. R.T. Iwar in the Department of Agricultural and Environmental Engineering, University of Ibadan.

Supervisor

K. Ogedengbe

B.Sc. (Ibadan), M.Sc. (Southampton), C.E.S (Strasbourg), Ph.D. (Ibadan)

Professor, Department of Agricultural and Environmental Engineering,

University of Ibadan.

DEDICATION

This Ph.D. thesis is dedicated to my late parents Chief and Chief (Mrs.) P.N. IWAR, on whose footsteps I started this journey of " knowledge seeking" and in memory of all those who have paid the ultimate prize in their quests for knowledge, which has in no doubt shaped today's world.

ACKNOWLEDGEMENTS

Firstly, I deeply and sincerely express my thankfulness to the everliving Father who is the creator and manager of the entire universe, He who knows the end even from the start of time and His most beloved Son, our Lord and Saviour Jesus Christ for His grace upon my life, which has enabled me to reach the peak of my academic pursuit.. May all the glory be yours for ever, Amen!

My sincere appreciation goes to my father, mentor and major supervisor, Prof. Kola' Ogedengbe who guided me technically and morally all through this research work. Your fatherly counsels and moral/spiritual support during my encounters with you cannot be forgotten in a hurry. May the Lord continuously extol and reward you and your household with good health and peace of mind at all times. I must also greatly acknowledge the sound inputs made by my Co-Supervisor, Dr. Oluseyi E. Ewemoje, which has resulted to the enhancement of this thesis.

My gratitude is specially extended to our amiable Head of Department, Dr. M. O. Omobowale for his sound administrative prowess, that have in no doubt fast-forwarded this PhD program, Thank you sir for all the support. I am and will always remain grateful to all the PG lecturers in the Department of Agricultural and Environmental Engineering namely; Professors A. Y. Sangodoyin, E. A. Ajav, Y. Mijinyawa, A. I. Bamgboye, A. O. Raji, A. K. Aremu and T. A. Ewemoje; Dr. B. O. Oyefeso for their sound technical inputs at various stages of my research presentations. If not for you, it would have been difficult to shape this research work. The Technical and Administrative support staff in the Department are also sincerely appreciated for their various contributions towards the actualization of this piece. God will continue to bless all of you. The Dean, Sub-Deans and the entire members of the PG Committee of the Faculty of Technology are deeply appreciated for the various roles they played towards the accomplishment of this piece.

The roles played by the Vice Chancellor and the entire management staff of the Joseph Sarwuan Tarkaa University Makurdi (JOSTUM) by providing financial support in form of tuition/allowances and for granting me training leave that enabled me to complete this PhD thesis is immensely appreciated. God bless all of you. Furthermore, my sincere gratitude goes to the Tertiary Education Trust Fund (TET-Fund) of the

Federal Republic of Nigeria for sponshoring my Bench Work at the Universiti Putra Malaysia (UPM), Serdang, Malaysia, which enabled me to complete this research.

This acknowledgement would not be completed if I do not appreciate the various technical supports I received from the following: I want to thank Mr. Utange of the Environmental Chemistry Laboratory at the BSU for his help during the batch adsorption experiments. Staff of Benue State Environmental Sanitation Agency (BENSESA) Laboratories, Makurdi especially Mr. Tivfa is deeply appreciated for providing facilities and for helping during the synthesis of the materials developed in this research. Mr. Orpin of the Benue State Rural Water Supply and Sanitation Agency (BERWASA), Makurdi is also appreciated for his contribution towards the characterization of groundwater samples. I wish to deeply appreciate Mr Isa Yakubu and Engr. Kamil Katibi of the National Research Institute for Chemical Technology (NARICT) Zaria and the Universiti Putra Malaysia (UPM), Serdang, Malaysia respectively for their huge assistance towards the advanced characterization of my activated carbon samples as well as for the provision of Aqua Chem (Aq*QA) version 2014 software for the hydro-chemical characterization of groundwater. I wish you divine rewards in abundance. Not forgetting the assistance and counsel I received from my colleague and friend, Engr. Dr. O. T. Iorhemen of the Department of Civil and Environmental Engineering, University of Nothern British Columbia, Canada.

I wish to acknowledge the contributions of some of my undergraduate students at the JOSTUM for helping out with data collection at different times during the course of this research work. I remain grateful to Oshido, Hangeior, Aboh, Ijoga and Ugwudike for assisting in this regard.

My profound gratitude is extended to my PhD mates at the Department of Agricultural and Environmental Engineering, University of Ibadan for their various contributions and the nice times we had when we all travelled from various locations to Ibadan for our annual seminar presentations. I will definitely miss, Audu, Kuti, Raphael, Mark, Olokoshe, Unisa, Simeon to mention a few. However, may God continue to guide and strengthen you in your future endeavours.

I wish to appreciate my colleagues back home in the Department of Agricultural and Environmental Engineering at JOSTUM for always reminding me that I had a task ahead to accomplish. Those constant reminders kept me on my toes until this research

piece was delivered. Professors M. O. Udochukwu, S. B. Onoja and T. K. Kaankuka are appreciated most specifically in this regard. The financial support I received from Engr. Prof. G. D. Akpen, Dr. Moses Ukeyima, Mr. Emmanuel Igbaukum, Dr. Aondowase Nyam, Engr. Drs. T. Utsev and T. Kureve which enabled me to complete my PhD. Journey during the trying times is deeply and sincerely appreciated. God will surely replenish your pockets in multiple folds.

I am grateful to my lovely wife, Ngodoo who always stood in for me during my long trips to and from Ibadan and sundry while pursuing this degree and who ensured that our kids were fine at all times. Finally to my lovely daughters: Vera, Sandra, Stephanie and Julie and my brother; Godwin, my cousin; Michael who would always accompany me on the long trips to and from Ibadan, I say thank you all for your love, prayers and understanding throughout the duration of my studies. You are the reason for all these struggles and successes.

ABSTRACT

Groundwater contamination with elevated levels of fluoride has been an age-long environmental problem in many countries including Nigeria. Adsorption is an effective defluoridation technique; however, most of the effective adsorbents are not readily available. It is therefore necessary to explore the adsorptive potentials of local materials such as Raffia Palm Shells (RPS) for fluoride containment in groundwater. This study was designed to produce and characterise activated carbon from RPS for groundwater defluoridation.

Fluoride contents of groundwater in Makurdi, Nigeria, were determined using 63 samples collected from boreholes in 21 locations following standard procedures. The USEPA Hazard Quotient (HQ) was used to evaluate the human health risk potentials in relation to fluoride contamination for infants, children, teenagers and adults. The RPS were sourced from Ugbema market in Benue state and processed into activated carbon using phosphoric acid as activating agent. Response Surface Methodology (RSM) was used to optimise the quality (Specific Surface Area (SSA) and Carbon Yield (CY)) of Raffia Palm Shell Activated Carbon (RPSAC). The surface of RPSAC was coated with aluminium hydroxide to produce Aluminium-oxide-Coated-RPSAC (ACRPSAC) using functionalization principle. Physical characteristics (Brunauer-Emmett-Teller Surface Area (BETSA), Bulk Density (BD), Moisture Content (MC), Total Pore Volume (TPV), Average Pore Diameter (APD) and pH_{pzc}) of the adsorbents were determined using standard methods. Adsorbents' surface compositions were determined by SEM/EDX, FTIR and XRD analyses. Groundwater defluoridation potentials of the adsorbents were evaluated using batch adsorption method in comparison with a Commercial Activated Carbon (CAC). Linear regression and ANOVA at $\alpha_{0.05}$ were used to analyse the data sets.

The fluoride contents in the water exceeded the WHO limit of 1.5 mg/L in 33.3 % of the samples and ranged from 0.32 – 2.06 mg/L (mean=1.26±0.41). The HQ exceeded the threshold value of 1 in 66.7, 71.4, 52.4 and 9.5 % of the water samples for infants, children, teenagers and adults, respectively. Optimum conditions for the synthesis of RPSAC were 524 ^{o}C, 77.0 %, 4.00 g/mL and 104 minutes for temperature, concentration, impregnation ratio and time, respectively. The optimized values of SSA and CY were 1762.93 m^2/g and 78.0 %, respectively. The physical characteristics of RPSAC and ACRPSAC were 456.1 and 715.8 m^2/g, 0.45 and 0.37 g/cm^3, 18.5 and 4.2 %, 0.25 and 0.47 cm^3/g, 2.13 and 1.85 nm, 2.10 and 4.05 for BETSA, BD, MC, TPV, APD and pH_{pzc} respectively. The SEM/EDX showed that the adsorbents had both micro and meso-porosities. The abundance of hydroxyl functional groups on the adsorbents' surface was evident. The RPSAC was found to be amorphous, while the ACRPSAC was microcrystalline due to the formation of graphite-like structures. Batch fluoride adsorption performances of the adsorbents were in the order of ACRPSAC > RPSAC > CAC (removal efficiency= 80.0–99.0%) and were significantly different. Fluoride removal obeyed the Langmuir (R^2=0.8802–0.9751) and Pseudo second order (R^2=0.9974–0.9999) models which signified that its adsorption by the adsorbents was chemisorption-controlled.

Aluminium-oxide-coated raffia palm shell activated carbon is a suitable adsorbent for groundwater defluoridation in batch systems.

Keywords: Batch adsorption, Defluoridation, Groundwater contamination, Raffia activated carbon.
Word count: 484.

TABLE OF CONTENTS

LIST OF TABLES

LIST OF FIGURES

LIST OF PLATES

LIST OF APPENDICES

LIST OF ABBREVIATIONS

AA	Activated Alumina
AAC	Activating Agent Concentration
AC	Activated Carbon
ACRPSAC	Aluminium (Hydr) Oxide-Coated Raffia Palm Shell Activated Carbon
ANOVA	Analysis of Variance
APD	Average Pore Diameter
APHA	American Public Health Association
ASTM	American Standard Testing Method
AT	Activation Temperature
ATT	Activation Time
AWWA	American Water Works Association
BD	Bulk Density
BET	Brunauer-Emmett-Teller
BETSA	BET Surface Area
BISWQI	Bureau of Indian Standards Water Quality Index
BPD	Bangham's Pore Diffusion
CA	Correlation Analysis
CAC	Commercial Activated Carbon
CCD	Central Composite Design
CDD	Chronic Daily Dose
CY	Carbon Yield
DMRT	Duncan Multiple range Test
DW	Distilled Water
EC	Electrical Conductivity
EDI	Estimated Daily Intake
EDX	Energy Dispersive X-ray
EPA	Environmental Protection Act
EPMA	Electron Probe Micro Analyzer
FAOSTAT	Food and Agricultural Organization Statistics
FTIR	Fourier Transform Infrared
GAC	Granular Activated Carbon
HCA	Hierarchical Cluster Analysis

HI	Hazard Index
HHRA	Human Health Risk Analysis
HQ	Hazard Quotient
IHE	International Higher Education
IR	Impregnation Ratio
IRIS	Integrated Risk Information System
ISE	Ion Selective Electrode
IUPAC	International Union of Pure and Applied Chemistry
MC	Moisture Content
NOAA	National Oceanic and Atmospheric Administration
NISDWQ	Nigerian Standard for Drinking Water Quality
RfD	Oral Reference Dose
PAC	Powdered Activated Carbon
PCA	Principal Component Analysis
PD	Pore Diffusion
PET	Potential Evapotranspiration
PFO	Pseudo First Order
pH	Free hydroxyl ion
pH_{pzc}	pH of point of zero charge
PHREEQC	pH-REdox-Equilibrium Code
PoS	Point of Service
PoU	Point of Use
PSO	Pseudo Second Order
RACRPSAC	Aluminium (hydr) Oxide Recoated ACRPSAC
RPSAC	Raffia Palm Shell Activated Carbon
RPS	Raffia Palm Shell
RSM	Response Surface Methodology
SEC	Specific Electrical Conductivity
SEM	Scanning Electron Microscopy
SSA	Specific Surface Area
STCAC	NaOH-Treated Commercial Activated Carbon
STRPSAC	NaOH-Treated Raffia Palm Shell Activated Carbon
STRACRPSAC	NaOH-Treated and Aluminium (hydr) Oxide Recoated ACRPSAC
TDS	Total Dissolved Solids

TF	Total Fluorosis
TISAB	Total Ionic Strength Adjustment Buffer
TPV	Total Pore Volume
UNESCO	United Nation Education, Scientific and Cultural Organization
USEPA	United States Environmental protection Agency
WHO	World Health Organization
WMIPD	Webber Morris Intra-Particle Diffusion
WQI	Water Quality Index
XRD	X-ray Diffraction
XRF	X-ray Fluorescence

CHAPTER ONE

INTRODUCTION

1.1 Background to the Study

Adulteration of aquifers with fluoride is recently acknowledged to be among the foremost worldwide ecological contamination problems (Mahamud, 2012). Aside arsenic and nitrates, the global governing body on health: the WHO has categorized fluoride as one of the pollutants of potable water that promotes large-scale wellbeing problems. Raised levels of F^- in aquifers are reported in several continents and nations of the globe and are mostly documented to be wide-spread in Asia, South America and Africa (Ali *et al.,* 2016; Dhanya and Shaji, 2017). On the African continent, studies have revealed high levels of fluoride in Uganda, Ethiopia, Sudan, Kenya, Nigeria, Tanzania, Malawi, Ghana, Algeria and South Africa and among others (Malago *et al.,* 2017).

Amit *et al.* (2011) posited that F^- is expansively dispersed in ecological media and released to aquifers by slow disintegration of fluorine-bearing minerals. Fluoride is the ionized form of fluorine among the known halogens. It is light and do not exist as an element in nature because of its extraordinary electronegativity and reactivity (WHO, 2006; Mohammed *et al.,* 2018). Fluoride is vital for calcification of teeth and bone improvement in humans when present in tolerable concentrations (Mandal and Mayadevi, 2009). It is deposited in water by nature-based events (volcanic activities) and industrial/anthropogenic undertakings (electroplating, steel and fertilizer industries) (WHO, 2006). It is a hard base that has enormous attraction to hard acids like Al^{+3} and Fe^{+3} which could be further ascribed to its lesser ionic size and robust electronegativity.

Based on the health implications of consuming groundwater polluted with questionable amounts of F^-, the WHO has stipulated a tolerable threshold of 1.5 mg/L for healthy consumption of fluoride holding water (WHO, 2008). Fluoride ion is vital and as well detrimental for teeth and skeleton establishment in persons. It is beneficial to human

health when in small concentrations (0.5 – 1.5 mg/L) because it foils dental caries and aids in the establishment of robust skeletons in both growing and fully matured humans. Nonetheless, consumption of materials (food and water) with exceeding amounts (1.5 mg/L) of fluoride promotes diverse human health issues including fluorosis, stumpy intelligent quotients in children, diminished maternity, nervous disorders, and gland damages among others (Mohammed *et al.,* 2018). Moreover and most importantly epidemiological evidence has revealed that unwholesome water intake is the main doorway of F^- into humans. Fluoride in drinking water occurs naturally through rock-water interactions or through the addition of fluoridated salts to drinking water.

The northern and southwestern parts of Nigeria are the most affected regions with regards to fluoride content in groundwater exceeding the WHO threshold value (Akpata *et al.,* 2009). For instance several local government areas in Gombe, Oyo, Ogun, Ondo, Lagos, Taraba, Plataeu, Adamawa, Benue, Katsina, Niger, Sokoto, Nassarawa and Borno states etc. of Nigeria have elevated F^- contents in groundwater. However, such groundwater are the major sources of domestic water provisions to over 90 % of the residents in these areas (Bura and Goni, 2012; Gbadebo, 2012; Tukur and Amadi, 2014;Amadi *et al.,* 2015; Okunola *et al.,* 2016; Olasehinde *et al.,* 2016; Gwaha, 2017; Bura *et al.,* 2018; Emenike *et al.,* 2018a; Emenike *et al.,* 2018b; Malum *et al.,* 2019).

As a collaboration of the foregoing assertions, several works and surveys have revealed medium to excessive occurrence degrees of fluoride-linked ailments (dental caries and fluorosis) in several parts of Nigeria. This suggests that fluoride enrichment of domestic water supplies in such areas is to blame (El Nadeef and Honkala, 1998; Wongdem *et al.,* 2000; Akpata, 2004; Umesi-Koleoso, 2004; Ajayi *et al.,* 2012; Ephraim-Emmanuel *et al.,* 2013; Danbature *et al.,* 2014; Dirisu *et al.,* 2016; Ephraim-Emmanuel *et al.,* 2016; Fulata *et al.,* 2017) Potable water obtained from aquifers and unwholesomely ingested is believed to be the main channel of F^- -linked ailments in most parts of Nigeria (Uriah *et al.,* 2014).

In the bid to avert the inherent risk of consuming fluoride laden water, there has been an age long battle by researchers globally to identify suitable and sustainable technologies/approaches for defluoridation of potable water sources in several places

of the globe including Nigeria. The foregoing has however been linked with limited degrees of successes, thus requiring further efforts in this regard.

1.2 Problem Statement

Up till now, there are minute or negligible inputs aimed at fluoride containment in potable water sources before its intake at the domestic or communal/municipal levels in remote and urbanized environments in the less developed countries. The foregoing has perpetually exposed such populations that depend on unwholesome groundwater sources for their potable uses to the spiteful effects of fluoride contamination.

Several expertise including adsorption, precipitation (Nalgongo technique), electro-dialysis, reverse osmosis and nano-filtration were tried for containing F^- in potable water (Mahamud, 2012). Among these technologies, adsorption sustained by Activated Alumina (AA) is viewed to be low-cost, simplistic and yet effectual for containment of F^- ions in drinkable water sources. In the past, a number of nature-based resources like clay, red mud, AA, bauxite, pumice, charcoal and lateritic soils etc. have been employed with relative success for fluoride removal in potable water (Onyango, *et al.*, 2004; Mandal and Mayadevi, 2009; Mwampashi, 2011; Mahamud, 2012). The uneven spread of such minerals around the world is responsible for the relativity in the efficacy of these techniques. The foregoing implies that dependency on nature-based adsorbents for potable water treatment could hamper the practicability and usefulness of these technologies in some locations.

Lately, scientists have adopted the metal precipitation norm to modify nature-based or biomass-derived activated carbon (AC) or composites for F^- containment in water with auspicious and workable outcomes. With the adoption of the metal precipitation principle, it is guaranteed that the oxides of metals such as Al, Mn, Fe, Ce etc are placed on both the exterior and interior portions of the adsorbents by precipitation reactions resulting from the hydrolysis of such metal salts. These metal oxides are recognized as possessing great attractions towards the extremely electronegative fluoride ions in water. Thus, in general, very high defluoridation rates could be achieved through ion exchange and pore diffusion mechanisms when a fluoride contaminated media is interacted with activated carbon-metal oxide composites (Salifu, 2017).

A chronicle of selected metal oxide-coated adsorbents explored in the past is highlighted as follows; bauxite coated with Al_2O_3 (Mahamud, 2012), charcoal decorated with Al_2O_3 (Mahamud, 2012), bark *of Morinda tinctoria* decorated with hydrous Al_2O_3 (Almaraj and Pius, 2016), nano particles of hydrous Al_2O_3 coated on tea biomass (Cai *et al.*, 2016), Al_2O_3 surface-decorated pumice (Salifu *et al.*, 2016), nano particles of Al_2O_3 (Rathore and Mondal, 2017).

Literature evidence has shown that the majority of these materials for sequestrating F^- in water were obtained from the nature-based minerals with only a handful of them synthesized from renewable materials such as agro-based biomass. It is thus sacrosanct to test the suitability of the available biomass leftovers including Raffia palm (*Raphia hookeri*) shells for the production and utilization of metal oxide coated activated carbon for drinking water defluoridation. The foregoing would heighten the effectiveness of the efforts geared towards fluoride removal in water especially in regions where water contamination with fluoride and prevalence of fluorosis is endemic.

Remarkably, owed to its high carbon, low ash content and abundance, Raffia palm (*Raphia hookeri*) shells (RPS) are viewed to be a promising candidate with potentials for transformation into adsorbing materials for groundwater defluoridation. RPS has inherent immediate compositions that qualify it to be efficaciously changed into AC for home and work-based water management uses. In spite of the enormous potentials inherent in Raffia palm shells for its exploitation in water treatment applications, only a few researchers have documented its uses as base-resource in AC synthesis for water management applications (Inyinbor *et al.*, 2016; Ghogomu *et al.*, 2016; Inyinbor *et al.*, 2017). Notwithstanding, none of these studies have attempted to apply the raffia palm shells-derived activated carbon or bio-sorbents for fluoride removal in water.

The current work was therefore designed to synthesize a tailored activated carbon obtained from RPS by initially stimulating it with H_3PO_4 and then functionalizing its surface with aluminium oxide to offer amplified affinities for F^- in solution. In the future, the fallouts of these microcosm scale experiments would be handy for building household-scale point of use F^- containment systems using the best-performing and newly synthesized adsorbent in this work. Furthermore, this study seeks to embark on an all-inclusive assessment of groundwater sourced from boreholes (a major source of

drinking water) in Makurdi metropolis, North-central, Nigeria, with a focus on its fluoride concentrations and linked human health issues. The novelty of the current research as started above would benefit the achievement of the age long goal of the search for a cheap, effective and workable local technology for fluoride containment in drinking water sources at decentralized/household levels.

1.3 Aim and Objectives of the Study

The current research aims to develop and evaluate new adsorbents derived from RPS, namely; Raffia Palm Shell Activated Carbon (RPSAC) and Aluminium (Hydr) Oxide-Coated Raffia Palm Shell Activated Carbon (ACRPSAC) for groundwater F^- containment through batch adsorption techniques. The research is thus intended to address three specific objectives:

1. To optimally produce and brand novel AC of RPS origin for batch-mode groundwater F^- sequestration.
2. To assess the efficacy of the as-synthesized AC for groundwater defluoridation using batch adsorption experiments.
3. To assess groundwater obtained from boreholes in Makurdi Metropolis, North Central-Nigeria and determine the health risk potentials with emphasis on fluoride content.

1.4 Justification of the Study

Previously, a number of biomass materials belonging to the palm family such as coconut shells, coconut husk, palm kernel shell etc were adequately transformed into AC and used for environmental remediation. However, not much of these have been achieved using RPS, especially for fluoride removal in water. Interestingly and as reported by Ogwuche (2016), RPS possesses useful proximate and ultimate compositions that make it stand out as a potent precursor for AC synthesis. Therefore, it can be effectively exploited for the synthesis of AC for domestic and industrial water treatment uses. These would go a long way in ensuring environmental sustainability by reducing the dependency on fossil resources for activated carbon production and would also ensure the safety of water bodies.

There is therefore the need for the production of tailored agro-based AC with efficient fluoride removal potentials for drinking water treatment in Nigeria where most of the naturally occurring adsorbents are found in limited quantities.

In the current study, two optimally tailored activated carbon RPS origins were developed, characterized and comparatively tested for F^- containment in potable water by batch adsorption methods. As it is with the custom of adsorption system designs, the outcome of this work will benefit the design and deployment of batch PoU defluoridation units at family scales.

Furthermore the quality valuation of groundwater in Makurdi metropolis and its environs would provide valuable insights into the underlying threat linked with the intake of F^- laden groundwater in several locations considered. The findings of this work would highlight the need or otherwise for the adoption of a suitable technology for the containment of fluoride contamination in groundwater at household and community scales. This is the first attempt towards a rounded valuation of groundwater quality from boreholes in Makurdi, Nigeria with a focus on its F^- levels and linked well-being issues. It is also the first attempt toward the synthesis of tailored AC of RPS origin for groundwater defluoridation, thus the novelty of the current research work.

1.5 Scope of the Study

The current work is constrained to the following activities and outcomes. Firstly, only raffia palm (*Raphia hookeri*) shells were used as precursor for the preparation of RPSAC and ACRPSAC employed for fluoride adsorption in the current effort, while H_3PO_4 was adopted as the sole stimulating mediator and aluminium sulphate adopted as starting material for coating the adsorbent surface with aluminium (hydr) oxide. Response Surface Methodology (RSM) was adopted for optimization of the adsorbent quality during the activated carbon production process. As such, only four factors (stimulation time, temperature, and stimulating agent concentration and impregnation ratio) presumed to affect the quality of activated carbons were optimized, while only two responses (carbon yield and specific surface area) which are major determinants of a quality activated carbon were considered. This was done to reduce process times and cost of the study.

The inherent composition of the precursor was ascertained while the categorization of the optimally blended AC was limited to the ascertaunment of its BET surface area, pH_{pzc}, porosities, FTIR spectrums, SEM-EDX, XRD, moisture content and bulk density.

Furthermore the study considered the comparative influence of temperature, contact time, carbon dosage, initial fluoride concentration and solution pH on the fluoride removal efficiencies and adsorption capacities of the adsorbent (RPSAC and ACRPSAC) using batch adsorption experiments with simulated fluoride solutions in comparison with a CAC (charcoal activated) from where the fluoride adsorption mechanisms, types and nature were again comparatively determined for all adsorbents considered in the study. Furthermore the study again employed RSM to optimize fluoride uptake on the most potent adsorbent (ACRPSAC) as evidenced in the initial comparative fluoride adsorption tests. Confirmation experiments at the established optimal conditions were also done on actual drinking water samples gotten from already known fluoride endemic regions in Nigeria. Possible regeneration studies for the novel adsorbents were also elucidated as well as the influence of rival anions in solution on the fluoride removal abilities of the adsorbents.

The characteristics of groundwater systematically sampled from selected deep wells (21 locations) in the Makurdi town with a focus on fluoride contamination and related human health risks as well as the sources of pollution were succinctly elucidated. It should be noted that this was the first study in the study location that focused on human health risk and exposures to fluoride contamination on the parts of residents of the town and it was also the first to employ multivariate statistics and water quality index tools to give a holistic outlook of the deep well water quality in the area.

Thus holistically, the study succeeded in developing efficient adsorbents that were utilized in batch adsorption systems for sustainable fluoride removal from drinking water sourced from boreholes and elsewhere. This was primarily undertaken to protect human health in developing countries where most residents source their domestic water from unwholesome sources.

CHAPTER TWO
LITERATURE REVIEW

2.1 Fluoride and its Health Effects

Fluorine as an element is known to be beneficial for healthy dental development. Intake of fluoride in low quantities encourages dental caries and as such, the usage of fluoride-inclusive pastes and mouth cleaners is popularly encouraged to minimize the problems of poor dental health. In most countries, augmentation of natural fluoride concentrations in drinking water sources is undertaken by fluoridation (addition of fluoride). Nonetheless, in spite of the paybacks, optimum prescriptions of fluoride seem to plunge within a slim range. Long term ingestion of high fluoride amounts has been documented to be responsible for teeth decay, and in extreme cases, skeletal fluorosis in humans. Although yet to be fully established, these high dosages have also been reported to be carcinogenic (Marshall, 1990: Hamilton, 1992).

Fluoride concentrations in natural water have values that typically range between 0.2 – 12 mg/L (Adimalla and Li, 2019). Thus water could be the foremost cause of fluorine toxicity to humans in areas where the concentrations are high and such water is unwholesomely consumed. Values of about 1.0 mg/L are usually considered as optimal, however, long term intake of water with fluoride values around or beyond 1.5 mg/L could be injurious to man's well being (WHO, 2006). The WHO has stipulated a threshold of 1.5 mg/L as the extreme acceptable boundary that will guarantee human health (WHO, 2006; WHO, 2017). Many countries of the world including Nigeria have adopted this limit as their national guideline values for fluoride control in drinking water (NISDWQ, 2007), while other countries have set lower or higher limits as their own national guidelines depending on the amounts of fluoride in their natural water supplies and also the availability and cost effectiveness of technologies for fluoride removal in drinking water supplies. Excessive fluoride levels are most times linked with groundwater as they are known to amass fluoride from rock dissolutions and geothermal processes. Regions with high fluoride content in groundwater have been identified across the globe. These include; China, Indonesia, India, Pakistan,

Ethiopia, Kenya, Tanznia, Nigeria, Ghana, Western USA, Mexico, Sri-Lanka and Argentina to mention a few (Makoba and Mazuka, 2018, Karunanidhi *et al.,* 2019; Malum *et al.,* 2019, Liu *et al.,* 2020;).

Defluoridation is undertaken in most nations. Nevertheless, because most of endemic regions are found in emerging nations, defluoridation activities differ greatly and most sources with elevated fluoride levels are consumed unwholesomely. Consequently, enormous groups of persons in the emerging nations grieve with the consequences of long-term endemic fluorosis. Figures are not properly documented, however, over two hundred million persons globally are suspected to access their potable water from sources with worrisome F^- levels. This figure caters for the over 60 million people reported for India (Bello, 2020), forty-five million in China (Su *et al.,* 2021) and about six million persons in Mexico (Limon-Pacheco *et al.,* 2018). In Africa, the number of persons is not known, however, it is estimated to also be in tens of millions (Diaz-Bariga *et al.,* 1997).

Irrespective of the strong proof of wellbeing glitches associated with the occurrence of F^- in potable water and the acquaintances concerning F^- incidence and mineral-water interaction, there are only a hand-full of updates on the hydro-geochemistry of F^-. The subsequent section seeks to address the hydro-geochemical phases of fluoride in water, with particular emphasis on groundwater.

2.2 Fluorine Chemistry

Several authors (Turner *et al.,* 2005; Reddy *et al.,* 2010a; Reddy *et al.,* 2010b) reported that fluorine is a more abundant halogen as compared to chlorine. It amounts to over 600 mg/kg beneath the surface of the earth, while that of chlorine is just 130 mg/kg. Chloride is greatly transportable in water and mostly occurs in the seas. Contrastively, fluorine is typically held-up in rock crystals. Fluorine is the lightest and most electron-lossing element in the halogen family. The size of its ion is quite comparable to hydroxyl ions and replaces freely in OH^- locations in recently-developed crystals of volcanic formations.

According to Kilham and Hecky (1973) fluorine is transportable at high-temperature settings and as a result of its dainty volatile nature, it could co-exist with boron and/or chloride in hydrothermal solutions.

Fluoride contents are mostly confined in its geological existence. Fluoride is mostly present in acidic volcanic rocks, mineralized strains and deposited landforms where bio-geochemical interactions have occurred. It exchanges with OH^- ions locations in mineral formations like biotites and amphiboles in the following manner: $K_2(MgFe)_4(Fe,Al)_2[Si_6Al_2O_{20}](OH)_2(F,Cl)$ (Handa, 1995).

Upon disintegration of the minerals formations, fluorine is preferably let out of the weathered formations and can find its way into water environment especially where the weathered formation (for example granite) contains biotites and/or amphiboles. High temperature fluorine-bearing minerals like Topaz have lower solubility. Apatite ($Ca_5(ClFOH)(PO_4)_3$), on the other hand can be formed at both elevated and lowered temperatures and could be another major source of fluoride in water. However, replaced apatite containing large amounts of fluorine seems to be a more soluble mineral as compared to purer (high-temperature) apatite. The chief fluorine-bearing mineral is Fluorite (CaF_2) and it exists in local subordinate hydrothermal strain deposits and also as a comparatively occasional antigenic rock crystal in deposits (Ashley and Burley, 1994).

Bio-geochemical processes requiring phosphorus recovery as well as adsorption of fluorine onto clays encourages the concentration of fluorine in marine deposits. Limestone is also known to possess localized amounts of fluorapatite, principally in the form of francolite. Conversely, sandstone contains negligible amounts of fluorine and thus the F^- contents in its neighborhood groundwater is usually negligible (Fawell *et al.,* 2006)

A strong relationship thus exists between the occurrence of F^- in water and the abundance of local fluorine-bearing minerals/landforms (Reddy *et al.*, 2010a) It is also sturdily correlated with the solubility of the minerals for which fluorite is known to be the least soluble with a positive kinetics of dissolution especially at mild heat conditions, Fluorite existence in mineral formations could be seen as the major controlling feature for the occurrence of fluoride in aqueous media. The solubility product ($K_{fluorite}$) determines the extreme limit on fluoride activities in aqueous and can be given as in equations 2.1- 2.3 (Handa, 1995; Turner *et al.,* 2005).

$$CaF_2 = Ca^{2+} + 2F^- \quad (2.1)$$

$$K_{fluorite} = (Ca^{2+}).(F^{-})^2 = 10^{-10.57}\ at\ 25\ °C \quad (2.2)$$

or

$$LogK_{fluorite} = Ca^{2+} + 2Log(F^{-}) = -0.57 \quad (2.3)$$

The foregoing shows a vital association as it demonstrates that with the existence of fluorite, the amounts of fluoride are directly relational to Ca^{2+} amounts. For instance, when Ca^{2+} is present at concentrations of 10 – 30 mg/L at 25°C, soluble fluoride ions would be around 3.1 mg/L. This suggests that the absence of Ca^{2+} in solution would likely be responsible for the heightened and stabilized amounts of F^- in solution, even though carbonate precipitation has also been associated with reduced fluoride concentrations in aqueous media (Adimalla and Venkatayogi, 2017; Emenike *et al.,* 2018b).

Generally, groundwater with diminished calcium content are prevalent in mountaneous areas subjugated by alkaline active formations as well as in situations where natural cation exchange processes are eminent in which Ca^{2+} removal is reached through ion exchange mechanisms with clay-mineral derived sodium ions (Kilham and Hecky, 1973; Ashley and Burley, 1994; Handa, 1995). In each case, the typical hydrogeochemical facies to be found is the Na-HCO_3 water type. This usually takes place in soils and in aquifers following established flow lines in retort with evolving chemical reactions (Edmunds and Walton, 1983) especially in areas associated with salt-water intrusions.

Also as asserted by Handa (1995), another controlling factor for fluoride levels in aqueous environments is the reaction time with the aquifer minerals. Consequently, elevated fluoride levels are expected in groundwater with lengthy reaction times in the host aquifer, which can further be described as digenetic reactions. Surface water and most shallow dug wells are known to contain low levels of fluoride because they epitomize fresh, newly permeated, rainwater. Thus, long-formed and deep-occuring groundwater as in deep wells is thus more probable to comprise elevated levels of F^-.

Table 2.1: Typical composition of ground water in areas with high fluoride levels

Parameter	Unit	Country					
		Ghana	**UK**	**Sri-Lanka**	**Argentina**	**Canada**	**Tanzania**
Water Type		Unconfined	Confined	Unconfined	Unconfined		Unconfined
Well Depth	M	26	99	Nd	16	>30	110
pH		6.63	8.32	6.96	8.1	9.2	8.86
Temperature	°C	31.2	11	29.5	-	-	27.7
*SEC	mg/L	348	-	3840	2610	598	1360
Ca	mg/L	27.6	2.0	173	24.1	4.3	17.6
Mg	mg/L	13.7	4.1	179	22.9	0.7	1.37
Na	mg/L	18.8	540	355	616	137	332
Ca	mg/L	1.56	4.0	3.02	12.6	0.4	2.07
HCO_3	mg/L	146	506	516	1180	232	845
SO_4	mg/L	1.65	33	15.5	190	13.6	20.8
Cl	mg/L	5.89	490	1050	113	56.7	13.6
NO_3-N	mg/L	4.92	<0.1	9.00	45.9	Nd	7.81
F	mg/L	3.6	5.6	4.4	15.8	10.9	17.5
Si	mg/L	34.4	6.0	45.0	28.1	3.5	54.2
Fe	mg/L	0.37	0.48	0.007	0.055	0.087	0.053
Al	µg/L	30	14	Nd	40	67	81
Be	µg/L	1	Nd	Nd	83	Nd	2
U	µg/L	1.3	Nd	Nd	71	Nd	Nd
B	mg/L	-	-	0.15	4.58	-	0.46

Nd: Not determined. Source: Bolye and Chagnon (1995)*is Specific electrical conductivity

However, where hydrothermal inputs are inevitable, all of surface water, shallow groundwater and deep groundwater could contain questionable levels of fluoride.

Arid climatic zones are also known to contain excessive amounts of fluoride in groundwater (Fuhong and Shuquin, 1988; Handa, 1995; Smedley *et al.*, 2002). This is because in such situations, groundwater flow and infiltration rates are generally slowwhich promotes extended rock-water interactions. Conversely, in humid/tropical environments, groundwater fluoride contents are lower due to the diluting effect of high precipitations on groundwater chemistry. Table 2.1 depicts the elemental structures of a number of characteristic fluoride-ladened groundwater in different regions of the world. The overriding effect of Na over Ca is illustrated in the data presented as well as the elevated amounts of HCO_3^- that symbolise fluoride-ladened water. Likewise, it shows the probable principal classes, estimated by the PHREEQC approach (Parkhurst and Appelo, 1999).

Unrestricted fluoride could be seen as the overpoweringly main form in most natural water that have negligible extra quantities of multiplexes containing key positively charged ions like Ca^{2+}, Mg^+ and Na^+. Nevertheless, the distribution of these ions is intensely pH-reliant. Strong complexation with hydroxyl and aluminium ions could take place under acidic situations (Deng *et al.*, 2011), whereby, hydrogen fluoride dominates at around pH of 3.5 (Hem, 1985). Fluorine also voluntarily combines with boron, vanadium uranium, iron, silicon etc. to create multiplexes in water which may encourage fluoride mobility when found in high concentrations in solution.

2.3 Raffia Palm Fruit

The Raffia palms (*Raphia hookeri*) are a major source of agro-waste especially during its harvesting season. The edible part of raffia palm fruits is the chewy portion. The shells are not edible and are typically thrown away as unwanted materials. Raffia palm has emerged as a vital species in the economic point of view. This is evident in its surged domestic demand in most countries including Nigeria Consequent upon the increased intake of the fruit's consumable portions, enormous volumes of Raffia palm shells are indiscriminately discarded in the environment (Ghogomu *et al.*, 2016)..

This practice promotes environmental degradation arising from the slow decay of the shells and ensuing discharge of odour. For enhanced beneficial utilization of cheap and

profuse agricultural biomass, Raffia palm shells could be converted into activated carbon for subsequent use in environmental remediation. This would solve the problems of agro waste management and curb environmental pollution. Conversely, only a few studies have been reported on the conversion of raffia palm shells into activated carbon for water purification, with none considering it for fluoride removal in water (Ghogomu *et al.,* 2016; Inyinbour *et al.,* 2016; Inyinbor *et al.,* 2017; Akpen *et al.,* 2018).

Raffia palm seed is characterized by a large ellipsoid seed within the oily mesocarp of the fresh fruit and a hard endocarp (Plate 2.1a). At maturity, the seed appear to be intermittently furrowed and ridged at the outer parts. The inner part houses the endosperm which has a deep but slender cogitation. The fruit is not much studied for its value as a source of food but is mostly used for beautifications. The endocarp is hard and presents handy for use in arts and actifacts development. The braches are soft and durable and can be easily sawn into usable shapes for furniture-making (Ghogomu *et al.,* 2016; Inyinbor *et al*, 2017).

The shells of raffia palm fruit are not known for much use. Despite their high carbon content, they are considered as waste (Ogwuche, 2016). The focus of this work was to convert the waste into wealth for a friendlier environment through activated carbon production using the shells. Plate 2.1b shows an image of raffia palm fruit, while plate 2.1c shows the image of Raffia palm shells (the starting material for AC synthesis in the current study).

2.3.1 Uses of Raffia Palm

There are many valuables derived from raffia tree around the world. Its economic value has been tested in the following endeavors:

A. Raffia Palm Fibre

Throughout the world, Raffia fibre is extensively utilized for making of twine, basket, brooms, ropes, hats, shoes, mats and clothing etc. Membranes of the downside of the palm leaves are mainly used for the fibre production. Removal of the membrane leads

Plate 2.1a: Image of Raffia Palm fruit endocarp
Source: Aniogbu, 2017

Plate 2.1b: Raffia palm fruit
Source: Aniogbu, 2017

Plate 2.1c: Raffia palm shells
Source: Ogwuche, 2016

to the formation of long thin fibres that could be coloured and converted into clothing materials and other products as mentioned earlier (Ogwuche, 2016).

Furthermore, in most nations, the fibres could be imported and utilized in form of natural strings for farmland separation and plant support during grafting or soilless culture in greenhouses (Ogwuche, 2016).

B. Raffia Wine

Raffia palm also serves as a source of a cherished local wine regularly consumed in east and southern regions of Nigeria. The juice contains sugars and is typically gotten by creating a box-like cutting on the topmost portion of the tree and then placing a big siphon that collects the whitish-milky outpour; a process that usually leads to the death of the plant as opposed to oil palms which survive similar exposures.. The collected liquid could be better enjoyed as a source of alcohol if allowed to ferment in
a few days as the freshly harvested sap is sugary and partially carbonated. During the fermentation process, most of the sugars are converted into alcohols and is natively referred to as "wine". The Wines of Raffia palm origin are usually sweeter no matter the age as compared to wines of oil palm origin. However, both kinds could be further distilled to produce spirits locally called "Ogogoro". As a tradition in most cultures where Raffia or oil palms are abundant, visitors and spirits are symbolically offered these wines derived from the palms (Ogwuche, 2016).

Most agricultural biomass including Raffia palm shells are also useful as materials for the synthesis of AC (Table 2.2). The produced AC is usually used for removing contaminants in various ecological media including soil, water and air (Rahmani *et al.,* 2009).

2.4 Activated Carbon

Activated carbon (AC) could be described as an amorphous material with a very huge inner surface area and pore volume. These exclusive features of AC account for its adsorptive potentials that could be explored in several liquid- and gas-phase uses. Usually, the adsorptive performances of ACs toward environmental remediation are enhanced by several factors including the type of starting material, the activation method and manipulation of preparation conditions (Okwuchukwu, 2017).

Table 2.2: Production of Activated Carbons from Biomass Residues

Author	Year	Precursor	Activation Method	Application
Erabee *et. al.*,	2017	Sargo palm bark	$ZnCl_2$	Not applied
Hu and Srivinasen	2001	Coconut and Palm kernel shells	$ZnCL_2$ and CO_2	Adsorption of phenol and methylene blue
Guo and Lua	2003	Palm shells	H_3PO_4	Ammonia adsorption
Mozammel *et. al.*	2002	Coconut shells	$ZnCL_2$	Adsorption of iodine
Hu *et. al*.	2001	Coconut and Palm kernel shells	$ZnCL_2$	Dye and phenol adsorption
Daud and Ali	2004	Coconut and Palm kernel shells	Physical activation	Nitrogen gas adsorption
Iwar	2015	Coconut, palm kernel shells and their mixture	H_3PO_4	Treatment of brewery wastewater
Ogwuche	2016	Raffia palm shells and seeds	$ZnCL_2$	Treatment of abattoir wastewater
Okwuchukwu	2017	Raffia palm shells	HNO_3	Cadmium adsorption
Alhogbi, *et al.*,	2021	palm tree fibre waste	H_3PO_4, H_2SO_4, KOH	Anionic and cationic dyes

2.4.1 Origin and History of Activated Carbon (AC*)*

ACs has been in use for ages to the extent that its place of beggining is not precisely established. However, the first knowledge of its use as charcoal was by the Egyptians and Samarians for the lessening of metals used in the production of bronze, as well as household charcoal for cooking (Oloworise, 2006).

Charcoal (carbon) has the ability to adsorb vapours from organic chemicals and decolorize aqueous solutions. Nevertheless, those derived from wood at that moment did not perform effectively in this regard, because of its poorly formed pore structure emanating from mere carbonization. Thus, consequent attempts to increase the porosity of these charcoals gave birth to activated carbon (Oloworise, 2006).

The first method of producing ACs using both heat-based and chemical procedures was done by heating plasma with ash to create AC that had over 50 times higher the colour removal performance of bone char (Oloworise, 2006). Thereafter, scholars and researchers started searching for ways of producing AC industrially from vegetable materials (agro wastes) with improved porosity (i.e. large surface area). In recent times, activated carbons production techniques employed the methods of incorporation of carbonaceous materials with activating agents such as; phosphoric acid, carbonate, salts, metallic chlorides, sulphuric acid, hydrochloric acid to yield activated carbons with superior/high adsorptive properties (Alkali, 2016).

2.4.2 Properties of Activated Carbon

AC is a material that has elevated carbon content and has been subjected to the activation/stimulating procedures. Alternatively, they could be viewed as materials whose adsorptive potentials have been enhanced by anthropogenic procedures. According to Soleimani and Kaghazchi (2008), AC is the professional designation for a carbonaceous material that has enhanced pore formations and huge surface area. Generally, they can be defined as non-hazardous, treated, carbon-rich materials with a great extent of pore formations with and extensive internal surface coverage. Thus they are capable of adsorbing a vast quantum of contaminants from the environment. AC is amorphous in structure which indicates the absence of regular atomic structures in them as compared to other forms (allotropes) of carbon such as diamond, fullerenes or nano-tubes. It is usually hydrophobic and non-polar in nature.

AC is extensively applied for various purposes with regard to its enhanced surface area and micro-pore structure (formed during carbonization/activation) which promotes adsorption or chemical reactions (Barret *et al*., 1951). It can be applied for water and wastewater purification, adsorption of toxic and emerging contaminant, air purification, separation of gases, and recovery of valuable organic and inorganic chemicals form air and water (Rahmani *et al*., 2009).

Similarly, it is used in the polishing of electroplating liquid as a major procedure for adsorption of organic contaminants in solution. Table 2.2 shows a summary of some previous studies on the use of some agricultural residues as low cost ACs.

2.4.3 Uses and Applications of Activated Carbon

AC is used in diverse applications including as filters in pressurized air, gas cleaning, refinement of gold, metal abstraction, caffeine removal, water/wastewater treatment, drug delivery and poison removal among other uses.

A. Industrial Uses

The main industrial use of AC is in the field of metal finishing where it is largely used in the polishing of electroplating liquids. As an instance, the use of AC is a major treatment procedure for eliminating organic contaminants in perky nickel plating liquids. During such procedures, a vast number of organic substances are mixed with the plating liquids to enhance its deposition abilities and improve metal features such as brightness, smoothness, ductility. The mechanisms are such that as direct current is passed and electrolytes interact at the anode and cathode, the added organic chemicals produce unsolicited degradation by-products in the plating liquids which must thereafter be removed by the use of AC. The extreme formation of these unwanted by-products can harmfully influence the features and quality of the finished metals if not removed by the use of activated carbon (Faraji and Ani, 2015; Maher *et al.*, 2021).

A. Medical Applications

In medicine AC is commonly utilized for the containment of ingested poisons or drug overdoses in humans and animals. Usually and in most developed nations, activated carbon capsules or tablets are used as a common drug to contain health conditions like dyspepsia, turgidity and diarrhea. On the contrary, AC performs poorly when used to

contain poisons such as glyphosate, strong acids and bases, cyanide, heavy metals, methanol and ethylene glycol (The American Society of Health-System Pharmacists). Furthermore, wrong uses of AC for medical purposes such as in the lungs could lead to respiratory injuries that can cause death if immediate medical attention is not sought (Elliott *et al*., 1989).

B. Environmental Applications

Activated carbon adsorption serves for a number of uses in the industrial and domestic fields aimed at eliminating contaminants in water and air media. Such application include, determination of radon quantities in air, oil spill cleaning, soil remediation from heavy metals, leachate treatment, groundwater treatment, air scrubbing, capture of volatile organic substances during gasoline dispensing and dry cleaning activities, nutrient recovery, wastewater/sewage treatment among others (Utsev *et al.,* 2020).

In the initial execution stages of the 1974 "Safe Drinking Water Act" in the USA, there was a strong rule that required all proposals aimed at the establishment of potable water treatment facilities to use granular activated carbon (GAC). This rule was enforced by the officials of the USEPA. However, the prohibitive costs of GAC led to strong negative agitations by the water supply industrialist including the biggest water utilities in California. The foregoing compelled the USEPA to set aside the rule.

C. Agricultural Applications

AC is a permitted material for use for organic farming toward the production of livestock and wine. It is applied as a pesticide, feed stabilizer (questionable benefit), handling aid, non-agricultural constituent and sterilizer in livestock production. For organic-based wine production, AC is unrestrictedly utilized as a process aid in organic wine making to adsorb tanned colour pigments from white grape distillates. It is also used for soil amendment towards effective soil fertilization (Dominguez *et al.,* 2020).

2.5 Production of Activated Carbon

Chemically and physically activated carbons are both widely used in contemporary technologies. Although products of high quality can be obtained from both activation methods, in most cases, these are not correspondingly decent for all application. For instance, in solvent recapture and/or adsorption refrigeration, Activated carbons of

chemical modifications perform better, while for wastewater management, both activation methods can suffice (Smisek and Cerny, 1970).

1. Physical/Thermal activation: In this method the precursor is converted into activated carbon by subjecting it to hot gaseous treatment after which air is applied to scrub the gasses by burning This process leads to the formation of a well-sorted, partitioned and dust-free AC . Usually one or a mixture of the following procedures is adopted:

i. Carbonization: The precursor with adequate proximate composition (carbon content) is carbonized at temperatures of 400 - 800 ˚C, in the presence of argon or nitrogen with limited or avoided oxygen supplies.
ii. Activation/Oxidation: The precursor or pyrolyzed product is subjected to oxidizing situations using steam or oxygen, usually at elevated temperature ranging from 600 to 1200 ˚C.

The stimulating/activating media destroys the volatile parts of the carbon network at raised temperatures. The interaction between the stimulating/activating media/agent and the carbonized material (intermediates) occurs at the interior portions and leads to the formation of additional adsorption sites with the liberation of H_2, CO_2, CO and O_2 from its matrix. The reaction that takes place between the activating agent and the carbonized intermediate is known as the "water-gas reaction".

2. Chemical activation: Here, before pyrolysis, the precursor is mixed with a chosen chemical substance which is usually an acid, strong base or salts (eg. HCL, NaOH, $ZnCl_2$, respectively). The next steps involve the subjection of the impregnated precursor to pyrolysis at moderate temperatures of 450 - 900 ˚C. The assumption is that both carbonization and activation occur at the same time. Usually, the mechanism for chemical activation involves the degradation or desiccation of the cellulosic matrix of the precursor (Hussein *et al.*, 1995). Scientist and industrialists choose chemical activation ahead of physical activation because of the lower temperatures and lesser processing times required in the former.

2.5.1 Phosphoric Acid (H_3PO_4) Activation

The synthesis of high quality AC using H_3PO_4 as activating mediator involves the optimal manipulation of influential factors such as The proximate composition of the precursor, the chemical (acid) to starting material ratio (impregnation ratio), activation

temperature and time as well as the heating rate. In general, wood and agro-biomass such as coconut shells, walnut shells, flamboyant pods and other carbon-rich precursors with appreciable volatile content are the utmost frequently used in the chemical activation method using H_3PO_4 (Menéndez-Díaz and Martín-Gullón, 2006). As posited by the authors, the following illustrate the general phases involved in the synthesis of AC using H_3PO_4 as activating agent:

i. Pulverization and characterization of the precursor;
ii. Interacting the precursor with the ideal concentrations and ratio of H_3PO_4
iii. Carbonizing the filtered, washed and dried material at lower temperatures of 400 – 500 $^{\circ}$C in the absence or limited supply of oxygen to avoid complete burn-out.
iv. Further carbonization at higher temperatures of 673 to 773 $^{\circ}$C.
v. Recovery of unreacted acids by repeated washing of the carbonized product with distilled water, then oven-drying and characterization.

Steps (iii) and (iv) above could be undertaken in the same furnace without requiring an initial cooling step. Residence times for steps (iii) and (iv) may be about one hour each. As a comparison with AC synthesized via thermal method, wood-derived AC by H_3PO_4 possess diminished densities and resistance to attrition, but have higher meso-pore structure formation. The highlighted features of AC are linked to the hollow fibrous configuration in wood, which is responsible for macro-pore volume formation in AC.

Within the past two decades, the impregnation of lignocellulosic precursors using H_3PO_4 as a chemical activation method for industrial-scale AC production has increased alarmingly (Table 2.3) This is attributed to the inherent ecological benefits of H_3PO_4 such as; the simplistic nature of the material recovery, reduced energy

Table 2.3: E**xperimental conditions of activated carbons activated with H_3PO_4**

Precursor	H_3PO_4 (%)	Impregnation ratio	Activation temperature (°C)	Heating rate (°C min^{-1})	Reference
Avocado Kernel seed	85	6	800	5	Elizalde-gonzalez *et al.*(2007)
China fir	50	4.6	475	5	Zuo *et al.*(2009)
Coconut fibre	30	4	900	20	Phan *et al.*(2006)
Fruit stones	60	1.02	800	-	Puziy *et al.*(2005)
Jackfruit peel waste	85	4	550	-	Prahas *et al.* (2008)
Jute	30	4	900	20	Phan *et al.*(2006)
Licorice residues	89	1.5	400	2.5	Kaghazchi *et al.*(2010)
Oil palm shell	85	1.09	450	5	Arami-Niya *et al*. (2011)
Olive stone	50	2	400	5	Yavuz *et al*. (2010)
Olive waste	75	2.4	500	10	Moreno-Castilla *et al*. (2001)
Pecan shell	50	-	450	-	Ahmendna *et al*. (2000)
Pine wood	85	1.5	400	-	Hared *et al.* (2007)
Pistachio-nut shells	89	0.5	400	5	Kaghazachi *et al*. (2010)
Sea-buckthorn stones	85	0.5	550	10	Mohammadi *et al*. (2010)
Stem of date palm	85	5	600	10	Jibril *et al.* (2008)
tea plant	85	3	350	-	Yagmur *et al*. (2008)

Source: Virginia *et al.* (2012)

Inputs and enhanced carbon yields.. As in Table 2.3, H_3PO_4 theatres dual distinct roles in the course of AC synthesis viz:

i. Acting as acidic promoter for bond cleavage, hydrolysis, desiccation and condensation, supplemented by interrelated reactions between H_3PO_4 and bio-based polymers;
ii. Template functioning due the volume occupied by H_3PO_4 in the inner parts of the activated originator which coincide with the micropore volume of the activated carbon produced (Zuo *et al*., 2009).

The features of AC derived from activation of precursors using H_3PO_4 are usually influenced by the synthesis conditions including acid concentration, activation time, impregnation ratio, pyrolysis temperature and heating rate. Similarly, some current studies have revealed the all-important influence of the atmospheric conditions during the pyrolysis state on the somatic and non-somatic features of AC (Zuo *et al*., 2009).

2.6 Factors Affecting Activated Carbon Production

Several conditions influence the quality of activated carbon synthesized irrespective of the synthesis route considered. These influential conditions are highlighted in the subsequent sections.

2.6.1 Nature of Precursor

A number of carbon-rich organic precursors which would not fuse after pyrolysis hold great potentials for conversion into AC (Rodriguez-Reinoso, 2002). The choice of precursor for synthesis of AC is usually influenced by various variables such as:

i. Raised amounts of fixed carbon.
ii. Less ash content.
iii. Raised density and high volatile matter
iv. The handiness and accessibility of precursor.
v. Probable degree of activation required.
vi. Low-cost
vii. Storability

The most widely employed precursor is lignocellulosic constituents, which represents about 45 percent of all unprocessed materials used in the production of AC. Low

organic matter percentage is crucial for producing activated carbon that contain reduced ash percentage, however, a reasonably high volatile percentage is also required for process control. Several forms of activated carbon are made from precursors (Table 2.4) such as oil palm fruit shells, walnut shells and date stones etc, which have a comparatively high density, rigidity, and percentage of unstable constituents, making them excellent for making rigid granular AC. Coconut shells, as well as peach and olive stones, are commercially employed to make micro-porous AC that can be employed in a variety of uses. Additional information on the proximate features of ideal precursors for AC synthesis is presented in Table 2.4.

2.6.2 Temperature

The features of the AC formed are prejudiced by temperature, notably the absolute activation temperature. This is commonly done with a combination of steam and CO_2 at temperatures higher than 800 $^{\circ}$C for industrial AC making (Miguel *et al.,* 2001; Miguel *et al.,* 2003). To save money and time, researchers have recently been focused on optimizing the absolute activation temperature. Activation temperature has been shown to have a considerable impact on both the product percentage and the surface coverage of AC, according to numerous publications. Temperatures as low as 200 $^{\circ}$C (Haimour and Emeish, 2006) and as high as 1100 $^{\circ}$C were employed in the past (Miguel *et al.,* 2003).

Studies in the past have posited that the optimal temperatures for various precursors were between 400 and 500 $^{\circ}$C, irrespective of activation duration and extent of impregnation (Srinivasakannan and Zailani, 2004). The product percentage is continually lowered with a hike in the activation temperature. According to Guo and Lua (2003), this is anticipated because when the temperature is raised upto 900 $^{\circ}$C, an increased amount of unstable materials are produced. The foregoing promotes the declinine in the product yield..

In the past, Haimour and Emeish (2006) submitted that the amount of unstable material content was reduced with a hike in pyrolysis temperature. Such reduction in the volatile was more evident in a pyrolysis temperature range of 200 and 800 $^{\circ}$C, which was ascribed to the speedy carbonizing effects. The feasibility of AC synthesis at pyrolysis/carbonization temperature above 800 $^{\circ}$C is doubtful as a result of the

Table 2.4: Proximate Features of Common Activated Carbon Precursors

Precursor	Carbon Content (%)	Volatile Content (%)	Density (kg/m^3)	Ash Content (%)	Appearance
Lenient wood	41-46	50-65	0.3-0.6	0.4-1.4	Lenient, enormous porosity
Tough wood	41-43	50-65	0.6-0.9	0.4-1.5	Lenient, enormous porosity
Lignin	34-41	55-60	0.2-0.45	----------	Lenient, huge porosity
Biomass shell	41-44	50-63	1.5 -2.0	0.6-0.8	Tough, enormous multiple porosity
Lignite	50-65	30-45	1.5-2.0	4-7	Tough, lesser porosity
Lenient coal	65-85	30-35	1.3-1.55	3-10	Partially hard, moderate micro-porosity
Petroleum coke	75-85	10-25	1.4-1.5	0.4-0.8	Partially hard, moderate micro-porosity
Partially durable coal	70-80	0-20	1..5-2.0	6-20	Tough, enormous porosities
Durable coal	90-95	6-12	1.5-2.0	3-10	Tough, huge pore volume

Source: Nurul'Ain (2007) as cited by Ogwuche (2016)

corresponding minute reductions in the volatile content at such high temperature. The foregoing occurred simultaneously with a rise in the fixed carbon and ash percent, as a result of the elimination of volatile contents during the pyrolysis step which lead to the formation of stabilized carbon and ash-producing minerals (Haimour and Emeish, 2006).

The Brauner-Emmet-Teller (BET) surface area is also a foremost characteristic that portrays similar influence of activation temperature on the AC features. The BET surface area usually rises as the activation temperature increases (Haimour and Emeish, 2006). This could be due to the formation of new pores consequent upon the evolution/elimination of volatile materials as well as the expansion of older pores when the activation temperature rises.

2.6.3 Activation Time

Other than the temperature of activation, the duration (activation time) similarly influences the pyrolysis step AC characteristics. Earlier studies have reported that the ideal duration of activation ranged from 1 – 3 hours for palm and coconut biomass-based precursors (Srinivasakannan and Zailani, 2004). Usually, it is documented that as the duration of activation is increased, there is a corresponding reduction in the AC yield and an increase in the BET surface area. This trend is linked with the formation and release of unstable materials from the precursor (Kim *et al.*, 2001).

2.6.4 Activating Agent Concentration

In any adsorption process, it is evident that the extent is mostly determined by the adsorbent's accessible surface. Adsorption is almost always reversible, and a defined equilibrium is quickly attained, depending on the initial adsorbate concentration in solution as well as the amount of adsorbent added (Bhatia, 2009).

2.6.5 Chemical Impregnation Ratio (IR)

This is the ratio of the weight of activating agent to the weight of starting material; be it of biological or non-biological origin. Thus aside temperature and the other process factors that influence AC synthesis, the IR is also critical in ensuring adequate porosity in AC and must be considered carefully (Bhatia, 2009).

2.7 Classification of Activated Carbon

Based on the functionality, surface features, and paramount criterion, AC can be hardly classified. Nonetheless, general grouping of AC could be done on the basis of size, means of synthesis, and commercial uses.

2.7.1 Granular Activated Carbon (GAC)

A typical SEM image of GAC is depicted in Plate 2.2. It possesses a comparatively higher particle size than PAC and accordingly, possesses a lesser exterior surface morphology which is responsible for the extent of dispersal of the target pollutant in adsorption process. GAC is ideal for gaseous/vapour-based adsorption uses, since they disperse more swiftly. They can also be applied in the treatment of water and wastewater, odour control, flow constituent split-and in speedy blend sinks. GAC come in extruded or granulated nature and could be in sizes like 8×20, 20×40, or 8×30 for liquid mode uses and 4×6, 4×8 or 4×10 for gas mode uses. The frequently used GAC for aqueous mode operations are the 12×40 and 8×30 sizes, owing to their balanced size, BET surface area and favourable pressure loss features (Srinivasakannan and Zailani, 2004).

2.7.2 Powdered Activated Carbon (PAC)

A typical micrograph of PAC obtained from SEM analysis is as shown in Plate 2.3. The fractal-like outline of the constituent-parts suggests its huge surficial area which is seemingly visible. Apart from being just about 0.1mm, every particle displayed on the micrograph possesses a large surface area in multiple square meters. Generally, AC is synthesized in particulate nature as dusts or fine grains of below 1.0 mm in size and an average radius of 0.075 - 0.125 mm. Therefore it has a huge area/capacity ratio accompanied by a diminished dispersion space. Furthermore they are better utilized in small-scale batch adsorber systems for water or gas purification (Srinivasakannan and Zailani, 2004). PAC is rarely deployed in uninterrupted flow-through water/wastewater purification schemes due to its propensity to encourage channeling and clogging of the system, thus hiking the process cost.

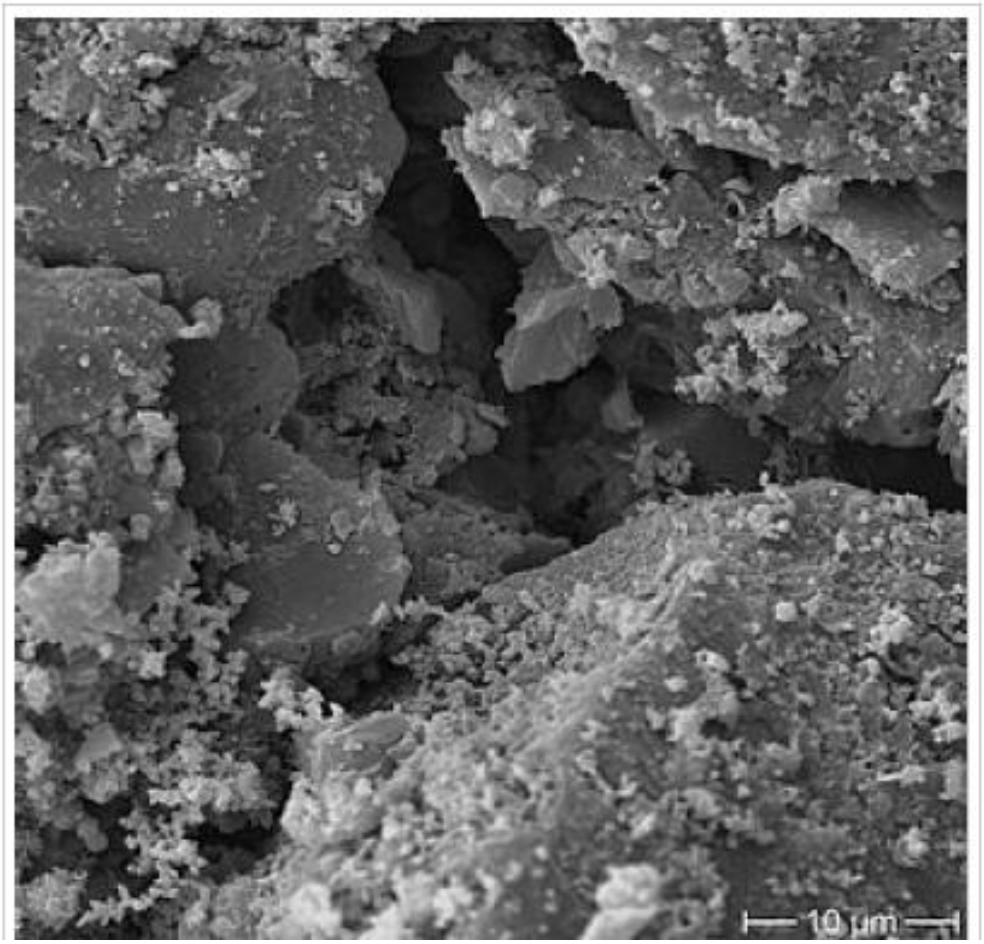

Plate 2.2: SEM micrograph of GAC

Source:https://www.sciencedirect.com/topics/social-sciences/scanning-electron-microscopy: Retrieved on 12th June, 2020

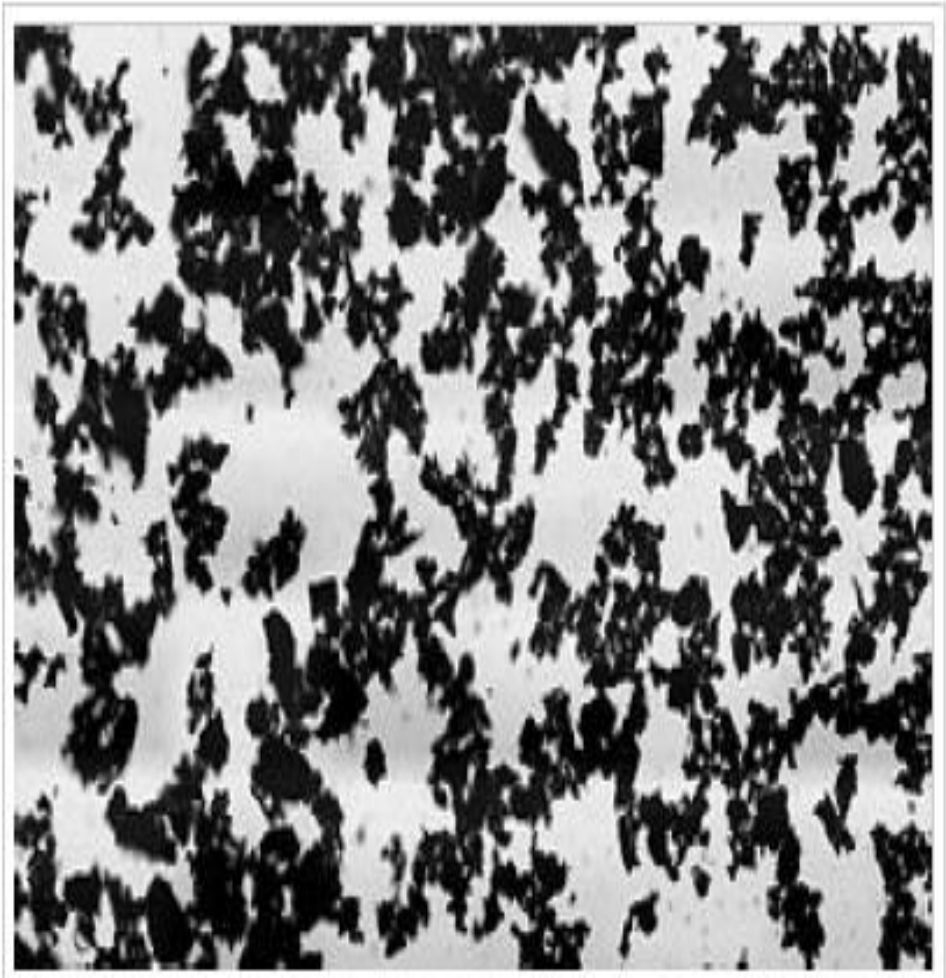

Plate 2.3: SEM micrograph of PAC

Source:https://www.sciencedirect.com/topics/social-sciences/scanning-electron-microscopy: Retrieved on 12th June, 2020

PAC consists mainly of crinkled or pulverized carbon bits, of which about 90 – 100 percent would pass through an assigned mesh size. Normally the American Society for Testing Materials (ASTM), groupsconstituent-parts that pass througha 0.78 mm sieve and the lesser as PAC. It is worthy to note that the application of PAC in continuous flow-through systems is unsatisfactory as a result of the associated huge pressure drops (Kim *et al.,* 2001). It can thus be otherwise efficiently applied in batch treatment operations such as in clarifiers, water intakes, speedy blend sinks and gravity filters.

2.8 Characteristics of Activated Carbon

The characteristics of AC that presents it as an excellent adsorbent are its, enormous internal surface area and pore-structure. AC could also be seen as froth solid with a huge surface area and firm particle assembly of comparatively lesser volume. Large surface area of AC is responsible for its excellent capabilities in the adsorption of pollutants in liquid or gaseous phases. Furthermore, the adsorption propensity of AC results from the large interior pore formations that ensue in the course of its synthesis (Cuhadar, 2005).

Based on the nature of the precursor and method used for AC synthesis, it may contain foreign materials in diverse proportions Activated carbon is not a pure carbon. Some of these impurities usually mixed with the carbon elements include: H, O_2, N_2 and S. The presence of such impurities in AC influences its catalytic or adsorptive performances in environmental matrix. Similarly, the type of precursor employed also impacts the surfacial appearance of the adsorbent material. Thus the features of CAC determine its most suitable application with regards to liquid or gas mode operations. The characteristics of AC are broadly classified to be either physical or chemical in nature.

2.8.1 Ash Content

When carbon-bearing material is burnt-off, the obtained residual matter is referred to as the ash content. It is capable of retarding the performance of AC in environmental remediation and prohibits the regeneration or reuse of AC. Metal oxides like Fe_2O_3 could be leached out of an AC matrix leading a secondary pollution problem in the treatment media. Water and acid-soluble ash content is of more significance in this regard as compared to the total ash content. For instance in aquaculture, the soluble ash in AC could be of great concern as they encourage algae blooms as a result of the

leaching of iron oxides. Thus AC with minimal soluble ash percent are recommended for use aquaculture wastewater treatment and reuse to avert the risk of heavy metal toxicity in fish as well as algae blooms (Nurul' ain, 2007).

2.8.2 Specific Surface Area (SSA)

According to Guo and Lua (2003), activated carbon adsorption capabilities are found to increase with increase in its SSA. Common CAC possess SSA of up to 2000 m^2/g (Nurul'ain, 2007). Pore volume of AC on the other hand determines the type of molecular sized compound that would be likely adsorbed by the AC. Thus the adsorption performance of activated carbon could be said to be greatly dependent on its SSA and pore capacity. The SSA (m^2/g) of AC is most customarily obtained from its gas adsorption extent based on the BET theory (Hu and Srinivasan, 1999). Interpretation of the equilibrium isotherm of nitrogen flows at 77 K is the usual method for unveiling the BET surface area of AC. However, apart from nitrogen, argon could also be used at a similar temperature (Ogwuche, 2016).

Other approximations have also been used in the past for obtaining SSA of AC where equipment for the BET method is not available. These methods include the Sear's method, the methylene blue and iodine number method. Details of these approximation-based procedures which should be used with caution as they only provide approximate values and not a true representation of the AC surface area could be obtained elsewhere (Itodo *et al.*, 2010a; Itodo *et al.*, 2010b; Mianowski *et al.*, 2007).

2.8.3 Moisture Content (MC)

The pricing of AC greatly depends on its MC as a moisture free AC is most desired, however, AC may sometimes contain MC in the range of 2 – 11 % which could be tolerated. Most activated carbons when kept in a humid environment may adsorb substantial moisture from the environment in a short time interval unless packaged in containers that are airtight. AC can adsorb upto 35% moisture and still look dry based on physical observations. However, in most instances, high moisture levels in AC do not affects its performance during use, but could certainly dilute the carbon nature. Thus an absolutely dry AC is recommended for any environmental remediation uses as

this would guaranty its repeated uses and consequently cut down on costs (Hu and Srinivasan, 2001; Okwuchukwu, 2017).

2.8.4 Iodine Number (IN)

Simply put, IN is the quantity (mg) of iodine taken up by a unit mass (g) of AC when the level of iodine in the resulting filtrate is 0.01 normal. It is a major characteristic feature of AC and could serve as an indicator of the AC pore volume. It is used to elucidate on the micro-pore extent in AC, found to be usually between 0 – 20 Å or 0 – 2 nm. This is equivalent to SSA 900 - 1100 m^2/g (Radovic, 2001). AC meant for water treatment applications usually have iodine numbers that fall between 600 and 1100 and can be used to infer the extent of exhaustion of an AC under operation. As stated earlier, this method must be employed with caution as foreign materials may also compete with iodine for the active sites on the AC surface and hinder its full adsorption leading to false outcomes. Thus, the adoption of iodine number method as a determinant of the exhaustion rate of an AC is only allowable if it is ascertained that foreign chemicals are not present (Ogwuche, 2016). Apart from the foregoing, an empirical association between IN and the extent of enervation must be previously ascertained for the intended use.

2.8.5 Surface Functional Groups

The selectivity of AC in adsorption processes rely heavily on its surface composition and spread of its pores (Radovic, 2001). Usually, AC surface appears to be nearly not charged in a way that it hampers on the adsorption of polar and ionic substances as compared to organic compounds. Thus AC is preferably supposed to be tailored in terms of its surface composition to promote the effectiveness of its intended use. The chemical configurations of precursors affect the surface chemistry of AC and offer a hypothetically more facile means of altering the qualities of AC. For instance, activated carbon fibers made from nitrogen-rich isotropic pitches are known for their hyper-active roles in the catalytic conversion of SO_2 to H_2SO_4 (Radovic, 2001).

Several oxygen, nitrogen and heteroatom-bearing functional groups have been found on the surfaces of most AC. In the course of AC production, the developed large pore structure of AC alongside its abundant chaotic sites is responsible for the voluntary combination of the heteroatoms on its surface (Yang and Lua, 2003). Heteroatoms are

fused into the grid and are also strongly attached to the boundaries of the planes. These heteroatoms so attached take the feature of the functional groups that are usually seen in aromatic compounds, and interact in a similar manner with most chemicals. The adsorption mechanisms of most ACs could be explained if the alterations in the functional clusters are noted at the end of an adsorption cycle (Yang and Lua 2003). Various procedures are available for ascertaining the surface functionalities of AC, but the most recent and frequently used is the Fourier transform Infra-Red (FTIR) method (Utsev *et al.*, 2020).

2.8.6 Porosity

The term 'pore' emanates from the Greek expression 'porous' connoting 'passage'. This It therefore shows the behaviour of a pore which is similar to that of a passage/channel for the exterior and the interior surfaces of a solid. This channel permits matter including liquids, gases and vapour to have access into, through or out of the matrix. Porosity is therefore a common attribute of any adsorbent employed for catalysis of decontamination uses. Thus creation of porosity on a solid matrix is most practicable means of creating huge internal and external surface area in solids including AC (Plate 2.4 and Fig. 2.1).

According to Guo and Lua (2003) in describing the availability and accessibility of porosity, five terminologies therefore come to play viz:

'**Open pore' –** This is a type of porosity that is linked to the exterior surface of a material, which permits the conduct of a contaminant in the material**.**

'**Closed pore'** – This is a pore in a solid matrix that is not linked with the exterior surface and as such exist in isolation.

'Transport pores – They are numerous in most solid materials and serve to interlink several points on the exterior portion of the matrix with the interior formed porosities.

'Blind pores' – These are linked with the transport pores but do not connect with any other porosity or material surface.

'internal surface' – This is made up of the region on the material that encompasses the closed pores and every openings and cracks that go down deeply into the inner portion of the solid matrix. They are usually deep with minimal width and 'external

Plate 2.4: Typical Pore Structure of Activated Carbon

Source: Ogwuche (2016)

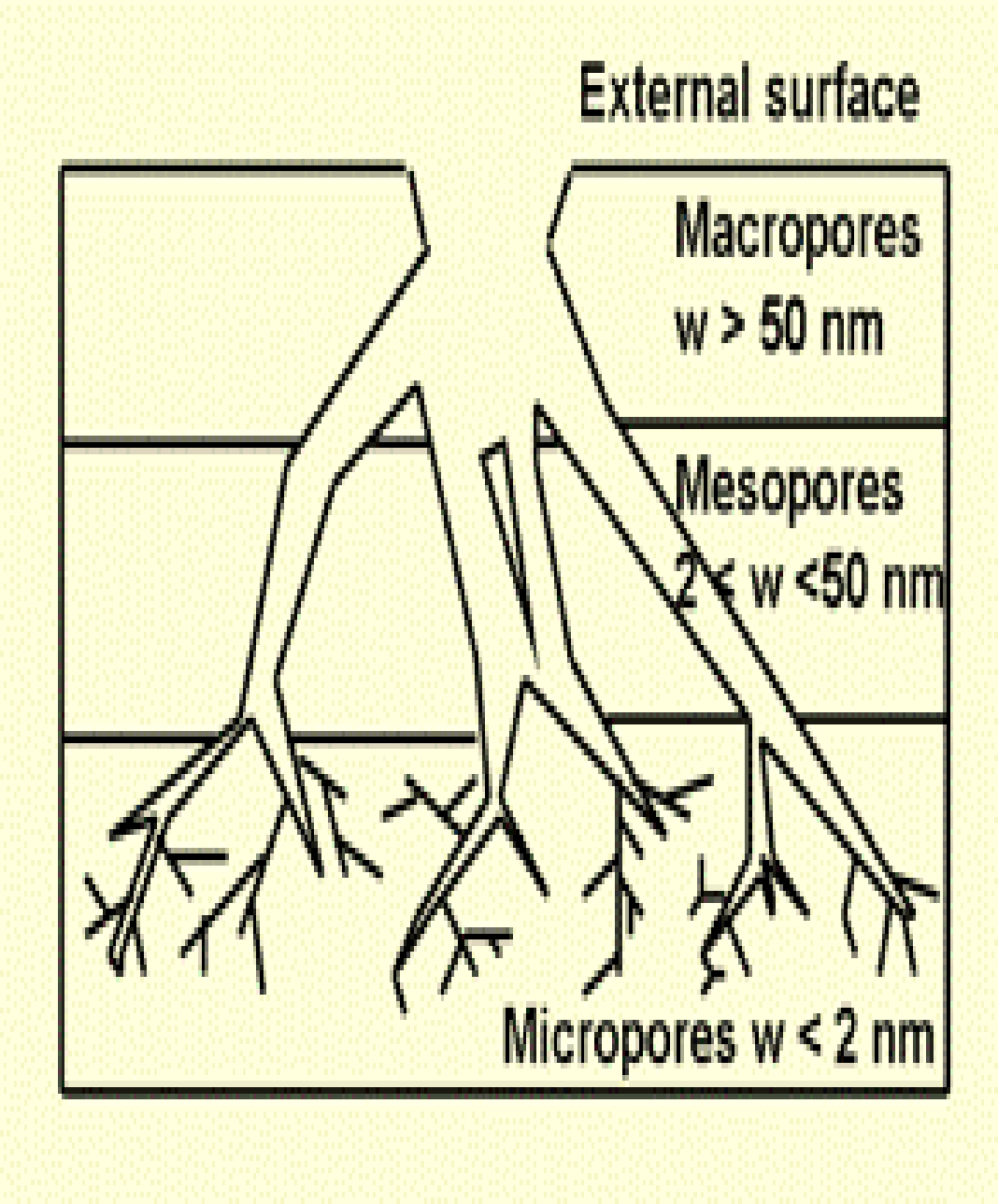

Figure 2.1: Interior pore formations in a typical AC

Source: Ogwuche, 2016

surface' – on the other hand have lager widths than depths and are made up of the emerging flanges and apparent fissures/openings on the material**.** Plate 2.4 shows the pore structure of AC and Fig. 2.1 is a graphic illustration displaying the pore network within a carbon adsorbent. The adsorptive potentials of AC towards molecular compound of varying shape and sizes is influenced by changes in the extent of pore opening in the AC and remain a paramount basis for the choice of adsorbent for a given application.

As pointed by IUPAC (Guo and Lua, 2003), porosity can be categorized based on pore size in terms of its width as follows (Fig. 2.1):

Micropores- < 2nm

Mesopores- 2 - 50nm

Macropores- > 50nm

2.8.7 Activated Carbon Morphology and Crystallinity

The morphology of AC is ascertained with the aid of scanning electron microscopy (SEM) which employs concentrated rays of high intensity electrons that yield a diverse array of indicators at the periphery of solid materials. These indicators so generated provide useful hints about the material including its texture, chemical make-up, crystallinity and alignment of the material constituents. Common uses of this technique require the collection of information around a region of interest on the material surface, which are then used to produce 2-D micrograph the shows spatial changes in the sample characteristic. Regions covering about 1 – 5 μm wide could be micro-graphed in a scanning-approach by means of normal SEM procedures, i.e intensities of 30X – 35000X and resolutions between 60 – 110 nm (Yihunu *et al.,* 2020). The SEM procedure could also be used to analyze the properties of points of interest on a material and is mostly applied in the quantitative or partially quantitative determination of chemical configurations (by means of EDX) and crystallinity (by means of XRD analysis). SEM instrument operates in a similar fashion with the EPMA and also have similar capabilities.

2.9 Response Surface Methodology (RSM)

RSM is an assembly of mathematics/statistics-based procedures for modeling, analysis and optimization of difficult situations where a parameter of interest (response) is affected by a number of factors (variables). It is commonly employed for multivariate

experimental designs, modeling and product/process optimization (Singh *et al*., 2010, Xin-hui *et al*., 2012). In such applications of RSM, product/process optimization requires that the parameter of interest should be maximized at the feasibly established levels of the influential factors. RSM has also been documented to be effective for adsorption processes as evidenced from the lesser variability and use resources involved (Anupam *et al*., 2011; Khataee, 2010).

Various experimental designs are inherent in RSM and the most suitable and robust is usually preferred. Common designs in RSM include; The Box Benkhen Design (BBD), Central Composite design (CCD), three-level factorial design, Optimal Design and Use of historical data (Ahmad *et al*., 2009, Khataee, 2010). Inspite of the application of RSM for optimization of activated carbon synthesis conditions, there is much still needed to be done in this regard as not all possible precursors of influential factors have been tested. The advantage of RSM for optimization uses comes to play in situations where the variables under study alongside their levels and the output of interest and not clearly understood. Ultimately, CCD is preferably used by many researchers for product and process optimization because of its robust nature even with a reduced number of experimental runs, which also saves the cost of experimentation (Alslaibi *et al.* 2013; Magoling and Macalalad, 2017).

2.10 Theories of Adsorption in Batch Systems

Metcalf and Eddy (2003) have defined adsorption is a phenomenon that describes the movement and adherence of dissolved substances on the periphery and interior portions of an adsorbent. It usually takes place in situations where the attractive forces at the periphery of the adsorbent overpower the attractive forces medium containing the adsorbate.

Usually, GAC is known to be the most suitable adsorbent owing to its enormous area to volume ratio. Typical surface area of CAC could be as high as 1000 m^2/g. Such large surface area allows for the buildup/accretion of a diverse number of pollutant fragments

The authors have also detailed the theories of adsorption to include the following sub-section

2.10.1 Adsorption Capacity

The ability of any adsorbent to remove pollutants from a polluted media depends largely on the definite surfacial area, the concentration of the pollutant in the aqueous media and the apparent molecular pull that exist. Adsorption isotherms are the main techniques used to test the efficacy of activated carbon for pollutant abstraction from the environment. Adsorption isotherms depict the experimentally-determined interactions amid the uptake capability (mg/g) of an AC and the equilibrium pollutant concentration. For liquid phase operations, this interaction can be represented as shown in equation 2.4 (Metcalf and Eddy, 2003).

$$\frac{X}{M} = KC^{1/n} \qquad (2.4)$$

Where:

X/M = Quantity of pollutant adsorbed in a single weight of adsorbent

C = Concentration of pollutant in solution

K, n - Experimental constants specific to the pollutant

The constants K and n are obtained from a Log-Log paper-based graph of the adsorption capacity against the pollutant concentration. From such graph the value of K is the intercept on the vertical axis, while the slope represents the value "1/n". These experimental constants without a dimension are valuable for comparatively relating the adsorption capacities for diverse pollutants or for evaluating the uptake capabilities of different adsorbents.

For a number of particular pollutants, corresponding liquid-mode equilibrium isotherms of commercially available activated carbon (CAC) have been determined and are available for use in design of adsorption systems employing such CAC. Thus adsorption isotherms are explicit to a given pollutant and the type of adsorbent employed (Metcalf and Eddy, 2003).

2.10.2 Activated Carbon Particle Size

Adsorption rate kinetics and access to AC surface area is higher and faster when the AC particle size is finer (Jiaping, 2012). However, this must be applied with caution in gas adsorption systems to avoid drastic head loss that could heighten the process costs. Cautious thought about the ideal particle size distribution of AC could offer substantial

working benefits. Nevertheless for adsorption of minerals like boron or gold, AC particle size distribution of 1.5 - 3.50 mm is ideal. On the other hand, AC of less than 1 mm is appropriate for doffing pollutants from an AC.

2.10.3 Types of Adsorption

Generally, two adsorption types exist, namely; physisorption and chemisorption (Jiaping, 2012). It depends on the mechanisms controlling the pollutant uptake onto an AC surface.

2.10.4 Physisorption (Vander Waals Forces)

Physisorption is said to occur when and where there exist some attractive inter-particle forces between adsorbent molecules and the pollutant adsorbed. Physisorption is always reversible and as such may not be a preferred mode of adsorption of AC for certain applications. However, such reversibility is useful on an industrial scale when useful resources like phosphorus could be recovered from the surface of an AC after its adsorption from solution (Bhatia, 2009).

2.10.5 Chemical Adsorption

This involves chemical associations involving the adsorbent and the adsorbed pollutant. When chemisorption is the driving tool during pollutant uptake, the pollutant uptaje heat and force of adhesion is usually higher as compared to mechanisms involving physisorption. Most often, chemisorption processes are irreversible and is of particular significance to catalytic processes. Certain pollutants may be removed from solution at low temperature by physisorption mechanisms and at higher temperatures by chemisorption or both (Metcalf and Eddy, 2003).

2.11 Regeneration of Activated Carbon

AC regeneration/reactivation is simply the restoration of the exhausted AC adsorption capacity by recovering the adsorbate from the periphery of the adsorbent. This can be achieved using either the thermal or chemical approaches (Sabio *et al.*, 2004).

2.11.1 Thermal Reactivation

Thermal reactivation is the most popular regeneration pathway in most industrial applications and it involves three basic steps (Sabio *et al.,* 2004) viz:

- Drying of exhausted media at around 110 °C
- Subjecting the dried media to high temperature treatment of around 400 – 1000 °C in the absence of oxygen.
- Left over organics gasification by an oxidizing vapour such as CO_2 or steam at high temperatures of over 900 °C.

The high temperature exposure phase utilizes the exothermically-lead adsorption and leads to elution, fractional cracking and polymerization of the adsorbed substances. The last phase helps to take-off the residuals produced in the pore matrix of the AC during the earlier phase of regeneration and as such brings back the actual surface features of the AC. This guarantees the reusability of the so regenerated carbon for several cycles. For each adsorption-thermal reactivation cycle, about 6 – 11 % by weight of the AC is lost, which also leads to a decrease in its adsorption capacity (Miguel *et al.,* 2001).

It is however, less popularized due to the huge energy and cost involvements and as such can only be practiced by large scale industries with such regeneration facility on site (Sabio *et al.,* 2004). Such onsite regeneration facilities could also serve for smaller industries that may transport their exhausted AC for regeneration for a fee that would be much profitable for them (Alvarez-Puebla *et al.,* 2004).

2.11.2 Chemical Regeneration

Reactivation of exhausted AC by chemical routes is also a viable alternative for the restoration of the uptake potentials of the exhausted adsorbent media. It has recently been proven to be the most preferred method by a number of scholars (Nabbou *et al.,* 2019: Gitari *et al.,* 2020: Kiram *et al.,* 2020). AC regeneration using chemicals involves the soaking of the exhausted media in a known molar acidic or basic solution for a predetermined period. The foregoing is done in order to enhance desorption of the adsorbed contaminant into the acidic or basic solution, thereby making available again the adsorption spots on the periphery of the AC (Adak *et al.,* 2017). Thus in this way

the adsorption/desorption experiments could be done in several cycles up to 6, depending on the quality of the AC (Adak *et al.*, 2017).

2.12 Factors Affecting Adsorption in Batch Systems

According to Bhatia (2009), many factors affect the adsorption process, these include, pH, contact time, adsorbent dosage, column height, or carbon bed depth adsorbate concentration, flow rate, temperature and particle size among others.

2.12.1 pH

The solution pH influences adsorption to a large extent. This influence is most evidenced in the adsorption capacity. It influences both the solution chemistry and the peripheral adsorption spots on the AC and rely on the adsorbent's ionic charge. Negatively-charged adsorbent surface favour the adsorption of pollutants at lower pH because in such circumstances the large number of hydroxyl ions existent in the lower pH range counterbalances the anionic state of the adsorbent surface, thus decreasing interruption to adsorbate diffusion for a significant adsorption to occur. Conversely, positively-charged adsorbent surface retards pollutant adsorption at lower pH of solution due to completion between the hydroxyl ions and the cationic surface of the adsorbent (Jiaping, 2012).

2.12.2 Contact Time

Usually, the quantity of pollutant taken up by the adsorbent exists in a condition of a changing equilibrium with the quantity taken off from the adsorbing material. Such time taken to reach the state of steadiness is referred to as the equilibrium/steadiness contact time and is a very significant factor in the adsorption process which varies from adsorbent to adsorbent and from pollutant to pollutant. The quantity of pollutant taken up by the adsorbent at the steadiness time represents the highest uptake capability of the material at the given conditions of operation (Bhatia, 2009).

2.12.3 Initial Adsorbate Content

The extent of adsorption mechanisms in any adsorption process relies heavily on the nature and composition of the adsorbent's surface. Usually, any adsorption process is reversible and a defined equilibrium point is quickly attained, with respect to the primary pollutant content in the reacting media and the amount of adsorbent added

(Bhatia, 2009). In most cases, a hike in the starting/primary pollutant concentration in solution is accompanied by a lowered adsorbate removal percent with a hike in the uptake capability.

2.12.4 Pressure and Temperature

Higher temperatures and lower pressures tend to favour the degree of adsorption of a given adsorbate from its aqueous solution. According to the Le Chatliers principle, such heat of adsorption is captivated in the process. Similar to the temperature of solution, the heat of adsorption could either be differential or integral and must be well-known. When the exact quantities of these heats of adsorption are known, the mechanisms of adsorption involved for a particular adsorbate could be precisely elucidated. As reported by Jiaping (2012), several researchers have attempted to empirically provide accurate estimates of the heat of adsorption of several adsorbates on different adsorbents, which lead to the precise elucidation of the adsorption mechanisms that are useful knowledge in the design of effective adsorption systems and processes.

2.12.5 Surface Area and Particle Size Distribution

The exterior surficial area of adsorbing materials tends to be better enhanced when its particulate size dispersal falls in the smaller range: A phenomenon that is responsible for the higher adsorption performances of small-particulate sized adsorbents as reported in several literatures for different adsorption experiments.

However, the use of adsorbent with small particle sizes is challenged when the adsorption process is designed to be continuous or semi-continuous. In continuous or semi-continuous adsorption processes, the use of small-sized adsorbents would promote channeling and pressure drop effects, which would decrease the process efficiency and increase cost. Thus, the use of small particle-sized adsorbents is only recommended for batch processes, while larger sizes or granulated adsorbents with tailored surface compositions to balance for the disparity in exterior surface area are preferred for continuous or semi-continuous systems (Jiaping, 2012).

2.13 Modeling Batch Adsorption Systems

This section gives a breakdown of basic adsorption models that are relevant for setting-up batch-mode adsorption processes/systems. These models are classified on an equilibrium isotherm, kinetic and thermodynamic basis.

2.13.1 Equilibrium Isotherm Models

Mathematical representation of adsorption equilibrium is of utmost importance within the field of adsorption basics as it provides relevant information for adsorption process design and assessment Adsorption equilibrium is directly influenced by the kind of pollutant/adsorbent interactions present and also by the external characteristics of the aqueous media including temperature, pH and contending adsorbates in solution. Single solute adsorption description is used as an ideal means for describing adsorption equilibrium even though this is not realistic in real water or wastewater adsorption systems as adsorbate competition is inevitable. This is largely because most aspects of the adsorption processes could better be described in a situation where only one adsorbate is considered. It also aids in effective comparisons in the capabilities of various adsorbents.

Finally, single solute adsorption equilibrium studies are useful for the formulation of mixed solute adsorption models. Thus it is useful to firstly study the single solute adsorbate/adsorbent interactions for any system before embarking on multiple solute experiments. Based on the forgoing, this study only gives a description of some of the most commonly applied single solute adsorption isotherm equilibrium models. Therefore, for a single solute adsorption setting, the general equilibrium description is given as in equation 2.5 (Metcalf and Eddy, 2003; Jiaping, 2012).

$$q_{eq} = f(C_{eq}.T) \qquad (2.5)$$

Where q_{eq} is the amount of pollutant adsorbed at equilibrium, C_{eq} is the adsorbate concentration at equilibrium and T is temperature (constant).

Many researchers have developed several specific equilibrium isotherms that have been deployed to describe many adsorption systems. Most of these models are typically formulated to be non-linear and are mostly linearized to ease their application in the description of adsorption data. Mathematical representations of the linearized form of some of these models are given in Table 2.5.

Table 2.5: Equilibrium Isotherm, Kinetic and Thermodynamic Model

S/No	Model	Equation	Definition of Parameters	Plots
1	Isotherm			
	(a) Langmuir	$\frac{1}{q_e} = \frac{1}{bq_mC_e} + \frac{1}{q_m}$	Where, Ce is concentration at equilibrium (mg/L), q_m is the single layer uptake capability (mg/g) and *b* is the Langmuir constant (L/mg). K_f is adsorption capacity (mg/g) and 1/*n* is the Freundlich constant. B_1 and k_T (L/g) represent the Temkin constants.	(a) $1/q_e$ vs $1/C_e$
	(b) Freundlich	$lnq_e = lnk_f + \frac{1}{n}lnC_e$		(b) lnq_e vs lnC_e
	(c) Temkin	$q_e = B_1 lnk_T + B_1 lnC_e$		(c) q_e vs lnC_e
2	Kinetic			
	(a) Pseudo First Order	$In(q_e - q_t) = Inq_e - k_{ad}t$	*β* is the desorption constant (g/mg). q_e is the uptake capability at equilibrium, *Ci* is the starting pollutant content (mg/L), *V* is solution volume (mL), m is the mass of sorbent (g/L), qt (mg/g) is the pollutant uptake at time *t (min)* and α, k_2, k_{ad}, *k0*, K_{ip} and C are constants	(a) ln(qe – qt) vs t
	(b) Pseudo Second Order	$\frac{t}{q_t} = \frac{1}{k_2 q_e^2} + \frac{1}{q_e}t$		(b) t/q_t vs *t*.
	(c) Elovich	$q_t = \frac{1}{\beta}In(\alpha\beta) + \frac{1}{\beta}In(t)$		(c) q_t versus *ln(t)*
	(d) Pore Diffusion			(d) $LogLog\left(\frac{c_i}{c_i-}\right.$ versus Logt
	(e) Intra-particle Diffusion	$LogLog\left(\frac{c_i}{c_i - q_t m}\right) = Log\left(\frac{k_o}{2.303v}\right) + \propto Logt$		(e) *qt* versus $t^{1/2}$
		$q_t = k_{ip}t^{1/2} + C$		
3	Thermodynamic			
	(a) Vant Hoff	$lnK_d = \frac{\Delta S^o}{R} - \frac{\Delta H^o}{RT}$ $\Delta G_o = -RTInK_d$ $K_d = \frac{q_e}{C_e}$ $\Delta H_o = \Delta G_o + T\Delta S_o$	R is worldwide gas constant (8.314 J/mol K), T is absolute temperature (Kelvin) and K_d is the coefficient of distribution (L/g), *qe* is adsorption capacity (mg/g), *Ce* is the final concentration (mg/L)	*lnKd* vs*1/T*

Source: Adapted from (Jiaping, 2012; Metcalf and Eddy, 2003).

2.13.2 Adsorption Kinetic Models

The adsorption equilibrium for most porous adsorbents is not attained instantaneously. The mass transfer resistance is known to constrain the mass transfer from solution to adsorbent surface. This ultimately determines the equilibrium time. This time progress of an adsorption process is referred to as the adsorption kinetics**.**

Adsorption rate is typically restricted by diffusion processes near the exterior adsorbent surface and inside the permeable adsorbent particles. Inquiries into the adsorption kinetics are essential to explain the rate-limiting mass transfer mechanisms and to appraise the typical mass transfer factors. The mass transfer factors and the equilibrium data are indispensable inputs necessary for ascertaining the requisite reaction times in slurry contactors and fixed-bed adsorber designs (Jiaping, 2012)..

Although diffusion/mechanistic models were previously seen too be more appropriate in the description of the adsorption process kinetics, presently, the simple reaction based kinetic models have been adopted and successfully utilized in this regard. Based on the foregoing, the current work seeks to basically highlight on some of the diffusion/mechanistic as well as the reaction-based kinetic models useful in the description of adsorption process. In this case, only the linear forms of such models are presented as shown in Table 2.5. Typical representations of reaction-based adsorption kinetic models according to the first and second order equations are as shown in equations 2.6 and 2.7 respectively. While that for the diffusion/mechanistic model is shown in equation 2.8 (Metcalf and Eddy, 2003)..

$$\frac{dq}{dt} = k_1(q_{eq} - q) \tag{2.6}$$

$$\frac{dq}{dt} = k_2(q_{eq} - q)^2 \tag{2.7}$$

$$\frac{dq}{dt} = k_s^*(q_{eq} - q) \tag{2.8}$$

Where k_1 and k_2 are the 1st and 2nd order kinetic constants respectively and k_s^* is the mass transfer coefficient.

2.13.4 Thermodynamic Models

Thermodynamic models are useful for describing the energy evolvement and type of the adsorption system. The models are useful in the design of effective batch and fixed

bed adsorption systems. They are mathematically stated according to the Vant Hoff equations as depicted in Table 2.5 above.

2.13.5 Design of Batch Adsorption Systems

Different process configurations and reactors are used in most batch adsorption designs. The choice of technology is positively inclined to the particle size of the chosen adsorbent(s). Succinctly, when powdered adsorbents are chosen, a batch/slurry adsorber is most suitable for design. On the other hand, granular adsorbents are better designed with fixed bed adsorber. Small particle-sized adsorbents like powdered activated carbon (PAC) are advantageous from the kinetic point of view because with them, the rate of adsorption is high and rapid and as such the contact times are shorter. Secondly, they are easier to deploy as compared to the fixed bed systems. However, PAC cannot be deployed in fixed bed systems because of the likely excessive increase in flow resistance that would be experienced. The most significant disadvantages of batch/slurry adsorption systems are that, firstly, the amount of adsorbent required to achieve a target treatment performance is higher and secondly, an additional filtration or flocculation stage is needed to separate the adsorbent from the liquid phase, which may give rise to additional costs. Irrespective of the foregoing, The batch asorption system is adopted over the fixed bed system in the current study owing to the singular advantage of simplicity and ease of deployment (Ozacar and Sengil, 2006; Bhatia, 2009).

Batch adsorption systems could be deployed such that the adsorbent (PAC) is constantly in contact with adsorbate solution until equilibrium is attained. Thus for a single solute solution, the batch adsorption system design is quite simple and involves just the combination of material balance and isotherm equation as given in equation 2.9 (Salman and Hussein, 2014).

$$m_A(q_{eq} - q_o) = V_L(C_o - C_{eq}) \quad (2.9)$$

Where, m_A is the quantity of adsorbent added, q_{eq} and q_o are the equilibrium and opening adsorbed amount, $V_L$is the solution volume, C_o and C_{eq} are the adsorbate concentration at the initial and equilibrium stages respectively.

2.14 Global Fluoride Distribution in Groundwater and Health Concerns

Heightened amounts of F^- past the safe boundary of 1.5 mg/L in potable water are responsible for fluorosis-related ailments in humans. Such high amounts have been documented to occur in several countries and parts of the globe. Similarly, reduced F^- amounts lower than the stipulated relevant dose of 0.50 mg/L that encourages dental caries has also been documented in literature across the globe. Based on the foregoing, fluoride content of drinking water is normally seen as a double-edged sword and as such it is imperative to monitor drinking water sources in order to maintain the safe limits for oral consumption**.** This study sought to review literatures published within the last decade (2011 – 2021) highlighting the concentration of F^- in aquifer water and its linked human wellbeing risk potentials in the various continents of the world and a particular paragraph dedicated to such scenarios in Nigeria.

In light of the above, high amounts of F^- in aquifer water has been predominantly reported to occur in Asia, South America and Africa particularly in absolutely and partially dry environments, while moderate to low levels are documented in North America, Europe, Antarctica, and Oceania (Adeyeye *et al.,* 2021; Islam and Mostapha, 2021). Geogenic fluoride occurrence is largely associated with volcanic activity, presence of fumaric acids and availability of thermal water. Probable immediate pointers to raised fluoride concentration in aquifer water include; lowered calcium and magnesium content, raised sodium and bicarbonate concentrations, alkaline pH (Malago *et al.,* 2017). However, Thole, (2013) cautioned that there could be some exceptions to this conditions in which high fluoride levels could be experienced in groundwater (Table 2.6).

Furthermore, Islam and Mostafa (2021) asserted that on a global scale, children are more prone to risk (78 %) of ailments related to excessive fluoride intakes as a result of the potable uses of fluoride loaded groundwater as compared to adults (22 %). Earlier, it was documented in 2015 that fluoride contamination and prevalence of fluorosis was endemic in over 25 countries of the world and that there are possibilities that more countries could join the league as geogenic activities, rising sea levels, desertification etc. continue to plague the globe (Babu *et al.,* 2015).

The thrust of this review therefore is to ascertain the latest trends for fluoride contamination of groundwater across the globe (mostly in developing countries in

Table 2.6: Global occurrence of Fluoride in groundwater and human health risk

S/No	Continent/Country/Location	No of Sampled wells	Fluoride Concentration Range (mg/L)	Mean Fluoride Concentration (mg/L)	Hazard Quotient (HQ)				Remark	Ref.
					Infant	Children	Teenagers	Adults		
1.	South America/ Mexico/ Lerma-Charpala Basin and valley of Mexico	27 and 9	0.02 – 1.31 and 0.29 – 1.06	0.30 ± 0.28 and 0.51 ± 0.31	*	*	*	*	Low levels of fluoride pollution	Valdez-Alegria *et al.*, (2019)
2.	Asia/ India/ Bihar district.	63	2.15 – 3.20	2.64 ± 1.81		>1	>1	>1	High levels of fluoride pollution in groundwater	Mridha *et al.*, (2021)
3.	Asia/ India/Punjab district	76	0.60 – 5.07	*	*	0.67 – 5.63	*	0.29 – 2.41	High levels of fluoride pollution in groundwater	Chetan and Suthar (2019)
4.	Asia/India/ Telangana state	105	0.50 – 3.50	*	*	0.87 – 7.08	*	1.17 – 9.57	High levels of fluoride pollution in groundwater	Adimalla and Li (2019)
5.	Asia/India/Andhra Pradesh	123	0.4 – 5.80	*	*	*	*	*	High levels of fluoride pollution in groundwater	Adimalla *et al.*, 2019
6.	Asia/Mongolia/Inner Mongolia	30	0.07 – 7.70	2.51 ± 1.80	*	*	*	*	Moderate risk for fluoride contamination	Nakazawa *et al.*, 2020
7.	Asia/India/ Shanmuganadhi	61	0.01 – 2.50	0.96 ± 0.70	*	0.07 – 7.66	*	0.10 – 5.67	Moderate fluoride contamination and risk of fluorosis	Kurunanidhi *et al.*, 2019

8	Asia/China/ Loess Plateau	128	*	3.8	*	> 1	*	> 1	High level of fluoride in water and a high risk to children and adults	Jia *et al* 2019
9	South America/Argentina/Santiago del Estero	110	0.01 – 2.80	0.90 ± 0.60	*	*	*	*	Moderate fluoride contamination and risk of fluorosis	Gomez *et al., 2*020
10.	South America/Argentina/Sla Ballenera catchment	34	1.10 – 2.50	1.90 ± 0.71	*	*	*	*	Moderate fluoride contamination and risk of fluorosis	Calvi *et al.,* 2016
11	South America/Brazil, Sao Joao do Rio do Peixe	111	0.11 – 9.33	1.64 ± 1.80	High	High	High	High	High fluoride contamination and risk of fluorosis	De Souza *et al.,* 2013
12	Asia/Pakistan/River Swat Flood Plains	53	0.7 – 6.4	1.65 ± 1.22	*	*	*	*	High risk of fluorosis	Rashid *et al.,* 2018
13	Asia/China/ Yuncheng Basin	79	0.10 – 14.1	2.32 ± 1.74	*	*	*	*	High to moderate risk of fluorosis	Liu *et al.,* 2020
14.	Africa/ Tanzania/Mt. Meru	65	1.50 – 84.0	24.1 ± 22.55[#]	*	*	*	*	High levels of fluoride pollution in groundwater	Makoba and Mazuka, 2017
15	Africa/Kenya/Nakuru County	32	0.5 – 72.0	11.08 ± 24.63	*	*	*	*	High levels of fluoride pollution in groundwater	Gevera and Mouri, 2018

16	Africa/Kenya/Bomet County	58	*	4.37 ± 0.57 and 4.51±0.50	*	*	*	*	Moderate risk for fluoride contamination	Mosonik, 2015
17	Africa/Ethiopia/Rift Valley	138	1.1 – 68.0	9.4 ± 10.5	>1	>1	>1	>1	Very high risk of fluorosis	Rango *et al.*, (2012)
18	Africa/Ghana/North-Easthern Region	88	0.05 – 13.29	3.26 ± 1.49	0.02 – 4.43	0.07 – 18.83	0.03 – 8.86	0.03 – 6.86	Very high risk of fluorosis	Sunkari *et al.*, 2019
19	Africa/Ghana/ Upper East Region	64	0.11 – 4.27	*	*	> 1	> 1	> 1	Moderate risk of fluorosis	Ganyaglo *et al.*, 2019
20	Africa/Ethiopia/ Southern Rift	29	0.2 - 5.60	2.1 ± 0.82	*	0.75 – 8.44	*	0.27 – 3.01 0.34 – 3.88	High risk of fluorosis in children	Haji *et al.*, 2021
21	Nigeria/Gombe State/Kaltungo	30	0.60 – 1.53	1.31 ± 0.08	*	*	*	*	Moderate fluoride contamination	Danbature *et al.*, 2014.
22	Nigeria/ Borno State/ Chad formation aquifers	127	0.00 – 9.00	*	*	*	*	*	Moderate to high risk of fluorosis	Bura *et al.*, 2018
23	Nigeria/Gombe State/Kaltungo	108	1.6 – 2.1 and 1.5 – 1.7	1.9 and 1.6[#]	*	*	*	*	Moderate prevalence of dental fluorosis	Malum *et al.*, 2019
24	Nigeria/Ogun State/Abeokuta South	63	0.48 – 1.84	1.23	0.90 – 3.02	0.37 – 1.38	0.21 – 1.03	0.28 – 1.14	Moderate risk of fluorosis	Emenike *et al.*, 2018a

*not reported, [#]Mean fluoride concentration in hand dug wells

Source: Author's Survey (2021)

Asia, South America and Africa) and its related health risk effects on humans based on reliably documented literatures. For this purpose only cases reported in the last decade were considered in this review.

Valdez-Alegria *et al.* (2019) gauged the longitudinal dispersal of F^- in groundwater within the Lerma-Charpala Basin and valley of Mexico. It was asserted that fluoride contents of water in the studied vicinity reached 0.02 – 1.31 and 0.29 – 1.06 with mean values of 0.30 ± 0.28 and 0.51 ± 0.31 for Lerma-Charpala Basin and the valley of Mexico respectively. No work on human health risk assessment was reported, however, it was concluded that water obtained in the studied regional aquifers was safe for potable uses in relation to its fluoride content.

Mridha *et al.* (2021) conducted an appraisal of groundwater pollution with fluoride in two regions of Bihar district in India. They reported a mean fluoride level of 2.64 ± 1.81 mg/L which surpassed the WHO tolerable threshold of 1.5 mg/L. It was specifically reported that 91 and 48.1 % of groundwater trials surpassed the acceptable limit threshold (1.50 mg/L) in Rajuali and Banky Bazar regions of the district respectively. The authors concluded that a good number of the population in the district were already suffering from fluoride related ailments and that all age groups in the population risked developing dental or skeletal fluorosis with a hazard index greater than 1 (Table 2.6).

Similarly, Chetan and Suthar (2019) undertook an assessment of fluoride adulteration in aquifer-derived water and its associated human wellbeing potentials on the population in 14 districts of Malwa region in Punjab, India. The researchers reported fluoride concentrations of 0.60 – 5.07 mg/L and asserted that several samples out of the total 76 surpassed the Indian allowable maximum of 1.0 mg/L. Additionally, the hazard quotient due to raised up fluoride contents in the water was estimated to be 0.29 – 2.41 for adults and 0.67 – 5.63 for children and concluded that the population residing in the area who secure their drinking water from groundwater sources were liable to develop fluoride-linked ailments like fluorosis and brain damage. The deployment of cost-effective technologies for groundwater defluoridation at source before its consumption was recommended for the study area.

Earlier, Adimalla and Li. (2019) examined fluoride and other ionic concentrations of groundwater in the mineral-dominated and partially dry area in Telangana municipal of

India. The water in the district was predominantly alkaline and was of the Ca·Mg–HCO_3 and Na–HCO_3 types. It was further reported that fluoride concentrations ranged between 0.5 – 3.50 mg/L in which around 48 % of the 105 trials had values that surpassed the postulated extreme boundary of 1.5 mg/L. The eastward sections of the studied location were recounted as having upper amounts of F^- in groundwater. With regard to risk posed to humans, it was observed that the total hazard index were 0.87 – 7.08 and 1.17 – 9.57 for adults and children respectively. It was concluded that water rock interactions were the major causes of fluoride enrichment of groundwater in the area and recommended the use of contaminant filters and the adoption of rainwater harvesting techniques to lessen the risk of compromised wellbeing in the populations residing in those locations.

Similarly, F^- amounts of 0.4 – 5.8 mg/L were documented in the rural portions of Andhra, Pradesh, India by Adimalla *et al.* (2019). No human health risk analyses were conducted; however a high prevalence of fluorosis already existing among the studied population was documented. It was also documented that the aquifer content was alkaline in nature with a pH range of 7.18 – 9.32 which favoured the dispersion of fluoride into groundwater. Furthermore, the water samples were predominantly of the Na^+-HCO_3^- and Ca^{2+}-HCO_3^- type and fluoride concentration were higher in the regions with the Na^+-HCO_3^- of groundwater. F^- was affirmatively associated with pH and HCO_3^- and was negatively correlated with Ca^{2+} and NO_3^-. The authors concluded that water-rock interaction was the main mechanisms for fluoride enrichment in groundwater.

Nakazawa *et al.* (2020) examined the quality of groundwater, surface water and tap water used for drinking purposes in Inner Mongolia. It was asserted that ground water was largely polluted with regards to fluoride (0.07 – 7.70 mg/L) and arsenic (0.31 – 47.0 µg /L). To avert the risk associated with the consumption of high fluoride bearing water, the use of snow as an alternative potable water source in the region and most specifically in the winter periods was recommended.

Kurunanidhi *et al.* (2019) carried out an assessment of fluoride concentrations and human wellbeing hazards analysis related to the intake of groundwater in the Shanmuganadhi watershed in Southwards of India. A total of 61 trials were made from sampled groundwater, which were analysed for various physical and chemical

variables including fluoride. Findings revealed that 23 % of the trials had F^- levels that surpassed the tolerable maximum (1.5 mg/L). Furthermore, it was reported that the HQ for risk of fluorosis was 0.07 – 7.66 and 0.1 – 5.67 for children and adults correspondingly, and over 80 % of sampled water were observed to surpass the allowable HQ limit of 1. In conclusion, the authors pointed that children in the area were at a higher risk of developing fluorosis as compared to the adults.

In Argentina, Gomez *et al.* (2020) assessed fluoride levels in ground water in the Santiago del Estero Province. Altogether, 110 samples were obtained from 23 diverse points in the study location and analysed for its physicochemical properties. Results indicated that the samples had moderate fluoride contamination ranging from 0.01 – 2.80 with a mean value of 0.90 ± 0.60 for combined sampling campaign covering both the waterless and rainy periods. It was further asserted that fluoride concentrations in the water surpassed the National permissible threshold of 1.00 mg/L in approximately 51 % of trials. PCA and HCA were found to be useful tools in providing understanding about the state and mechanisms of contamination of the studied samples.

Similarly, another research group (Calvi *et al.*, 2016) considered the fluoride concentration in groundwater around the La Ballenera catchment in South-Easthern Argentina and reported that fluoride concentration ranged from 1.10 – 2.50 mg/L (mean = 1.90 mg/L). It was asserted that the water was of the Na-HCO_3 type, having a mean pH value of 8 and concluded that the differences in the F^- levels of the water were as a result of the geological**,** geomorphological and the geochemical factors in the catchment.

de Souza *et al.* (2013) undertook a groundwater quality assessment in partially-dry area in northwards of Brazil. In all, about 110 trials were made from various groundwater sourced in the area for ascertaining the physico-chemical compositions and variations. It was reported that F^- contents were in the range of 0.11 - 9.33 mg/L and around 30 % of trials surpassed the safe extreme of 1.50 mg/L. Similarly, 12 % of the samples had calcium to fluoride ratio that was suitable for the inhibition of dental caries, while there was a minimal risk of fluorosis in this population. However, based on a mapping of fluoride distribution in the area, it was reported that about 2465 and 1057 persons had heightened tendencies of portraying symptoms of teeth and skeleton

fluorosis separately. It was thus concluded that majority of drinking water sources were unsafe for such purposes in the study area.

Ranasinghe *et al.* (2019) gauged the longitudinal spread of fluoride content in groundwater and the populace that risked having dental caries and fluorosis in Sri-Lanka using the spatial mapping approach. It was found that 12 % of children below the age of 12 years could suffer from fluorosis, while more than 84 % of the population that lived in the areas with low fluoride levels in groundwater could suffer tooth decay (dental caries). It was concluded that the spatial approach was useful for controlling inherent fluorosis in the region.

In Pakistan, Rashid *et al.* (2018) assessed the prevalence of fluoride in underground aquifers in the vicinity of a fluorite excavating region in the inundation savannahs of River Swat. An aggregate of 53 samples were acquired from superficial, mid and subterranean aquifers in the region and tested for its fluoride and other physico-chemical compositions using standard procedures. F^-concentration in the samples were 0.70 – 6.40 mg/L (mean = 1.65 mg/L) and about 64 % of the total trials were found to have fluoride concentrations that surpassed the threshold limit (1.50 mg/L). Predominantly, the water was of the $NaHCO_3$ type. The Dean's classification method proved that most of the water was unsuitable for potable uses. It was concluded that fluorite-bearing rocks had strong influence on the spread of fluoride-related ailments in the area and rock weathering (granite and gneisses) as well as dissolved silicate materials and ion exchange were responsible for the poor quality of the water especially with regards to its fluoride levels.

Similarly, Liu *et al.* (2020) explored the processes controlling fluoride enrichment in groundwater using Principal Component Analysis (PCA) in the Yuncheng Basin in China. The authors reported low – high amounts of F^- in the shallow groundwater of the various regions considered. Multivariate statistics were deployed to trace fluoride origin. The authors asserted that numerous hydro-chemical processes including weathering and evaporation controlled groundwater fluoride enrichment in the area.

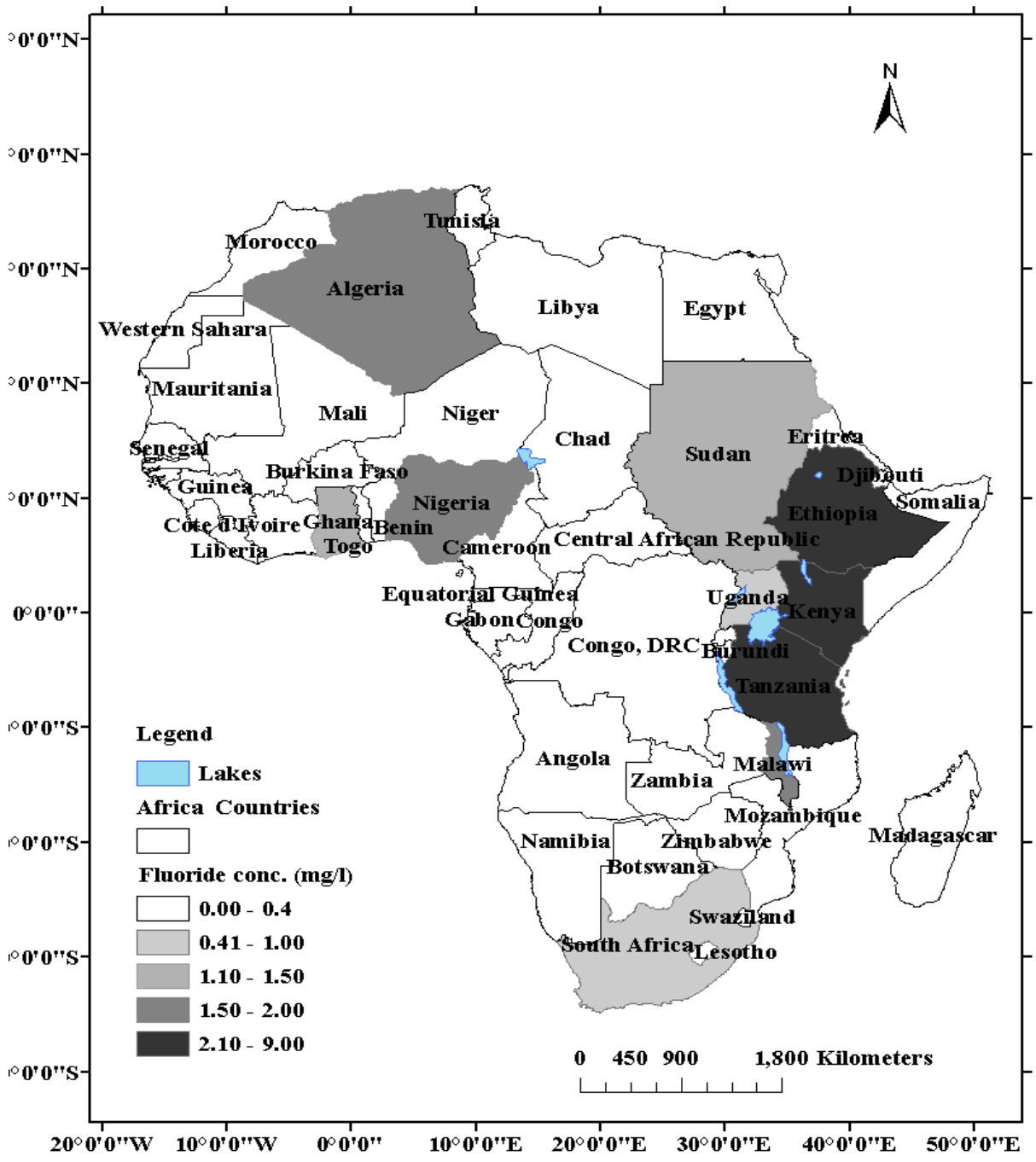

Figure 2.2: Incidence of Fluoride in Groundwater in Africa
Source: Malago *et al.* (2017)

It was concluded that groundwater sourced from shallow aquifers presented very high risk of fluorosis to the population.

Again, in China, Jia *et al.* (2019), investigated the fluoride hydro-geochemistry of groundwater around the southwards end of the Loess plateau. It was observed that 64.0 % of the studied water had fluoride concentration that exceeded the allowable threshold. The authors asserted that groundwater enrichment with fluoride was mainly dependent on the dissolution of fluoride-containing minerals, alkalinity of the water which promotes rock-water interface and ion exchange by calcium removal processes. Human health risk (HQ) for children and adults were reported to be > 1 in 94 and 60 % of the samples respectively. Popularization of fluoride removal techniques and the optimization of water supply strategies by relevant bodies in the area were highly recommended.

In Africa, excessive groundwater F^- contents are documented in countries such as the East African Valley, Ethiopia, Ghana, Nigeria, Tanzania, Sudan, Uganda, Kenya, Malawi, Algeria and South Africa (Fawell *et al.*, 2006: Thole, 2013). Very high levels (2 – 9 mg/L) are reported around the Eastern Africa (Figure 2.2) including Kenya and Tanzania, high levels (1.5 – 2 mg/L) around West and North Africa including Nigeria, Tunisia and Algeria, moderate levels (1.1 – 1.5 mg/L) in Sudan and Ghana and low levels (0.4 – 1 mg/L) in Southern Africa. Specific countries scenarios for groundwater contamination in Africa are presented in the subsequent paragraphs.

Rango *et al.* (2012) evaluated the quality of groundwater and the pervasiveness of teeth fluorosis in countryside occupants of the main Ethiopian Rift valley. Extremely raised intensities of F^- in shallow groundwater (1.1 – 68 mg/L) with an average quantity per unit volume of 9.4 ± 11.5 mg/L were reported. It was also confirmed that extreme F^- contents were obtained in samples with alkaline pH, high salinity, high Na^+, HCO_3^-, and SiO_2 contents with a corresponding reduction in Ca^{2+} contents. Signs of dental fluorosis in all individuals between the ages of 7 – 40 years in the area were also found.

Makoba and Mazuka (2017) evaluated the features of undergroundwater in the vicinity of Mt Meru in Northwards Tanzania.It was asserted that fluoride (mean concentration 17.6 mg/L) was the major naturally occurring inorganic contaminant bedeviling water

quality for domestic use in the area, while the raised Na^+, potassium and HCO_3^- contents in the water were the limiting factors for irrigation.

Similarly, Gevera and Mouri (2018) assessed the natural occurrence of fluoride as a potential harmful contaminant in groundwater around Nakuru-County, Rift Valley, Kenya. It was observed that out of the 32 samples collected from borehole sources; a total of over 86 % had fluoride concentrations surpassing the safe maximum (1.5 mg/L). F^-contents were reported to range between 0.5 – 72 mg/L (mean = 11.08 mg/L) and showed resilient affirmative correlations with the main physicochemical variables and a damaging relationship with ca^{2+}. In conclusion, the authors asserted that the buildup of liquefied solids in the water bearing rocks and evaporative fortifications as a result of raised heat levels were responsible for the heightened fluoride contents in groundwater.

Mosonik (2015) also undertook the valuation of potable water bases in the low-lying areas of Bomet County, Kenya. High mean levels of fluoride (4.37 ± 0.57) in the rainy term and 4.51±0.50 in the arid stint were reported. It was concluded that residents of the area were highly probable of manifesting signs of fluorosis if their groundwater intake patterns were not checked.

Sunkari *et al.* (2019) evaluated the incidence, wellbeing risk and ecological modes of F^- enrichment in groundwater in a Northeastern region in Ghana. A total of 88 samples were retrieved from functional boreholes which served as foremost cradle of drinking water for the inhabitants and analysed for its hydrogeochemical parameters with a special focus on its fluoride levels. Findings revealed that the grology of the region comprised shale, sandstones, mudstones and carbonate-bearing rocks of the Oti/Pendjari Group. It was found that the groundwater was largely alkaline and of the Na-HCO_3 type. F^-contents were 0.05 - 13.29 mg/L (mean = 3.26 mg/L) with 70 % of trials having F^- values higher than the tolerable threshold. The authors also asserted that children stood a higher chance of manifesting fluorosis (HQ: 0.07 – 18.83) as compared to infants (HQ: 0.02 – 4.43), teenager (HQ: 0.03 – 8.86) and adults (HQ: 0.03 – 6.86) and concluded that the pH, rock-water interface, evaporation, dissolved minerals, precipitations, intense weathering and contributions from human undertakings including those from industrial releases and home-based sewage were some of the mechanisms of fluoride enrichment in the water. Complete defluoridation

of the water to avert the threat ascribed to high fluoride contents was strongly advocated.

Similarly, Ganyaglo *et al.* (2019) investigated groundwater pollution with respect to F^- and the probabilistic health risk to humans in a Ghanaian province using the Mont-Carlo simulation technique. It was reported that 27.27 and 15.38 % of the studied water contained excessive F^- amounts in the Bongo and Kassena Nankana West districts respectively. Furthermore, they posited that the non-cancer risk connected with the ingestion of F^- showed a mean Hazard Quotient (HQ) > 1 for children in both areas suggesting possible wellbeing risk to this population.

Haji *et al.* (2021) overhauled the quality of potable water in the Bilate watershed, southwards of the Ethiopian Rift Valley using multivariate techniques. About 29 samples of groundwater were randomly obtained from dug wells and tested for its physical and chemical parameters with a focus on F^- concentrations and related risk to human well-being. It was observed that 59 % of the studied water displayed F^- concentrations in exceedance of the tolerable benchmark value. F^- Contents varied from 0.20 to 5.60 mg/L (average = 2.1 mg/L). Similarly, sodium and HCO_3^- were the major ions controlling the water chemical interactions in the study area. Well-being risk analyses revealed that the HQ was 0.75 – 8.44, 0.34 – 3.84, 0.27 – 3.01 for kids, adult females and adult males separately. Rock-water interfaces were the dominant mechanism governing groundwater chemical compositions in the region.

In Nigeria, several studies have revealed the incidence of F^- ions at elevated levels in undergroundwater which is mostly sort as a major potable water source in the country. Several studies have also indicated the occurrence of dental and skeletal fluorosis in Nigeria as well as an alarming potential risk to human wellbeing linked with the intake fluoride-rich water. These studies cut across the northern and southern parts of Nigeria, thus making groundwater pollution with F^- an important national issue.

For instance, Danbature *et al.* (2014) undertook a bill of undergroundwater fluoride concentration in Kaltungo area of Gombe state. On the whole, about 30 groundwater samples were retrieved from four separate settlements within the region and tested for its F^- concentrations. Fluoride concentrations that varied from 0.6 – 1.53, an alarming dominance of fluoritic disease conditions with an increased level of bone fracture due

to reduced bone strengths in the resident was reported. The foregoing observations were ascribed to the unwholesome intake of F^--ladened groundwater.

Similarly, Bura *et al.* (2018) undertook a survey of the incidence and spread of F^- in aquifer water within the Chad founding aquifers in Borno state, North-Eastern, Nigeria. An aggregate of 127 water trials were obtained from boreholes and shallow wells, then subjected to physico-chemical characterization with a special focus on fluoride concentrations. It was found that F^- contents in the samples were within the safe limit in the upper zone aquifer except for one sample that had an elevated fluoride amount of 1.8 mg/L. In the mid and lower zone aquifers, it was found that fluoride concentrations were as high as 4.6 - 9.0 mg/L. It was further asserted that there was evidence of teeth and skeleton-related fluoride effects especially in the New Marte settlement where the highest fluoride concentration (9.0 mg/L) was recorded. The authors concluded that the raised F^- amounts in the trials was influenced by its alkaline nature, moderate EC, and leaching from confined clay layers, long residence time and high temperature.

Similarly, Malum *et al.* (2019) assessed the temporal spread of F^- in groundwater within the Kaltungo area in Gombe state, northern-Nigeria. Water trials were obtained from shallow wells and boreholes for duration of 12 consecutive months giving rise to a total of 108 samples. The samples were analysed for its physical and chemical features with a special focus on F^- concentrations. The researchers documented that F^- concentrations were 1.6 - 2.1 mg/L (mean = 1.9 mg/L) in the samples from the hand dug wells and from 1.5 - 1.7 mg/L (mean = 1.6 mg/L) in the borehole samples.
It was concluded that the high F^- amounts in the groundwater of Kaltungo town is responsible for teeth mottling among the people and recommended that a central water treatment plant be installed in the area to reduce high fluoride content before pumping the water for public consumption.

Emenike *et al.* (2018a) assessed the ionic and fluoride concentration of groundwater obtained from 21 locations in Abeokuta South, Ogun State, southwards, Nigeria. It was perceived that F^- concentrations in the samples (n = 63) was strongly and positively correlated with pH and TDS. Furthermore, the authors found fluoride concentrations of 0.48 - 1.84 mg/L with 33 % of the samples violating the recommended limits. The authors adopted the HQ approach to ascertain the dangers of human wellbeing linked

with fluoride contact through the dermal and oral routes. Findings showed that HQ for infants (6–12 months) in over 91% of the studied locations exceeded the allowable threshold (<1). Conversely, the HQ for the other populations (11–16 years, > 65years, 18–21 years, 21 years, 16 –18 years) were greater than 1 in 95.2, 90.5, 80.95 and 100 % of the locations considered respectively. It was concluded that the HQ established in their work could provide preliminary knowledge for water governance, policy, and the larger society headed for averting or controlling such contamination problems (Table 2.6).

2.15 Empirical Review of Technologies for Fluoride Removal in Water

Globally, the main technologies for fluoride removal in water are reverse osmosis, ion exchange, electrodialysis, coagulation/precipitation and adsorption (Loganathan *et al.,* 2013; Vithanage and Bhattacharya, 2015: Kumar *et al.,* 2019). These methods especially adsorption employing several different adsorbent materials have been conveniently and successfully used by several researchers across the globe for treatment of high fluoride levels in groundwater sources meant for drinking. This work focused mainly on the adsorption technologies used for water defluoridation.

According to Kumar *et al.* (2019), several adsorbents have been tested for their effectiveness in groundwater defluoridation with a special focus on the affordability and efficiency. Some of the tested adsorbents include: Activated alumina, modified activated alumina, nano-composites, nano-sorbents, iron-based adsorbents, activated carbons, bio-sorbents, agro-biomass-based sorbents, industrial waste-based sorbents, metal oxide functionalized materials etc. Most defluoridation techniques are associated with high costs and secondary pollution issues which make them less attractive.

Several authors have elaborated on the various techniques for water defluoridation (Yadav *et al.,* 2019) and hypothesized that coagulation was the most popular defluoridation method but was limited by the poor and unsatisfactory fluoride removal performance (Ayoob *et al.,* 2008). Membrane-based procedures comprising reverse osmosis and electrochemical processes such as electro-dialysis for fluoride removal in water are associated with prohibitive cost implications and skilled manpower requirements which limit its adoption in most climes. Therefore, of the several defluoridation technologies, adsorption seems to hold great potentials for adoption and wide utilization due to its cheap and easy mode of operation (Mohammed *et al.,* 2018).

However, one promising endeavor for a wide adoption of the technique is the need for synthesis of locally available, efficient and affordable adsorbents for fluoride abstraction in aqueous media. Fig. 2.3 is an abridged symbolic representation of the various techniques used for fluoride exclusion in water (Kumar *et al.*, 2019), while Fig. 2.4 illustrates some of the mechanisms involved during fluoride adsorption from aqueous media. Table 2.7 shows a summative comparison of the most recent and widely used defluoridation techniques.

2.15.1 Carbon-Based Adsorbents, Composites and Bio-sorbents

Activated carbons (ACs) are promising candidates for water treatment because of the raised carbon content, porosity and huge surface area they poses. ACs can be synthesized from both natural and biomass materials, they can also be further functionalized for specific application by coating its surface with metallic oxides or their nano-forms. Similarly, unmodified biomass and micro-organisms could also be used as bio-sorbents for environmental remediation. Based on the foregoing, AC obtained from coal, biomass-based AC, AC composites and bio-sorbents have beenwidely synthesized and studied by various researchers for abstraction of F^- in water using batch adsorption techniques.

Notably, Rajkumar *et al.* (2019) used thermally treated (300 - 700 °C) carbon derived from cow dung (CDC) for F^- abstraction from synthetic fluoridated water. The CDC was characterized by SEM, EDX, BET and FTIR techniques, where the material carbonized at 500 ^oC was selected and used for fluoride adsorption experiments. Optimum F^- removal capability of 15.5 mg/g was reported at pH 7.25, while removal efficiency of 80 % was also achieved. Fluoride adsorption was suitably represented by the Freundlich, PSO and intra-particle diffusion models. Presence of HCO_3 was observed to most significantly retard the process efficiency. Regeneration of the

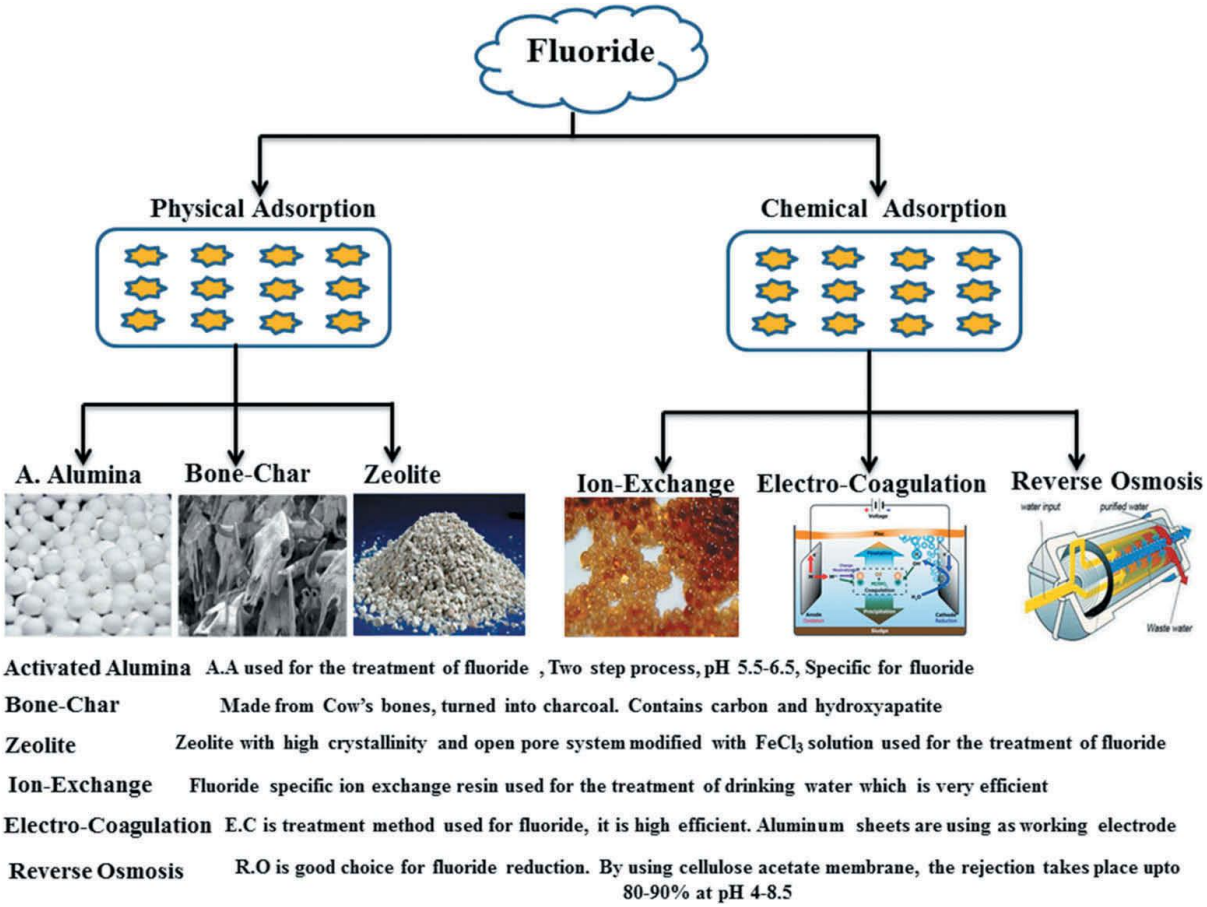

Figure 2.3: Techniques for Fluoride Removal in Water
Source: Kumar *et al.* (2019).

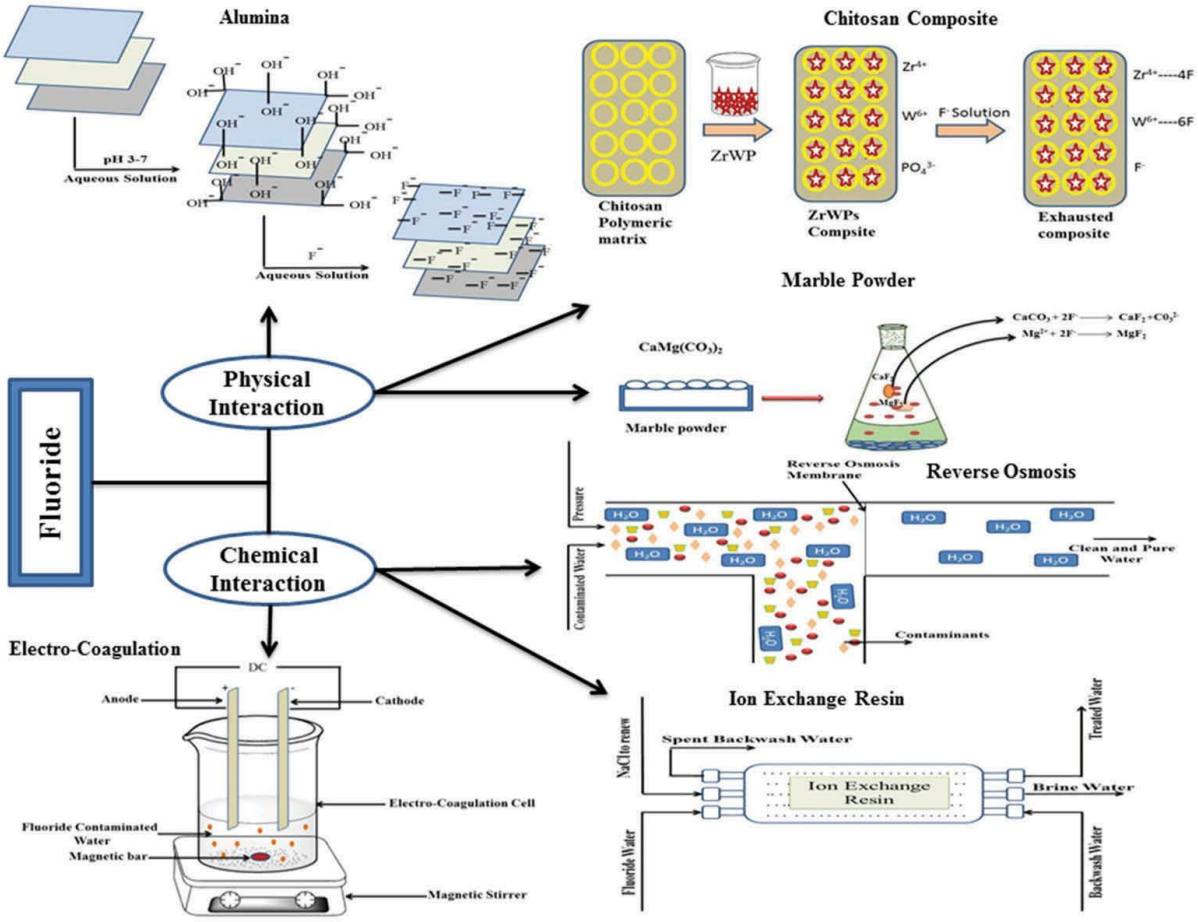

Figure 2.4: Mechanisms for Fluoride Removal from Water by Adsorption Technique

Source: Kumar *et al.* (2019).

Table 2.7 Comparison of Various Technologies for Fluoride Removal in Water

Technology	Advantages	Disadvantages
Coagulation/Precipitation	Extensively utilized, high efficiency, commercially available technique	Costly as a result of huge chemical requirements. Effectiveness is pH-dependent and competing ion could also retard efficiency. Tiresome due to pH adjustments requirements. Sludge disposal issues are eminent. Not suitable for water with low F^- levels (< 5 mg/L).
Membrane processes: reverse osmosis, nano-filtration	Highly efficient, eliminate other contaminants. No chemicals required.	Prohibitive initial and running costs due to huge energy and maintenance requirements. Disposal problems related to concentrates generated. It is not selective. May be pH dependent and unattractive. Associated with fouling, clogging and scaling problems.
Electrochemical treatments: dialysis, Electrodialysis	High efficiency and selectivity. No chemical required. No waste production	High cost during installation, operation (energy) and maintenance. Not selective. Requires skilled man-power. Issues of polarization.
Ion exchange	Highly efficient, simple and flexible design.	Expensive due to the resins. Competing ions retard removal efficiency of target pollutant. Regeneration or replacement of exhausted media leads to secondary pollution problems. Process depends on pH.
Adsorption	Affordable, available and simple to design and operate.	High efficiency often demands adjustment and readjustment of pH. Interferences of competing ions. Issues connected with exhausted adsorbent replacement or regeneration including disposal issues.

Source: Halla *et al.* (2015)

exhausted media was found to be possible by soaking the fluoride loaded adsorbent in alkaline solution made using NaOH. Fluoride removal mechanism was controlled by outer surface complexation. The authors concluded the richness of the grasses consumed by the ruminants (cow) in essential cations which also remained inherent in the dungs were responsible for the high F^- scavenging prowess of CDC and as such CDC could be effectively deployed for fluoride containments in rural environments.

In a separate work, byproducts (chars) of the rapid heat-treated (400 - 450 °C) pine wood (PW) and pine bark (PB) were obtained by Mohan *et al.* (2012), checked for its inherent features and applied as adsorbent for fluoride containment in water. Temperature, pH and dosage were varied during the batch empirical studies. The highest F^- uptake capability (7.66 and 9.77 mg/g for PW and PB respectively) was noticed at pH 2 and heat treatment (25 °C), while equilibrium was reached after 48 h at a dosage of 10 g/L. The kinetic data obtained fitted excellently with the PSO model. Fluoride sorption on the sorbents was noticed to hike with a hike in its initial concentration (1 – 100 mg/L) and decreased with rising temperatures. The steadiness single temperature data was suitably represented by the Langmuir and Toth models for PW and PB adsorbents respectively. It was concluded that F^- adsorption on the adsorbents was higher than conventional AC with larger BET surface area and that the underlying process mechanisms were ion exchange and metal precipitation.

Similarly, Mondal and Kundu (2016) investigated fluoride uptake onto lichen and Ca-loaded lichen using batch adsorption systems. The operational factors including rotating speed, dosage, pH, initial F^- concentration, particulate size and temperature were influential to the extent of F^- uptake by the adsorbents. The rate kinetics was modeled using PFO, PSO and intra-particle diffusion models. SEM technique was helpful in understanding the superficial make-up of the materials. The bio-sorption studies evidenced that the Ca-loaded lichen removed more fluoride (78.3 %) at pH 6. The adsorption figures complied with the Langmuir model for each bio-sorbent with a supreme capability of 0.81 and 1.72 mg/g for lichen and Ca-loaded lichen respectively. The adsorption rate followed the PSO model. The mechanism for fluoride adsorption on Ca-treated lichen proposed to be electrostatic attraction. Regeneration of the adsorbent was feasible using NaOH solution. The Ca-treated lichen was effective in lowering the fluoride contents of groundwater obtained from two villages below the stipulated safe limits.

Also recently, Yihunu *et al.* (2020) utilized *Eragrostis tef* as starting material to synthesize two new adsorbents viz: activated biochar (BTS) and hydrochar (HTS) for F^- sequestration in water. The activated biochar produced through heat treatment of the precursor was established to be meso-porous with a huge superficial area of 627.71 m^2/g, while the hydrochar was produced through an acid-enhanced hydrothermal carbonization procedure. Both adsorbent materials exhibited enormous fluoride removal abilities at process conditions of 2, 120 minutes and 200 rpm for pH, interaction time and rotation speed respectively. The process was seen to be thermodynamically exothermic with the empirical data connoting the Freundlich and Langmuir isotherms for the BTS and HTS respectively. The highest monolayer uptake capabilities were 212 and 88.70 mg/g for BTS and HTs separately. The superior superficial area of BTS was concluded as being responsible for its better performance in F^- removal in water.

Cai *et al.*, (2016) synthesized a cheap and efficacious ball-milled tea powder bio-sorbent, packed with zirconium (UTP-Zr) for F^- sequestration in potable water. The features of the prepared bio-sorbent were scrutinized using advanced material characterization techniques, including, FTIR, BET, SEM, XRD, XPS etc. The effects of bio-sorbent amount, interaction time, pH, starting F^- content and competing ions were studied experimentally. The pH (3 – 10) did not affect the F^- uptake efficiency of UTP-Zr and was able to remove fluoride to insignificant levels (0.01 mg/L) in water. The empirical data was well represented by the Langmuir ideal with a supreme capability of 12.43 mg/g at 25 °C. The PSO model was appropriate for recounting the adsorption rates. They posited that UTP-based bio-sorbents was valuable and benign for F^- uptake in potable water.

Suneetha *et al.* (2015) prepared an AC (NVNC) using *Vitex negundo* bark as precursor and nitric acid as stimulating agent and explored its fluoride uptake potentials in water. The highest F^- uptake percent was noticed at neutral pH (7.0), adsorbent amount: 4.0 g/L; interaction time: 50 minutes, Particulate size: 45µm and temperature: 30 ± 1°C. The experimental figures were sufficiently collaborated with the Langmuir and Freundlich ideals. The rate was controlled by the PSO dynamic ideal. Phosphate and bicarbonate were the most influential competing anions towards fluoride adsorption by NVNC. They concluded that NVNC was efficient in sequestrating F^- in water.

In another study, Sahu *et al.* (2021) probed the efficacy of a magnetic activated carbon composite of *Pisum sativum* peel origin for fluoride uptake in water. The adsorbent was synthesized at a temperature of 500 °C and characterized for its surface morphology and functionality. Batch-mode adsorption performance showed that the composite's highest F^- uptake capacity was 4.71 mg/g, achieving also a removal efficiency of up to 100 % at pH of 2. The empirical data obtained was adequately explained by the Freundlich and the PSO models (R^2 = 0.995 – 0.975). The process mechanisms were complex and explained as complexation, hydrogen bonding, electrostatic attraction and ion exchange.

Earlier, Getachew *et al.* (2015) studied the ability banana peel and coffee husk as adsorbents for fluoride uptake in solution. These bio-sorbents were produced through heat treatment of the precursors to enhance the surface morphology and compositions. Best F^- removal performance of the adsorbents was observed at pH 2 at a dosage of 96 g/L and 13 hours interaction time for banana peel, while the best performance of coffee husk bio-sorbent were found at 2, 72 g/L, and 3 hours for pH, dosage and interaction time respectively. At the optimal process conditions, these bio-sorbents were found to remove up to 84 % of F^- in actual water samples obtained from different industries having initial F^- concentrations ranging from 6.72 – 12.54 mg/L. The uptake statistics were soundly described using the Langmuir and PSO models. Based on the smaller dosage involved and shorter time taken to equilibrate, the coffee husk derived bio-sorbent was concluded to be a better material for F uptake in water as compared to banana peel.

Almaraj and Pius (2017) investigated the viability of a cheap AC obtained from the wail of *Morinda tinctoria* and enhanced with Al_2OH_3-coatings for F^- sequestration in aqueous media without pH regulations. IR, SEM/EDAX techniques were applied to scrutinize the morphology and functionality of the adsorbent prior to and after F^- adsorption experiments. The fluoride uptake ability of the material was studied at varying process conditions (interaction time, dosage and F^- concentration). The data obtained revealed enormous adsorption capacity of about 26.0 mg/g at pH 7 and the process was well represented by the Freundlich, intra-particle diffusion and the PSO models (Table 2.8). The influence of competing anions did not have significant hindrance to the F^- uptake capacity of the new material.

Table 2.8: Activated Carbon, Composites and Bio-sorbents for Fluoride removal in Water

S/N	Adsorbent Class/Type	Effective pH Range	Maximum Adsorption Capacity (mg/g)	Removal Efficiency (%)	Influential Competing Ions	Suitable Isotherm/Kinetic Models	Regeneration/ Reusability	Removal Mechanisms	Reference
(a)	Cow dung carbon (CDC)	7.25	15.5	80.0	Bicarbonate	Freundlich, PSO and Intra-particle diffusion	NaOH	Outer sphere surface complexation	Rajkumar *et al.* (2019)
(b)	Pine wood and Pine bark chars	2.0	7.66 and 9.77	NR	None	Langmuir, Toth and PSO	ND	Ion exchange and metal fluoride precipitation	Mohan *et al.* (2012).
(c)	Ca-Treated Lichen	6.0	1.72	78.3	ND	D – R, Langmuir and PSO	NaOH	Electrostatic attraction	Mondal and Kundu (2016).
(d)	Teff straw Biochar (BTS)	2.0	212.0	NR	ND	Freundlich and PSO	NaOH	Electostatic attraction and Ion exchange	Yihunu *et al.* (2020)
(e)	zirconium(IV) loaded ultra-fine tea powder (UTP-Zr)	3 – 10	12.43	NR	Bicarbonate	Langmuir and PSO	NaOH up to 5 cycles	Chemisorption and Electrostatic attraction	Cai *et al.* (2016)
(f)	*Vitex negundo* Activated carbon (NVNC)	2 – 6	NR	97.0	Sulphate and Bicarbonate	Langmuir, Freundlich and PSO	ND	Chemisorption	Suneetha *et al.* (2015)
(g)	Magnetic activate carbon of *Pisum sativum* peel	2.0	4.71	100	NR	Freundlich and PSO	ND	Complexation, hydrogen bonding, ion exchange and electrostatic attraction	Sahu *et al.* (2021)
(h)	Banana peel and coffee husk activate carbon	2.0	0.395 and 0,415	NR	ND	Langmuir and PSO	ND	Chemisorption	Getachew *et al.* (2015)
(i)	Morinda tinctoria bark coated with $Al(OH)_3$	7.0	26.03	ND	Bicarbonate	Freundlich, Intra-particle diffusion and PSO	ND	Electrostatic attraction	Almaraj and Pius (2017)

In another study, Inaniyan and Raychoudhury (2018) systematically investigated the suitability of a new cerium infused AC-composite for F^- uptake in polluted groundwater. To accomplish the aim, firstly the authors made a number of groundwater tests to confirm fluoride contamination of the water from two separate regions in India. The foregoing was then followed up with F^- batch adsorption tests utilizing the newly synthesized adsorbent material at varying process conditions and pH adjustments. The authors posited that the F^- concentrations in the water samples had strong relationship with the water pH, alkalinity level and presence of sodium ions. Fluoride sorption capacity of the adsorbents was greatly retarded at high pH, CO_3^{2-} and HCO_3^- levels. The pH adjustment to the acidic range was found to favour fluoride uptake except for the problem of cerium leaching into solution which also relied on the working content of fluoride in the samples. A summary of activated carbon, bio-sorbent and composites used for water defluoridation is presented in Table 2.8.

CHAPTER THREE
MATERIALS AND METHODS

3.1 Production and Characterization of RPSAC

Table 3.1 highlights on the resources adopted for synthesis and descriptions of RPSAC ACRPSAC. Every chemical utilized in the research was of diagnostic quality. Table 3.2 further reveals the origin, manufacturers and intended use of all chemicals adopted in the current study.

3.1.1 Experimental Background

The emphasis of this work work was to ascertain the appropriateness or otherwise of RPSAC (synthesized via chemical activation route) for decontamination of fluoride laden potable water. The activating agent (phosphoric acid) used for the production of RPSAC was formulated in five separate concentrations as 20, 40, 60, 80 and 100%.

3.1.2 Synthesis of Oxidizing/Activating Agent

Phosphoric acid (H_3PO_4) was utilized as the acidic oxidizing mediator. It was prepared in five different levels as stated above with the aid of distilled water (DW). To achieve this, 20, 40, 60 and 80 milliliters of H_3PO_4 were mixed with 80, 60, 40 and 20 milliliters of DW to obtain 20, 40, 60 and 80 % by volume content of H_3PO_4. The oxidizing agent (H_3PO_4) was used without any dilution with DW to obtain a concentration of 100 %.

3.1.3 Sample Collection and Preparation

Raffia palm fruit bunches were obtained at Ugbema market in Buruku district, Benue state. The shells were retrieved from the fruits, washed and dried under the sun for seven days as shown in Plates 3.1(a-b) (Inyibour *et al.,* 2017). After dehydration, the shells were ground to reduced particle sizes with the aid of a pestle and mortar and further kept in the sun for 3 hours to expel all dampness. They were then kept in the oven at 80 ^oC for 3 hours. The material was then sieved to obtain particles of 3 – 6mm and stored in air tight vessels for further empirical uses (Nwabanne, 2010).

Table 3.1: Constituents and Gadgets for Creation and Description of Adsorbents

S/No	Constituent/Gadget	Depiction	Quantity
1	pH meter	Elico pH meter-Model L1 – 120	1
2	Crucibles	250ml capacity	10
3	Adhesive	-	2
4	Measuring Beaker	250ml capacity	2
5	Measuring cylinder	30ml capacity	5
6	Sieves	Sizes 6mm and 3mm, made by ENDECOTTS Ltd. 667924, London, England	1
7	Activating agent	Phosphoric acid	4Litres
8	Digital Weighing balance	25kg capacity, Mettle Telode-AB204	1
9	Raffia Palm Shells	Freshly collected from local markets in Benue State	20kg
10	Furnace	Carbolite- Model GPC 12/81+103, Max Temp. 12000^0C, Sheffield, England	1
11	Oven	Gallenkamp Oven, Made in Germany	1
12	Scanning Electron Microscope	Phenom ProX	1
13	Infrared spectrometer	Agilent Cary 630 FTIR	1
14	Surface Area and Porosity Analyzer	Quantachrome Novawin Version 11.0	1
15	X-Ray Powder Diffractometer	Rigaku Mini Flex	1
17	Vacuum Filter	Model QF 120C	1
18	Whatman Filter Paper	No 42	1 Pack
19	Glass Column Set-up		1
20	Stop-Watch		1

Table 3.2: List of Reagents, Suppliers and Intended Uses

S/No	Reagent	Supplier	Purpose
1	Sodium Fluoride	Guanzough JHD Chemical Co. Ltd., China	Preparation of synthetic Fluoride solutions
2	Aluminium Sulphate	PVT. Ltd., India	Coating of Adsorbents
3	Sodium Hydroxide	BDH, Dubai, UAE	pH adjustment
4	Hydrochloric Acid	BDH, Dubai, UAE	pH adjustment
5	Palintest No. 1 Tablet	Wagtech Ltd., U.K	Fluoride Test
6	Palintest No.2 Tablet	Wagtech Ltd., U.K	Fluoride Test
7	Sodium Chloride	Guanzough JHD Chemical Co. Ltd., China	Determination of pH_{pzc} and preparation of chloride ion solutions
8	Charcoal Activated carbon	Loba Chemie Pvt. Ltd., India	Fluoride Adsorption Test
9	Potassium dihydrogen Phosphate	BDH, , Dubai, UAE	Preparation of phosphate ion solutions
10	Sodium bicarbonate	MERCK KGAA, Germany	Preparation of bicarbonate ion solutions
11	Anhydrous Sodium Sulphate	Fisher Chemicals, Germany	Preparation of sulphate ion solutions
12	TISAB I	Orion Group, Korea	Buffering of Fluoride solution

Plate 3.1(a): Raffia Palm Fruits under Sun-drying

Plate 3.1(b): Raffia Palm shells under sun-drying

The prepared material was later infused with different concentrations of the H_3PO_4 activating agent (20, 40, 60, 80 and 100 %). To achieve this, 50 g of the as prepared precursor was measured and impregnated separately at activation ratios of 1:1, 1:2, 1:3, 1:4 and 1:5. For the purpose of this work the ratios were convenience in the present work they were labeled as ratios 1, 2, 3, 4 and 5 mL/g respectively. The H_3PO_4 infused precursor was let to interact for 24 hours without heat treatment after which the mixture was clarified and dried in the room for 3 days. The dried materials was then subjected to carbonization in a muffle furnace at varying temperature conditions (200 – 1000 °C) at intervals of 200 °C each at residence times ranging from 30 – 150 minutes.

At the end of carbonization, the furnace was switched-off, allowed to cool and then the heat-treated materials were taken out and rinsed severally with DW to attain a neutral pH in the wash water. The washed activated carbon was then oven heated at 105 °C for 1 hour, pulverized to particle sizes of 0.85 - 2.0 mm (granular activated carbon) using a standard sieve 200 µm. The sieved material was designated as RPSAC and put in airtight vessels for continued empirical studies. Plates 3.3 - 3.5 show some of the steps taken to produce RPSAC.

3.1.4 Determination of Proximate Composition of Precursor

Proximate content of the raffia palm shells precursor was done with a view to ascertain the initial features of the precursor. It was necessary to classify the shells in terms of its moisture content, volatile content, percentage ash and fixed carbon; a pre-indication of the of the suitability or otherwise of a biomass derived precursor for AC synthesis. The inherent make-up of the starting material was determined in harmony with the approaches described by Alkali, (2016).

A. Determination of Moisture Content (MC)

A pre-determined amount of the precursor was weighed and its weight detailed as W_1 (g). It was then subjected to oven heat at 105 °C for 1 hour. After heating, the material was subjected to cooling and final weight measurement. The weight obtained after cooling was designated as W_2 (g). The MC was thereafter estimated from equation 3.1 (Kwaghger, 2012).

Plate 3.2(a): Pulverized Sieved Precursor

Plate 3.2(b): Weighing Balance and Activation Process

Plate 3.2(c): Phosphoric Acid-modified and Carbonized RPSAC in Preservation Bags

$$Moisture\ Content\ (\%) = \frac{W1-W2}{W1} \times 100 \quad (3.1)$$

B. Ash Content Estimates

5g of the sample was evaluated and put on a ceramic receptacle and transmitted into a muffle furnace operated at 600 ^{O}C for 60 minutes in order to reduce mineralization. After the designated time, the content was retrieved from the heat chamber and left to remove heat in desiccators (Ogwuche, 2016). The weight of the ash obtained was taken and the ash content estimated in accordance with equation 3.2.

$$\%\ \text{Ash Content} = \frac{\text{Wash}}{\text{X g}}\ \text{X}\ 100\ \% \quad (3.2)$$

Where; W_{ash} is the weight of ash (g)

X g is the weight of material transferred to the furnace without heat.

C. Determination of Volatile Matter (VM)

The muffle furnace was kept at 600 °C before the precursor sample was transferred into it and allowed to heat for half an hour. The precursor was put in half sealed ceramic receptacle and the initial weight obtained before inserting it in the furnace. At the end of the heat treatment, the ceramic receptacle containing the precursor was taken out and allowed to cool in desiccators. Then the final weight of the material was determined and the weight difference noted. Thus the VM was estimated from 3.3 (Leco, 2010).

$$\text{Volatile content} = \frac{\text{W1}-\text{W2}}{\text{W1}}\ \text{X}\ 100\ \% \quad (3.3)$$

Where; W_1 is weight of ceramic receptacle and sample (g)

W_2 is weight of ceramic receptacle and the ash (g)

D. Fixed Carbon Content (FCC) Estimates

The FCC of the starting material was estimated using the expression below;

100 – [Ash content + Volatile content + Moisture content] (Leco, 2010).

3.2 Physical Characteristics of RPSAC and ACRPSAC

3.2.1 Moisture Content (MC) Estimates

Effective moisture levels for CAC ranges from 3 – 10 %. Thus beyond this limits the quality and of course demand for CAC is diminished. Activated carbon usually take-up moisture from the atmosphere when exposed to a humid environment over time. Such moisture absorptions could be as high as 20 – 35 % and yet display the AC to appear dry by mere observation (Alkali, 2016). To estimate the moisture content of the adsorbents, the initial weight of the material was recorded as W_1 (g) using a digital weighing balance. Then it was subjected to heat in an oven at 110 °C for a 24 h duration after which its temperature was steadied with that of the room. Then the final weight of the adsorbent was again taken and designated as W_2 (g). The adsorbent MC was then estimated using eq. 3.4 for both RPSAC and ACRPSAC.

$$\% \text{ MC } = \frac{W1-W2}{W1} \text{ X } 100 \% \quad (3.4)$$

3.2.2 Determination of Ash Content

The level of ash in the synthesized materials (RPSAC and ACRPSAC) RPSAC was ascertained following the ASTM D2866-94 (2004) standard method. Succinctly, a ceramic receptacle initially subjected to heat maintained at about 500 °C. The crucible was the left in desiccators to extract the excess heat before its final mass was noted. Then about 1.5 g of the materials was taken and put on ceramic receptacle and its total weight noted. Both the ceramic receptacle and its material content were again exposed to heat treatment in a muffle furnace at 500 °C for 1h. Finally, the heated materials were the ejected from the furnace, temperature equilibrated with the room using desiccators and weighed again. The amount of ash present was estimated with eq. 3.5.

$$Ash\ content\ (\%) = \frac{Ash\ weight\ (g)}{Oven\ dry\ weight\ (g)} \times 100 \quad (3.5)$$

3.2.3 Bulk Density Estimations

A Pre-weighed gauging tube was filled with the prepared ACs (RPSAC and ACRPSAC) and softly crammed to a point where there was no observable variation in the depth of the sample in the gauging tube. The sample filled volume was then depicted as V_s. The weight of the unfilled gauging tube was recorded as W_c, while the combined weight of gauging tube with sample was denoted as W. Thus the weight

(W_s) of AC sample was estimated using eq. 3.6. Thereafter, the bulk density of AC was estimated with the aid of eq. 3.7 (Ahmedna *et al.,* 2000).

$$W_s = W - W_c \quad (3.6)$$

$$B_d(g|mL) = \frac{W_s}{V_s} \quad (3.7)$$

3.2.4 Determination of Carbon Yield

The carbon yield of the adsorbents was estimated following the methodology described by Tan *et al.* (2007). Weight (g) of dry starting material was determined using a digital weighing balance and denoted W_p. After AC synthesis, its final weight (g) was determined and denoted as W_f. Then the carbon yield was obtained using eq. 3.8.

$$\frac{W_f}{W_p} \times 100 \quad (3.8)$$

3.2.5 Estimation of Specific Surface Area (SSA)

To ascertain the the SSA of the samples, the Sear's methodology was employed. About 2.0 g of every single sample was variegated with drops of dilute hydrochloric acid (HCl), up to a point when a pH range of 3 – 3.5 was attained. Then, thirty grams of NaCl was spiked under constant stirring to the mixture: then DW was spiked with the mixture to increase its capacity to the 150 mL mark. Then titration of the solution with NaOH (0.1 mol) was done to a point when a solution pH of 9 was attained (Mohammed *et al.,* 2015). The capacity of NaOH consumed to arrive at such pH values was recorded. Thus the SSA of AC sample was estimated using eq. 3.9.

$$S = 32V - 25 \quad (3.9)$$

Where, V is the capacity of NaOH consumed to heighten the solution pH to 9, and S is the SSA (m^2/g).

3.3 Optimization of Synthesis Condition for the Production of RPSAC

Design-Expert 10 statistical software was used to guide the optimal synthesis of RPSAC using Response Surface Methodology (RSM). RSM is an assemblage of mathematical procedures that are suitable for demonstrating and investigating difficult situations in which an interesting parameter is prejudiced by numerous other variable factors (Montgomery, 2001). It is a tool used to unravel the interrelationships among

various variable process or product factors that have been optimized. This method is suitable for fitting various models and also for providing optimal values of the effective parameters, with an advantage of a reduced number of experiments (Azargohar and Dalai, 2005). It is also used to determine which factors and interactions between factors have significant effects on the process. These results help in focusing on what is important, so that money and time could be saved, thus creating the best product and enhancing efficiency. A response surface analysis helps to determine the combination of factors that are necessary to achieve the best response.

In this work, quadratic and 2FI models as suggested in design-expert software were derived with the aid of the Central Composite Design (CCD) in RSM comprising of 30 empirical runs for the activating agent considered for the production of RPSAC.

The adequacy of the developed models in predicting the AC SSA and yield was additionally warranted using analysis of variance (ANOVA). The ANOVA was used to identify which factors or their interactions in the model were significant in obtaining a particular response. The ANOVA was carried out at 95% confidence level from where the factors or combinations of factors that significantly influenced the studied responses were determined.

Design expert 10, was also used to achieve optimization. The terms in the model having P values ≤ 0.05 were taken as significant factors. This is because, ascertaining the competence of models is an imperative aspect in data processing, as it would lead to over or under estimations if its adequacy is not justified/proven. The best optimization results as indicated from the analysis were selected and RPSAC produced at those optimum conditions for validation of the models, further characterization of the optimal product was done and a second adsorbent (ACRPSAC) was synthesized from the optimally produced RPSAC by coating it with aluminium hydroxide following the method described by Salifu (2017) as described below in details. This adsorbent was so prepared in order to improve its affinity for fluoride adsorption in aqueous solution and compared its performance in terms of fluoride adsorption with that of the optimally synthesized RPSAC.

3.3.1 Design of Experiment for Optimization of RPSAC

This was done following the "Central Composite Design" (CCD) in RSM. The CCD is robust and easily unravels the interactive outlook of the variables considered, while ensuring a reduced quantum of experiments to save time and cost of research in accordance with equation 3.10.

$$N = 2^n + 2n + 6 \quad (3.10)$$

Thus, "N" is the overall quantum of experiments to be conducted and "n" is the number of independable factors (4) chosen in this work (Table 3.3).

In the current work, the autonomous factors that were optimized were the AT (^oC), ATT (hours), AAC (%) and IR (g/mL). The dependent variables were CY (%) and SSA (m^2/g). Thus 'N' was computed Putting n = 4 (variables) to give thirty experimental runs (Table 3.4) as follows:

$N = 2^4 + 2x4 + 6 = 30$ (Experimental runs).

3.3.2. Regression Model Development

Relationships in form of experiment-based models were provided to show the interactions of the autonomous and dependent factors in accordance with a general quadratic illustration as in equation 3.11 with all variablescontained there-in as defined by Mohammed *et al.* (2014).

$$Y = b_o + \sum_{i=1}^{n} b_i X_i + \sum_{i=1}^{n} b_{ii} X_i^2 + \sum_{i=1}^{n-1} \sum_{j=i+1}^{n} b_{ij} X_i X_j \quad (3.11)$$

3.3.3. Statistical and Graphical Analysis

Standard statistical and graphical illustrations were deployed to analyse and interprete the data in accordance with the suggestions of De Lima *et al.* (2011) as well as that of Hassani *et al*. (2014) and Roy *et al*. (2014).

3.3.4. Process Optimization for Synthesis of RPSAC

The production conditions of RPSAC which gave the optimal SSA and yield were established using the desirability option in the software that was described earlier. Suitable goals were set for all variable categories (Appendix A). Similarly, suitable limitations for each variable were adopted as depicted in Table 3.3 (Hassani *et al.*, 2014).

Table 3.3: Process Variables and stages Adopted for the CDD in RSM

Variable	Stage				
	-α	α	0	α	+α
*IR (g/mL)	1	2	3	4	5
AT (°C)	200	400	600	800	1000
ATT (minutes)	30	60	90	120	150
AAC (%)	20	40	60	80	100

*IR is impregnation ratio, AT is activation temperature, ATT is activation time and ACC is activating agent concentration.

Table 3.4: CCD Scheme for RPSAC Production

RUNS	Variable 1 A: Activation Temperature °C	Variable 2 B: Activation Time Minutes	Variable 3 C: Chemical Impregnation Ratio g/mL	Variable 4 D: Activating Agent Concentration %
AC1	800	120	2	40
AC2	800	60	4	40
AC3	800	120	4	40
AC4	600	90	3	60
AC5	600	90	1	60
AC6	800	60	4	80
AC7	1000	90	3	60
AC8	600	90	3	60
AC9	400	60	2	80
AC10	600	90	3	60
AC11	600	150	3	60
AC12	400	120	4	40
AC13	400	120	2	40
AC14	200	90	3	60
AC15	600	90	3	100
AC16	400	120	4	80
AC17	600	30	3	60
AC18	800	120	4	80
AC19	600	90	5	60
AC20	400	60	2	30
AC21	400	120	2	80
AC22	600	90	3	60
AC23	800	60	2	40
AC24	600	90	3	60
AC25	800	120	2	80
AC26	800	60	2	80
AC27	600	90	3	60
AC28	400	60	4	40
AC29	600	90	3	20
AC30	400	60	1	80

3.3.5. Model Authentication

This was used to validate the reliability of the models. As such confirmatory experiments were re-conducted at the model indicated optimal conditions and a comparison through error analysis was made between the model-derived and experimental optimal values of the dependent variables (Roy *et al.,* 2014).

3.3.6 Functionalization of RPSAC with aluminium oxide to produce ACRPSAC

The as-synthesized RPSAC was reacted with a solution of Al_3SO_4 in order to form oxides of aluminium on its surface to produce a composite called ACRPSAC in accordance with the functionalization principle (Amalraj and Pius, 2017; Salifu, 2017). To achieve this, 550 mL of Al_3SO_4 (0.6 M) was shaken in reacting vessel. Then 100g of the as-synthesized RPSAC was gently added to the contents of the reacting vessel under constant stirring to guaranty the wholesome soaking of RPSAC in the solution. Afterwards, the slow addition of a 3M NaOH solution to the reactor contents was carried-out with further constant mixing at 250 rpm until the solution pH of 7 was reached. At this point the mixture was guaranteed to contain a mixture of ACRPSAC and excess sodium salts. The generated mixture was then alienated with the aid of vacuum separator; a process which yielded a sieve lump of ACRPSAC. The ACRPSAC cake was thereafter dehydrated for three hours in an oven set at 110 °C. Thereafter, it was carefully washed using distilled water to eliminate all salt impurities. The washing of ACRPSAC was continued until the wash water had a concentration of sulphate ions that was lower than 1 mg/L and oven-dried for 3 hours at 100 °C.

The ACRPSAC alongside the optimally synthesized RPSAC were characterized using advanced techniques for ascertaining the surface area/porosity, surface morphology/elemental composition, crystallographic/mineral composition and surface functional groups of materials with the aid of the Brunauer-Emmett-Teller (BET), SEM/EDX, XRD, Fourier Transform Infra-Red (FTIR) methods respectively. Other physical characteristics of the adsorbents such as pH_{pzc}, bulk density, moisture content, and percentage ash and particle size were also ascertained following standard procedures. The adsorbents were at this point used for batch F^- sequestration in simulated and actual drinking water trials.

3.3.10 Characterization of Produced Activated Carbon and Composite

As earlier stated, the adsorbents (RPSAC and ACRPSAC) synthesized in the current (Plate 3.3 (A and B) respectively, were characterised using SEM/EDX, FTIR, BET and XRD methods. These analyses were sacrosanct as they were aimed at providing more insights as to the likely mechanisms to be encountered when deploying the adsorbents for groundwater defluoridation in batch systems.

3.3.8 SEM and FTIR Analyses

In a bid to unravel the functionalities on the adsorbents' exterior, the FTIR analysis was deployed, while the surface appearance was scrutinized via the SEM analyses. The Infra-Red (IR) spectrums were detailed using a Nicolet Avatar FT-IR (4000 and 400 cm^{-1}). Potassium bromide disk were adopted as the reference. The complete instrument set-up for FTIR analysis is as in Plate 3.4A. The surface appearances of the adsorbents were scrutinized with a SEM set up (Phenom Pro X) at appropriate magnifications and pressure. The materials were treated with gold before subjecting it to the SEM procedure (Giwa *et al.*, 2013).

3.3.9 Determination BET Surface Area and Porosities

Nitrogen uptake at 77 °C was used to estimate the BET surface area, summed pore volume and mean pore-diameter of the adsorbents (RPSAC and ACRPSAC) with the aid of a Quantachrome Novawin Version 11.03 analyser following the procedures of Kang *et al.* (2013) as shown in Plate 3.4B.

3.3.10 X-ray Diffraction (XRD) Analysis

The mineral and crystallographic make-up of the synthesized materials (RPSAC and ACRPSAC) were scrutinized using a Rigaku Mini Flex X-ray Diffractometer and in accordance with the methods of Kang *et al.* (2013) with slight modifications. Briefly, the samples were crushed and regimented before the mean bulk configuration was ascertained. The finely grounded samples were then arranged with the aid of the sample grounding block and trampled in the level sample holder to form a level, exterior that was afterwards fixed on the sample stage in the XRD cabinet.

The reflection-transmission rotator stage was used to analyse the samples at the ɵ - ɵ settings. The 2ɵ opening spot was 4 degrees and terminated at 75 degrees with a 2ɵ

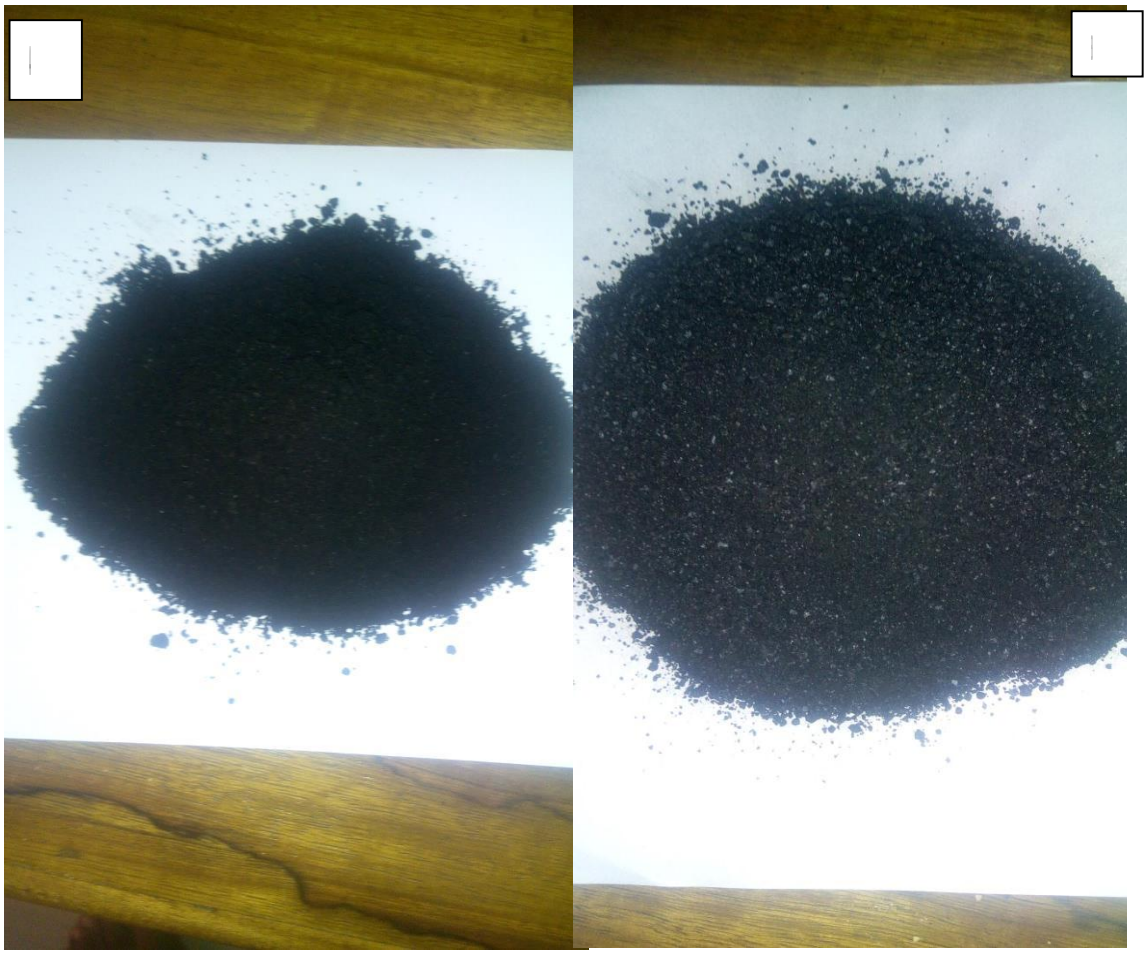

Plate 3.3, (A): A sample of RPSAC, (**B):** ACRPSAC

Plate 3.4, (A): FTIR Instrumental Set-up, (**B):** BET Surface Area and Porosity Analyser

step of 0.026261 at 8.67s/step. Current supply in the tube was set at 40mA with a tension of 45VA. The 2λ spot of the diffraction peak was usually measured as the centroid of the peak at 80% peak height.

3.3.11 Measurement of Adsorbents' pH_{pzc}

This was done by means of the salt addition method for the newly synthesised adsorbents (RPSAC and ACRPSAC) and a commercial activated carbon (CAC). Plate 3.5 shows a sample of the CAC used in this study. Precisely, fifty milliliters of NaCl solution (0.01 mol/L) was reassigned into a number of laboratory flasks. The pH of the flask contents was controlled with HCL and NaOH solutions. Thereafter, 0.6 g of the sample was put in the mixture and shaken on a rotary spinner for an hour and left to settle and equilibrate quiescently at room conditions for about 48 hours. The solution pH was then noted for the sample in question. A plot of the starting pH (pH_o) against the change in pH after addition of adsorbent (ΔpH) was made from where the pH_{pzc} for each sample (adsorbent) was taken as the spot where ΔpH = 0 (Abia and Asuquo, 2007).

3.4 Batch-Mode Adsorption of Fluoride using RPSAC and ACRPSAC

Table 3.5 shows the materials and instruments that were utilized for testing the adsorption of fluoride in simulated ground water by the synthesized adsorbents (RPSAC and ACRPSAC). The experiments were carried-out in both batch equilibrium isotherms, kinetic and thermodynamic experiments using simulated fluoride contaminated water. The best performing adsorbent (ACRPSAC) with regard to the F^- uptake capability and removal percent was selected from the batch adsorption experiments for further studies (batch adsorption modeling and optimization and experiment with actual groundwater samples).

3.4.1 Comparing Fluoride Adsorption onto ACRPSAC, RPSAC and CAC

The optimum RPSAC and ACRPSAC were evaluated in batch operation mode in the laboratory for F^- uptake from simulated aqueous media in comparison with a CAC (Plate 3.5). The essence was to elucidate on the commercial value or otherwise of the newly produced adsorbent materials. The influence of process parameters (interaction period, pH, temperature, carbon amount per given solution volume and primary fluoride levels) on the adsorbents' adsorption capacity and fluoride removal efficiency

Plate 3.5: Sample of the purchased Commercial Activated Carbon (CAC)

Table 3.5: Materials and Instruments for Batch Fluoride Adsorption Studies

S/No	Resources/ Gadgets	Detail	Number
1	pH, TDS and EC meters	Hanna -ModelHI98107, HM Digital TDS-4 Pocket Size, Suntex model SC-120	1 each
2	Crucibles	250ml capacity	10
3	Adhesive	-	2
4	Measuring Beaker	250ml capacity	10
5	Measuring cylinder	100 ml capacity	50
6	Glass columns	Locally made, 3cm diameter and 30cm	3
7	Peristaltic pump		1
8	Isothermal Magnetic shaker	Model HY-2	1
9	Digital Watch		1
11	Reagents	Analytical grade	
12	Activated Carbons	RPSAC ACRPSAC Activated Charcoal and Activated Alumina	3kg 3kg 1kg each
14	Portable Data logging Spectrophotometer	HACH model, 2300	1
15	Thermostatic Water Bath		2
16.	Digital Analytical Balance	Adam model PW 184	1
17.	Photometer	Wagtech, Model 7100	1
18.	Palintest Fluoride No. 1 Tablet	Wagtech	100 Tablets
19.	Palintest Fluoride No. 1 Tablet	Wagtech	100 Tablets
20.	UV-Visible Spectrophotometer	UNICO, model 2800P	1
21	Fluoride Ion Selective Electrode	Orion, Model 25100	1
22	pH/Multimeter	Xplorer GLX, Model PS-2002	1

were evaluated. The experimental results obtained were snugged with existing unit temperature, dynamic and temperature-dependent dynamic ideals in other to elucidate on the F^- uptake scenarios of the tested adsorbents and also provide data for design of adsorption systems targeted at fluoride removal in drinking water. The adsorption parameters determined for the best performing adsorbents from the batch experiments undertaken in the current work would be useful for the development of a household-Point of Use (PoU) adsorption system for F^- containment in drinking water.

3.4.2 Conditioning Main F^- Solution

A 1000 mg/L stock solution of F^- ions was prepared by liquefying 2.21g of NaF (without initial water) in a litre of DW. Thereafter, aliquots of desired F^- contents were made from the stock by serial dilution and utilized in the batch F^- uptake tests. Every chemical utilized was of approved quality.

3.4.3 Batch Equilibrium Isotherm, Kinetic and Thermodynamic Experiments

Batch adsorption and modeling experiments were undertaken extensively in the laboratory (Environmental Chemistry Laboratory, Benue State University, Makurdi) using several laboratory flask (capacity = 250 mL) holding about 100 mL of the F^- solutions. F^- c oncentrations ranging from 2 – 10 mg/L were separately reacted with a known dose (2 g/L) of the adsorbing media (RPSAC, ACRPSAC and CAC) and agitated at a speed of 150 rpm on a constant-temperature (303 K) shaker (model HY-2) (Table 3.5) for 120 minutes at a constant pH of 6.0.

After agitation, the mixture was separated using a separating media (Whatman No 4) and the residual concentration of fluoride in the filtrate determined with the aid of Orion 25100 ISE connected to an Xplorer GLX, PS-2002 multimeter (ASTM D9214). The filtrate solution was diluted with a TISAB I solution (at 1:1). The instrumental set-up was attuned with a known F^- solution standard in a manner which allowed the fluoride concentration of the unidentified to be within the limit of the standard. The batch adsorption tests were helpful in the estimation of preliminary optimal operating conditions with regard to the primary F^- content, adsorbent dosage, interacting period, pH and temperature that would lead to high fluoride adsorption capacity and removal efficiency by the adsorbents. Furthermore, acquired data after the variations of initial F^- concentration were used for adsorption isotherm modeling; those from the

variations of contact time and temperature were utilized for kinetic and thermodynamic modeling respectively. To guaranty the reproducibility and quality of the experimental data, all assays were repeated thrice and average values recorded.

3.4.4 Influence of Solution Hydroxyl Ions (pH) on F^- Uptake Ability

The influence of pH on F^- uptake percent and adsorbents' uptake capability was investigated by agitating 100 mL of fluoride solution on a thermostatic horizontal mechanical shaker at initial pH ranges of 3-11 to cover both the acidic and alkaline range (Salifu, 2017). The carbon dosage (g/L), pollutant concentration (mg/L), agitation time (minutes), temperature (K) and speed (rpm) were kept constant at 2, 5, 120, 303 and 150 respectively. At the stop of agitation, the solutions were filtered and analyzed for residual fluoride concentrations using a fluoride Ion Selective Electrode (ISE) (Orion Model 25100). The pollutant removal efficiencies and activated carbon adsorption capacities were calculated using equations 3.12 and 3.13 respectively.

$$R = \frac{(C_i - C_t)}{C_i} \times 100 \quad 3.12$$

$$q_t = \frac{(C_i - C_t)V}{m} \quad 3.13$$

Hence;

R is F^- removal efficiency (%),

q_t is F^- uptake capacity (mg/g),

C_i and C_t are the starting and end F^- concentrations (mg/L) respectively,

M is the carbon dosage (g),

V is F^- volume of solution (L).

3.4.5 Effects of Initial Fluoride Concentration

The influence of initial fluoride content on the removal percent and uptake capability was studied in comparison with a CAC in separate 2-10 mg/L F^- solutions. The chosen range was a reflection of the ideal F^- contents in real potable water samples across the globe (Adimalla *et al.,* 2019). The carbon dosage (g/L), solution pH, agitation time (minutes), temperature (K) and speed (rpm) were kept constant as earlier described. 100 mL solutions at the various fluoride concentrations were agitated with a known quantity of the adsorbents on a shaker. After agitation, the mixtures were filtered and checked for residual F^- concentrations. The pollutant

removal efficiencies and activated carbon adsorption capacities were calculated using equations 3.12 and 3.13 respectively.

3.4.5 Effects of Adsorbent Dosage

The influence of the quantity of adsorbent added per given capacity of F^- laden solution on the F^- removal percent and adsorbents' uptake capability was investigated by agitating 100 mL of fluoride solution on an isothermal magnetic shaker at initial dosages of 0.5 – 2.5 g/L. The pollutant concentration (mg/L), agitation time (minutes), temperature (K) and speed (rpm) were kept constant at 5, 120, 303 and 150 respectively (Inyinbor *et al*., 2016) At expiration of agitation, the mixtures were separated by filtration and remaining fluoride contents in the filtrate determined potentiometrically using the fluoride ISE as described earlier. The pollutant removal efficiencies and activated carbon adsorption capacities were calculated using equations 3.12 and 3.13 respectively.

3.4.6 Effects of Contact/Agitation Time

The influence of reacting/agitation period on fluoride removal percent and adsorbents' uptake capability was examined by agitating 100 mL of fluoride solution on a thermostatic horizontal mechanical shaker at contact times of 30 – 150 minutes. The pollutant concentration (mg/L), adsorbent dosage (g/L), temperature (K) and speed (rpm) were kept constant at 5, 2, and 303 and 150 respectively (Inyinbor *et al.*, 2017). When agitations ended, the mixtures were separated by filtration and tested for remaining F^- content in the filtrate as described earlier. The pollutant removal efficiencies and activated carbon adsorption capacities were estimated from equations 3.12 and 3.13 respectively.

3.4.7 Effects of Temperature

Influences of heat treatments on F^- removal percent and adsorbents' uptake capability was investigated by agitating 100 mL of fluoride solution on a thermostatic horizontal mechanical shaker paced in a thermostatic water bath and operated at varying temperatures of 303 – 323 K. The pollutant content (mg/L), carbon amount per given volume (g/L), agitation period (minutes), and speed (rpm) were kept constant at 6, 2, 120, and 150 respectively (Chubaakum *et al.*, 2018). At the end of shaking, the solutions were filtered and checked for residual F^- concentrations as described earlier. The pollutant removal efficiencies and activated carbon adsorption capacities were calculated using equations 3.12 and 3.13 respectively. The performance of the

adsorbents was further compared using ANOVA at P = 0.05 level of significance using the SPSS software (Version 21).

3.6 Equilibrium Isotherms Modeling

The linear forms of the Langmuir, Freundlich and Temkin models were adopted in modeling fluoride uptake on the adsorbents (RPSAC, ACRPSAC and CAC). The linearized model formats are as shown in expressions 3.14, 3.15 and 3.16 respectively.

$$\frac{1}{q_e} = \frac{1}{bq_mC_e} + \frac{1}{q_m} \quad 3.14$$

Here, Ce is the steady state F^- content (mg/L), qm is the Langmuir uptake capability (mg/g) and *b* is the unchanging Langmuir parameter associated with the free vigor of adsorption (L/mg).

$$lnq_e = lnk_f + \frac{1}{n}lnC_e \quad 3.15$$

Where, K_f is the uptake capability (mg/g) and 1/*n* is the strength of the adsorption.

$$q_e = B_1 lnk_t + B_1 lnC_e \quad 3.16$$

Here, $B_1 = R_t/b_t$, k_t (L/g) and b_t ($kJmol^{-1}$) are the unchanging Temkin parameter and R_t is the global unchanging gas parameter.

3.7 Adsorption Kinetic Modeling

In the current study the kinetics of F^- uptake using the present adsorbing materials was scrutinized using the linear forms of the pseudo-first-order (PFO), pseudo-second-order (PSO), Elovich, Bangham's Pore Diffusion (BPD) and Webber- Morris Intra-particle Diffusion (WMID) models as shown in equations 3.17, 3.18, 3.19, 3.20 and 3.21 respectively.

$$In(q_e - q_t) = Inq_e - k_{ad}t \quad 3.17$$

Here, k_{ad} is the PSO rate persistent parameter; q_e is the uptake capability; and q_t is the uptake capability at any given period (t). k_{ad} is the slope of the linear plot of $ln(q_e - q_t)$ vs *t*.

$$\frac{t}{q_t} = \frac{1}{k_2 q_e^2} + \frac{1}{q_e}t \quad 3.18$$

Here, k_2 is the PSO rate constant; q_e is Steady state uptake capability; and q_t is the uptake capability at any given period (t). The parameters were approximated from the slope and intercept of the graph of t/q_t vs t.

$$q_t = \frac{1}{\beta} In(\alpha\beta) + \frac{1}{\beta} In(t) \quad 3.19$$

Here, α is the primary uptake rate (mg/g.min) and β is the unchanging desorption parameter (g/mg). q_t was graphed against *ln (t)* and the slope and intercept were taken to represent1/β)and (1/β) ln (αβ) correspondingly.

$$LogLog\left(\frac{c_i}{c_i - q_t m}\right) = Log\left(\frac{k_o}{2.303v}\right) + \propto Logt \quad 3.20$$

Here, *Ci* is the primary levels of the pollutant in aqueous media (mg/L), *V* is the solution volume (mL), m is adsorbent dosage (g/L), qt (mg/g) is the adsorption capacity at time "*t"* (min) and α (less than 1) and k_o are the unchanging parameters.
Rate of sorption is frequently used to analyze the kind of rate-limiting stage involved. In most cases the WMID model is readily utilized to ascertain the rate-limiting steps in any adsorption system and it is given as in the Weber-Morris equation (equation 3.21) below:

$$q_t = k_{ip} t^{1/2} + C \quad 3.21$$

Where, *C* is estimated from the intercept and provides information about the border cover solidness and *kip* is the intra-particle diffusion-unchanging rate parameter. In the accordance with the model assumptions, when an adsorption process is intra-particle diffusion-controlled, then a plot *qt* versus $t^{1/2}$ should yield a straight line.
Note that: from the second order kinetic model, $t^{1/2}$ is the period necessary for an adsorbing material to adsorb about 50 % of pollutant at its steady-state value. This parameter is taken as an estimate of the uptake rate and is given as in equation 3.22.

$$t^{1}/_{2} = \frac{1}{k_2 q_e} \quad 3.22$$

3.7 Thermodynamic Modeling

Three temperature ranges (303 – 323 K) were utilized to generate the thermodynamic parameters of F^- uptake by the three adsorbents. Other conditions were left to be 6.0 mg/L, 2.0 g/L, 2.0 hours for starting F^- concentration, dosage and contact time

respectively without pH adjustments. For this study, *lnKd* vs*1/T* was plotted in accordance with the Vant Hoff's equation (equation 3.23) and the values of ΔS° ΔH° were taken as the intercept and slope of the linear graph correspondingly. The value of ΔG° (kJmol^{-1}) and K_d on the other hand were estimated with expressions 3.23 -3.25 respectively.

$$lnK_d = \frac{\Delta S^o}{R} - \frac{\Delta H^o}{RT} \quad 3.23$$

$$\Delta G_o = -RTInK_d \quad 3.24$$

$$K_d = \frac{q_e}{C_e} \quad 3.25$$

Here, R is the unchanging global gas parameter (8.3 Jmol^{-1} K^{-1}), T is absolute temperature (Kelvin) and K_d is the dispersal coefficient (L/g), *qe* is the adsorption capacity (mg/g), *Ce* is the steady state adsorbate content (mg/L). ΔH_o (kJmol^{-1}) was thus estimated from equation 3.26.

$$\Delta H_o = \Delta G_o + T\Delta S_o \quad 3.26$$

For a known temperature, pollutant uptake is assumed to be unprompted if the ΔG° is negative. On the other hand, positive values of ΔH° entail an endothermic adsorption process, while negative values of ΔH° suggests an exothermic adsorption process (Chubakuum *et al.*, 2018).

Also, having been known that the magnitude of the diffusion coefficient (D) relies majorly on the adsorbents' surface compositions and that it is an inevitable parameter that provides useful insights as to the diffusion mobility. Thus in this work an attempt was made to estimate the coefficients for film diffusion (D_f) and intra-particle diffusion (D_p) using equations 3.27 and 3.28 respectively.

$$D_f = {0.23 r_o \partial q_e}\Big/{t^{1/2} C_o} \quad 3.27$$

$$D_p = {0.03 r_o^2}\Big/{t^{1/2}} \quad 3.28$$

Where; r_o (cm) is adsorbent particle radius (assuming its spherical in shape), ∂ is the thickness of the film (10^{-3} cm), q_e (mg/g) is the steady state uptake capability, C_o (mg/L) is the primary F^- content, $t^{1/2}$ is the 50 % life as estimated from eq. 3.24 above, D_f and D_p are the film and intra-particle diffusion coefficients correspondingly in

cm^2/h. It should be noted that the values of D_f and D_p are very useful for the development of full-scale adsorber systems.

3.8 Effects of Competing Anions on Fluoride Removal

The influence of interfering/competing ions on F^- uptake abilities of the adsorbents was studied at an initial F^- content of 6 mg/L at hydroxyl ion concentration (pH) of 7 and contact time of 120 minutes to depict real drinking water parameters. The mixed-ions were prepared at 30 mg/L concentrations each using $NaNO_3$, Na_2SO_4, $NaHCO_3$ and NaCl to represent the influence of anion (nitrate, sulphate, bi-carbonate and chloride) in drinking water. The foregoing was premised on the occurrence of these ions in such concentrations in actual groundwater samples meant for drinking in Nigeria (Malum *et al.,* 2019).

3.9 Regeneration of Adsorbents

In this study, the surfaces of the studied adsorbents were exhausted with fluoride ions by mixing in a beaker and shaking about 2g each of RPSAC, ACRPSAC and CAC with a known volume (100 mL) of the fluoride solution (6 mg/L) for 18 h. All regeneration experiments were conducted using DW to avoid external contaminations. Firstly, each fluoride-laden adsorbent were reacted with varying levels of sodium hydroxide with stirring for one hour to rejuvenate the adsorbent. The exhausted samples (reacted with NaOH) were washed with DW up to a neutral pH point and dehydrated in an oven set at 120 ^oC for 480 minutes and made available for reutilization for F^- uptake (Chubaakum *et al.,* 2018).

For estimating the removal efficiency of F^- onto rejuvenated adsorbing materials, 0.002 kg of each rejuvenated material was put in a 100 mL F^- solution (6 mg/L) and shaken for 2 hours under constant temperature (303 K) and pH 7. Additionally, rejuvenation was also accomplished by treating the exhausted and sodium hydroxide reacted-ACRPSAC with fresh aluminum sulphate to precipitate aluminium oxide on its surface again. Likewise, a part of the F^- loaded-ACRPSAC was rejuvenated by reacting it with aluminium sulphate to deposit aluminum oxide on its surface without any prior reaction with sodium hydroxide. All the as rejuvenated adsorbing materials were comparatively evaluated for their reusability for F^- uptake in aqueous media (Salifu, 2017).

3.10 Optimization of Fluoride Uptake onto ACRPSAC

From the equilibrium isotherm, kinetic and thermodynamic studies, it was observed that ACRPSAC performed better as compared with RPSAC and CAC. Thus, ACRPSAC was chosen for further studies. Again RSM using the CCD of experiment was deployed to model and optimize fluoride uptake onto ACRPSAC since it performed betterthan the other adsorbents in the earlier batch uptake studies. The software and optimization handle as earlier explained in section 3.3 above were again upheld for these studies.

Table 3.6 reveals the choosen variables (independent) and the constraints, while Tables 3.7 and 3.8 shows the empirical runs and the goals for optimization of both the independent and independent variables correspondingly. Model validation for F^- uptake by ACRPSAC was carried out at the predicted optimal conditions using both simulated and actual F^--ladened potable water samples and compared with the performance of CAC and AA.

Actual F⁻ladened potable water samples were obtained from Kaltungo and Langtang which are documented areas in northern-Nigeria with prevalence of fluoride-related ailments due to the consumption of F^- enriched groundwater (Wongdem *et al.,* 2000; Dibal *et al.,* 2012a; Dibal *et al.,* 2012b; Dambature *et al.,* 2014; Urial *et al.,* 2014; Dibal *et al.,* 2016; Goyit *et al.,* 2018; Malum *et al.,* 2019).

The obtained potable water samples from these locations were firsly checked for its physical and chemical compositions following customary procedures (APHA, 2005).

3.11 Assessment of Groundwater in Makurdi, North Central-Nigeria

Potable water sourced from boreholes was systematically collected from 21 localities in and around Makurdi metropolitan area in north-central Nigeria in the month of October. The water samples were further characterized for its parametric constitution with a focus on F^- contamination, possible causes of contamination and associated risk to human health. The month of October was chosen because it is the peak of raining season (Isikwue and Onyilo, 2010; Iorliam et al., 2013; NOAA, 2016) in the area and it is expected that groundwater contamination from all sources should peak at this time and could represent the worst-case scenario for the area in terms of groundwater pollution.

Table 3.6: CCD* Factors and Levels for Fluoride Adsorption using ACRPSAC*

Factors	Levels				
	-α	**-1**	**0**	**+1**	**+α**
Adsorbent Dosage (g/L)	0.5	1	1.5	2	2.5
Initial Concentration (mg/L)	2	4	6	8	10
pH	2	5	7	9	11
Contact Time (minutes)	30	60	90	120	150

*CCD is "Central Composite Design", *ACRPSAC is "Aluminum Oxide-coated Raffia Palm Shell Activated Carbon

Table 3.7: CCD Matrix for Fluoride Adsorption on ACRPSAC

Run	A:pH	B:Concentration	C:Dosage	D:Contact Time
		mg/L	g/L	Minutes
1	7.0	2.0	1.5	90
2	9.0	8.0	2	120
3	7.0	6.0	1.5	90
4	7.0	6.0	1.5	90
5	9.0	4.0	2	60
6	5.0	4.0	2	60
7	5.0	4.0	1	120
8	7.0	10.0	1.5	90
9	7.0	6.0	1.5	30
10	5.0	8.0	1	120
11	3.0	6.0	1.5	90
12	5.0	4.0	1	60
13	5.0	8.0	2	120
14	11.0	6.0	1.5	90
15	9.0	8.0	1	60
16	5.0	8.0	1	60
17	7.0	6.0	2.5	90
18	9.0	8.0	1	120
19	5.0	8.0	2	60
20	7.0	6.0	1.5	150
21	9.0	4.0	1	120
22	7.0	6.0	1.5	90
23	7.0	6.0	0.5	90
24	7.0	6.0	1.5	90
25	7.0	6.0	1.5	90
26	9.0	4.0	1	60
27	9.0	8.0	2	60
28	5.0	4.0	2	120
29	7.0	6.0	1.5	90
30	9.0	4.0	2	120

Table 3.8: Optimization Goals for Fluoride Adsorption on ACRPSAC

Factor/Response	Goal	Minimum	Maximum
Carbon Dosage (g/L)	Empirical Range	0.5	2.5
Interaction Period (minutes)	Empirical Range	30	150
Primary Adsorbate Content (mg/L)	Empirical Range	2	10
pH	Empirical Range	2	11
Removal Efficiency (%)	Maximize	82.38	99
Adsorption Capacity (mg/g)	Maximize	1.29	9.98

3.11.1 Description of the Study Area

Fig. 3.1 shows the map of Makurdi revealing the 21 sampling points. The GPS coordinates of the sample collection points are shown on Table 3.9. The studied location is the governmental headquarters of Benue state, in North-central (Middle belt) Nigeria and has therefore been associated with speedy urbanization activities in the last two decades which have largely altered its natural ecosystem. It is situated within Latitude 7.733^{o}N and longitude 8.5391^{o}E of the Greenwich meridian and has a total land area of about 36 km^{2}. The vegetation cover is that of the guinea savanna with well separated arid and rainy spells. The arid spell spans from the months of November – early April each year, while the rainy spell commences in mid-April and finishes in October. Peak rainfall amounts are usually encountered in September and October each year. Mean yearly rainfall in this location is estimated at 1,237 mm (NOAA, 2016).

Most periods in the dry spell (November – February) are usually associated with hamartan which makes the season to be relative cold (Isikwue and Onyilo, 2010). The area is characterised by a plain topography with a slope of about 0 – 2.5 % and a shallow aquifer depth. The average temperatures in a month are high (18 – 37 °C) owing to the closeness of this location to the Benue River; a condition that favour land and sea breezes (reflection of solar radiation back to land). The area is endowed with numerous solid minerals including glass, limestone, salt, barite and sand etc, which are locally exploited and marketed by the residents for improved livelihoods. The human population in Makurdi was estimated in 2007 to be about 500,978 people and is projected to grow to about 1million people by the year 2025 (The World Gazetteer, 2010). The total yearly consumptive use in the area is estimated to be 2603 mm, while the average relative humidity per year is given as 40.8 % (Isikwue and Adakole, 2011). The geology of the area is predominantly comprised of sandstone, emanating from the Nigerian sedimentary basin. The sandstones are fine to medium grained, micaceous, calcareous, feldspathic, shelly, mildly organized and in some instances contain cement-like oxides like Fe_2O_3, SiO_2, CO_3 (Iorliam *et al.,* 2013).

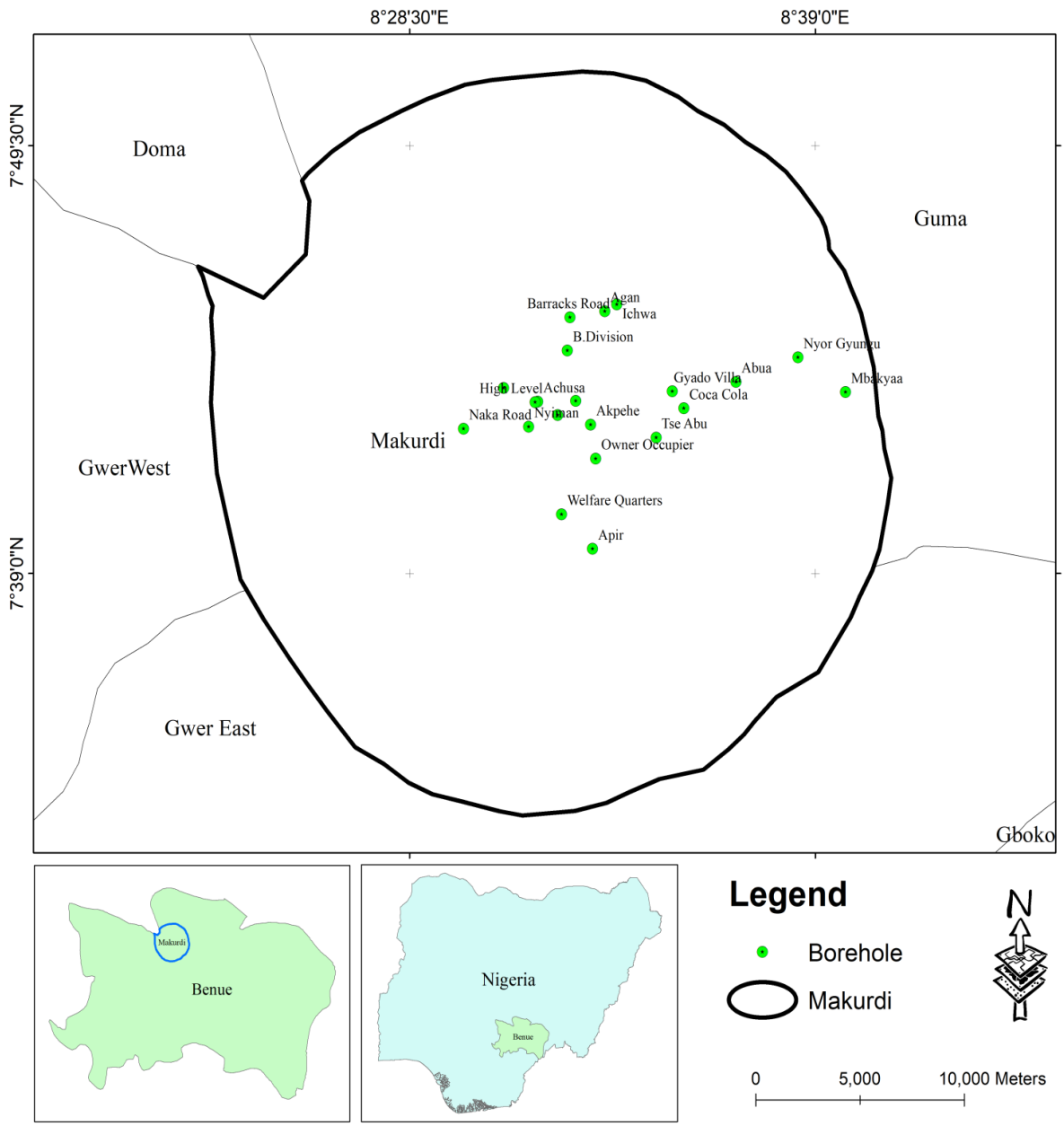

Figure 3.1: Map of Study Area showing the Sampling Points

Table 3.9: GPS Coordinates of Sampling Points in the Study Area

S/No	Location	Latitude	Longitude	Groundwater Source
1	Achusa	7º N 42’ 73’’	8º E 31’ 49’’	BH*
2	Ichwa	7º N 45’ 36’’	8º E 33’ 52’’	BH
3	B.Division	7º N 43’ 88’’	8º E 32’ 35’’	BH
4	Barracks Road	7º N 45’ 17’’	8º E 32’ 39’’	BH
5	Logo I	7º N 42’ 53’’	8º E 32’ 20’’	BH
6	Wurukum	7º N 43’ 14’’	8º E 32’ 48’’	BH
7	Nyiman	7º N 42’ 36’’	8º E 31’ 35’’	BH
8	Gyado Villa	7º N 43’ 28’’	8º E 34’ 78’’	BH
9	Welfare Quarters	7º N 40’ 27’’	8º E 32’ 26’’	BH
10	Akpehe	7º N 42’ 39’’	8º E 33’ 11’’	BH
11	Coca Cola	7º N43’ 03’’	8º E 35’ 36’’	BH
12	Nyor Gyungu	7º N 43’ 78’’	8º E 38’ 33’’	BH
13	Mbakyaa	7º N 43’ 27’’	8º E 69’ 47’’	BH
14	Modern market	7º N 43’ 33’’	8º E 30’ 56’’	BH
15	Tse Abu	7º N 42’ 20’’	8º E 34’ 53’’	BH
16	Owner Occupier	7º N 41’ 49’’	8º E 33’ 19’’	BH
17	Abua	7º N 43’ 42’’	8º E 36’ 57’’	BH
18	High Level	7º N 43’ 12’’	8º E 31’ 45’’	BH
19	Naka Road	7º N 42’ 33’’	8º E 29’ 54’’	BH
20	Agan	7º N 45’ 26’’	8º E 33’ 33’’	BH
21	Apir	7º N 39’ 36’’	8º E 33’ 14’’	BH

*BH means “Borehole”

3.11.2 Field Sampling and Laboratory Analysis

Triplicate groundwater samples from systematically selected boreholes were obtained at each of the 21 sampling points (totaling 63 samples) (Fig.3.1) in October, 2019. The samples were retrieved from the connected borehole taps at each location. Before sampling commenced, the taps were turned on and left to flow on to the bare surface for a period of 12 minutes, before the samples were taken in the newly bought and cleaned polyethylene containers (1L capacity).

The polyethylene containers were firstly eroded with a composite of DW and HNO_3 (15 %), then further cleaned with DW and dehydrated in the air for about 24 hours before the commencement of sampling works. At the point of sample collection, the vessels were firstly washed for about thrice using the sample water prior to fetching the desired trials. The trials so obtained were then correctly branded using concealing adhesives and indicator ink and then transported within freeze coolers to the laboratory for checks. In order to avert further deterioration of the samples under laboratory conditions, they were krefrigerated at about 4 ^{o}C before the commencements of laboratory tests.

The physical and chemical composition of the water samples including; Total Dissolved Solids (TDS), pH and Electrical Conductivity (EC) were potentiometrically measured and recorded in the field, just after the sample collection. Thus TDS, pH, EC were determined using a HM digital TDS-4 pocket size meter, Hanna meter model HI98107 and Suntex meter model SC-120 respectively. The concentration of anions and cations in the trials were scrutinized in compliance with approved procedures as given in APHA (2005). Fluoride was also potentiometrically measured in accordance with the ASTM standard procedures (ASTM 1996).

3.11.3 Determination of Water Types and Quality Index

The water types (hydrogeochemical facies) of samples obtained from each selected location were ascertained and presented in form of Piper diagram and Durov plots. These diagrams are useful for understanding the ionic composition of the water. The Aqua Chem version 2014 software was deployed to elucidate the sample hydrogeochemical facies.

Recently, the need to present a clear picture of water status in a single look has favoured the adoption of the Water Quality Index (WQI) criteria as a suitable instrument for achieving this objective. Several water quality indexes have been developed for different regions of the world over the last 2 decades. However, these indexes have also been proven to be applicable to other regions of the world without a locally developed index. Some of the commonly used indexes include, the BISWQI, OWQI and CCMEWQI among others. However, in this study, the BISWQI was embraced since it was developed in India, which has the most similar climatic conditions with that of the current study location as compared to the other indexes. Thus for estimating the WQI in this study, five consecutive stages were trailed: Stage 1 involved the assignment of load (w_i,) to the water quality parameters. The loads assigned ranged from 1 – 5 depending on the relative impact of the parameter in question. The next step involved the computation of the comparative loads for each parameter. The stage three involved the estimation of the water feature score, then the calculation of the sub-index for each factor considered, while the final step was the computation of the WQI.

Thus in this work 13 water quality parameters were considered. Table 3.10 shows the assigned weights to 12 of the parameters with the respectively computed relative weights. One of the parameters (bicarbonate) was not included in the computation of WQI because it does not have a bench mark regulation according to the WHO (2008). Therefore in this study, the relative weight (Wi) and water quality rating (qi) were estimated by eqs. 3.29 and 3.30 separately (Mahmud *et al.*, 2020).

$$W_i = \frac{w_i}{\sum_{i=1}^{n} w_i} \tag{3.29}$$

Where, W_i is the comparative load w_i is the parametric allotted load, while n represents the quntum of the sample features considered.

$$q_i = \frac{C_i}{S_i} \times 100 \tag{3.30}$$

Here, qi represents the feature score; Ci represents the parametric concentrations (mg /L) in the individual water samples, with the exemption of pH, while Si represents the WHO (2017) parametric limits for each varible (Table 3.10). Table 3.11 shows the BISWQI classifications from where the final inference about the computed WQI would be deduced.

Table 3.10: Assigned Parametric Weights and Relative Weights

S/No	Water Feature	*WHO Standard	Load (w_i)	Comparative Load (W_i)
1	pH	6.5 - 8.5	5	0.1
2	TDS	1000	5	0.1
3	EC	1500	5	0.1
4	Chloride	200	5	0.1
5	Fluoride	1.5	5	0.1
6	Nitrate	50	5	0.1
7	Sulphate	250	4	0.08
8	Potassium	50	4	0.08
9	Bicarbonate	500	3	0.06
10	Sodium	200	3	0.06
11	Calcium	75	3	0.06
12	Magnesium	150	3	0.06

*WHO (2011). All units are in mg/L except for EC (µs/cm) and pH without unit.

The parametric sub-indexes as well as the overall WQI were estimated using equations 3.31 and 3.32 respectively.

$$SI_i = W_i \times q_i \quad (3.31)$$

$$WQI = \sum_{i=1}^{n} SI_i \quad (3.32)$$

Where, SIi is the parametric sub-index (Keta-Rokbani *et al.,* 2011; Al – Omran *et al.,* 2015).

3.11.4 Human Health Risk Linked to Groundwater Contamination with Fluoride

Scientists have developed a methodology for ascertaining the risk posed to humans in relation to the contamination of different environmental media with toxic substances. This methodology is termed as "Human Health Risk Assessment (HHRA)". It is aimed at providing useful insights on the immediate or long-term harmful health impacts on humans that come in contact with toxic substances in polluted matrixes in the environment.

Thus, in this work, the danger posed to humans due to short or elongated ingestion of F^- contaminated groundwater was assessed for the first time in Makurdi metropolis, North-central, Nigeria. The data generated (concentration of fluoride in the different water samples) during the water quality tests were utilized for the HHRA. The human population was fragmented into four categories with respect to age, body weights and social differences in compliance with the procedure given by Yousefi *et al.* (2018).

Table 3.11: WQI Classification based on the Bureau Indian of Standards Water Quality Index (BISWQI)

Water Quality Index	Category	Remark
Less than 50	1	Outstanding Water
From 50 to 100	2	Decent Water
From 100 to 200	3	Lowly Water
From 200 to 300	4	Very Lowly Water
Greater than or equal to300	5	Non-consumable water

Source: Al – Omran *et al.,* 2015

The Calculated Daily fluoride Consumption (CDC) in mg/kgB_x//d was determined based on three criterions viz; the average quantity of water consumed per person per day (C_y), The content of F^- in the potable water (C_j) and average body weight of individuals (B_x). A mini-questionnaire (See Appendix F for details) and digital weighing balances (bathroom floor type model BME-S1 for adults and baby type model TC-M397 for infants) were deployed on the various populations in the study area to ascertain the required parameters (water consumption and average body weight). The average water consumptions were obtained for the infants, children, teenagers and adults as; 0.50, 1.0, 2.00 and 2.50 L/day, correspondingly. Furthermore, the average body weights were obtained for infants, children, teenagers and adults as 10, 18, 45 and 70 kg for respectively.

Equation 3.34 was then used to compute the non-carcinogenic risk posed to humans due to interaction with F^- contamination in potable water by estimating the Hazard Quotient (HQ).

$$HQ = \frac{CDC}{RfD} \qquad 3.34$$

Where RfD is the oral reference dose which approximates the acceptable daily human exposure to substances which do not pose a significant harmful effect to them all their life. The fluoride oral reference dose adopted in this work was 0.06 mg/kg/d (USEPA, 2011; IRIS U, 2017). The calculated HQ values that are less than 1 imply no significant health risk, while HQ values higher than 1 indicate adverse health impacts. (Yousefi *et al.,* 2018).

3.11.5 Data Analysis

Data obtained in this work were treated descriptively. The percentage desecration or compliance of the studied water features to the WHO standard limits was also estimated. The associations among the sample parameters was scrutinized using the Pearson's pair wise correlation analysis at P = 0.05. All these were done using SPSS software version 21.

The likely sources of pollutants in the water samples were elucidated using Principal component analysis (PCA). Principal factors were extracted by the Varimax orthogonal rotation method again using the SPSS software version 21.

Additionally, the interrelationships among water quality features, which led to the groupings of similar parameters and points was ascertained using the Hierarchical Cluster Analysis (HCA) in accordance with the method of Emenike *et al.* (2018b) also with the aid of the SPSS software version 21. The water types and facies were described with Piper, Schoeller and Durov plots with the aid of the Aqua Chem (Aq*QA) version 2014 software.

CHAPTER FOUR

RESULTS AND DISCUSSION

4.1 Proximate Composition of Precursor (RPS)

The outcome of the inherent composition of RPS is given in Table 4.1. This was used to ascertain the inherent Moisture Content (MC), Volatile Matter (VM), Fixed Carbon (FC) and ash content in the precursor. From Table 4.1, it was observed that the precursor had elevated amounts of FC, moderate VM and low levels of ash and MC. The proximate composition of RPS further indicated that it is an ideal starting material for AC synthesis. This was collaborated with the elevated FC (68.8 %), negligible ash content (1.37 %) and low MC (7.7 %). Furthermore, the high VM content of 22.03 % was an indication that RPS could be a suitable candidate for renewable energy (syngas, pyro-oil) harvesting during its carbonization/activation for the purpose of converting it into activated carbon. The findings are in tandem with those of Akpen *et al.* (2018) that reported the same proximate compositions of RPS obtained in the same study area.

4.2 Statistical Models and Optimal Setting for Synthesis of RPSAC .

Table 4.2 shows the experimental design matrix for RPSAC synthesis. The ANOVA for the responses: CY and SSA are as shown in Tables 4.3 and 4.4 respectively. Other results can be found in Appendix A. Interactive factor or polynomial equations were analysed in order to scrutinize the interactive influence of the process factors and also identify the significant contributions of each factor to the developed models towards forecasting the SSA and CY.

4.3 Percentage CY of H_3PO_4 Amended RPSAC

Model P-value of 0.0024 (Table 4.3) indicates the significance of the developed model for predicting SSA as a function of the studied factors. It was evidenced from Table 4.3 that model terms B, C and AC corresponding to Impregnation Ratio (IR), Activation Temperature (AT) and the interactive effect of activation temperature and

Table 4.1: Proximate Conformation of RPS

Characteristics (%)	
MC	7.77 ± 1.816
AC	1.37 ± 0.547
VC	22.03 ± 0.821
FC	68.83 ± 0.582

Table 4.2: Results of Yield and SSA of RPSAC

Run	*A (%)	B (g/mL)	C (°C)	D (Mins)	CY (%)	SSA (m^2/g)
1.0	60.0	3.0	600.0	90.0	79.1	1786.0
2.0	40.0	2.0	800.0	60.0	71.0	1801.0
3.0	60.0	3.0	600.0	90.0	79.6	1750.0
4.0	80.0	2.0	400.0	120.0	76.3	1742.0
5.0	40.0	4.0	400.0	120.0	72.8	1684.0
6.0	40.0	4.0	400.0	60.0	74.3	1714.0
7.0	80.0	2.0	400.0	60.0	76.7	1667.0
8.0	40.0	4.0	800.0	60.0	72.8	1796.0
9.0	80.0	4.0	800.0	60.0	68.1	1795.0
10.0	60.0	3.0	600.0	90.0	70.8	1769.0
11.0	40.0	2.0	800.0	120.0	67.2	1788.0
12.0	60.0	3.0	600.0	90.0	77.3	1767.0
13.0	40.0	2.0	400.0	120.0	72.7	1687.0
14.0	80.0	4.0	400.0	60.0	75.5	1746.0
15.0	80.0	4.0	400.0	120.0	78.9	1739.0
16.0	60.0	3.0	600.0	90.0	76.1	1766.0
17.0	80.0	2.0	800.0	60.0	66.1	1835.0
18.0	40.0	2.0	400.0	60.0	73.25	1725.0
19.0	60.0	3.0	600.0	150.0	70.4	1753.0
20.0	60.0	5.0	600.0	90.0	79.8	1788.0
21.0	60.0	1.0	600.0	90.0	69.5	1776.0
22.0	80.0	2.0	800.0	120.0	63.6	1795.0
23.0	100.0	3.0	600.0	90.0	73.6	1753.0
24.0	60.0	3.0	200.0	90.0	77.6	1394.0
25.0	80.0	4.0	800.0	120.0	69.1	1810.0
26.0	60.0	3.0	1000.0	90.0	67.4	1852.0
27.0	20.0	3.0	600.0	90.0	70.1	1750.0
28.0	60.0	3.0	600.0	30.0	68.6	1759.0
29.0	40.0	4.0	800.0	120.0	72.8	1818.0
30.0	60.0	3.0	600.0	90.0	71.2	1780.0

*A, B, C, and D represent Activating Agent Concentration (AAC), Impregnation Ratio (IR), Activation Temperature (AT) and Activation Time (ATT) respectively.

Table 4.3: ANOVA for CY of RPSAC as Affected by Process Factors

Source of Variation	Sum of Squares	Degree of freedom	Mean Square	Fischer-value	Probability-value	
Model	441.22	14	31.51	4.75	0.002	significant
*A	0.78	1	0.78	0.11	0.734	
B	61.05	1	61.05	9.21	0.008	
C	204.27	1	204.27	30.86	< 0.000	
D	0.010	1	0.010	0.0017	0.967	
AB	0.011	1	0.011	0.0018	0.966	
AC	61.22	1	61.22	9.24	0.008	
AD	3.47	1	3.47	0.52	0.479	
BC	9.63	1	9.63	1.45	0.246	
BD	6.57	1	6.57	0.98	0.334	
CD	2.52	1	2.52	0.37	0.545	
A^2	26.84	1	26.84	4.05	0.062	
B^2	2.11	1	2.11	0.31	0.581	
C^2	18.40	1	18.40	2.77	0.116	
D^2	67.87	1	67.87	10.24	0.005	
Residual	99.30	15	6.61			
Lack of Fit	26.75	10	2.67	0.18	0.9886	not significant
Pure Error	72.52	5	14.50			
Cor Total	540.51	29				

Values of "Prob > F" < 0.05 shows significant model terms.*A, B, C, and D represent AAC, IR, AT and ATT correspondingly.

Table 4.4: ANOVA for SSA of RPSAC as Affected by Process Factors

Source of Variation	Sum of Squares	Degree of freedom	Mean Square	Fischer-value	Probability-value	Source of Variation
Model	0.000014	14	10590.67	4.31	0.004	significant
A	620.16	1	620.16	0.24	0.624	
B	308.16	1	308.16	0.12	0.729	
C	0.000011	1	0.000011	46.04	< 0.000	
D	32.66	1	32.66	0.012	0.909	
AB	100.01	1	100.01	0.040	0.844	
AC	169.01	1	169.01	0.068	0.797	
AD	650.24	1	650.24	0.27	0.615	
BC	240.24	1	240.24	0.097	0.760	
BD	16.01	1	16.01	0.0064	0.937	
CD	16.01	1	16.01	0.0064	0.937	
A^2	9.32	1	9.32	0.0037	0.951	
B^2	1848.04	1	1848.04	0.74	0.400	
C^2	27288.04	1	27288.04	11.07	0.005	
D^2	80.04	1	80.05	0.032	0.859	
Residual	36946.57	15	2463.11			
Lack of Fit	36165.24	10	3616.53	23.14	0.001	significant
Pure Error	781.32	5	156.27			
Cor Total	0.000018	29				

Values of "Prob > F" < 0.05 shows significant model terms.*A, B, C, and D represent AAC, IR, AT and ATT correspondingly.

.

Activating Agent Concentration (AAC) respectively were also significant process factors for the synthesis of RPSAC as the P-values were lower than 0.05. Fig. 4.1a displays the effects of AT and IR on CY of RPSAC at the temperatures studied, while Figure 4.1b clarifies on the effect of ATT and AAC on CY at the temperatures studied (other factorial effects can be found in Appendix A).

It was observed that CY decreased as the ATT was raised at all the ATs considered. The interactive effects of AAC and AT were highly influential to the model. This could be due to the increased probability of carbon to interact with the steam environment at such increased ATs (Abdel *et al.,* 2010). This ultimately increases the likelihood for activation reactions to occur in the interacting media. In the course of activation, increased temperatures and reaction period create opportunities for enhanced reactions in the form of gasification which leads to an increase in ash production. Thus it implies that an uncontrolled rise in AT and ATT would lower the CY and favour the production of ash, which may not be desirable for an activated carbon synthesis process as is the case with the current study. Thus such factorial influences must be managed with care (Chan *et al.*, 2006).

Similar trends were observed previously by several authors who used biomass and non-organic precursors for AC synthesis as a function of AT, ATT, AAC and IR (Chan *et al.,* 2006; Adel *et al.,* 2010; Kwaghger and Ibrahim, 2013). The observation elucidated from Fig. 4.1a agrees with that of Sundaryanto *et al.* (2006) who also posited that AT portend significant influence on the CY in any activated carbon production process. Sundaryanto *et al.* (2006) further asserted that an increase in temperature would release accumulative volatiles due to rising dehydration reaction: a phenomenon that is favoured when H_3PO_4 is utilized as the activation agent.

A hike in AT could favour elimination reaction, increased C- H_3PO_4 reaction rates and a quickened gasification of carbon which ultimately results to the lowering of the CY (Adinata *et al.,* 2007; Bacaoui *et al.,* 2001; Lua and Yang, 2004). Sentorun-Shalaby *et al*. (2006) also recounted a decreased CY with an attendant increase in the porosity of apricot stones and fir wood -derived AC as AT and ATT were heightened. Similarly, in this study, it was noticed that an increase in IR favoured the CY as documented by Prahas *et al.* (2008) during the conversion of Jack fruit peel into

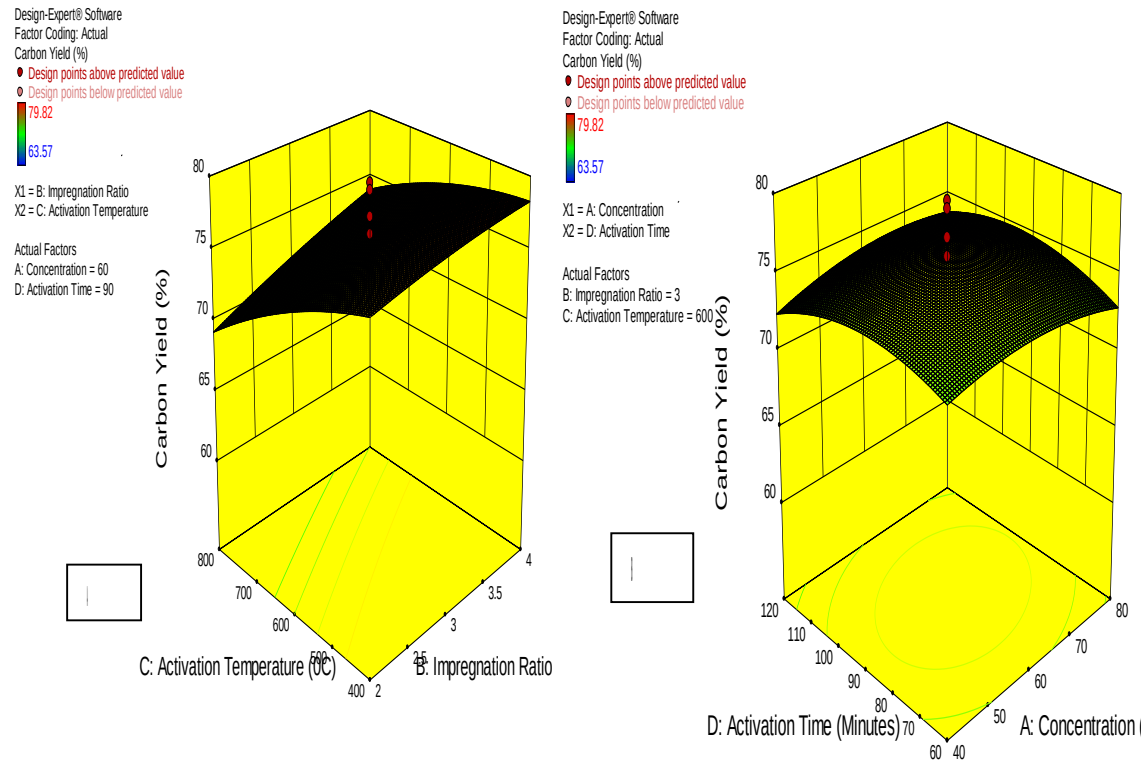

Figure 4.1: (A); Effects of AT and IR on the CY of RPSAC, (B); Effects of ATT and AAC on the CY of RPSAC

AC employing phosphoric acid as the activating instrument.

The observations noted in the present work could be explained in a chronological fashion as documented by Jagtoyen and Derbyshire (1998) who asserted that the outcome in terms of the CY is ascribed to the interaction of lignocelluloses with phosphoric acid, which commences immediately after mixing of biomass with the acid. Succinctly, the acid initially attacks the lignin and hemicelluloses while exempting cellulose due to its resistance to acid hydrolysis. Here, the acids will hydrolyze the glycosidic linkages in the lignocellulosic materials and disconnect the aryl ether bond in lignin. These reactions are convoyed by extra chemical alterations such as degradation, condensation (leading to the activation of gaseous phases) and dehydration, which promotes the reduction in CY. Although it is widely documented that increase in AT and ATT lead to a lowered CY, Adel *et al. (*2010) posited that there was an increase in the CY of HCL modified rice husk activated carbon when the AT was raised. This could be ascribed to inherent lignocellulosic content and ultimate composition of the starting material (rice husk), which differs greatly from most biomass materials.

The model prediction accuracy for CY as a function of AAC, IR, AT and AAC was further collaborated with the perfect match (straight line) of the plot of predicted CY against the experimental (actual) values (Fig, 4.2). This indicated that the model has good predictive power for the response (CY). The observed discrepancies were thus ascribed to noise. In this study a "power two" polynomial expression suitable for forecasting the CY as a function of the studied process variable was developed in terms of the coded factor values as shown in equation 4.1. Therefore, equation 4.1 could be useful in the future for the prediction of CY of activated carbon made from RPS and also for other biomass materials of similar characteristics with RPS.

$$\textbf{Carbon Yield} = 75.66 + 0.18A + 1.59B - 2.92C - 0.022D + 0.028AB - 1.96AC + 0.47AD + 0.78BC + 0.64BD - 0.40CD - 0.99A^2 - 0.28B^2 - 0.28C^2 - 1.57D^2 \qquad (4.1)$$

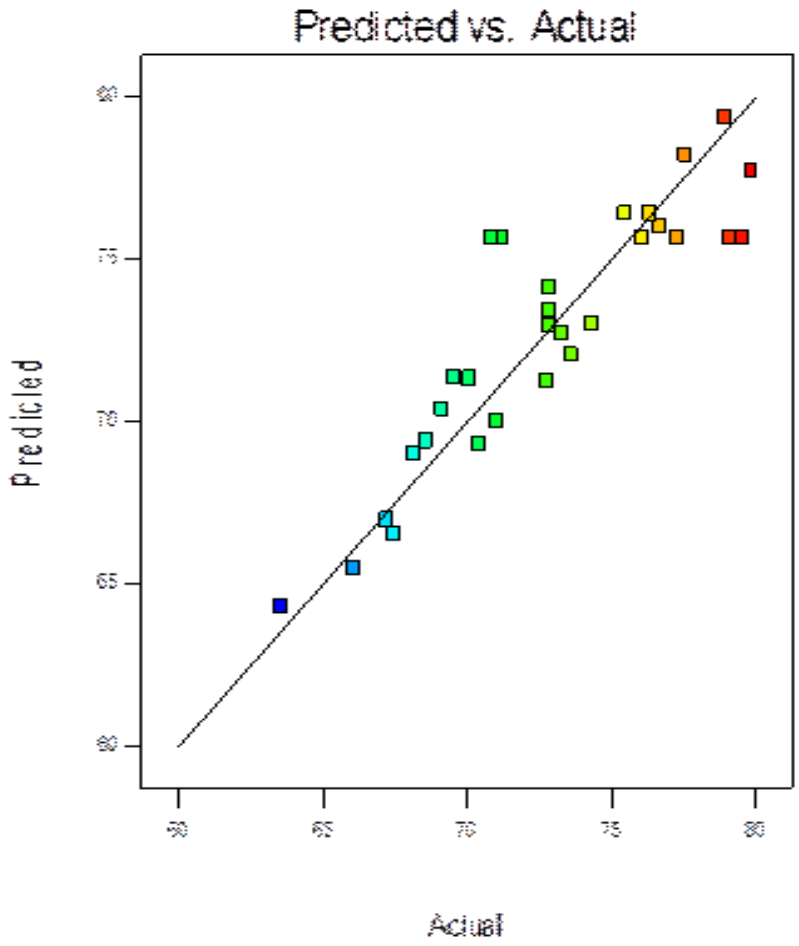

Figure 4.2: Model Prediction and Experimental Values for CY (%) of RPSAC

4.4 SSA of H_3PO_4 Amended RPSAC

Similarly, the results of ANOVA for SSA of RPSAC as a function of AAC, AT, ATT and IR suggest an adequately developed model. Model terms such as AT and its interaction, were as well very significant in influencing the SSA of the synthesized RPSAC (Table 4.4). The rise in AT enhances the enlargement of the already developed porosities, which ultimately leads to higher SSA and higher adsorption rates. The factorial effects on the SSA of the adsorbent (RPSAC) are as shown in Figs. 4.3a-b where it was found that the SSA was amplified with a rise in the AT (Fig. 4.3a). This was probably as a result of the radical enlargement of the carbon matrix which encouraged the establishment of enormous SSA in the synthesized AC.

Such comparable remarks were documented by Diao *et al.* (2002) in their works on sorghum-based precursor for activated carbon production. The authors posited that micro-porous carbon matrix with reduced SSA were produced at lower ATs (<500 °C), while large SSA were developed in the carbon matrix at ATs higher than 500 °C. Similarly, Laine *et al.* (1989) established that when AT was increased from 200 – 450 °C, the SSA of H_3PO_4 modified-coconut shell activated carbon was also found to increase. Several other authors have documented such trends in their separate studies (Srinivasakannan and Zailani, 2004; Prahas *et al.*, 2008).

The findings of this study were attributed to the destruction of cellulosic polymers during the various reactions that took place as heat treatments were raised. This likewise led to the deposition of tars in the reacting media. It is worthy to state that the AT has enormous stimulus towards the development of porosities in heat-treated adsorbent materials and as such must be optimized to a point that is suitable for volatiles and moisture removal from the precursor. The optimal removal of moisture and volatiles from activated carbon precursors is the main mechanism responsible for pore formation in activated carbon. Thus activation should be restricted up to the intrinsic point where complete volatile content is evolved. This is because; ATs higher than the intrinsic values would favour the expansion of pores at the expense of the SSA.

The model prediction accuracy for SSA as a function of AAC, IR, AT and AAC was further collaborated with the perfect match (straight line) of the plot of predicted SSA against the experimental (actual) values (Fig, 4.4). This indicated that the model has

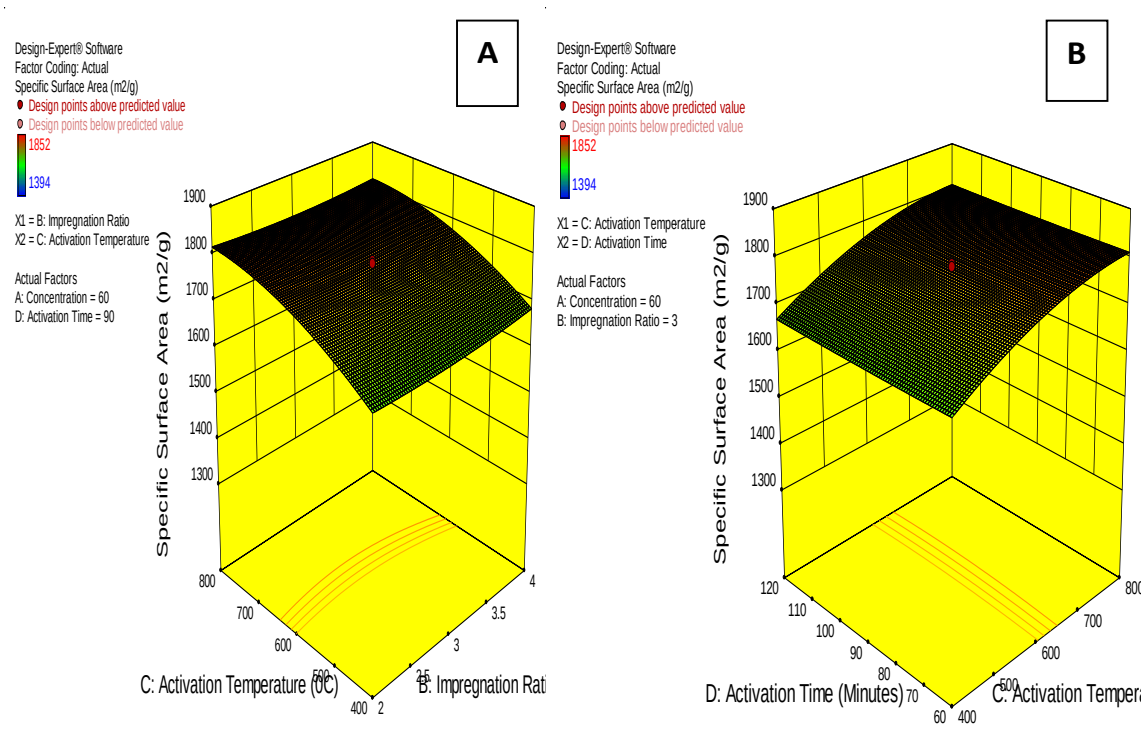

Figure 4.3: (A); Effects of AT and IR on the SSA of RPSAC, (B): Effects of AT and ATT on the SSA of RPSAC

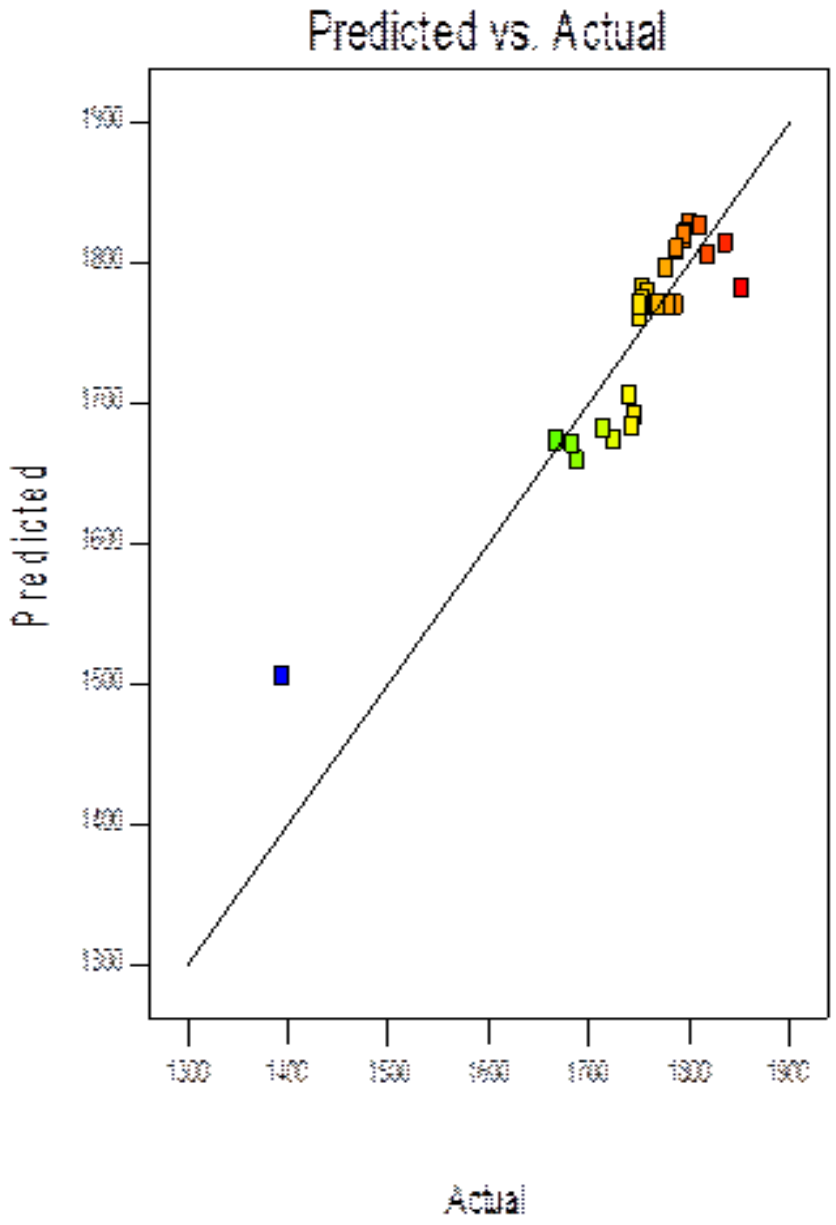

Figure 4.4: Model Prediction and Experimental Values for SSA of RPSAC

good predictive power for the response (SSA). Discrepancies in the model predictive power were thus ascribed to noise. In this study, a "power two" polynomial expression suitable for forecasting the SSA of AC as a function of the studied process variable was developed in terms of the coded factor values as shown in equation 4.2. Therefore, equation 4.2 could be useful in the future for the prediction of the SSA of activated carbon made from RPS and also for other biomass materials of similar characteristics with RPS.

$$SSA = 1769.68 + 5.08A + 3.58B + 68.75C - 1.17D + 2.50AB - 3.25AC + 6.38AD - 3.87BC + 1.00BD - 1.00CD + 0.58A^2 + 8.21B^2 - 31.54C^2 + 1.71D^2 \quad (4.2)$$

4.5 Optimization of Phosphoric Acid Modified RPSAC and Validation

The most desirable qualities in commercial activated carbon production are the SSA and CY as these ensure the economic viability and effectiveness (increased adsorption capacity) of the products (Kwaghger and Ibrahim, 2013). A major focus of this work was to ascertain the optimum points for all influential process variables at which the synthesized RPSAC would possess sufficient yields and SSA. However, it is challenging to optimize these targets under the similar operating circumstances, because these targets have extremely differing interest points and thus may not converge. Therefore, while enhanced SSA of AC is desired, the yield must also be able to justify its economic viability or cost effectiveness.

The desirability criterion in the design Expert (Version 10) software was used to ascertain the optimum factor settings that would yield the desired levels of the responses. The optimization constraints were set to been in the range of the factor levels considered, while the optimization goals were to maximize both CY and SSA. Usually, the desirability values range from 0 – 1 and the ones closer to unity are the preferred optimization solutions.

In this study the predicted optimal settings for the synthesis of RPSAC were found to be 77.0 %, 4.0 g/mL, 524 °C and 104 minutes for AAC, IR, AT and ATT respectively. These resulted in predicted response values of approximately, 78 % and 1762.93 m^2/g for CY and SSA respectively with a desirability value of 0.845 as the preferred optimization solution (Figs 4.5 and 4.6 a - b).

Through the process optimization, RPS was upheld as an ideal precursor for AC manufacturing with huge SSA and CY as desired. The predicted optimal settings with respect to RPSAC synthesis were authenticated empirically following the recommendations of the optimization schedule. We found that the empirically produced RPSAC had a SSA of 1815.6 m^2/g and CY of 79.4 %, which did not differ significantly from the model suggested values as shown in Table 4.5. The percentage errors/variations found between the predicted response values of and the experimentally determined values which were 1. 46 and 52.69 % for CY and SSA respectively were negligible and further assured the reliability of the models developed in the current study.

4.6 Characteristics of the Optimally Produced Activated Carbon

The optimal samples of RPSAC and ACRPSAC were characterized for the purpose of determining the BD, MC, pH and pH_{pzc}. The synthesized materials were also subjected to some advanced characterization procedures such as FTIR, SEM/EDX, BET and XRD analyses which respectively revealed the functional groups, surface morphology/elemental composition, surface area and phase/mineral composition of the materials. The features of the as-synthesized materials were compared with the manufacturer provided values for the CAC (Charcoal Activated) used in this work (Table 4.6).

The surficial area (BETSA) of the adsorbents was 402.23, 456.10 and 715.80 m^2/g for CAC, RPSAC and ACRPSAC respectively (Table 4.6). The increase in the BETSA of ACRPSAC which was due to the functionalization of RPSAC was indicative of the extra micro-porosities that were formed on ACRPSAC. The increase in micro-porosity of ACRPSAC was ascribed to the reactions between the oxides of aluminium and the major constituents of the precursor which encouraged the development of porous inorganic constituents such as Nitrolite, Erionite, Apatite, hydroxyapatite and quartz on its surface as also evidenced from the results of the XRD analysis. Nitrolite, Erionite, Apatite, hydroxyl apatite are known to possess zeolitic surfaces which are usually micro-porous in nature and were therefore reasons behind the increased BETSA and micro-porosity in ACRPSAC.

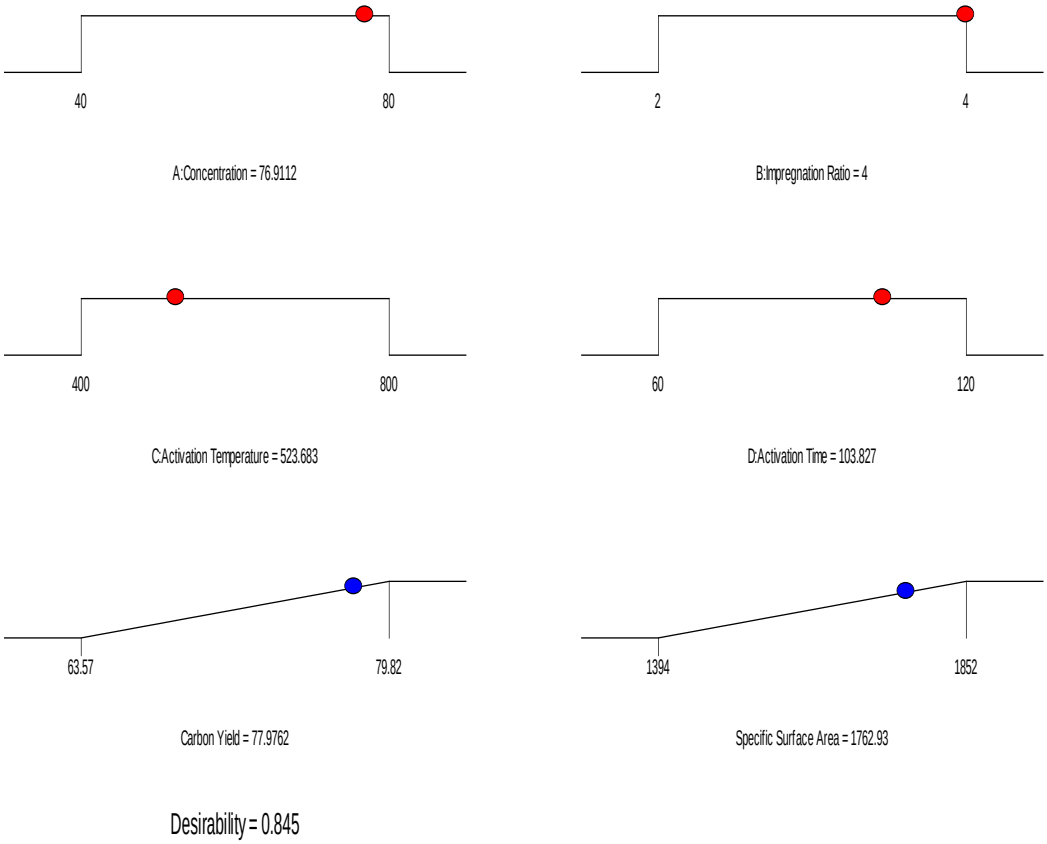

Figure 4.5: Predicted optimal factor and response levels for production of RPSAC

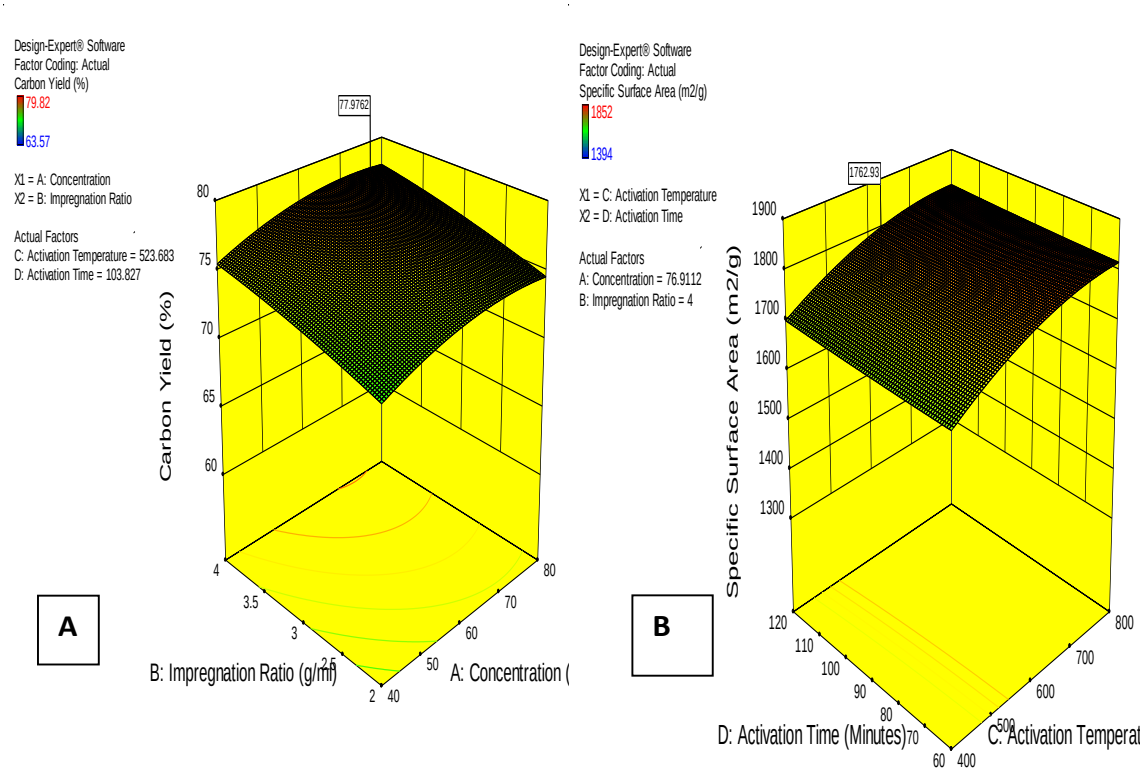

Figure 4.6: (A); Optimization of RPSAC as a Function of IR and AAC, (B); Optimization of RPSAC as a Function of AT and ATT

Table 4.5: Optimum Predicted and Experimental Factor Settings for RPSAC

Factor/Response	Model Prediction	Experimental	Error (%)
*AT (°C)	524.00	524.00	0.00
AAC (%)	77.00	77.00	0.00
IR (g/mL)	4.00	4.00	0.00
ATT (min)	104.00	104.00	0.00
CY (%)	78.00	79.16	±1.46
SSA (m^2/g)	1762.92	1815.61	±52.69

Note: desirability = 0.845
*AT, AAC, IR, ATT, CY and SSA represent Activation Temperature, Activating Agent Concentration, Impregnation Ratio, Activation Time, Carbon Yield and Specific surface Area, respectively.

Table 4.6: Physical and Chemical Compositions of the Produced Adsorbents

S/No	Property	Activated Carbon Type		
		RPSAC	**ACRPSAC**	**CAC**
1	BD (g/cm^3)	0.45	0.37	0.48
2	pH	2.0	3.89	5.74
3	pH_{pzc}	2.10	4.05	6.10
4	MC (%)	18.50	4.20	11.50
5	*BETSA (m^2/g)	456.10	715.80	402.23
6	DR-MPA (m^2/g)	491.30	1066.00	-
7	BJH-TPV (cc/g)	0.25	0.47	-
8	BJH-APD (nm)	2.13	1.85	-
9	MPV (cc/g)	0.17	0.38	-
10	MPD (nm)	6.24	6.93	-
11	CY (%)	79.44	72.23	-
12	*PSD (µm)	100-300	100-300	100-300

*PSD is particle size distribution, MPD is Micro-pore Diameter, MPV is Micro-pore Volume, APD is Average Pore Diameter, TPV is Total Pore Volume, MPA is Micro-pore Area, MC is Moisture Content, BD is Bulk Density and BETSA is BET Surface Area. *BET surface area is reported with respect to the Multi-Point Data.

Revelations of this work differ with those of Salifu (2017) who noticed a decline in the BETSA and pore formation during a similar experiment in a rural Ghanian settlement. The foregoing indicates that the inherent mineral/elemental compositions of precursors for activated carbon synthesis and functionalization have enormous influence on the BETSA, porosity and phase composition of the finished product. Thus the starting material (RPS) adopted in the current study is superior to that adopted by Salifu (2019) interms of reactivity towards enhance BETSA of activated carbon composites.

The synthesized adsorbents had moisture content values of 4.20, 11.50 and 18.50 % for ACRPSAC, CAC and RPSAC respectively (Table 4.6). The low moisture value of ACRPSAC was indicative of its relative non-hygroscopic nature and could therefore retain its quality while in storage for a longer time as compared to CAC and RPSAC. This also suggests the economic superiority of ACRPSAC over RPSAC and CAC as also informed by Inyinbor *et al.* (2016) and Bello *et al,* (2021) in their distinct works.

The bulk density on the other hand were 0.37 – 0.48 cm^3/g in range and were such that the minimum and maximum values were found for CAC and ACRPSAC separately (Table 4.6). High bulk density suggests better packing potency in the synthesized materials. The pH of RPSAC was lowest (2.0), while that of CAC was highest (5.74).

The pH of ACRPSAC was also in the acidic range (4.05) as shown in Table 4.6. The acidic nature of the RPSAC and ACRPSAC was ascribed to the residual activating agent (H_3PO_4) utilized for the production of the adsorbents. The PSD of each material produced spanned 100 – 300 µm. A rise in p/p_0 was accompanied with higher N_2 uptake, which favoured the spread in porosity of the materials (see Appendix B).

The pH_{pzc} of the studied materials were in the range of 2.1 - 6.1 with RPSAC and CAC accounting for the lower and upper limits separately (Table 4.6). This indicated that the exterior of each adsorbent would be positively ionized when reacted with an acidic solution; a condition that would promote the removal of pollutants like F^- in aqueous media (Fig. 4.7).

The APD, TPV and CY were approximately, 2.1 nm, 0.3 cc/g and 79.0 % for RPSAC, while those for ACRPSAC were 1.85 nm, 0.47 cc/g and 73.23 %. These

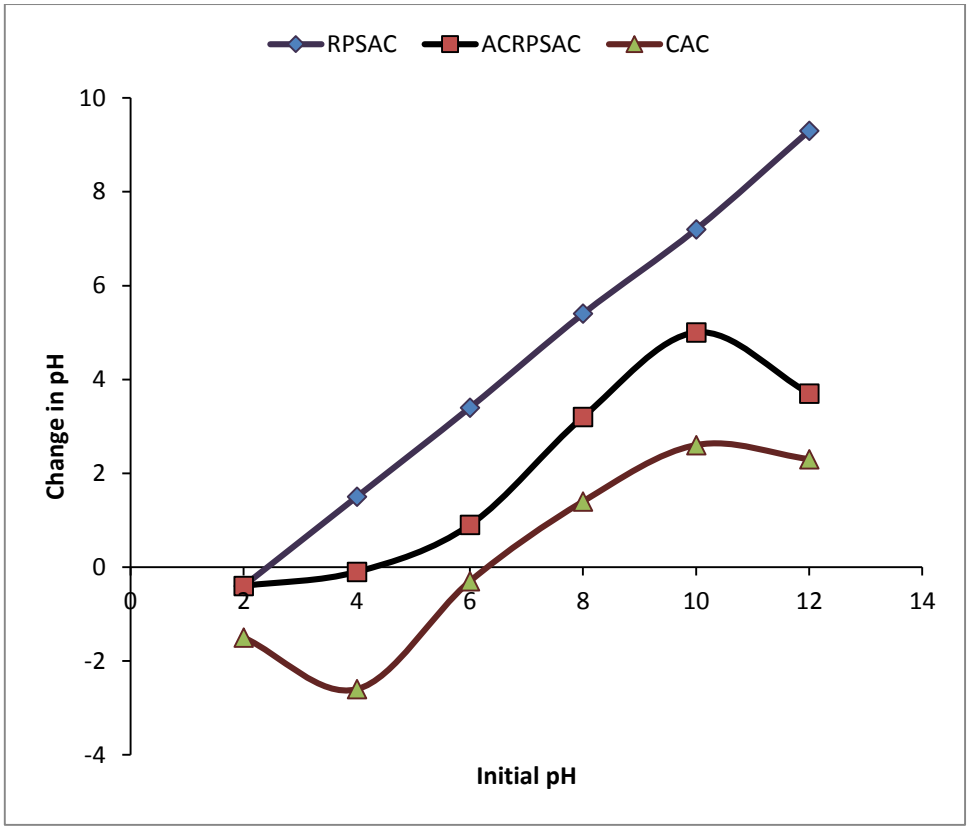

Figure 4.7: Adsorbents pH_{pzc} (ACRPSAC = 4.10, RPSAC = 2.10, CAC = 6.10)

properties of activated carbon were however not provided for CAC by the manufacturer (Table 4.6). The value of the average pore diameter of ACRPSAC obtained in this study (1.85 nm) was a further confirmation of its micro-porous dominance and increased BET surface area, while that of RPSAC was of the meso-micro-porous nature. Such porosities portray the suitability of adsorbing materials when the target adsorbate is/are of small size in molecules as is the case with F^- that was targeted in this study. The formation of micro-pores on the exterior of ACRPSAC was also found to account for its increased total pore volume and the implied higher adsorption capacity for the targeted pollutant (fluoride). Thus micro-porous nature, higher micro-pore area (Table 4.6) and suitable average pore diameter (greater than the molecular size of fluoride) of ACRPSAC portend it as a superior material in water defluoridation when likened to RPSAC and CAC. Other pore properties of the adsorbents can be found in Appendix B (pages 236 – 261).

4.6.1 Morphological Compositions of the Adsorbents (SEM/EDX)

The morphological arrangements (SEM) of RPSAC and ACRPSAC are presented in Figs. 4.8a and 4.8b, while the EDX bands are as presented in Fig. 4.9. From Figs. 4.8 a-b, RPSAC comprised mostly of micro/meso-pores. The surface of ACRPSAC was however dominated with micro-pores and had homogeneous whitish coverings which proved that the aluminium (hydr) oxides surface coating of RPSAC to produce ACRPSAC was successful.

The elemental composition of RPSAC showed that it was dominated by phosphorus, oxygen, carbon and silicon in that order. While potassium, calcium, aluminium, iron, sulphur, nitrogen, magnesium, sodium and chloride were found in trace levels (Fig. 4.8a). The elevated level of phosphorus in RPSAC was attributed to the unreacted H_3PO_4 that was deployed as the activating agent (Inyinbor *et al.*, 2017). The foregoing may also be the reason behind lower carbon content and BETSA of RPSAC as compared to ACRPSAC.

From Fig. 4.9, it was noticed that the weight concentration of aluminium in ACRPSAC increased from 1.18 % to 1.34 % as a result of the successful coating of its surface with aluminium oxide. This was further confirmed by the corresponding increase in the sulphur value of ACRPSAC to 0.83 % from 0.69 % in RPSAC. As a

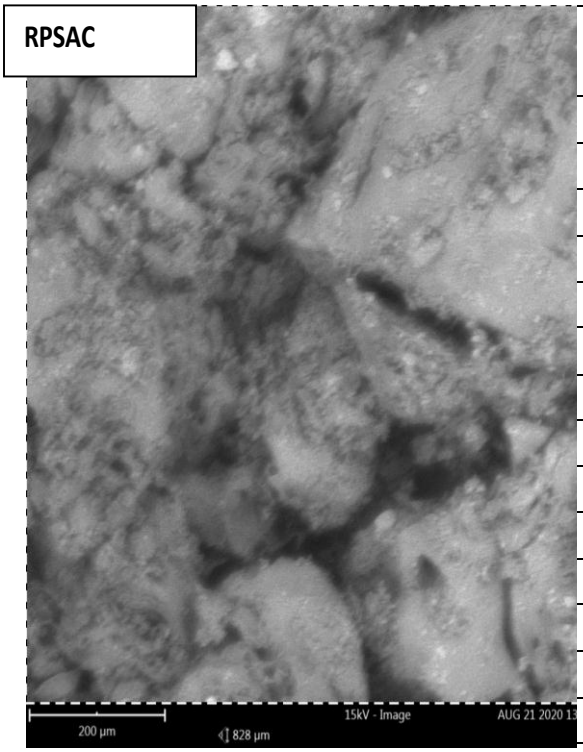

Element Number	Element Symbol	Element Name	Atomic Conc.	Weight Conc.
15	P	Phosphorus	33.96	48.36
8	O	Oxygen	37.03	27.24
6	C	Carbon	18.78	10.37
14	Si	Silicon	4.28	5.53
19	K	Potassium	0.94	1.69
20	Ca	Calcium	0.88	1.63
13	Al	Aluminium	0.95	1.18
26	Fe	Iron	0.46	1.17
16	S	Sulfur	0.47	0.69
7	N	Nitrogen	1.04	0.67
12	Mg	Magnesium	0.54	0.61
11	Na	Sodium	0.41	0.43
17	Cl	Chlorine	0.25	0.41
22	Ti	Titanium	0.00	0.00

Figure 4.8a: SEM Micrograph of RPSAC and Elemental Composition

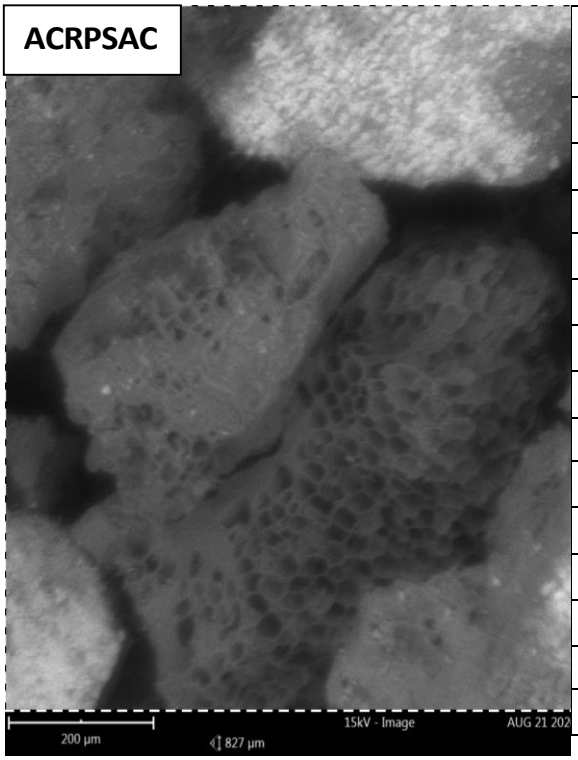

Element Number	Element Symbol	Element Name	Atomic Conc.	Weight Conc.
6	C	Carbon	48.53	32.05
15	P	Phosphorus	13.98	23.80
8	O	Oxygen	19.64	17.28
14	Si	Silicon	10.33	15.95
7	N	Nitrogen	2.65	2.04
20	Ca	Calcium	0.69	1.52
26	Fe	Iron	0.49	1.51
17	Cl	Chlorine	0.73	1.43
13	Al	Aluminium	0.90	1.34
11	Na	Sodium	0.88	1.11
16	S	Sulfur	0.47	0.83
12	Mg	Magnesium	0.48	0.64
19	K	Potassium	0.23	0.49
22	Ti	Titanium	0.00	0.00

Figure 4.8b: SEM Micrograph of ACRPSAC and Elemental Composition

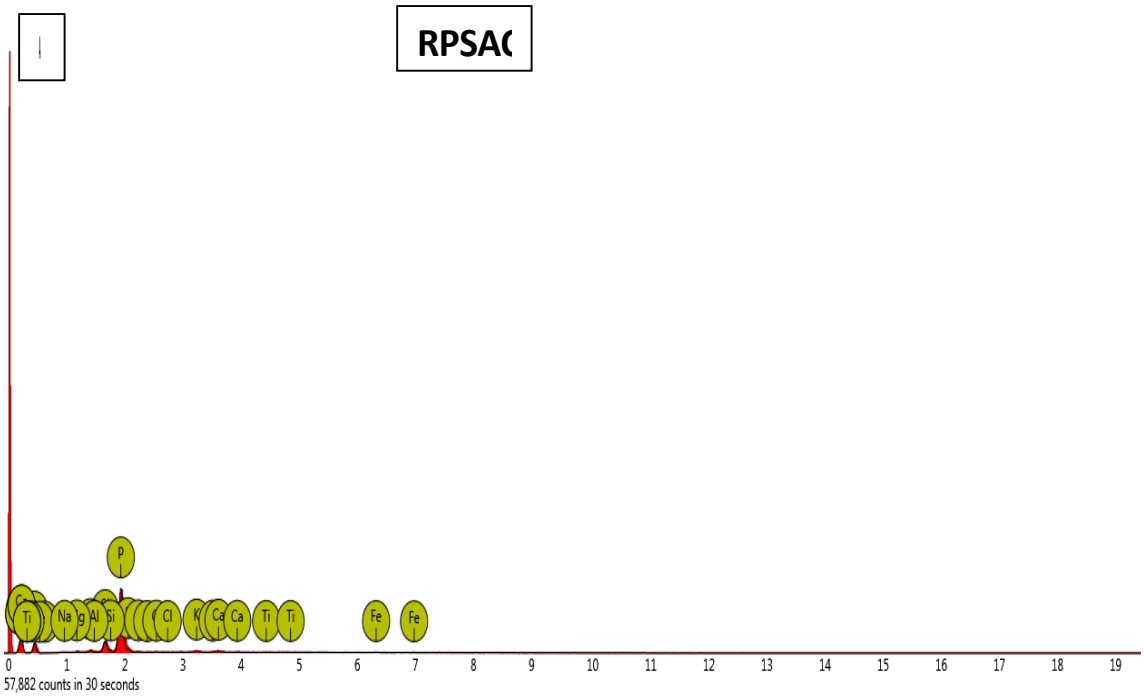

Figure 4.9 (A): EDX Spectrum of RPSAC

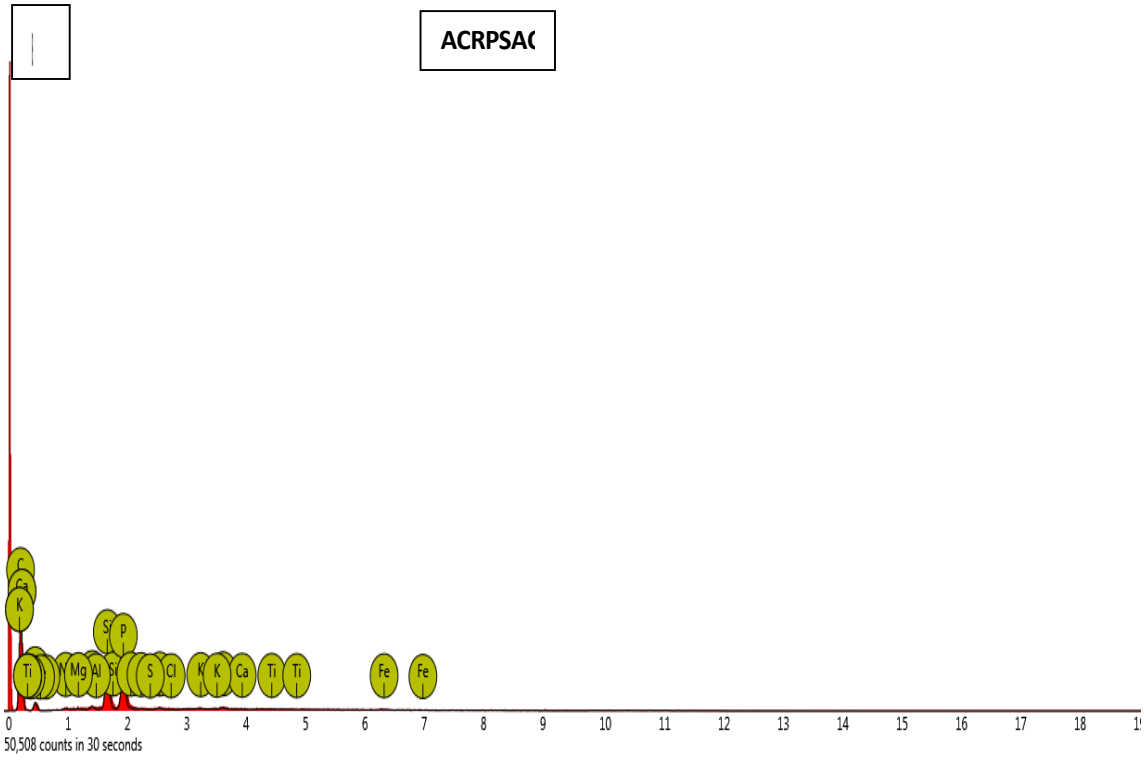

Figure 4.9 (B): EDX Spectrum of ACRPSAC

consequence of the foregoing, there was also a reduction in the phosphorus value of ACRPSAC which was ascribed to the interaction of the residual phosphorus in RPSAC to form zeolitic micro-porous compound such as apatite, hydroxyapatite and Erionite etc on ACRPSAC. The foregoing observations indicated the effectiveness of the $Al_2 (SO_4)_3$ functionalization procedure.

Succinctly, the EDX analyses proved ACRPSAC to be enriched with aluminum, which was linked with an increase in the sulphur and carbon contents in ACRPSAC which served as a proof that ACRPSAC has been effectively coated with aluminum (hydr) oxide. Revelations expunged in this work are collaborated with those of Salifu, (2017) who reported a comparable mechanism for the uptake of fluoride in groundwater by aluminium oxide coated pumice.

4.6.2 Functional Groups on the Adsorbents Surface (FTIR Analysis)

The FTIR spectrums of the as-synthesized materials are shown in Figures 4.10a and 4.10b for RPSAC and ACRPSAC respectively. Both adsorbent materials were found to comprise of complex chemicals as each had over five (5) peaks on the FTIR spectrum (Nandiyanto *et al.*, 2019). As fallout of the success of the coating process, newer and additional peaks were found to dominate on the surface of ACRPSAC than RPSAC. This was ascribed to interactions between aluminium sulphate and the inherent compounds on RPSAC to form numerous metal oxides including aluminium oxide on ACRPSAC. Such metal oxides were responsible for the micro-porosity, increased BETSA, TPV and increased adsorptive potentials of ACRPSAC as stated earlier.

For RPSAC, the strong peaks at 3213, 2344, 2117, 1990, 1625, 1121, 969 cm^{-1} were allotted to hydroxyl elongating vibrations, triple carbon and nitrogen bonds, mono-substituted terminal alkyne stretch, transition metal carbonyl stretch, primary amine N-H bend and non-ringed phosphate elongations respectively. The modest rise at around 879 cm^{-1} was allotted to the ringed phosphate elongation (Coates, 2000).

For the ACRPSAC, the rise around 3682 cm^{-1} was allotted to hydroxyl stretch of phenols, that at 3623 cm^{-1} was linked to the secondary alcohol O-H stretch, the hike at 3093 cm^{-1} was assigned to methyl and vinylidin elongations of C-H. That at 2981 cm^{-1} was given to the secondary amine C-N/ aliphatic nitro compound. The rise found

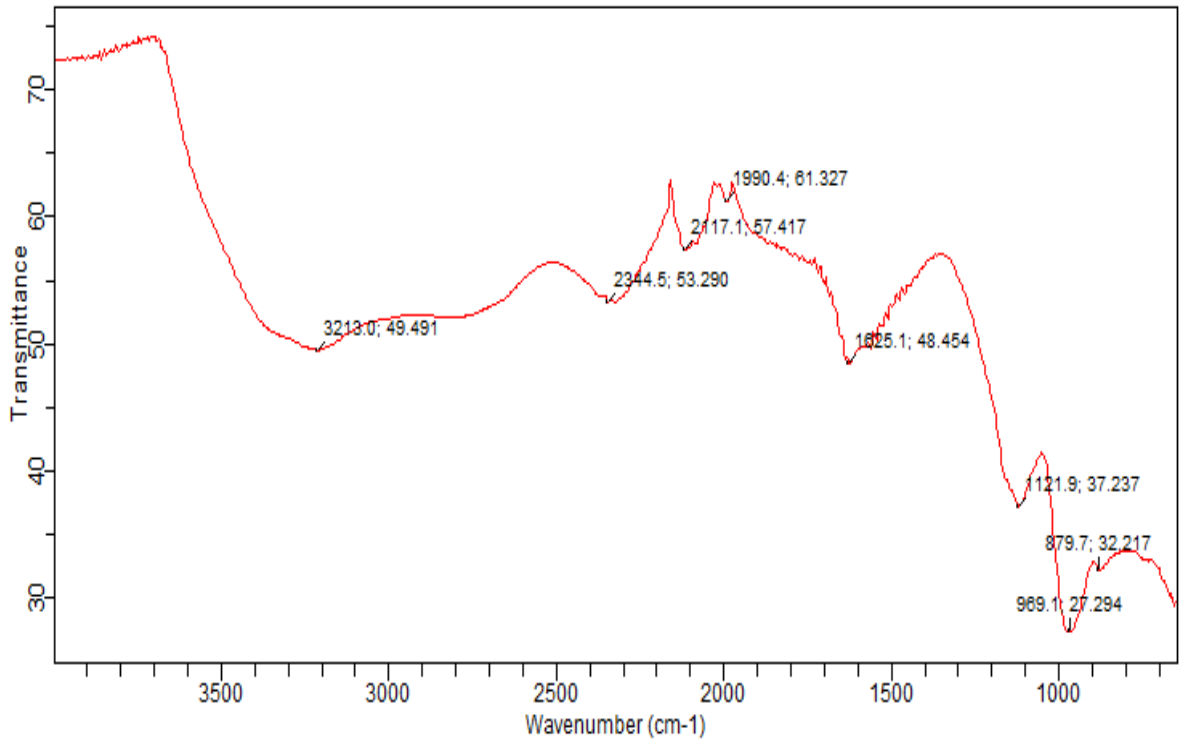

Figure: 4.10a: FTIR Spectrum of RPSAC Elucidating on the Functional Groups

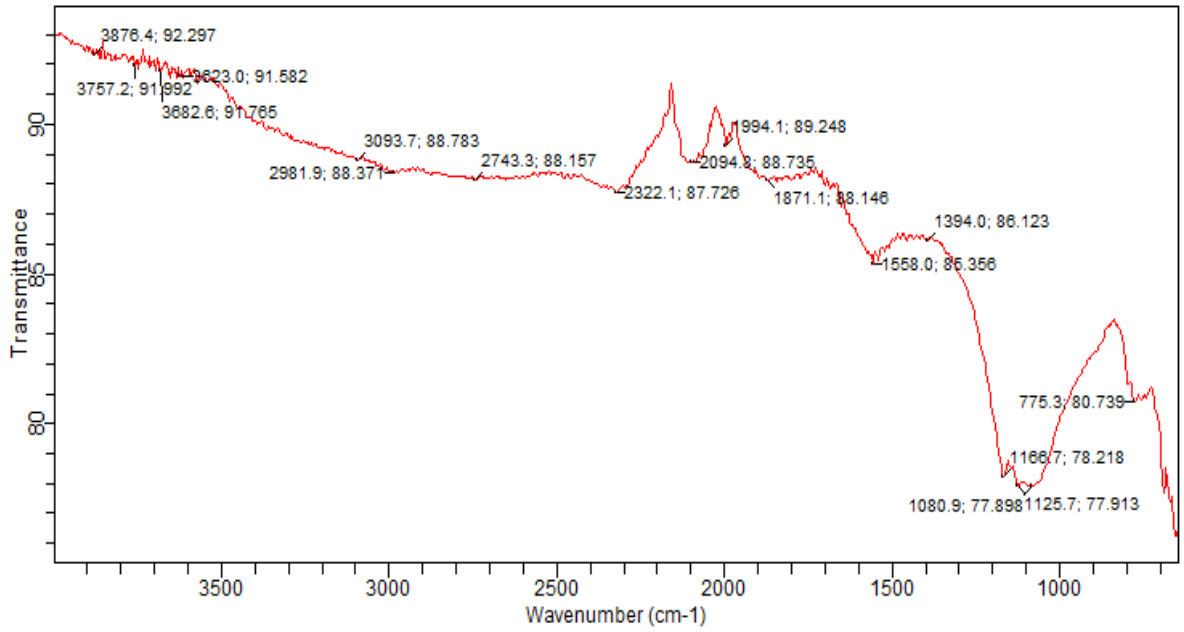

Figure: 4.10b: FTIR Spectrum of ACRPSAC Elucidating on the Functional Groups

around 2743 cm^{-1} was ascribed to the phenol/tertiary alcohol O-H bend, that at 2322 cm^{-1} was assigned to the organic siloxone/silicone elongations (Coates, 2000).

On the whole the adsorbents were confirmed to originate from organic matter as was evidenced in the dominance of O, C, H_2, and N_2 containing functional groups. Such functional groups were previously documented by Olugbenga *et al.* (2017) for raw *Moringa oliefera* seed pod and its H_3PO_4 modified part as adsorbents for Rhodamine B dye containment in wastewater. Similar reports were given by Okoye *et al.* (2019).

4.6.3 Crystallographic Make-ups of the Adsorbents (XRD)

The XRD spectrum for RPSAC and ACRPSAC are given in Figures 4.11a and 4.11b respectively. Details about the phase proportion as well as the peak angles can be found in Appendix B (Pages 236 – 261).

The RPSAC was observed to be largely amorphous in nature (Fig. 4.11a), while the ACRPSAC exhibited some degree of micro-crystalinity (Fig. 4.11b) which was due to the formation of graphite-like structures and zeolitic minerals in the matrix. This was further attributed to inherent silica-based complexes in the precursor as already exemplified in the EDX analysis. Triple large summits were formed on the surface of RPSAC and conformed to $2\theta = 15.2$, 23.3 and 26.7^o. Similarly, three broad crests that were analogous to $2\theta = 15.29$, 23.28 and 26.84^o where found on the XRD spectrum for ACRPSAC. The coating of ACRPAC with aluminium oxide was found to be largely responsible for the slight differences recorded in the peak angles of the two adsorbents (Salifu, 2017).

The peaks close to $2\theta = 24.0$ and 25.0^o match with the graphitic framework and the ones close to $2\theta = 15.0^o$ were ascribed to the smaller-sized porosities and crystallinity of the materials which occurred as a result of the multiple-stage piling of graphite-like small-sized-crystalline arrangements, especially with regards to ACRPSAC (Mopoung *et al.,* 2015). Details of the inorganic phases of the adsorbents (Appendix B) show that apatite (46%) and hydroxyapatite were the main complexes on RPSAC surface. These minerals have been shown to be of high affinity for fluoride ion in solution. Similarly, ACRPSAC was observed to be composed mainly of amorphous graphite and apatite which also have abilities for fluoride adsorption from

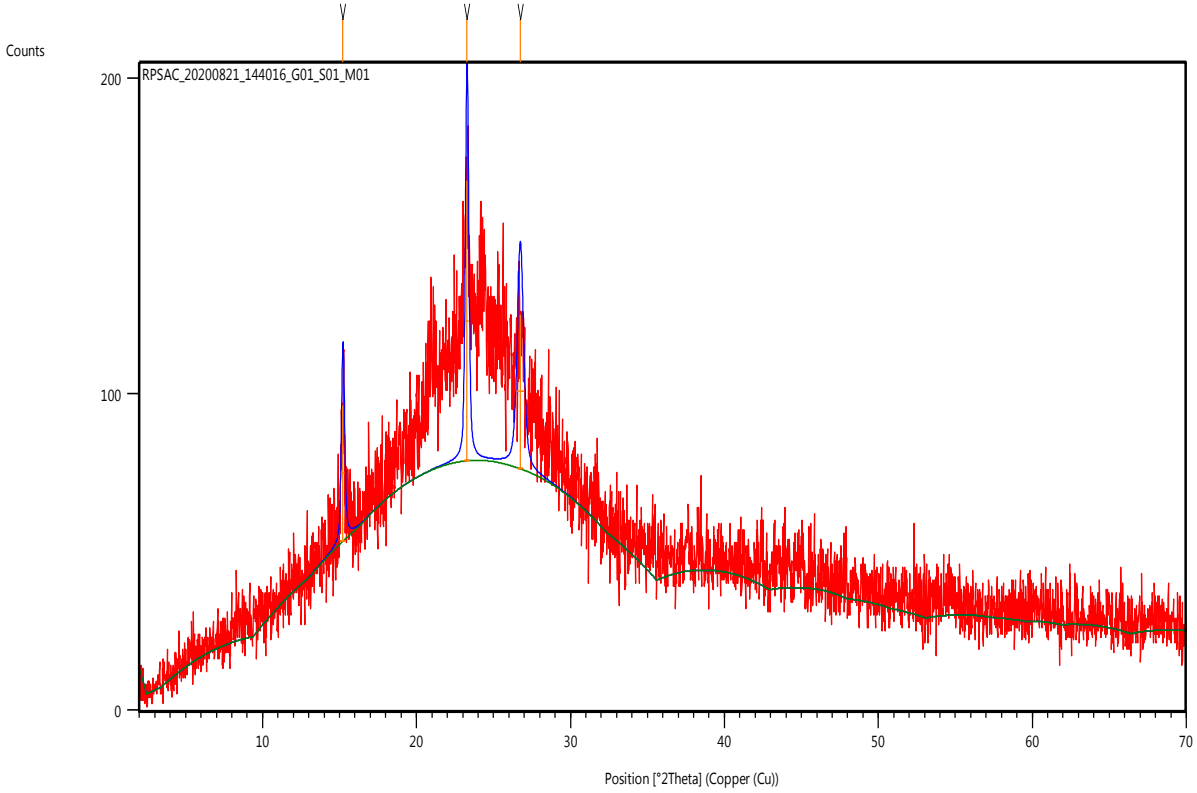

Figure 4.11a: XRD profile for RPSAC

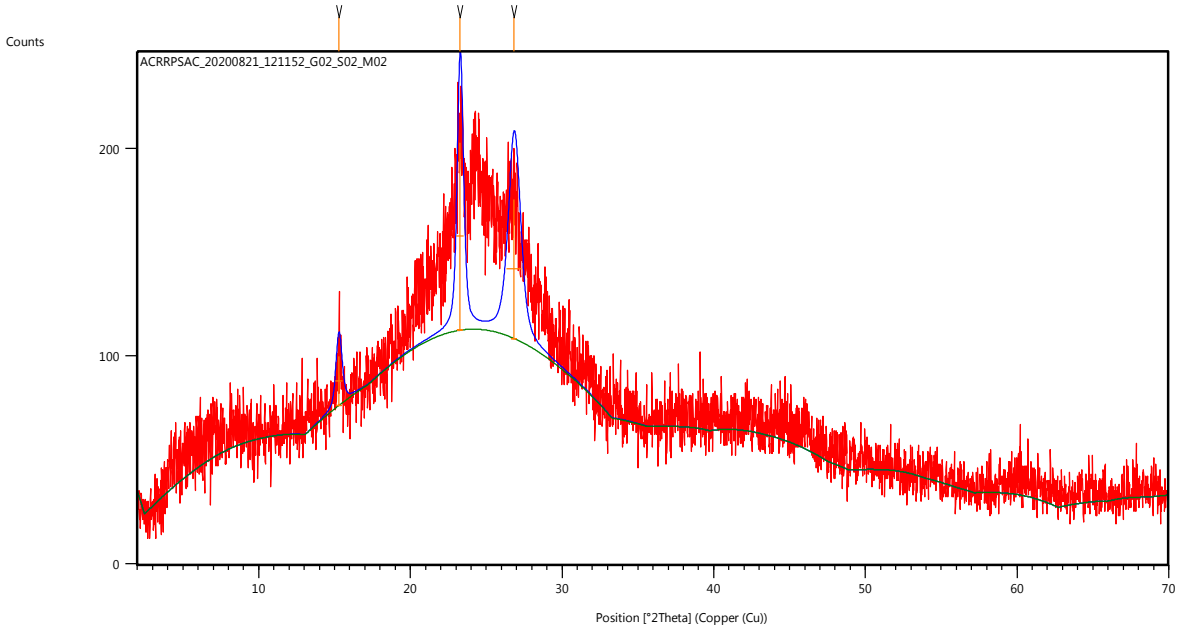

Figure 4.11b: XRD profile for ACRPSAC

aqueous media. Thus from the evidence gathered in this work, both RPSAC and ACRPSAC hold great potentials for use as fluoride scavenging agents in drinking water treatment processes.

4.7 Results of Batch Adsorption Experiment

In this section we present the findings from the experiments on the comparative batch uptake of F^- onto the as-produced AC. The influence of controlling process factors such as interaction period, pH, adsorbing material dosage, primary F^- content and temperature on process outcomes (F^- removal efficiency and uptake capacity) are also scrutinized with a view to ascertaining the optimal process settings that would ensure high removals and uptake capability for fluoride ions in water. In furtherance of the foregoing, the adsorption type, nature and mechanisms were also scrutinized by subjecting the obtained data to isothermal, kinetic and thermodynamic model fitting using regression analysis.

4.7.1 Interaction Period Effects on F^- Adsorption

Influential attributes of interaction period (30 – 120 minutes) on F^- uptake in aqueous solution was evaluated at a primary fluoride content of 6.0 mg/L, carbon addition of 2.0 g/L and temperature of 303 K with an unmodified pH. The obtained results are presented in Fig. 4.12. Both F^- uptake percent and uptake capability heightened with a rise in the contact time (interaction period). The steady state interaction period was 2 hours (120 mins) with corresponding uptake efficiencies/percent of 95.83 – 99.83. 87.67 – 99.67 and 73.41 – 90.22 % for ACRPSAC, RPSAC and CAC respectively. The uptake capbility at equilibrium was perceived to rise from 2.88 – 3.0, 2.63 – 2.99 and 2.21 – 2.68 mg/g in correspondence with ACRPSAC, RPSAC and CAC.

In accordance with the submissions of Yusuff *et al.* (2018), such increase in the F^- uptake efficiency and adsorption capacity as the contact time was elongated was ascribed the increased pore diffusion rates which paved way for the creation of more adsorption sites. Similar scenarios were documented previously (Getachew *et al.*, 2015; Yusuff, 2019).

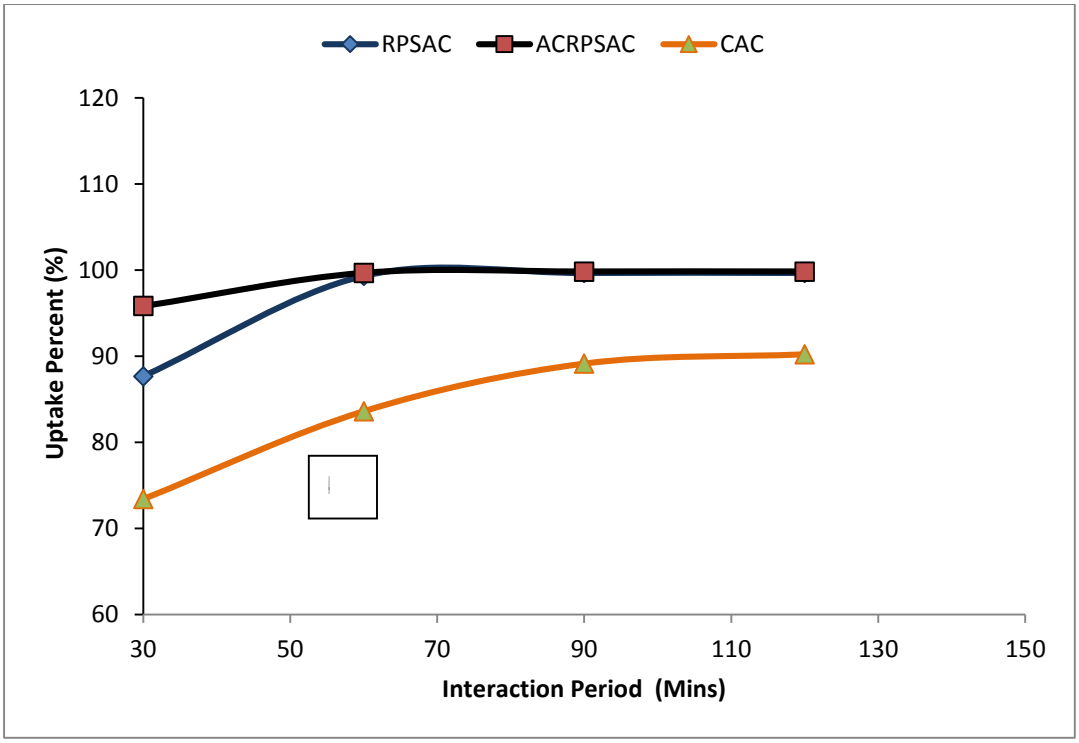

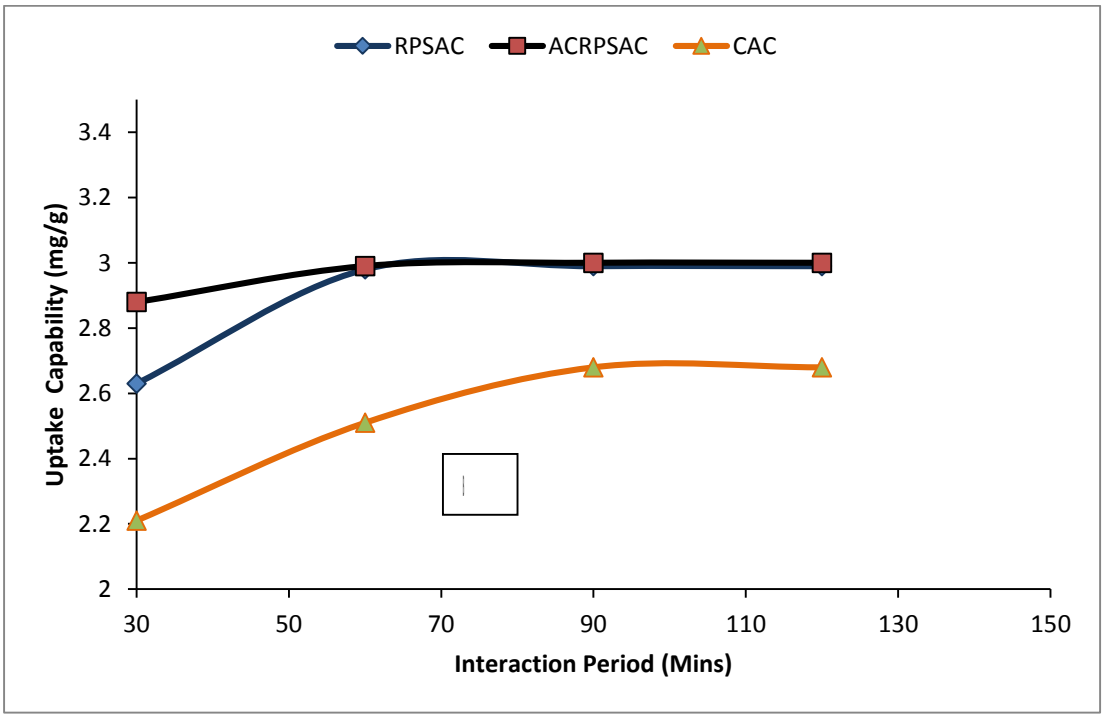

Figure 4.12: Influence of Interaction Period on (A): F^- Uptake Percent and (B) Uptake Capability (Primary F^- Content = 6.0 mg/L, Adsorbent Dose = 2.0 g/L, Temperature = 303K, without pH alteration).

4.7.2 Fluoride Adsorption as Influenced by Carbon Dosage

Efficient deployment of batch-wise adsorption schemes depend largely on the amount of adsorbing material added per volume of solution (g/L). In this work, adsorbing material dosage impacts (0.5 – 2.0 g/L) on fluoride elimination efficiency and adsorption capacity was evaluated for RPSAC. ACRPSAC and CAC at constant initial fluoride content (6.0 mg/L), interaction period (2 hours), heat treatment (303 K) without pH control (Fig. 4.13). Noticeable F^- uptake percent improved from 94.4 – 99.8, 86.2 – 99.8 and 69.2 – 89.2 percent for ACRPSAC, RPSAC, and CAC separately and corresponded with surges in the carbon dosage. This was likely due to the increased accessibility of active superficial pore spaces for cleavage of fluoride ions when the carbon dosage was increased (Salifu *et al.,* 2016; Yusuf *et al.,* 2017). The changes in the removal efficiency were negligible at dosages greater than 2.0 g/L, as such 2.0 g/L was taken as the optimum carbon dosage in the current system (Salifu, 2017).

On the contrary, fluoride adsorption capacity was found to be lowered from 11.30 – 2.99, 10.30 – 2.99 and 8.30 – 2.70 mg/g for ACRPSAC, RPSAC, and CAC respectively at raised carbon doses of 0.50 to 2.00 g/L. Similar findings were documented by several other authors in their separate studies on pollutant adsorption on activated carbon (Mohammed-Ridha *et al.,* 2017; Salifu, 2017; Yusuff, 2019). Yusuff (2019) asserted that the inconsistencies in relation to the accessibility of uptake sites and capacity of adsorbents are largely responsible for the low fluoride uptake capacity at higher carbon dosage. Nevertheless, when the carbon dosage is reduced, additional fluoride ions are held by the unsaturated extra surface centres (Mohammed-Ridha *et al.,* 2017).

The lowered uptake capability recorded with decreasing adsorbing material additions affirms the assumptions of superficial spot heterogeneity model which posits that the peripheral of the adsorbent contains adsorbing spots with a vast band of cleavage vitalities and proves that the materials were of heterogeneous surfaces. Thus, at reduced carbon doses, every adsorption site is completely open for fluoride uptake with quickened surface saturation. This ultimately results to higher adsorption capacity (q_e).

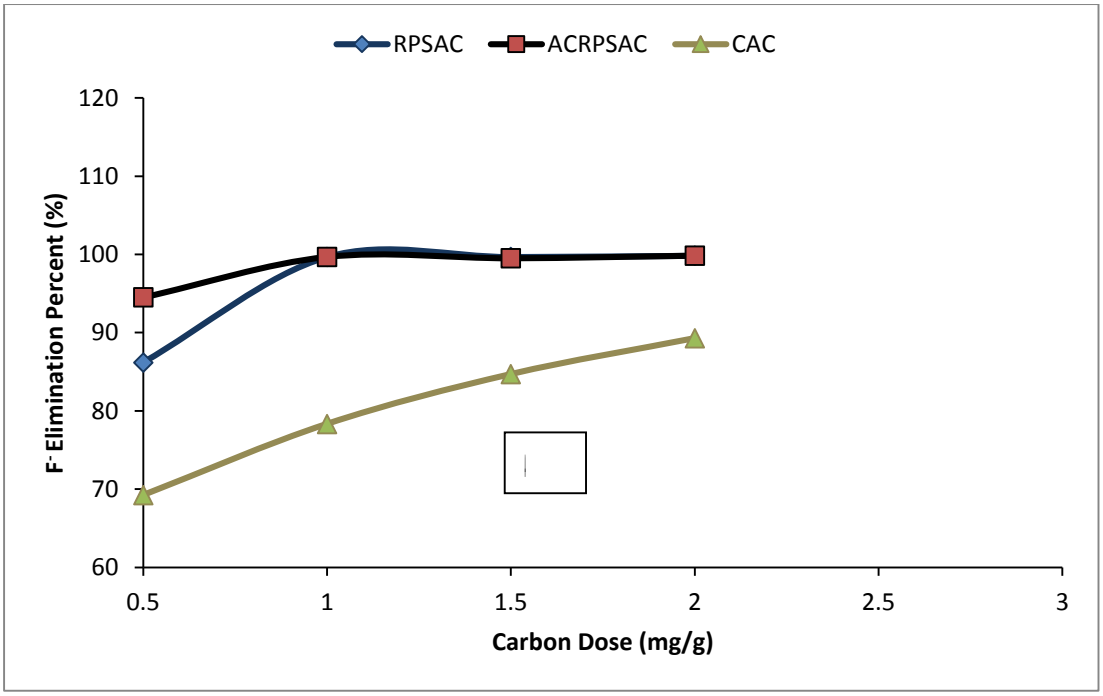

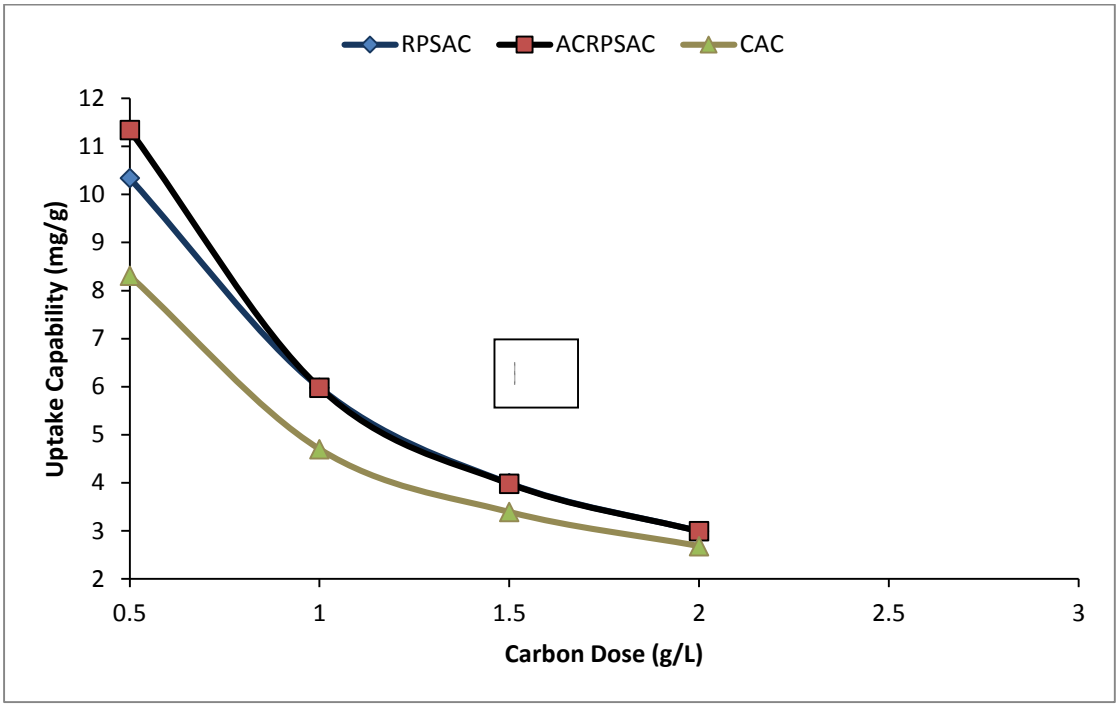

Figure 4.13: Influence of Carbon Dose on (A): F^- Elimination Percent and (B) Uptake Capability (Primary F^- Content = 6 mg/L, Interaction Period = 2 hours, Temperature = 303K, without pH alteration)

However, when the dosage is increased, there is a corresponding reduction in the available upper vitality spots which warrants a huge segment of the lesser vitality spots to be taken up by the fluoride ion, thereby leading to a lowered uptake capacity (Biswas *et al.*, 2009; Wang *et al.*, 2010; Salifu, 2017).

Additionally, as reported by Getachew *et al.* (2015); "to maintain high fluoride adsorption capability and elimination percent, the superficial stacking which is the ratio of adsorbate mass eliminated to mass of adsorbing material added is required to be less than the optimal dose". It was however, almost impossible to achieve the foregoing, moreover that the removal/elimination efficiency was taken to be more critical than the uptake capability in any adsorption scheme. Thus, in this study a dosage of 2.0 g/L was taken as ideal for further experiments.

4.7.3 pH Effects on Fluoride Adsorption

The pollutant uptake capabilities of AC is greatly influenced by the hydroxyl ion content of reacting media due to alteration of the activated carbon's surface charge. It is thus imperative to consider its effect in any adsorption studies. In this work, the pH effects (2 – 8) on the fluoride uptake potentials of ACRPSAC, RPSAC and CAC was evaluated, while maintaining a fixed primary fluoride content (6.0 mg/L), interaction period (2 hours), carbon dose (2.0 g/L) and temperature (303 K).

A decrease in the removal efficiency ranged as 99.7 – 89.8 and 98.7 – 76.3 % for ACRPSAC and RPSAC respectively as the pH was raised (Fig. 4.14). This implied that there was a preferential fluoride adsorption in the acidic than alkaline conditions of the solutions for both ACRPSAC and RPSAC. The foregoing was ascribed to the already acidic pH_{pzc} of the two adsorbents (4.05 and 2.1 respectively). Theoretically and as earlier stated, the exterior of materials including AC are positively ionized when reacted in a media having a pH lesser than the adsorbent's pH_{pzc}; a situation that favour the adsorption of deleteriously excited ions like F- in such media. Conversely, fluoride adsorption onto CAC (pH_{pzc} = 6.1) did not show a clear trend as pH was increased from 2 – 8. Concisely, fluoride removal efficiency by CAC was initially lowered from 67.9 – 62.6 % (at pH 2 - 4) and was later increased up to 76.4 % at the extreme alkaline pH conditions of the F^--ladened solutions.

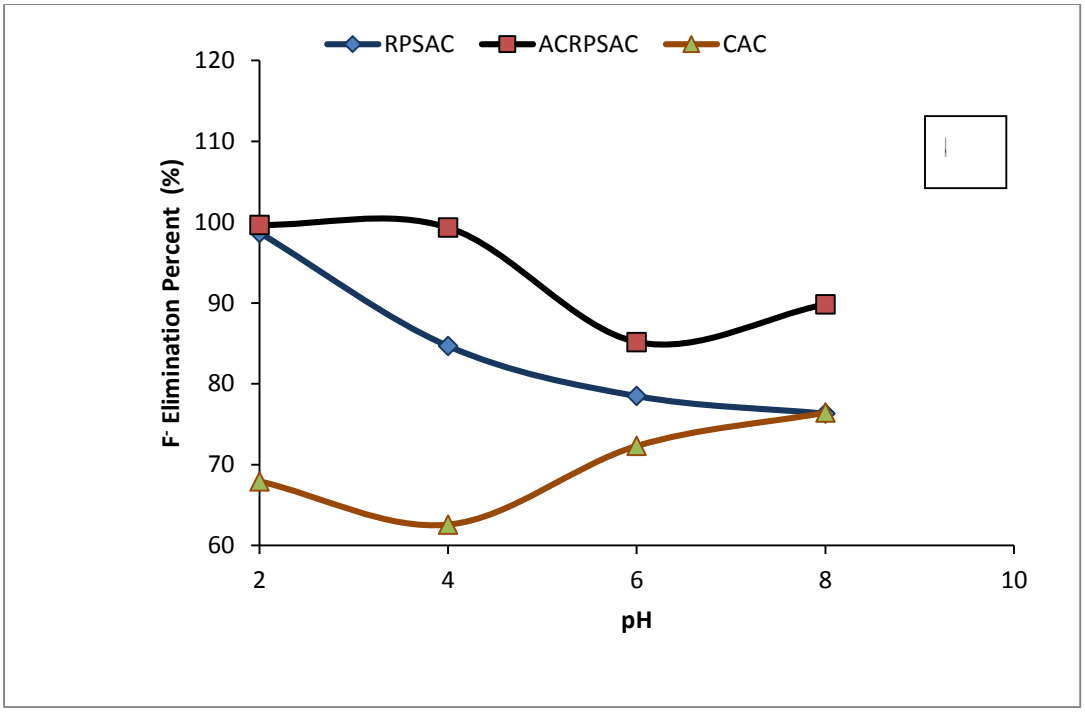

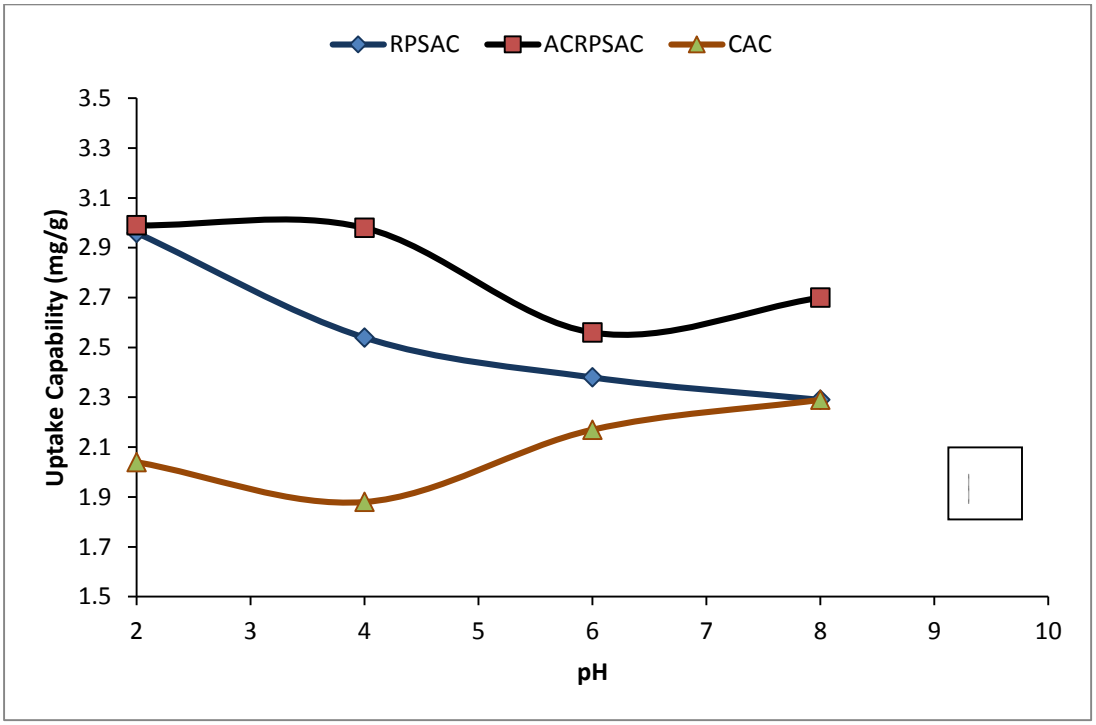

Figure 4.14: Influence of pH on (A): F^- Elimination Percent and (B) Uptake Capability (Primary F^- Content = 6 mg/L, Interaction Period = 2 hours, Carbon dose = 2.0 g/L, speed = 150 rpm and Temperature = 303K)

The F^- adsorption capability of the studied materials was also observed to display the same tendency as was with the removal efficiency. Thus in this work the pH 6 is recommended as the optimum for favourable fluoride adsorption onto any of the studied adsorbents. This decision was premised on the fact that removal efficiency higher than 70 % and final F^- content lower than the tolerable limit (1.5 mg/L) were achieved for all the adsorbents at pH 6 – 7, which conforms to the natural pH values of potable groundwater in most places where F^- enrichment in aquifer water is documented.

The foregoing was presumed to enhance the cost effectiveness of fluoride removal by the adsorbents as pH adjustments would not be needed for groundwater defluoridation, especially in rural settings. Thus in this work other experiments were conducted with no pH adjustments. Kanaujia *et al.* (2015) also experienced such pH effects in their study.

4.7.4 Temperature and Concentration Effects on Fluoride Adsorption

Presently, the impact of heat treatments (303 – 323 K) and initial/primary F^- contents (2 – 8 mg/L) on fluoride uptake abilities of ACRPSAC, RPSAC and CAC were comparatively evaluated and the related results are as presented in Figs. 4.15 and 4.16. For each of the adsorbents, a hike in the F^- elimination percent was noticed as the temperature was increased. Such increase in fluoride removal efficiency as temperature increased was observed to be higher at lower fluoride concentrations for ACRPSAC and RPSAC, but was not the same trend with the CAC. Fluoride removal efficiency ranged from 88.8 – 99.0 % at all initial concentration levels considered for ACRPSAC, while it was 83.9 – 98.6 % and 62.8 – 83.4 % for RPSAC and CAC respectively (Appendix C).

Likewise, the uptake capability rose with a rise in the primary F^- contents for all solution temperatures (303 – 323 K) considered (Fig. 4.16). At higher initial concentrations, ACRPSAC exhibited the greatest adsorption capacity for F^-. Thus hierarchy in the adsorption capacity was found to be ACRPSAC $\geq$ RPSAC > CAC. Nevertheless, it was noteworthy to mention here that at lesser concentrations of fluoride (1 - 6 mg/L), which coincide with the mean ranges reported for most Nigerian groundwater (Malum *et al.*, 2019), ACRPSAC, demonstrated excellent

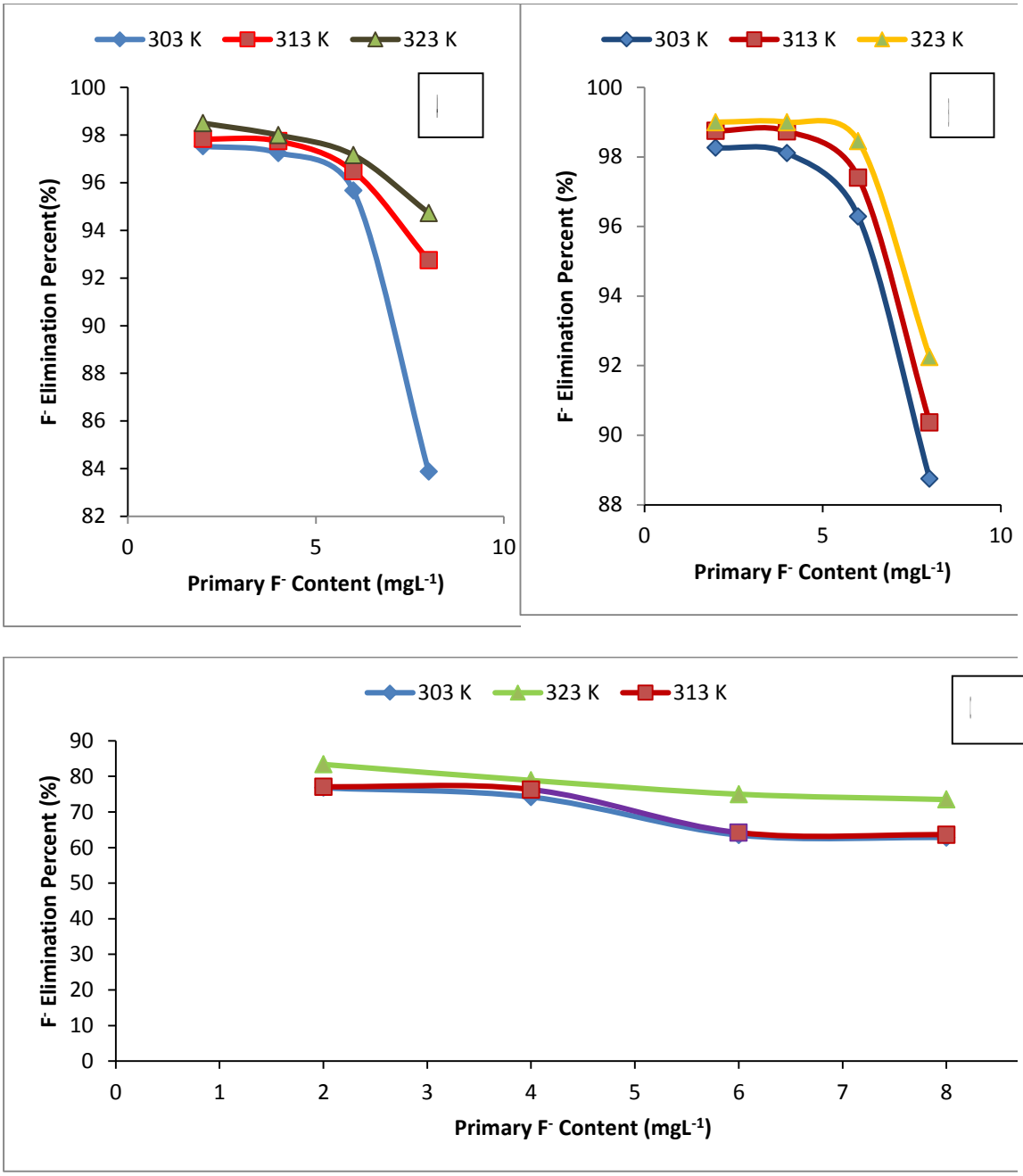

Figure 4.15: Influence of Primary F^- Content and Heat Treatments on F^- Elimination Percent from aqueous solution using (A) RPSAC, (B) ACRPSAC and (C) CAC (Interaction Period = 2 hours, Carbon dose = 2.0 g/L, rotation = 150 rpm, without pH alteration = 4.0)

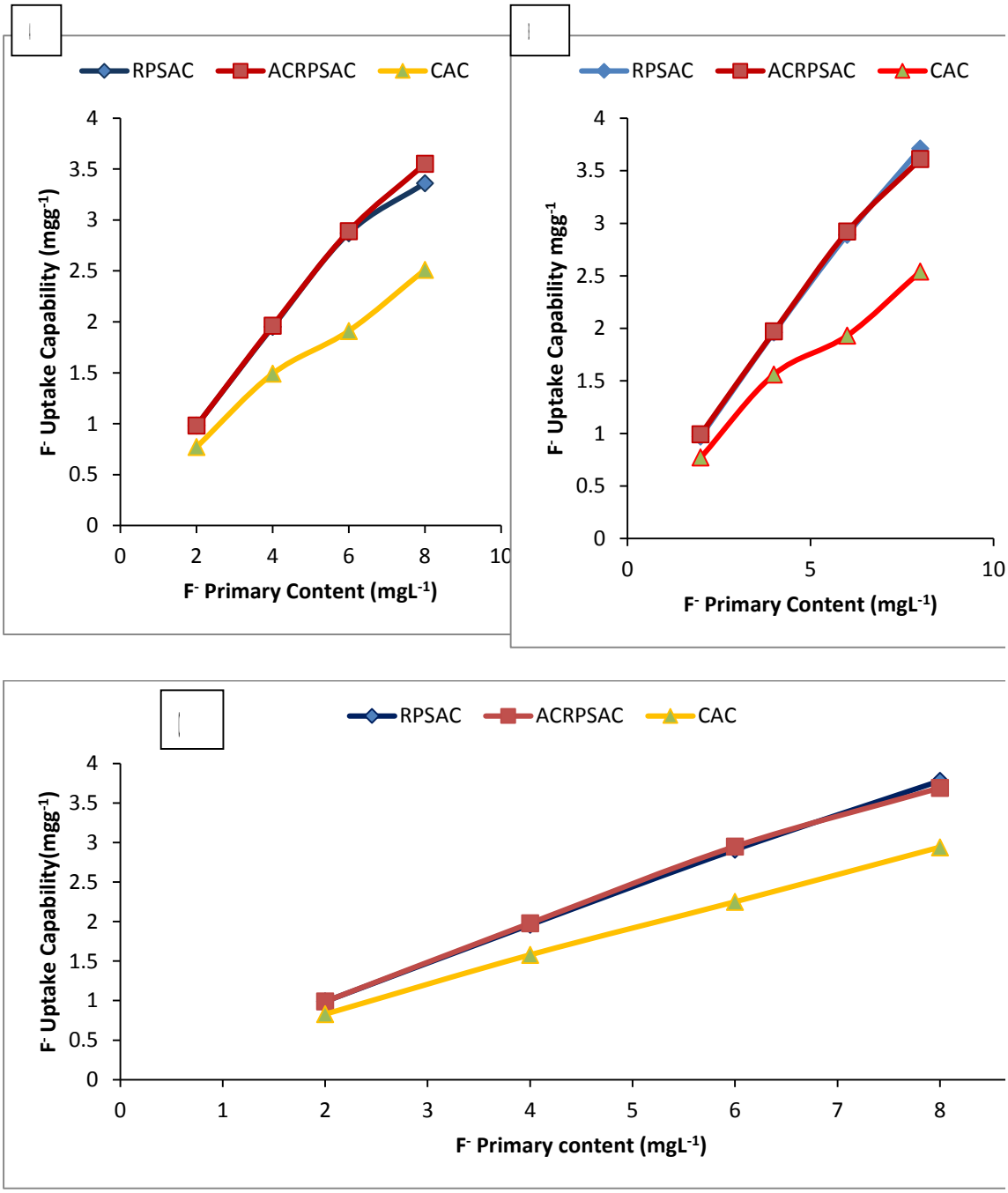

Figure 4.16: Influence of F^-Primary content on Uptake Capability of the Adsorbents at (a) 303 K, (b) 313 K and (c) 323 K (Interaction Period = 2 hours, Carbon dose = 2.0 g/L, Rotation= 150 rpm, without pH alteration = 4.0)

fluoride adsorption capacity ahead of RPSAC and CAC. This shows that ACRPSAC has great potency for use as fluoride ion scavenger in actual pollution control scenario. The applausive influence of heat treatments on F^- containment by these novel materials indicate that the superficial active sites on the adsorbents enlarge with rising temperature and as such create room for more adsorption to occur (Yusuf *et al.,* 2017).

While the adverse Influence of primary F^- content on its elimination percent as well as its favourable effects on the adsorption capability at variable heat levels was ascribed to the occurrence of the identical energetic centres on the exterior of the materials which promotes the inundation of available lively uptake spots. Conversely, a decline in the removal efficiency as concentration was raised is a reflection that there was an expansion in the adsorbent's pore diameter with a corresponding drop in the BETSA owing to the dominance of protons in the acidic medium (Salifu, 2017). This observation was also made by several other researchers in earlier studies (Ghasemi *et al.,* 2015; Gorzin & Abadi, 2017; Yusuf, 2019).

4.7.5 Statistical Comparisons of the Adsorbents' Fluoride Uptake

Analysis of Variance (ANOVA) was performed at the established optimum process settings for each of the adsorbents (ACRPSAC, RPSAC and CAC) at $p = 0.05$. Results of ANOVA and mean separation for removal efficiency and fluoride adsorption capacity using Duncan Multiple Range Test (DMRT) are presented in Appendix C. It was observed that there was a significant difference ($p = 0.05$) in the performance of the adsorbents. Mean removal efficiencies were 99.13 ± 0.31, 94.57 ± 1.06 and 80.37 ± 0.71 % for ACRPSAC, RPSAC and CAC correspondingly. Similarly, mean uptake capability was found to be 3.35 ± 0.22, 2.93 ± 0.06 and 2.27 ± 0.23 mg/g for ACRPSAC, RPSAC and CAC respectively.

Therefore as already established in the preliminary experiments, the adsorbents performance with regards to fluoride removal in aqueous solution was such that ACRPSAC $\geq$ RPSAC $\geq$ CAC, which was also attributed to the enhanced functionalities on the surface of the ACRPSAC when compared to the other adsorbents.

4.8 Modeling Isotherm, Kinetics and Thermodynamics of Fluoride Adsorption

The empirical data generated in the current work as described in section 3.8 were fitted to existing linear forms of some selected (Langmuir, Freundlich and Temkin) equilibrium isotherm models in order to provide insights on the prevailing adsorption modes.

Similarly, the mechanisms of F^- uptake by the adsorbents were validated using the rectilinear modes of the PFO, PSO, WMID and Elovich dynamic models. While the temperature-dependent equations as described in section 3.8 were considered for estimating the heat exchange mode, feasibility and self-driving ability of the fluoride adsorption process. All model fitting obligations were analysed curve fitting procedures using the R^2 values as indicator statistic, wherein the model derived design parameters were estimated.

4.8.1 Adsorption Data Fits to the Isotherm Models

The model parametric estimates were obtained with the aid of Fig. 4.17 for each tested AC (Table 4.7). Model analysis indicate that fluoride uptake was more collaborated with the Langmuir expression (R^2 = 0.88 – 0.98) for all adsorbing materials tested. The foregoing was an indication that each of the adsorbing materials had homogeneous adsorption sites that enhanced the monolayer fluoride uptake by the adsorbents. Table 4.8 depicts the model regression equations and R^2 values from where all model parameters and inferences were deduced.

The values of separation factor (RL), which were 0.050, 0.030 and 0.30 respectively for RPSAC, ACRPSAC and CAC at optimum conditions, show that fluoride uptake was favourable for all the adsorbents, which was further corroborated by Freundlich exponent (n) which were higher than unity and viz: 2.120, 1.850 and 1.260 for ACRPSAC, RPSAC and CAC separately. In a like vein, fluoride adsorption by the materials was moderately explained by the Freundlich model (R^2 = 0.8464 - 0.9416).

Similarly the fit of the fluoride adsorption data to the Temkin model was poor and was such that CAC > RPSAC > ACRPSAC with R^2 values of 0.6975 - 0.785. Such

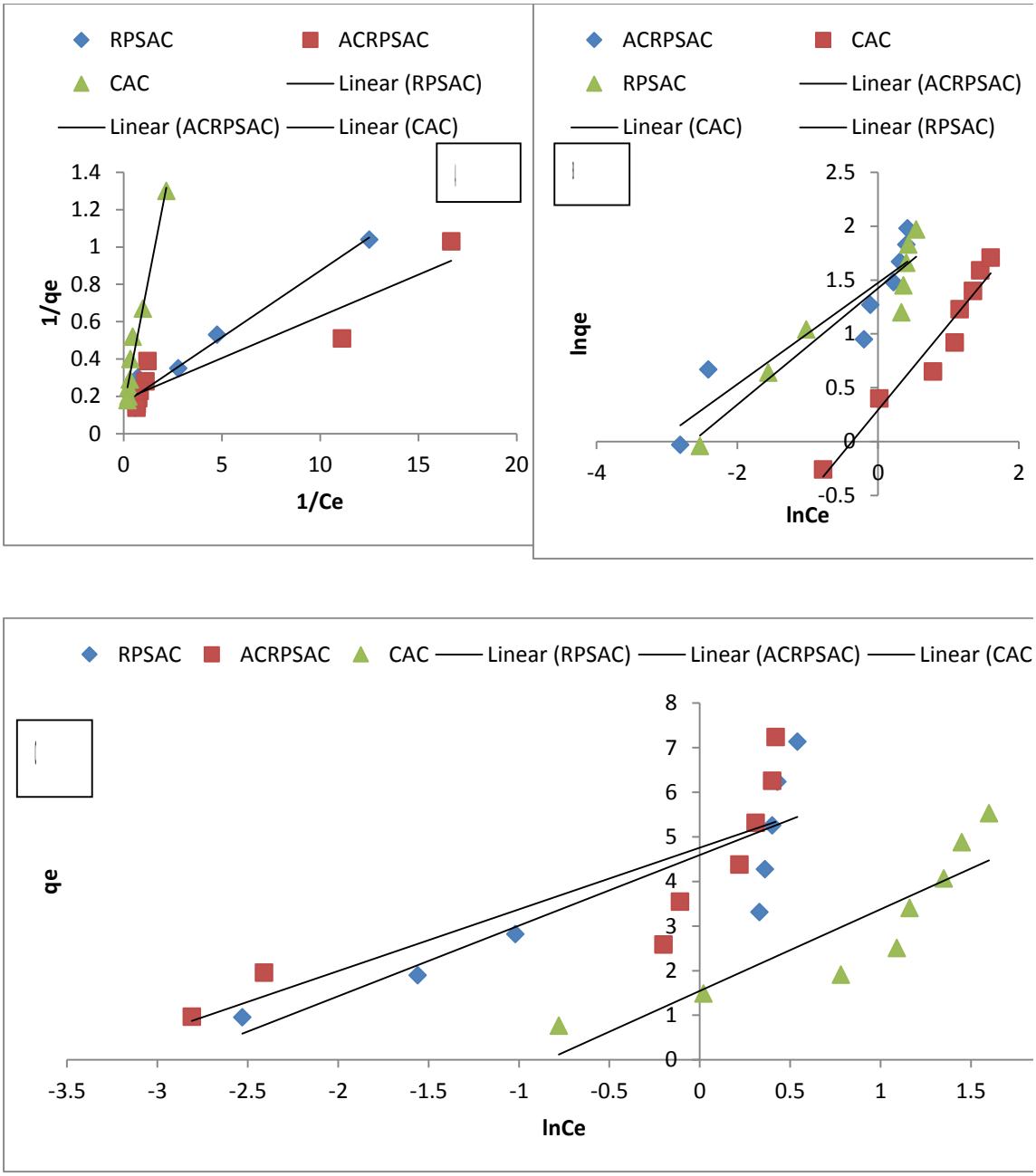

Figure 4.17: Fluoride Adsorption Model Fit using: (A) Langmuir, (B) Freundlich and (C) Temkin Models

Table 4.7: Isothermal Model Parameters for Fluoride Uptake by the Adsorbents

Serial	Parametric Estimates	Material Type		
		ACRPSAC	**RPSAC**	**CAC**
	$q_{e\ empirical}$ (mgg^{-1})	3.0	2.99	2.6
1.0	**Langmuir**			
	Q_m (mgg^{-1})	4.1	2.26	2.24
	K_L (Lmg^{-1})	5.49	6.27	7.18
	R_L	0.03	0.05	0.32
	R^2	0.88	0.98	0.97
2.0	**Freundlich**			
	K_f (mgg^{-1})	4.365	4.159	1.340
	n^{-1} or n	0.47 or 2.12	0.54 or 1.85	0.79 or 1.26
	R^2	0.85	0.89	0.94
3.0	**Temkin**			
	K_T (Lg^{-1})	31.21	18.20	2.33
	B_T ($kJmol^{-1}$)	6.01	5.25	4.55
	R^2	0.69	0.75	0.79

Table 4.8: Isotherm and Kinetic Model Equations for Fluoride Adsorption

Model	Model Regression Equations and R^2 Values		
	ACRPSAC	**RPSAC**	**CAC**
Langmuir	y = 0.0447x + 0.1821 R^2 = 0.8802	y = 0.0713x + 0.1595 R^2 = 0.9751	y = 0.5434x + 0.1393 R^2 = 0.9652
Freundlich	y = 0.4711x + 1.4736 R^2 = 0.8464	y = 0.5416x + 1.4252 R^2 = 0.896	y = 0.7934x + 0.2935 R^2 = 0.9416
Temkin	y = 1.3823x + 4.756 R^2 = 0.6975	y = 1.5833x + 4.5936 R^2 = 0.7499	y = 1.8276x + 1.5475 R^2 = 0.7851
Pseudo First Order	y = -0.0176x - 0.3365 R^2 = 0.9693	y = -0.0364x + 0.4366 R^2 = 0.9246	y = -0.0133x R^2 = 0.9684
Pseudo Second Order	y = 0.3274x + 0.6153 R^2 = 0.9999	y = 0.3173x + 1.404 R^2 = 0.9989	y = 0.3615x + 2.139 R^2 = 0.9974
Intra-Particle Diffusion	y = 0.0329x + 2.6751 R^2 = 0.8948	y = 0.068x + 2.3349 R^2 = 0.8164	y = 0.0953x + 1.754 R^2 = 0.9769
Pore Diffusion	y = 0.0027x - 0.0149 R^2 = 0.8816	y = 0.0405x - 0.077 R^2 = 0.9275	y = 0.0399x - 0.1004 R^2 = 0.9422
Elovich	y = 0.1345x + 2.403 R^2 = 0.975	y = 0.2885x + 1.7348 R^2 = 0.9226	y = 0.3127x + 1.2353 R^2 = 0.9445

findings were in the past reported by other researchers (Inyibor *et al.,* 2016; Salifu, 2017; Yusuff, 2019). Generally, the fluoride adsorption routine of the studied materials was explained by the various models in the fashion of the Langmuir ≥ Freundlich ≥ Temkin models.

4.8.2 Modeling Fluoride Adsorption Kinetics

Here the F^- uptake data for ACRPSAC, RPSAC and CAC was modeled using the linearized formats of PFO, PSO, WMIPD, BPD and the Elovich dynamic expressions and results were as shown in Tables 4.8 - 4.9 and Fig. 4.18 for regression equations, estimated model parameters and model plots respectively.

The WMIPD and BPD models offered insights on the controlling modes of F^- uptake by the adsorbents. All kinetic models tested sufficiently explained F^- uptake for all the adsorbent materials tested (R^2 = 0.82 – 1.00). Precisely, the PSO kinetic model was observed to best describe the fluoride uptake rate (R^2 = 0.99 – 1.00) in a fashion that revealed ACRPSAC ≥ RPSAC ≥CAC. Such findings were also documented by Araga *et al.* (2017) as well as by Thakur *et al.* (2020).

The greatest collaboration of the kinetic statistics to the PSO and its additional good fit to the Elovich model was an indication that chemisorption was the major mechanisms of fluoride uptake by the studied adsorbent (Salifu, 2017).
Furthermore and more precisely, from Table 4.9 the good explanation of the kinetic data by the WMIPD and BPD models ((R^2 = 0.86 – 0.98) was an indication that both pore and particle-particle movement of the F^- ions on the adsorbents' peripheral were the controlling mechanisms for fluoride uptake.

Precisely fluoride adsorption mechanisms by ACRPSAC and RPSAC involved ion exchange between fluoride and the hydroxyl functional groups on the adsorbents exterior, electrostatic attraction between the positively charged metal ions and the negatively charged fluoride ions in solution, hydrogen bonding and fluoride complexation.

Additionally for ACRPSAC other likely mechanisms included the Lewis acid-base interaction and ion/ligand exchange (formation of inner sphere surface complexes) mechanisms (Wang *et al.,* 2020). The foregoing is premised on the fact that chemisorption was the main F^- uptake pathway as elucidated earlier and as such Van

Table 4.9: Parametric Estimates for Fluoride Adsorption Kinetics

Serial	Parametric Estimates	Material type		
		ACRPSAC	**RPSAC**	**CAC**
1.	**PFO**			
	$q_{e(cal)}$ (mg/g)	2.46	2.73	1.52
	K_1 (min^{-1})	0.04	0.08	0.04
	R^2	0.97	0.92	0.97
2.	**PSO**			
	$Q_{e(Cal)}$ (mg/g)	3.05	3.15	2.77
	K_2 (g/mg/min)	0.17	0.07	0.06
	R^2	1.00	0.99	0.99
3.	**WMID**			
	K_{ip} ($mgg^{-1}min^{-0.5}$)	0.03	0.07	0.10
	C (mg/g)	2.68	2.33	1.75
	R^2	0.89	0.82	0.98
4.	**BPD**			
	K_o(mLg/L)	0.23	0.21	0.21
	α	0.003	0.04	0.04
	R^2	0.88	0.93	0.94
5	**Elovich**			
	B	7.43	3.47	3.20
	α(mg/gmin)	7.64	118.58	16.28
	1/β ln(αβ)	2.40	1.73	1.23
	R^2	0.98	0.92	0.94

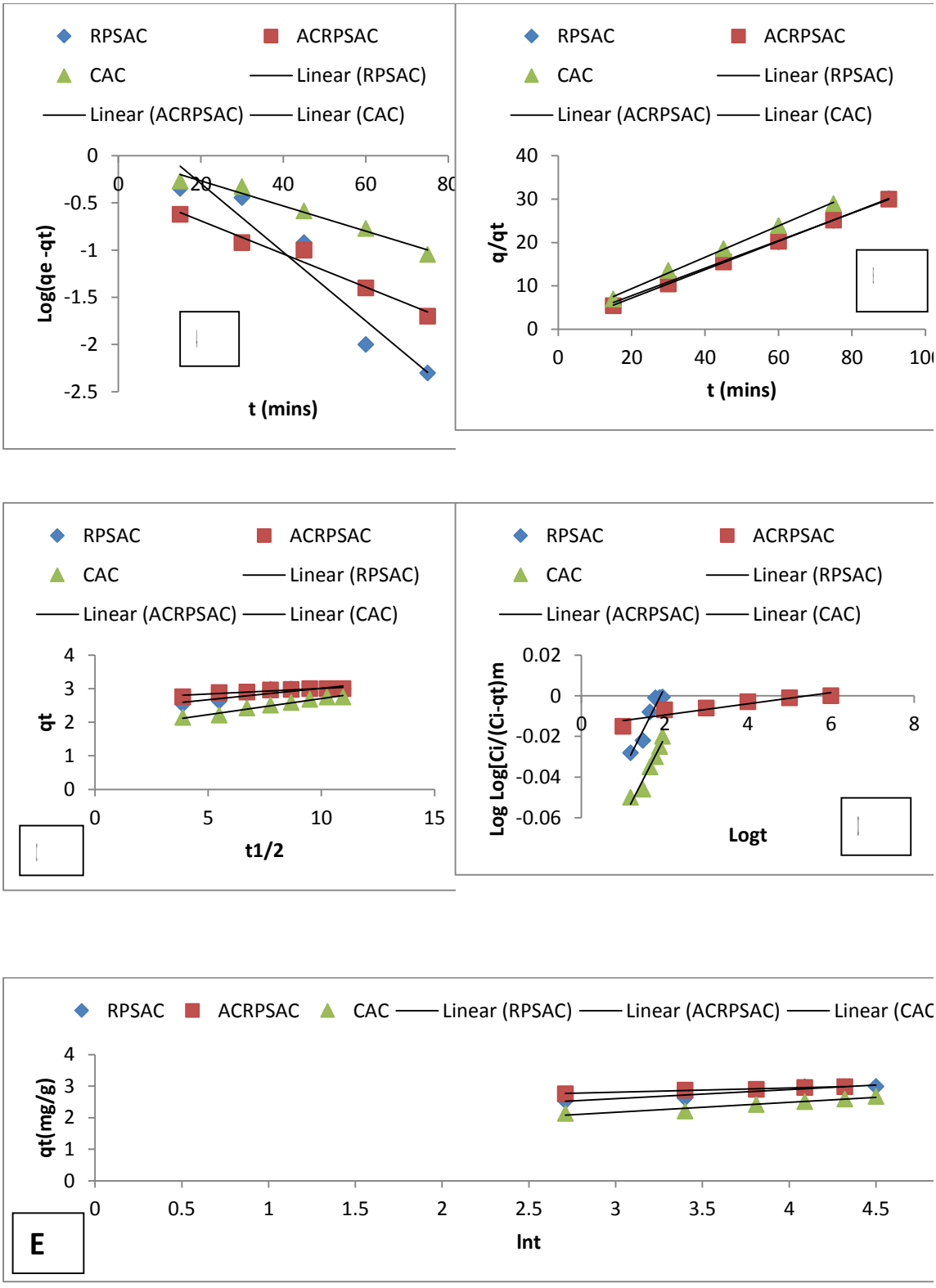

Figure 4.18: Kinetic Model Fits of the Adsorbents (A) PFO, (B) PSO, (C) WMID, (D) BPD and (E) Elovich Models

der Waals force (physio-sorption) were only mildly involved in the fluoride uptake by the studied adsorbents (Sahu *et al.*, 2021).

The involvement of complex modes of F^- adsorption on the studied materials was also confirmed by the non-passage of the linear plot of the WMID model through the origin (Fig 4.18). This suggested that all diffusion steps contributed to the rate-controlling phase in the fluoride uptake process. In the earlier phase of adsorption, film movement controlled the process, whereby the fluoride ions were diffused across the border regions adjoining the adsorbent particles, and were thus up taken and adsorbed at the exterior of the materials. Subsequently, the materials' exterior coverings became laden with F^- ions and the adsorption was then controlled by intra-particle and pore diffusion at the inner surfaces of the adsorbent up to the equilibrium point.

In the present work, the boundary layer thickness (C) which is an indicator for the likelihood of the adsorbate (fluoride) to either remain in solution or become adsorbed onto the adsorbent were 2.675, 2.335 and 1.754 mgg^{-1} for ACRPSAC, RPSAC and CAC correspondingly (Table 4.9). This was an indication that there was higher fluoride uptake on the ACRPSAC than RPSAC and CAC. These observations are closely collaborated with reports by other authors (Doke and Khan, 2012; Inyinbor *et al.*, 2016; Salifu, 2017; Sahu *et al.*, 2021).

4.8.3 Modeling Adsorption Thermodynamics

In the current study, three separate temperatures (303 – 323 K) at intervals of 10 K were used to model the thermodynamics of fluoride uptake by ACRPSAC, RPSAC and CAC. The Vant Hoff's model was used for parametric estimates (Table 4.10). The enthalpy change (ΔH^o) was observed to be positive for each adsorbent, which confirmed the endothermic mode of F^- uptake by the materials as was also evidenced from the rise in the spread parameter (k_d) when heat levels were raised (Appendix C). The positive values of ΔH^o also approved the chemisorption-controlled disposition of studied adsorption process, which were ascribed to the raised electronegativity of F^- ions that supported ion interchange for fluoride and the hydroxyl groups on the adsorbents' exterior coverings.

Similarly, there was also a positive entropy change (ΔS^o) (72.1 – 131.0 J/mol/K) for each adsorbent, which shows that the interior arrangement of the materials were

altered owing to fluoride uptake. Such huge values of entropy (131.0 J/mol/K) especially for ACRPSAC were an indication for huge affinities existing between F^- ions in aqueous media and the material's peripheral. There was however an observed negative values of the Gibb's free energy (ΔG^o) for fluoride uptake at all temperatures by ACRPSAC and RPSAC (Table 4.10), which supported the spontaneity of the uptake route.

The entropy (ΔG^o) was positive in the case of CAC at lower temperature (303 K), which portended the non-spontaneity of the process and diminished fluoride uptake rates at such temperature for CAC. Similar observations were made in the past by other researchers (Daifullah *et al.*, 2007; Mariappan *et al.*, 2015; Salifu, 2017; Chubakuum *et al.*, 2018) who studied the thermodynamics of fluoride uptake onto various adsorbents.

4.9 Influence of Contending Anions on Fluoride Adsorption

Contending anions such as bicarbonate, chloride, sulphate and nitrate are found to co-exist with fluoride in groundwater in real drinking water samples. These anions compete with the target pollutant; in this case fluoride over the available uptake spots on AC when such water is subjected to adsorptive treatment processes. Thus in this study, the stimulus of competing anions (HCO_3^-, Cl^-, SO_4^{2-} and NO_3^-) on the F^- uptake ability of ACRPSAC, RPSAC and CAC was scrutinized using simulated drinking water and results are shown in Fig. 4.19.

For all the adsorbents studied, a retarding impact on F^- uptake was observed when each of the contending anions was mixed with F^-. Generally, Fluoride removal efficiency were found to be 66.5 – 84.6, 68.8 – 89.3, 76.8 – 94.2 and 82.3 – 95.1 % when HCO_3^-, SO_4^{2-}, NO_3^- and Cl^- were respectively mixed with F^- solutions. In all cases considered, the highest fluoride removals were obtained by ACRPSAC while the lowest values were found for CAC.

The greatest inhibitory effects were found when SO_4^{2-} and HCO_3^- were interacted with the F^- media, while F^- adsorption was negligibly hindered when NO_3^- and Cl^- were mixed with F^- in aqueous media. The foregoing trend was linked to the magnitude of the ratio of ionic charge o the ionic radius of the ions as higher ratios

Table 4.10: Estimates of Thermodynamic Parameters of Fluoride Adsorption

Serial	Material type	ΔH^o (KJ/mol/K)	ΔS^o (J/mol/K)	ΔG^o (KJ/mol/K)		
				303 K	313 K	323 K
1	ACRPSAC	33.3	131.0	-6.4	-7.7	-9.0
2	RPSAC	15.8	72.1	-6.0	-6.8	-7.5
3	CAC	22.5	72.3	0.5	-0.2	-0.9

encourage stronger interfaces among the competing anion and the adsorbents (Wang *et al.,* 2020).

This is also collaborated with the closeness of the electronegativity values of bicarbonate and sulphate to the electronegativity of F^-. The foregoing builds comparable attractions between these anions and cations on the materials' exterior. Conversely the negligible hindrance to F^- adsorption when NO_3^- and Cl^- were present was likely due to the development of outer domain exterior multiplexes that encourage F^- uptake (Alagumuthu *et al.,* 2011; Chubaakum *et al.,* 2018).

4.10 Regeneration/Reuse of the Adsorbents

Varying concentrations (10 – 20 %) of sodium hydroxide were used for initial regeneration of the spent adsorbents (ACRPSAC, RPSAC and CAC) and optimum values were identified as depicted in Fig. 4.20.

There was an evident rise in the reusability of the regenerated adsorbents when they were treated with higher concentrations of sodium hydroxide (Fig. 4.20). Precisely, fluoride removals were raised from 65.2 – 97.4, 64.1 – 94.8 and 46.5 – 78.5 % for regenerated ACRPSAC, RPSAC and CAC respectively as the concentration of sodium hydroxide was raised up to 20%, which was then assumed to be the optimum. The foregoing indicated that adequate concentrations of NaOH was needed for an effective fluoride desorption from the spent adsorbents (Chubaakum *et al.,* 2018).

The optimum settings for the regeneration of the spent materials using sodium hydroxide served as a benchmark for testing other regeneration options. The results of reusability potentials for F^- uptake on the differently/further regenerated materials are shown in Fig. 4.21. It was noticed that there was an increased performance of the regenerated materials as removal efficiency was found to be 100.00, 100.00, 95.10 and 77.80 % for STRACRPSAC, RACRPSAC, STRPSAC and STCAC correspondingly after one cycle of the reusability experiment. On the whole, by simply re-coating the surface of the exhausted ACRPSAC with aluminium oxide was a more efficient regeneration technique as compared to its treatment with 20 % NaOH solution with or without recoating of its surface (Salifu, 2017).

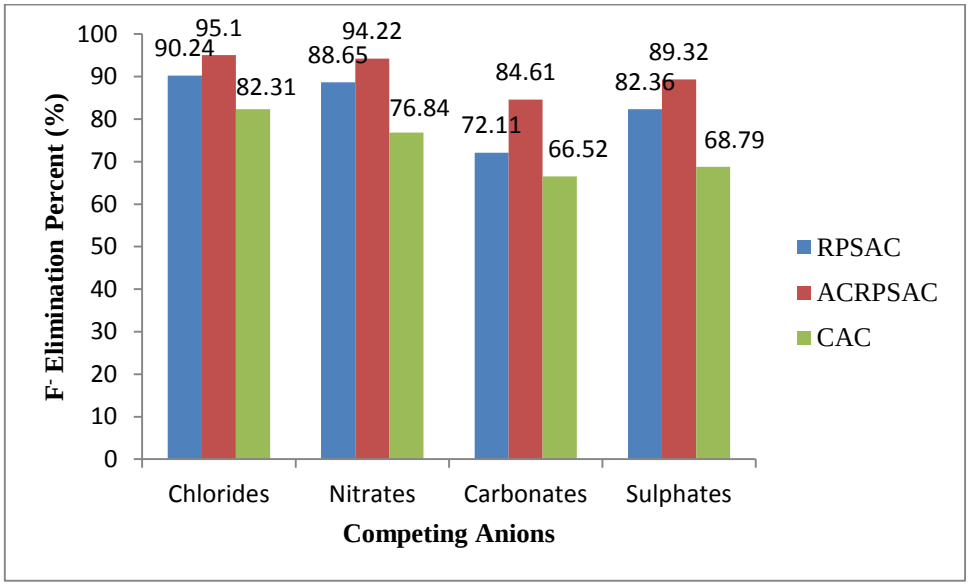

Figure 4.19: Ionic Competitions with F^- in Aqueous Media

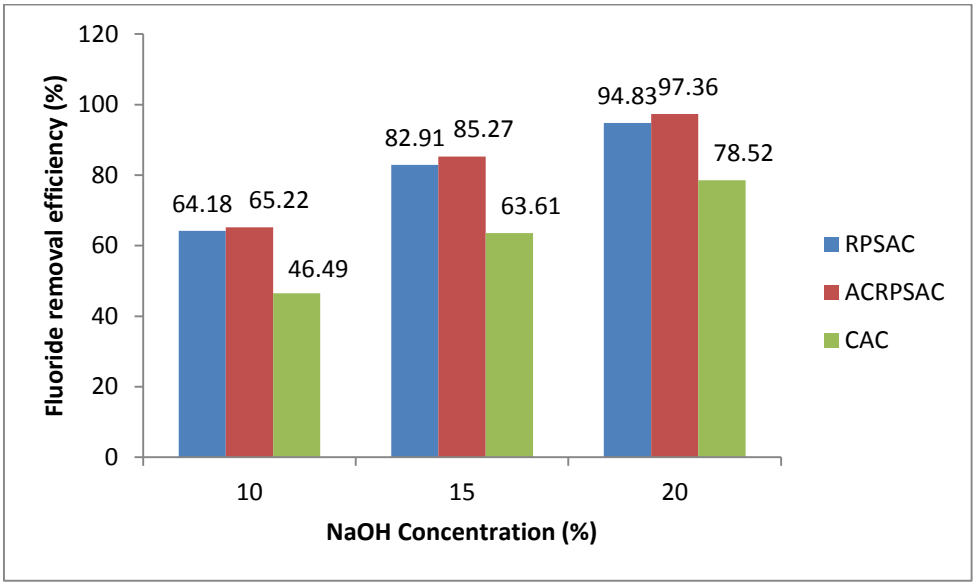

Figure 4.20: Effects of NaOH Concentration on Regeneration and Reusability of the Adsorbents

It is therefore established that the reusability of spent ACRPSAC is better enhanced when the exterior of the exhausted AC is re-coated with aluminium oxide as previously detailed in Chapter three of this work. Moreover, all evidenced gathered in the current research indicate that ACRPSAC is the most efficient adsorptive material for sequestration of F^- in water when likened with RPSAC and CAC, thus it was selected for the batch optimization studies using RSM and testing with real fluoride-ladened portable water at the optimum settings as presented in the subsequent sections of this Thesis.

4.11 Model Development and Optimization of F^- Uptake onto ACRPSAC

Results of the empirical runs for modeling and optimizing the fluoride uptake ability on ACRPSAC are presented in Table 4.11, while Tables 4.12 - 4.13 are the ANOVA for the outcomes correspondingly. Other results are presented as plates and figures (Appendix C). Two-factor interaction expressions have been developed to relay the influence and contributions of the variables in the model.

4.11.1 F^- Uptake Efficiency onto ACRPSAC

The analysis of variance for F^- uptake efficiency as contained in Table 4.12 indicates the significant and non significant model terms (P = 0.05). Thus the primary F^- concentration, carbon dosage and the model itself were the significant terms, while the interaction time, hydroxyl ion concentration and lack of fit were not significant. Some interactive effects were also noted to either be significant or insignificant (Table 4.12). The effects of factor interactions on fluoride uptake efficiency can be found in the Appendix C.

Figure 4.22 is the curve fit between the actual and model-predicted values for F^- uptake efficiency which yielded an almost straight line, which potends the model power of prediction. Thus the two-factor interaction model (in coded factor forms) revealing the interrelationships amoung the variables for predicting the F^- uptake efficiency is given in equation 4.3.

Thus the derived expression with regard to rebranded factor levels for fluoride removal efficiency using ACRPSAC was found to be:

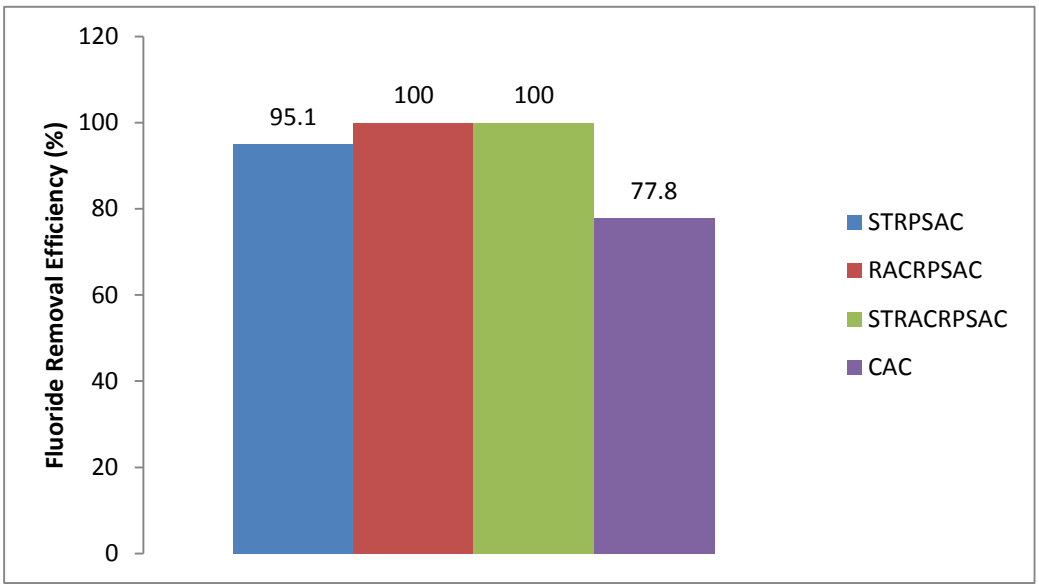

Figure 4.21: Comparative Reusability Potentials of Rejuvenated Materials for One Round F^- Uptake

Table 4.11: Empirical Runs for Modeling F^- Uptake onto ACRPSAC

Run	A:pH	B:Primary Concentration	C: Carbon Dosage	D:Interaction Time	Uptake Efficiency	Uptake Capacity
		mg/L	g/L	Minutes	%	mg/g
1	7	2	1.5	90	97	1.29
2	9	8	2	120	82.38	3.3
3	7	6	1.5	90	84.5	3.38
4	7	6	1.5	90	84.5	3.38
5	9	4	2	60	99	1.98
6	5	4	2	60	98	1.96
7	5	4	1	120	96.5	3.86
8	7	10	1.5	90	85.2	5.68
9	7	6	1.5	30	89.67	3.59
10	5	8	1	120	90.5	7.24
11	3	6	1.5	90	98.5	3.94
12	5	4	1	60	91.75	3.67
13	5	8	2	120	94.75	3.79
14	11	6	1.5	90	98.17	3.93
15	9	8	1	60	90	7.2
16	5	8	1	60	95.13	7.61
17	7	6	2.5	90	99	2.38
18	9	8	1	120	83.25	6.66
19	5	8	2	60	92.88	3.72
20	7	6	1.5	150	95.5	3.82
21	9	4	1	120	93.25	3.88
22	7	6	1.5	90	90.17	3.61
23	7	6	0.5	90	83.17	9.98
24	7	6	1.5	90	90.83	3.63
25	7	6	1.5	90	91.5	3.66
26	9	4	1	60	98	3.92
27	9	8	2	60	90.75	3.63
28	5	4	2	120	98.75	1.98
29	7	6	1.5	90	94	3.76
30	9	4	2	120	98.25	1.97

Table 4.12: ANOVA for F^- Uptake Efficiency by ACRPSAC

Source	Sum of Squares	Df	Mean Square	F	p-value	
Model	646.6	14	46.2	3.7	0.008	Significant
A-pH	24.1	1	24.1	1.9	0.184	
B-Primary Concentration	250.0	1	250.0	20.1	0.000	
C-Carbon Dosage	96.2	1	96.2	7.7	0.014	
D-Interaction Time	1.6	1	1.6	0.1	0.724	
AB	57.7	1	57.7	4.6	0.048	
AC	1.3	1	1.3	0.1	0.748	
AD	34.1	1	34.1	2.8	0.118	
BC	10.0	1	10.0	0.8	0.385	
BD	20.0	1	20.0	1.6	0.224	
CD	1.5	1	1.5	0.1	0.734	
A^2	142.4	1	142.4	11.5	0.004	
B^2	6.1	1	6.1	0.5	0.496	
C^2	6.0	1	6.0	0.5	0.499	
D^2	19.4	1	19.4	1.6	0.230	
Residual	186.3	15	12.4			
Lack of Fit	110.2	10	11.0	0.72	0.690	not significant
Pure Error	76.09	5	15.22			
Cor Total	832.88	29				

Table 4.13: ANOVA for Fluoride Adsorption Capacity of ACRPSAC

Source	Sum of Squares	df	Mean Square	F Value	p-value Prob> F	
Model	105.14	4	26.28	230.62	< 0.0001	Significant
B-Primary Concentration	34.34	1	34.34	301.34	< 0.0001	
C-Carbon Dosage	56.76	1	56.76	498.06	< 0.0001	
BC	2.92	1	2.92	25.58	< 0.0001	
C^2	11.11	1	11.11	97.51	< 0.0001	
Residual	2.85	25	0.11			
Lack of Fit	2.73	20	0.14	5.61	0.0324	Significant
Pure Error	0.12	5	0.024			
Cor Total	107.99	29				

Uptake Efficiency = 88.4 + -3.0A + 3.16B + 3.3C + 0.1D + -0.5AB + -0.3AC + -0.1AD + -0.8BC + -0.01BD+ 0.02CD + $0.6A^2$ + $0.1B^2$ + $1.9C^2$ + $0.0009D^2$ (4.3)

Here; A, B, C and D are pH, primary fluoride concentration (mg/L), carbon dosage (g/L) and interaction time (minutes) correspondingly. The derived expression is useful for predicting fluoride uptake efficiemcy as a dependent of the factors considered for ACRPSAC and other similar adsorbing materials.

4.11.2 F^- Uptake Capabilityy of ACRPSAC Composite

The effect of various investigational factors (as with the elimination percent) on the F^- uptake capability is displayed with the aid of 3-D plots (Appendix C). The uptake capability was found to heighten with a corresponding hike in the primary concentration of fluoride in solution and the interaction time. However and oppsite trend was observed when the solution pH and carbon dosage was increased. This implied that fluoride ions were better up-taken on the novel material under acidic pH situations of the interacting solutions.

The analysis of variance for F^- uptake capability (mg/g) as contained in Table 4.13 indicates the significant model terms (P = 0.05). Again the primary F^- concentration, carbon dosage and the model itself were the significant terms. Some interactive effects were also found to be significant (Table 4.13). The effects of factor interactions on fluoride uptake capability can be found in the Appendix C. The model lack of fit was noticed to be significant; a condition that necessitated the reduction or removal of the non-significant model terms in the expression with a view to improving the predictive power of the model. Other model analysis parameters such as adequate prescision and coefficient of determinations were in favour of the model reliability.

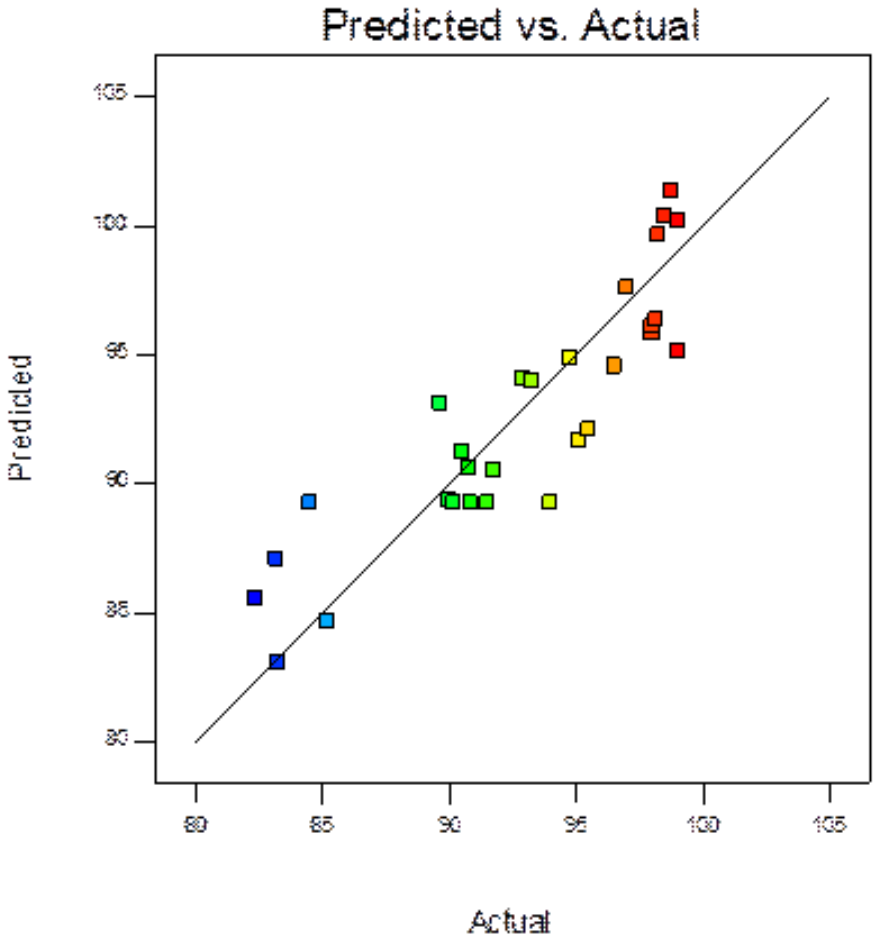

Figure 4.22: Curve Fitting for F^- Uptake Efficiency onto ACRPSAC

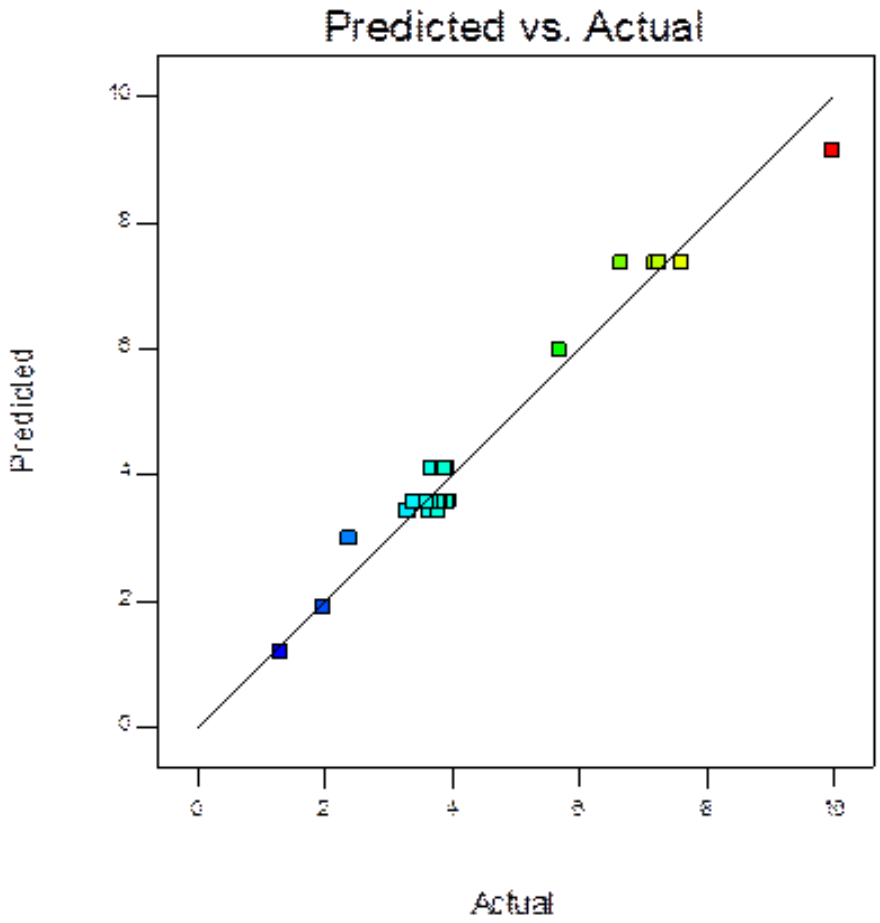

Figure 4.23: Curve Fitting for F^- Uptake Capability onto ACRPSAC

Similarly, Figure 4.23 is the curve fit between the actual and model-predicted values for F^- uptake capability of ACRPSAC which yielded an almost straight line, which potends the model power of prediction. Thus the two-factor interaction model (in coded factor forms) revealing the interrelationships amoung the variables for predicting the F^- uptake capability is given in equation 4.4.

Thus the derived expression with regard to rebranded factor levels for fluoride uptake capability using ACRPSAC was found to be:

$$\text{Adsorption Capacity} = 6.4 + 1.2\ B + -8.0\ C + -0.4\ BC + 2.5\ C^2 \quad (4.4)$$

Here; B, and C, primary fluoride concentration (mg/L) and carbon dosage (g/L) correspondingly. In the same vein, the derived expression is useful for predicting fluoride uptake capability as a dependent of the factors considered for ACRPSAC and other similar adsorbing materials.

4.11.3 Process Optimization for F^- Uptake onto ACRPSAC

The mathematical style of optimization was deployed to establish best F^- uptake criterion as a function of the already mentioned influential procedural factors. See Fig. 4.24 for details of the optimized points. The optimal points for both factors and responses were established with a desirability value of 1.0 in the current work. The optimization results were authenticated by undertaking separate batch fluoride uptake investigations at the stipulated optimal settings using both simulated and actual ground water contaminated with fluoride (Table 4.14).

The influence of every of the experimental variable on teach target outcome considered can be found in Appendix C. From Fig. 4.24, optimum values of the variables were established as 6.00, 4.00 mg/L, 2.00 g/L and 120.00 minutes respectively for pH, primary F^- concentration, carbon dosage and interaction time. The optimum dependable variable outcomes were 99.00 % and 2.0- mgg^{-1} for F^- elimination percent and uptake capacity correspondingly.

The estimated and experimental values of the responses; uptake efficiency and adsorption capacity did not differ as percentage errors were found to be ±0.4 and ±0.0

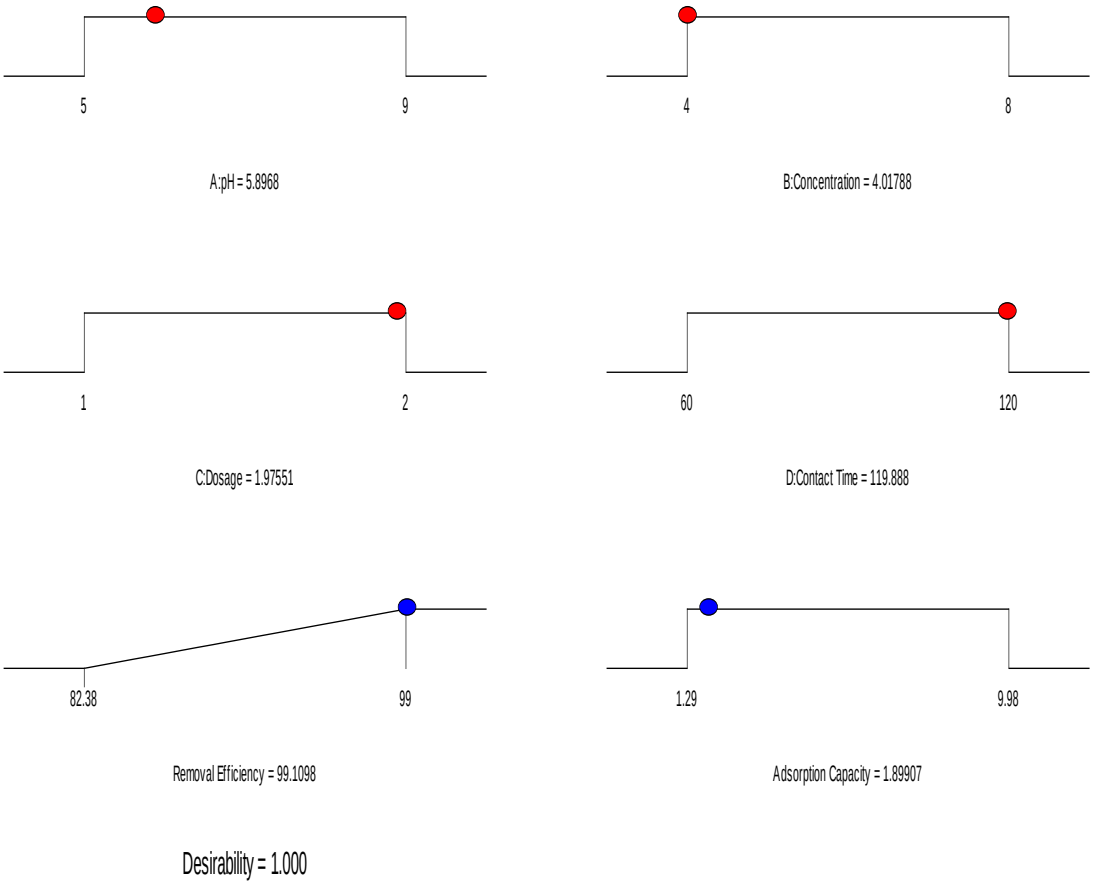

Figure 4.24: Optimal Conditions for F^- Uptake onto ACRPSAC

Table 4.14: Model-derived and Empirical Optimums for F^- Adsorption on ACRPSAC

Material	Optimum Variable Setting	Model-derived Outcome		Empirical Outcome		Deviations (%)	
		Uptake Efficiency (%)	Adsorption Capacity (mg/g)	Uptake Efficiency (%)	Adsorption Capacity (mg/g)	Uptake Efficiency (%)	Adsorption Capacity (mg/g)
ACRPSAC	Carbon Dosage = 2.0 g/L, Primary F^- Concentrationt = 4.0 mg/L, pH = 6.0 and Interaction Time = 120.0 minutes	99.0	2.0	98.6	2.0	±0.4	±0.0

respectively (Table 4.14). Furthermore, findings from the optimization routine also pointed to the feasibility of deploying these conditions for F containment in actual fluoride-ladened water samples. This is because these values, especially pH are practicable and in most cases in tandem with the actual composition of drinking water.

4.12 Confirmatory Experiments for F Adsorption onto ACRPSAC using Field Water Samples

The possibilities of deploying ACRPSAC as a suitable adsorbent for F^- removal in actual contaminated drinking water was further scrutinized by adopting the established process optimums described in section 4.11.3 above. This was done using groundwater samples pumped out from selected boreholes in Langtang and Kaltungo districts in Northern Nigeria, which are established to have elevated F^- levels in its groundwater meant for drinking (Dibal *et al.,* 2016; Malum *et al.,* 2019). The physical and chemical compositions (Table 4.15) of the samples were initially ascertained in accordance with decent procedures as documented in APHA (2005). It was observed that a good number of the water features inclusive of F^- were excedence of the stipulated thresolds for potable water (WHO, 2008). Although there are no available data to buttress on the number of individuals at risk of fluorosis in these areas, consuming groundwater with elevated F^- concentrations would expose the resident populations to such health risks (Dibal *et al.,* 2016). The physiognomies of the studied water samples in the current work were similar to those already reported by other scholars for the two locations (Danbature *et al.,* 2014; Dibal *et al.,* 2016; Goyit *et al.,* 2018; Malum *et al.,* 2019).

Results indicating the performance of ACRPSAC for F containment in actual groundwater in comparison with CAC and AA (which can be purchased from the market and are readily used for fluoride adsorption in water) are presented in Fig. 4.25A. The order of fluoride uptake efficiency was such that AA $\geq$ ACRPSAC > CAC. Thus ACRPSAC was proven to lower groundwater F concentratios from as high as 7 mg/L to levels below the WHO limit of 1.5 mg/L (Fig. 4.25B). Thus it can be considered as an excellent fluoride scavenger in aqueous media which could be reliably deployed for sustainable groundwater defluoridation in batch systems.

Table 4.15: Physico-chemical Features of Groundwater in Northern Nigeria

S/No	Parameter	Mean Value		WHO Limit	Remark
		Kaltungo	Langtang		
1	Fluoride (mg/L)	4.06	7.24	1.50	**
2	Nitrate (mg/L)	0.95	12.6	45.00	*
3	Phosphate (mg/L)	2.05	4.12	-	
4	Bicarbonate (mg/L)	64.7	188.16	-	
5	Sulphate (mg/L)	8.49	16.72	400	
6	Chloride (mg/L)	89.35	125	500.00	*
7	Arsenic (mg/L)	0.04	0.14	0.01	**
8	TDS (mg/L)	210.34	246.16	500.00	*
9	Electrical Conductivity (µs/cm)	304.60	382.91	1000.00	*
10	Turbidity (NTU)	1.07	1.28	5.00	*
11	pH	7.00	6.25	6.50 – 8.50	*
12	Total coliform	ND	ND	0	

Note: * means within limit, ** means above limit and 'ND'means not detected

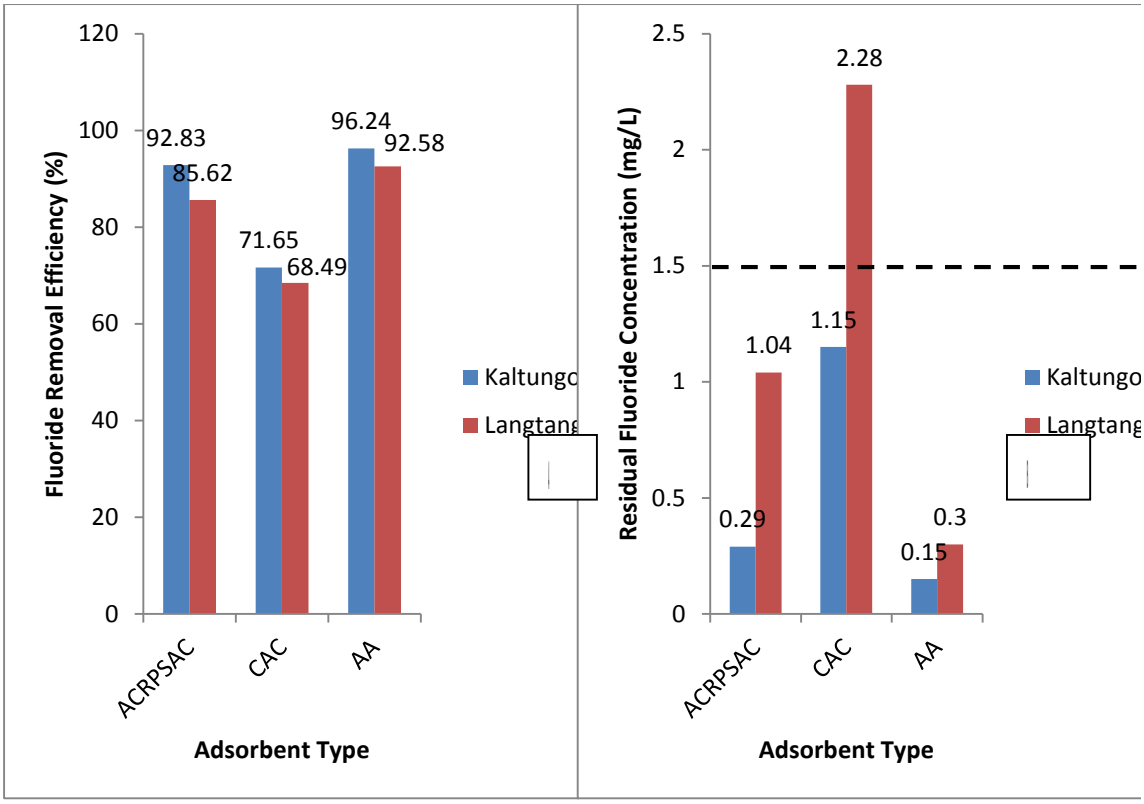

Figure 4.25: Actual Northern-Nigeria Groundwater F^- Removal by ACRPSAC, CAC and AA (A): Uptake Efficiency, (B) Final F^- Concentration (Initial F^- Concentration = 4.1 mg/L and 7.2 mg/L for Kaltungo and Langtang Areas congruently, Carbon dosage = 2.0 g/L, Interaction time = 120 minutes, Shaking Speed = 150 rpm)

The F^- uptake efficiency by ACRPSAC were approximately 93.0 and 86.0 % for samples obtained from selected deep wells in Kaltungo and Langtang areas, separately (Figure 4.25A). Similarly, the residual F^- content in the ACRPSAC-treated samples obtained from Kaltungo and Langtang area were decreased from 4.1 to 0.3 mg/L and from 7.2 to 1.0 mg/L respectively under inherent conditions of pH (Figure 4.25B). It was noticed that the performance of ACRPSAC for fluoride scavenging in water was lowered once the initial fluoride concentration were higher than the established optimum of 4.0 mg/L, thus suggesting an increase in the carbon dosage and/or interaction time when such higher concentrations were involved as shown in Fig 4.25.

4.13 Assessment of Groundwater for Fluoride Contamination in Makurdi-Nigeria

Results of groundwater features for water sourced from boreholes in twenty one locations across Makurdi town are presented systematically in the following sub-sections.

4.13.1 Physico-Chemical Variations in Groundwater Quality at Makurdi

The unprocessed data of the water quality features in the sampled (21) locations are shown in Appendix D. Table 4.16 displays the descriptive statistics of the groundwater quality. The sample pH ranged from 6.2 to 6.83 (mean = 6.5 ± 0.2) across the 21 locations as shown in Fig. 4.26. Overall, the pH values of samples were lower than the WHO endorsed threshold (6.5 – 8.5) for potable water quality in almost 52.4 % of the samples. Such non-alkaline pH could be detrimental to sound metabolic activities in humans if such water is unwholesomely consumed (WHO, 2017). The likely cause of slight acidity in the samples was ascribed to farmers' indiscriminate uses of fertilizer and herbicides in the study area (Chabukdhara *et al.*, 2017).

Table 4.16: Expressive Data for Groundwater Quality at Makurdi

S/No	Variable	Range	Average	S.D	WHO Threshold	% Exceedance
I	pH	6.2 - 6.8	6.5	0.2	6.50 – 8.50	52.4
Ii	TDS	90.0 -1472.0	708.0	405.1	1000	28.6
iii	EC	158.0 - 2487.0	1233.5	701.6	1500	38.1
Iv	Cl^-	38.0 - 533.0	165.1	110.0	200	28.6
V	CO_3^{2-}	0.0 - 196.0	18.7	25.5	-	-
vi	HCO_3^-	95.0 - 601.0	331.6	131.9	500	9.5
vii	SO_4^{2-}	40.0 - 492.0	283.9	122.1	250	71.4
viii	NO_3^-	0.6 - 16.0	5.9	3.4	50	0.0
Ix	F^-	0.3 - 2.1	1.3	0.4	1.5	33.3
X	Na^+	34.0 - 403.0	211.9	98.6	200	57.1
xi	K^+	1.5 - 11.5	5.0	2.3	50	0.0
xii	Ca^{2+}	46.0 - 221.0	102.8	44.8	75	47.6
xii	Mg^{2+}	29.0 - 238.0	90.0	48.5	150	14.3

Note: Total = 63 samples, Each Parameter is in mg/L except for EC (µs/cm) and S.D is “Standard Deviation”. TDS is “Total Dissolved Solids”, EC is “Electrical Conductivity”

The TDS and EC of the samples varied from 89.8 to 1471.5 (mean = 708.0 ± 405.1 mg/L) and from 158.4 to 2487.4 (mean = 1233.5 ± 701.6 µs/cm) correspondingly. These figures were higher than the WHO acceptable threshold for potable water in 28.6 and 38.1 % of the trials respectively. In as much as adverse health consequences are not associated with excessive TDS and EC values in water, however, high values are discouraged these hamper on its aesthetics for inake purposes, moreover high values of TDS and EC are linked with scaling issues in drinking water supply fittings including pipelines (WHO 2017). Recently, research has linked issues of renal disorders in humans and gastrointestinal malfunctions to the consumption of TDS-laden water (Chebet *et al.,* 2020). Anion dissolutions from geogenic and human activities, uncontrolled application of herbicides and fertilizers, ion exchange and rainwater percolations were suspected to be the major mechanisms affecting these water features in the samples (Chebet *et al.,* 2020; Egbueri and Mgbenu, 2020; Emenike *et al.,* 2018b).

Salty sensation in potable water is related to high chloride concentrations in it, especially when it is found to be in the region of 200 – 300 mg L (WHO, 2017). In this study the mean chloride content of groundwater was found to be 165.1 ± 110.0 mg/L with 28.6 % exceeding the allowable maximum of 200 mg/L. De-icing salts released as runoff or effluents from industrial, commercial or agricultural undertakings are majorly responsible for high chloride concentrations in drinking water. Other causes of groundwater enrichment with chlorides could be geogenic dissolution of chloride-containing rocks (Asuma *et al.,* 2020).

The mean CO_3^{2-} and HCO_3^- concentrations were 18.7 ± 25.5 mg/L and 331.6 ± 131.9 mgL^{-1} correspondingly (Table 4.16 and Fig. 4.20). Carbonate content in drinking water is not strictly regulated, not withstanding, for bicarbonate, a 9.5 % violation of the tolerable value was observed in the samples. The interaction of groundwater with runoff and irrigation water through seepage and geogenic dissolution of minerals were suspected to be the main origin of bicarbonate in the trials (Akoteyon, 2013; Rasool *et al.,* 2016).

The levels of SO_4^{2-} in the water was found to range from 39.6 – 492.1 mg/L (mean = 283.9 ± 122.1 mg/L) and surpassed the recommended maximum limit of 250 mg/L in over 71 % of the samples. Extremely high SO_4^{2-} concentrations in drinking water can be

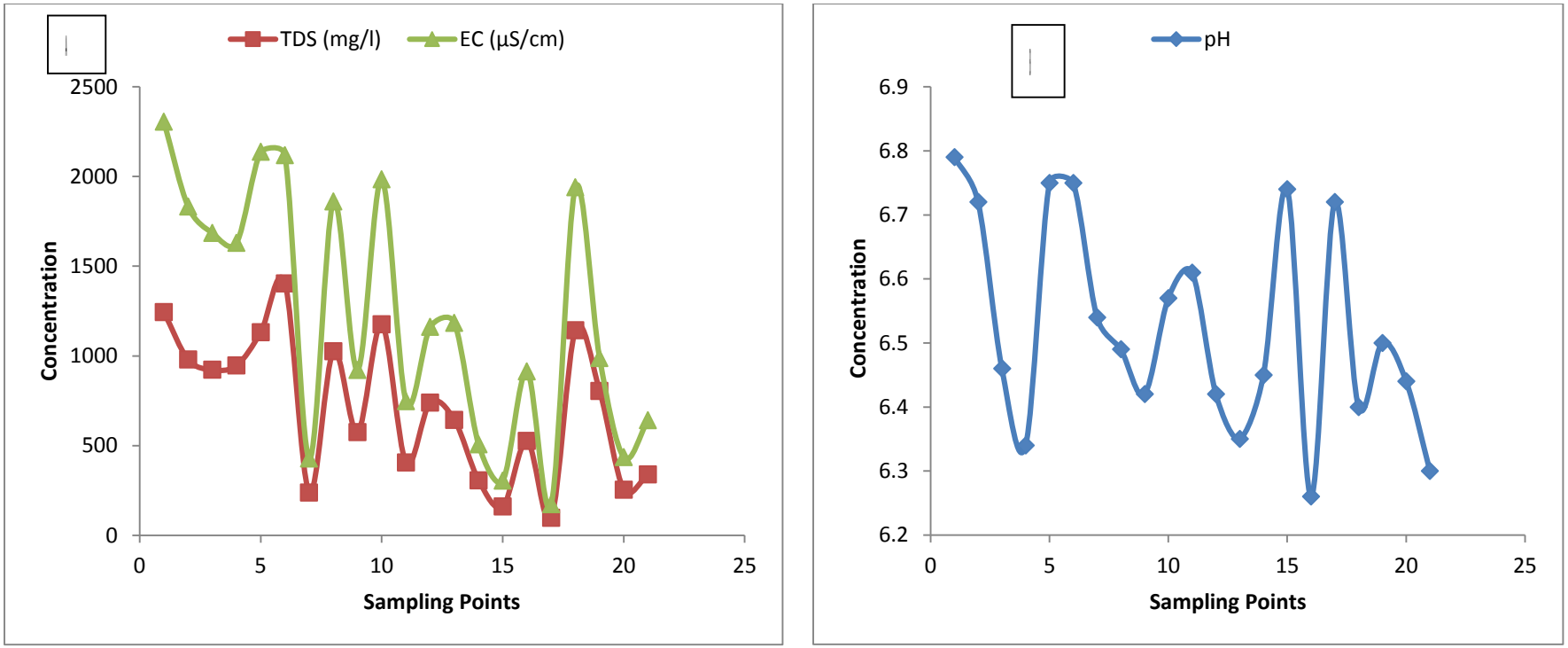

Fig. 4.26: Physico-chemical Features of Groundwater: (A) pH, (B) TDS and EC, (C) Anions and (D) Cations

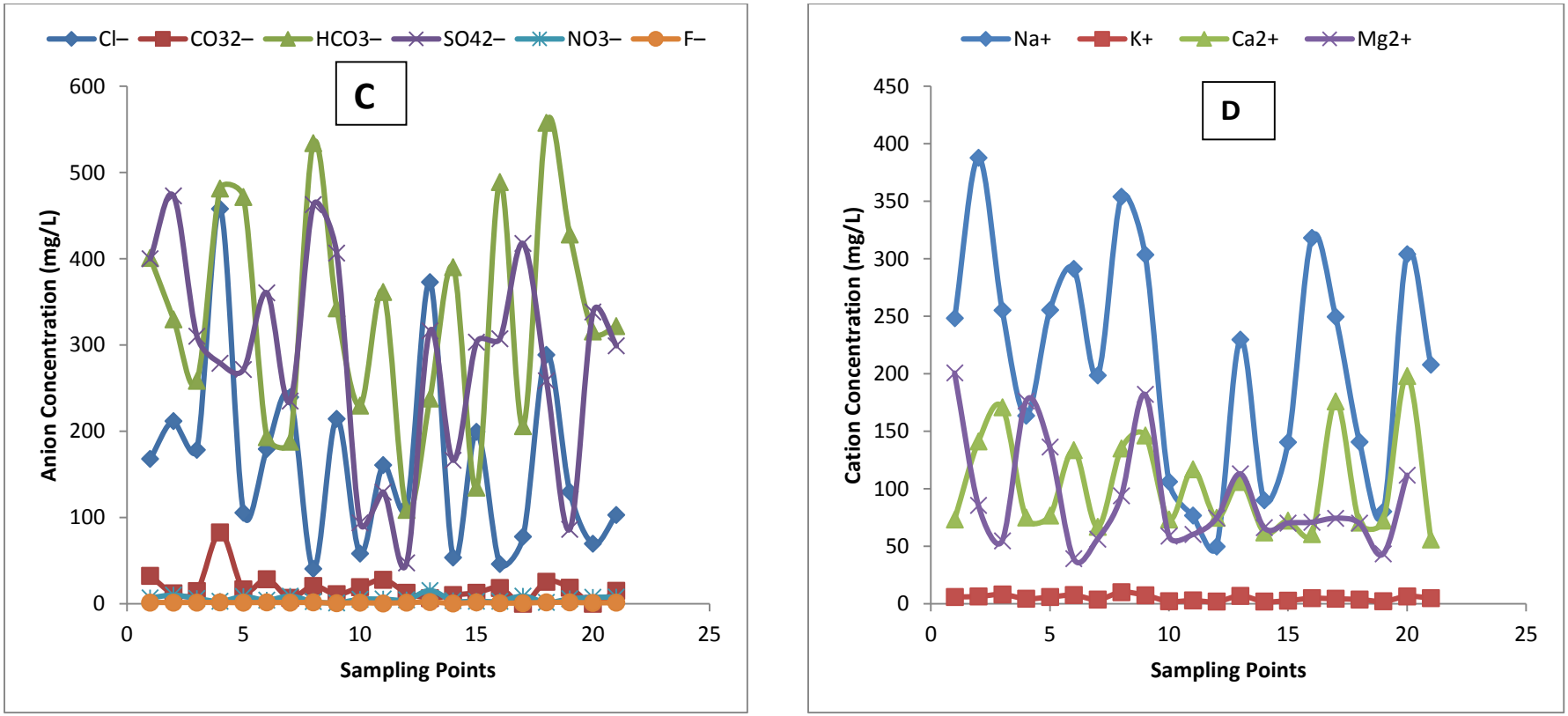

Fig. 4.26: Physico-chemical Features of Groundwater: (A) pH, (B) TDS and EC, (C) Anions and (D) Cations

responsible for purgative and respiratory health issues in human beings, while modest concentrations would prompt salty taste in drinking water (Emenike *et al.,* 2018a). Similarly, its occurrence in the studied groundwater was ascribed to basement mineral dissolutions and uncontrolled uses of fertilizer/herbicides by farmers.

Nitrate is a sternly monitored parameter in drinking water as it is recognized to be responsible for methamoglobinemia (blue baby syndrome) in younger humans when consumed in water with NO_3^- concentration in exceedance 55 mgL^{-1} (Adimalla and Li, 2019). In the current study, all samples were found to comply with the maximum tolerable threshold (45.0 mg/L) for NO_3^- in ingestible water irrespective of the unwarranted usage of inorganic soil enrichers and herbicides in most of the sample locations. Such diminished amounts of NO_3^- in the trials were ascribed to the adsorptive removal of nitrate by soil layer in the course of deep percolation and seepage of agricultural water (Achary *et al.,* 2016).

The concentrations of F^- as arrange were 0.2 – 2.1 mg/L (mean = 1.3 ± 0.4 mgL^{-1}). F^- values in potable water is considered a double-edged sword because a minimum of 0.5 mg/L is necessary for curtailing teeth caries in humans, while its presence in drinkable water at levels in exceedance of 1.0 mg/L promotes the molting of human teeth and skeleton. Recent documented evidence has also associated many cancers in human to the intake of fluoride laden water (WHO, 2004; USNRC, 2006). Thus in this work over 33 % of the trials had F^- that suppased the permitted maximum, while most samples had sufficient F^- contents for prevention of dental caries. Fluoride enrichment in the water was ascribed to both anthropogenic factors and the dissolution of fluoride-bearing mineral in the underlying aquifers.

Mean Na^+ concentration in the water was obtained as 211.9 ± 98.6 mg/L, with lowest and highest figures reaching 34.3 and 403.1 mgL^{-1} respectively. Noticeable variability was observed for Na^+ in the study location as over 57% of the trials were higher than the acceptable maximum (200 mg/L) in water. Groundwater chemistry and interference with anthropogenic generated effluents were suspected to be the major motives promoting raised Na^+ levels inaquifer-based water (Tirkey *et al.,* 2017).

Average K^+, calcium, and magnesium contents, which are main indicators of water hardness in the trials, were found to be 5.0 ± 2.3, 102.8 ± 44.8 and 90.0 ± 48.5 mg/L respectively. K^+ content was observed to fully comply with the stipulated limits in

drinking water at all locations considered, while over 47 and 14 % of the samples exceeded the set thresholds for calcium and magnesium in potable water. Thus based on the elated cation levels in the water samples, the studied aquifer were adjudged to be relatively hard and tasty water, which was caused by ion exchange and basement rock dissolutions (Magesh *et al.*, 2017).

4.13.2 Hydrogeochemical facies and Water Quality

The Bureau of Indian Standards Water Quality Index (BISWQI) approach and piper diagrams were adopted for assessing groundwater in the current work. The results of BISWQI are shown in Fig. 4.27. Appendix D contains the exclusive compilations and remarks for BISWQI of the samples. Bulk of the trials (95 %) were categorized as "good water" and corresponded to the BISWQI Class II, while the sample from P14 was observed to be excellent water (Class I of the BISWQI rating). The main donors to the general WQI of the samples were SO_4^{2-} > EC > Cl^- > Ca^{2+} > F^- > TDS > pH > Na^+. Lower contributions emanated largely from Mg^{2+}, HCO_3^- and NO_3^{2-} which were collaborated with the position of Adimalla *et al.* (2018) in another study.

Despite falling in Class II of the BISWQI ratings, samples L1, L2, L4, L6, L8, L13 were found to be at the verge of falling into class III ("poor water") in a short time if pollution sources were not checked. Thus we hypothesize a need for the deployment of simplistic and efficient technologies such as sand filtration and adsorption for containing the major contributing parameters (especially SO_4^{2-} and F^-) to the contaminant status of the water, with a view to providing excellent drinking water to the residents.

From the Piper plot (Figure 4.28) sodium > calcium > magnesium ions were noticed to be the dominant cations, while the main anions were found to be sulphate > chloride > bicarbonate. Calcium and sodium ionic dominance in the samples was indicative of the involvement of ion interchange and rock disintegration processes in the groundwater chemistry. On the other hand, the anionic dominance of sulphate and chloride was ascribed to silicate weathering (Achary *et al.*, 2016).

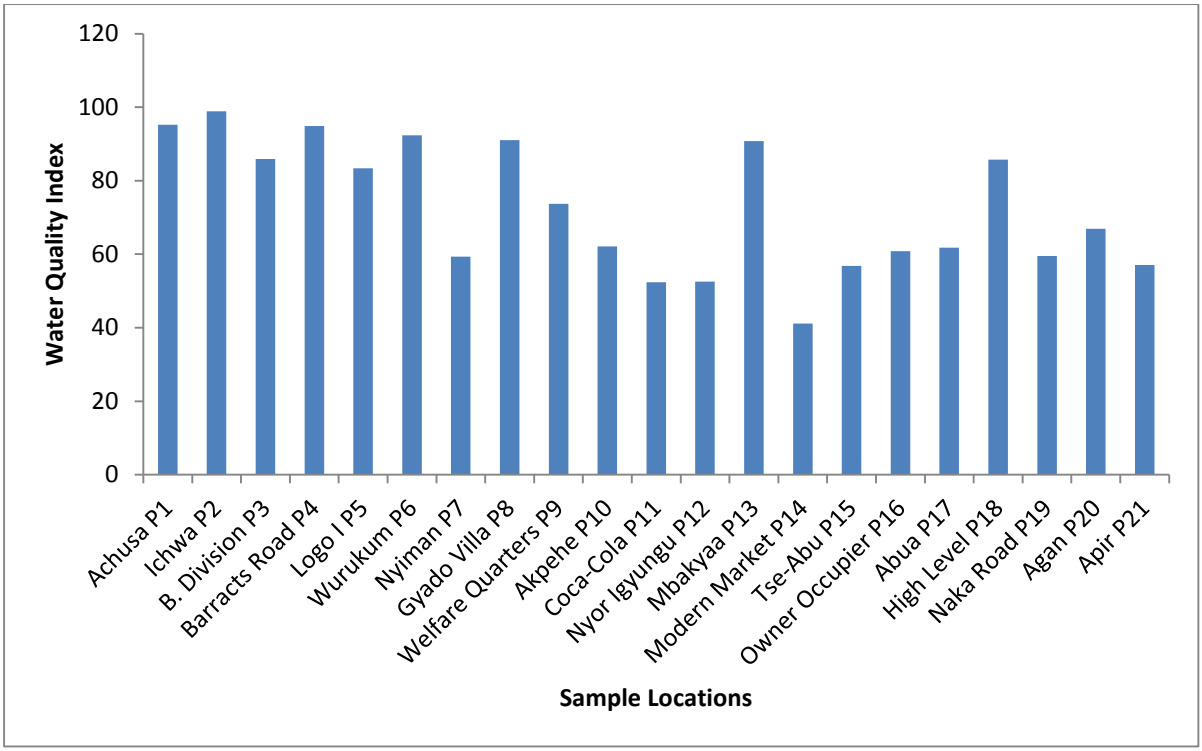

Figure 4.27: Water Quality Index (WQI) of groundwater from selected wells in Makurdi

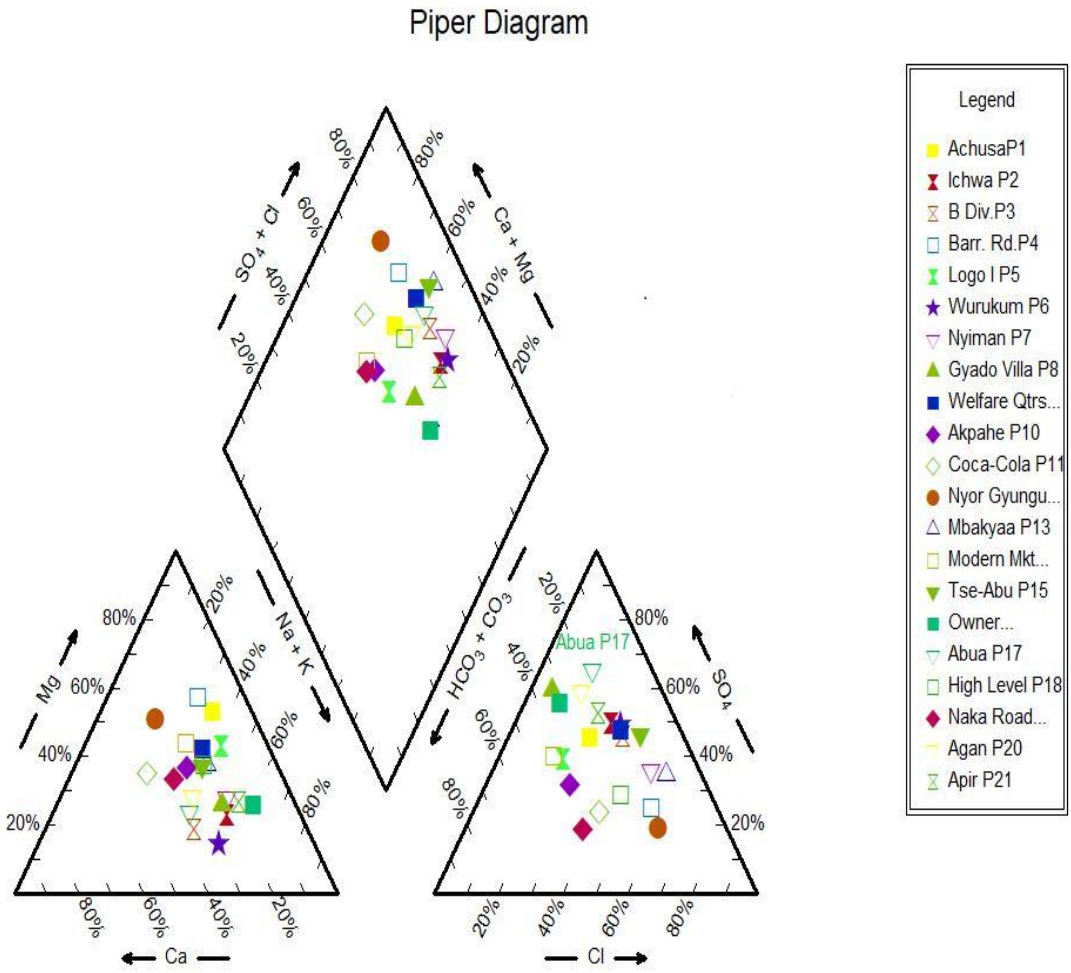

Figure 4.28: Piper Plots for Hydrogeochemical Description of the Water Samples

Moreover, the high Ca^{2+}/Mg^{2+} ratio (0.6 – 3.4 in over 80 % of samples) obtained in the current work was another confirmation of involvement of dolomite and silicate rock weathering in the groundwater chemistry (Aghazadeh *et al.,* 2016). Water type (hydrogeochemical facies) show that the dominant facies in the study area were Na-SO_4, Na- Cl, Mg-HCO_3, Ca-HCO_3, Mg-SO_4, Mg-Cl, Ca-Cl and mixed water types (Fig. 4.28), which were the reasons for the salty sensations in groundwater obtained from boreholes in the region.

4.13.3 Application of Multivariate Statistics for Groundwater Assessment

Source apportionment and interrelationships among the pollutants in groundwater were elucidated in the current study using Correlation Analysis (CA), Principal Component Analysis (PCA) and Hierarchical Cluster Analysis (HCA) as also utilized by several other authors in previous studies (Ali and Ali, 2018; Emenike *et al.,* 2018b). Feeble, modest and robust relationships are inferred when r is < 0.3, 0.3 – 0.7 and > 0.7 respectively in any correlation analysis.

4.13.4 Results of the Pearson's Correlation Analysis

In this work, fluoride exhibited a moderate and positive relationship with TDS, EC, Cl^- and NO_3^- (Table 4.17), which indicated that these pollutants alongside with fluoride originated majorly from geogenic activities as was also reported by Bempah (2014) for a Ghanaian region. Also, there was a weak and positive association of F^- with sulphate, bicarbonate, pH and each positive ion excluding calcium, which again attributed their sources into groundwater to be from geogenic activities. On the contrary, there was an observed weak and negative association between F^-, HCO_3^- and Ca^{2+}, which shows that they were contributed from divergent origins: Fluoride from natural processes and bicarbonate and calcium from anthropogenic contribution (Adimilla and Venkatayogi, 2017; Emenike *et al.,* 2018b).

Additionally, robust affirmative relationships were found for various ionic groups in the trials (Table 4.17), which indicated that the concerned pollutants originated from same or similar sources. Strong and moderate negative relationships among the groundwater pollutants were not established in the current study; however, weak negative associations were seen in a few ionic groups (Table 4.17) which shows that these were from diffuse sources.

Although higher F^- in groundwater were found in the current study as compared to previous works (Schen and Schafer, 2015; Emenike *et al.*, 2018b), it has been documented that F^- in water usually rises as the TDS/EC figures also rise (Schen and Schafer, 2015); an inclination that was as well established in this work. Raised F^- concentrations in the trials were also favoured because of the prevailing water pH (6.2 – 6.8) which encourages fluoride solubility in water (Saxena and Ahmed, 2001). The disbandment originating from shale and quartzite (the dominant ecological formations in the locality) as documented by Eneji *et al.* (2011) was also responsible for F^- enrichment in the aquifer.

4.13.5 Results of PCA for Pollutant Source Apportionment

Four Principal components (PCs) that accounted for over 71 % of the overall discrepancy were mined as depicted in Table 4.18 and the scree plot in Fig. 4.29. A summation of 13 factors were extracted, with only four attaining Eigen values that were higher than 1. Fig. 4.30 displays the component loadings in rotated space. Other details can be seen in Appendix D. There were strong affirmative loadings of SO_4^{2-}, Na^+, Ca^{2+}, K^+ and Mg^{2+} in PC1 that explained 24.7 % of the overall variability, which pointed to the role of mineral disintegration and ionic interchange processes in the groundwater chemical interactions and as well support the origination of cations in the water from geological sources.

Similarly, there were strong positive loadings of pH, TDS, EC and F^- that explained 19.6 % of the total variance in PC2. This indicated that these contaminants were from the same natural and anthropogenic sources. The controlling influence of pH on F^- fortification in the undergroundwater (Emenike *et al.*, 2018b) was also evidence from the robust affirmative pillings of pH and $fluoride^-$ in PC2. Additionally, the factor loadings in PC2 confirmed the claim that F^- content in water is favoured in the event of increasing TDS and EC values as earlier explained. Thus TDS and EC could be viewed as the main indicators of ionic compositions of drinking water (Rafique *et al.*, 2009).

Table 4.17: Correlation Matrix of Groundwater Quality Parameters

	pH	TDS	EC	Cl^-	CO_3^{2-}	HCO_3^-	SO_4^{2-}	NO_3^-	F^-	Na^+	K^+	Ca^{2+}	Mg^{2+}
pH	1												
TDS	0.229	1											
EC	0.235	0.980**	1										
Cl^-	-0.133	0.162	0.159	1									
CO_3^{2-}	-0.130	0.326**	0.324**	0.378**	1								
HCO_3^-	-0.196	0.290*	0.338**	0.012	0.205	1							
SO_4^{2-}	0.197	0.113	0.158	0.094	-0.023	0.142	1						
NO_3^-	0.131	-0.134	-0.076	0.147	-0.241	-0.322**	0.117	1					
F^-	0.004	0.472**	0.484**	0.457**	0.142	-0.085	0.087	0.279*	1				
Na^+	0.105	0.184	0.223	-0.017	-0.108	0.176	0.869**	0.176	0.068	1			
K^+	0.011	0.341**	0.361**	0.067	-0.004	0.177	0.756**	0.122	0.239	0.805**	1		
Ca^{2+}	0.148	-0.074	-0.071	-0.099	-0.218	-0.179	0.499**	0.156	-0.117	0.512**	0.540**	1	
Mg^{2+}	0.039	0.200	0.252*	0.352**	0.129	0.295*	0.374**	-0.040	0.018	0.259*	0.285*	0.070	1

** Significant at P = 0.01 (2-tailed). * Significant at P = 0.05 (2-tailed)

Table 4.18: Principal Components and Factor Loadings of Groundwater

Variable	Extracted Principal Components			
	PC1	**PC2**	**PC3**	**PC4**
pH	0.11	**0.43**	-0.51	0.25
TDS	0.10	**0.95**	0.09	-0.18
EC	0.14	**0.94**	0.11	-0.17
Cl^-	0.01	0.14	**0.85**	0.24
CO_3^{2-}	-0.15	0.29	**0.53**	-0.31
HCO_3^-	0.16	0.18	0.21	-0.74
SO_4^{2-}	**0.91**	0.07	0.07	-0.00
NO_3^-	0.18	-0.03	0.08	**0.77**
F^-	0.01	**0.59**	**0.43**	**0.47**
Na^+	**0.92**	0.11	-0.05	-0.02
K^+	**0.87**	0.24	0.10	-0.01
Ca^{2+}	**0.70**	-0.15	-0.24	0.20
Mg^{2+}	**0.41**	0.09	**0.45**	-0.25
% of Variance	24.70	19.60	13.70	13.50
Cumulative %	24.70	44.30	58.10	71.50

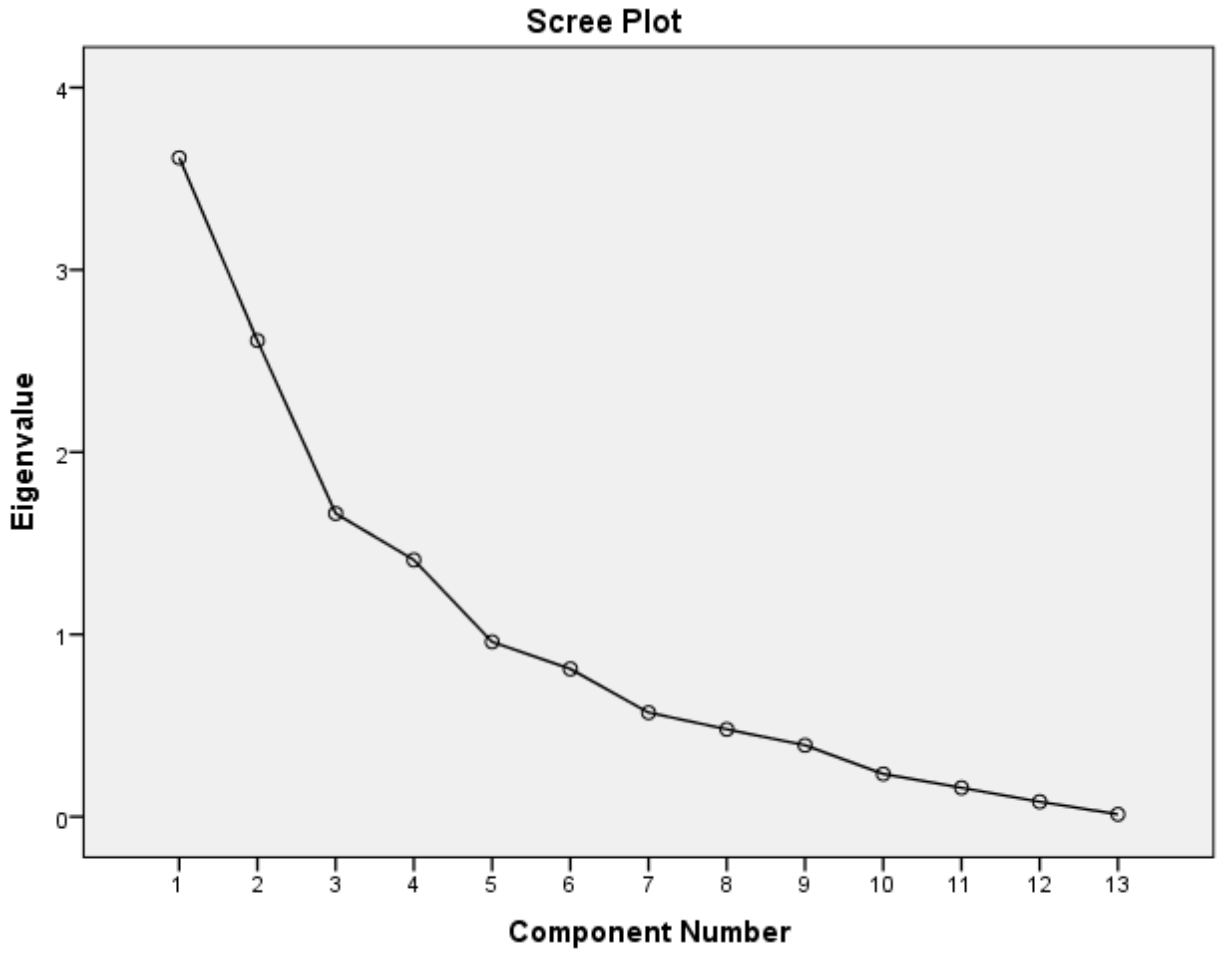

Figure 4.29: Scree diagram of Mined Components with Eigen Values

There were poor contributions to the overall water quality from PC3 (13.7 %) and PC4 (13.5 5) and were strongly and positively loaded with Cl^-, CO_3^{2-}, NO_3^-, F^- and Mg^{2+}. A quasi-independent behaviour between Mg^{2+} and F^- was seen in PCs 1, 2, 3 and 4, which was indicative that they found their way into groundwater from both geological/geogenic and human activities (Hosseini *et al.*, 2019).

4.13.6 Results of HCA for Pollutant Interrelationships

The Ward's methodology which requires the selection of the squared Euclidean distance as the interval was adopted in the current work for HCA. Associations among the various water quality features were established via the Variable-mode of the HCA, while similarities in the sampled (21) locations were ascertained using the Case mode of the HCA. Normalization of the data was done prior to analysis (Sharaf and Subyani, 2011: Bempah, 2014). The dendrogram showing the interrelationship among the variables is as presented in Figure 4.30, while that exposing the similarities in the locations is contained in Fig 4.31. Other details of HCA including the proximity matrix, agglomeration schedule and cluster membership details for the two scenarios are presented in Appendix D.

Two clusters were identified in the variable-mode. Cluster 1 comprised pH, K^+, NO_3^-, F^-, CO_3^-, Ca^{2+}, Mg^{2+}, Cl^-, SO_4^{2-}, Na^+ and HCO_3^- in accordance with their concentrations in water. The closeness of pH, nitrate and potassium shows that they originate mainly from both natural human activity-related sources. The closeness envisaged between Na^+, SO_4^2 and HCO_3^- further proved their origin to be from mineral disintegration and ionic interchange as also collaborated by the CA and PCA. These were also responsible for the prevalence of Na-SO_4 and Na-HCO_3 water facies in the locality.

Close clustering of Cl^-, CO_3^-, NO_3^-, F^-, K^+, Ca^{2+}, Mg^{2+} with pH was also indicative of the role of pH in the abundance or otherwise of these pollutants in the sampled water as pH is known to control the movement and spread of these ionic features in water. Additionally, short connection space existing for F^- and NO_3^- shows that F^- got into groundwater from fertilizer uses as well. The second and most significant cluster on the other hand housed TDS and EC. The grouping of TDS and EC in the same cluster was ascribed to their high concentrations in water and strong correlations with most of

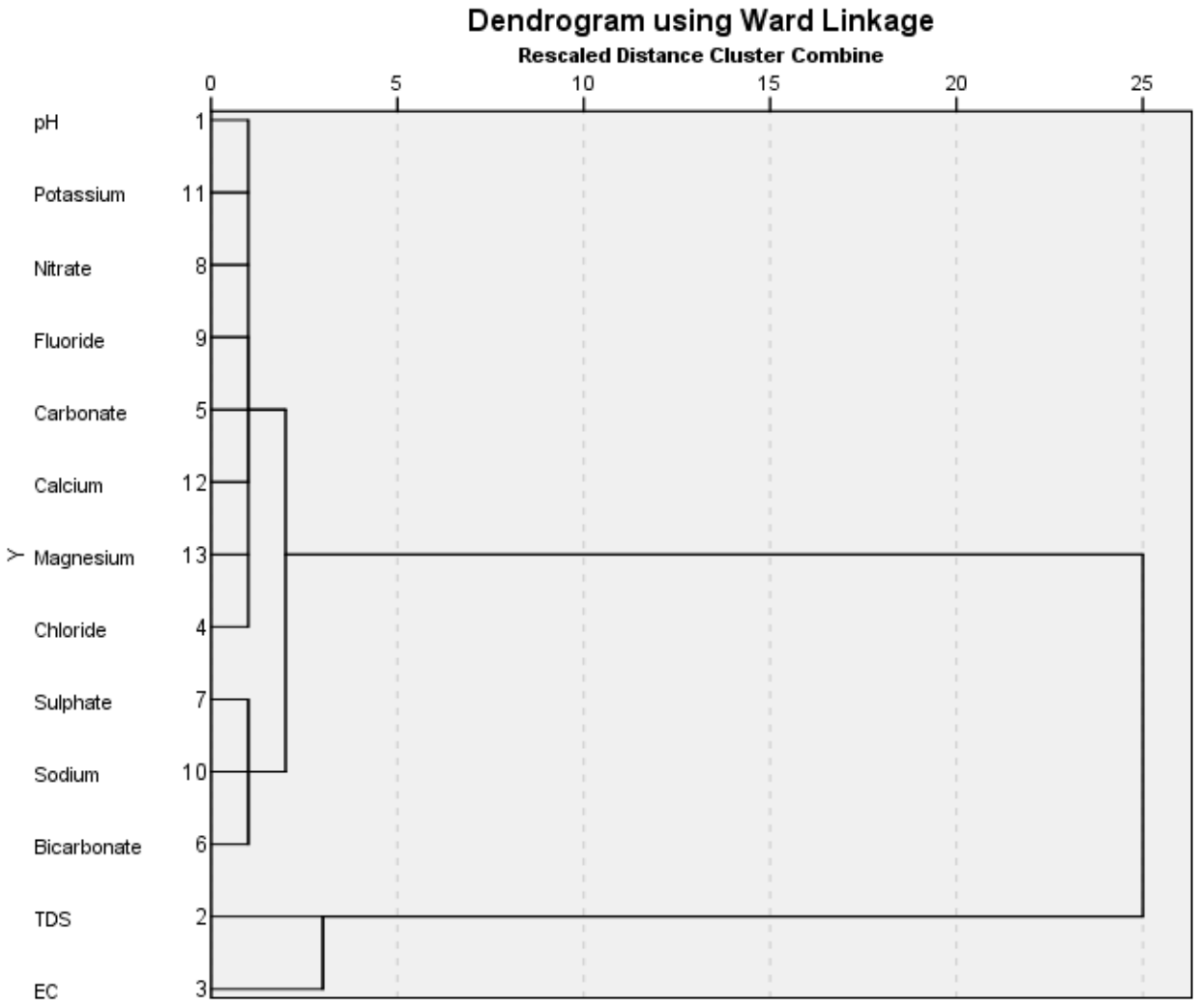

Figure 4.30: Hierarchical Cluster Analysis of the Water Quality Composition

the other water quality features. It also proved that natural processes were the major tools guiding the water chemistry and influencing salinity in the water (Bempah, 2014).

Similarly, the sampling points were grouped into two comprising a total of four clusters based on the salinity levels of the water samples (Fig. 4.31). Group 1 contained clusters 1 and 2, made up of sampling points S1, S2, S3, S4, S5, S6, S8, S10, S12 and S18. This group represented the saline water types. Group 2 on the other hand comprised clusters 3 and 4, made up of S7, S9, S11, S13, S14, S15, S16, S17, S19, S20 and S21. This group on the contrary represented the non-saline water types in the study area.

4.13.4 Well-being Risk Linked with Fluoride Levels in Groundwater

Irrespective of the apparent good nature of the studied water samples for potable uses as shown via the BISWQI analysis, it was necessary to overhaul the health risk posed to the inhabitants as a result of the consumptionof F^--ladened water. The foregoing need was envisaged as most of the inhabitants of the study area relied largely on sources for their cooking and potable needs with the wrong presumption that groundwater was wholesome for drinking purposes. It was also observed that about 33.0 % (7 locations) had F^- contents in exceedance of the safe limits for preventing dental fluorosis; as such there was a need to assess the risk posed to humans in this regard.

Results of the Estimated Daily Intake (EDI) of fluoride for the various age categories studied are given in Fig. 4.32, while that for the Hazard Quotient (HQ) is as shown in Fig. 4.33. See also Appendix D.

The EDI estimates were found to be excessive in most locations, most specifically with regards to infants and children. Modest EDI estimates were obtained for teenagers in majority of the locations, while values lesser than the oral reference dose (RfD) of 0.06 mg/kg/d were obtained in all locations for adults with the exception of location P13. The EDI estimates varied between 0 and 0.1 mg/kg/d for all population categories.Sampling points P14 and P13 were observed to have the least and uppermost estimates of the EDI correspondingly.

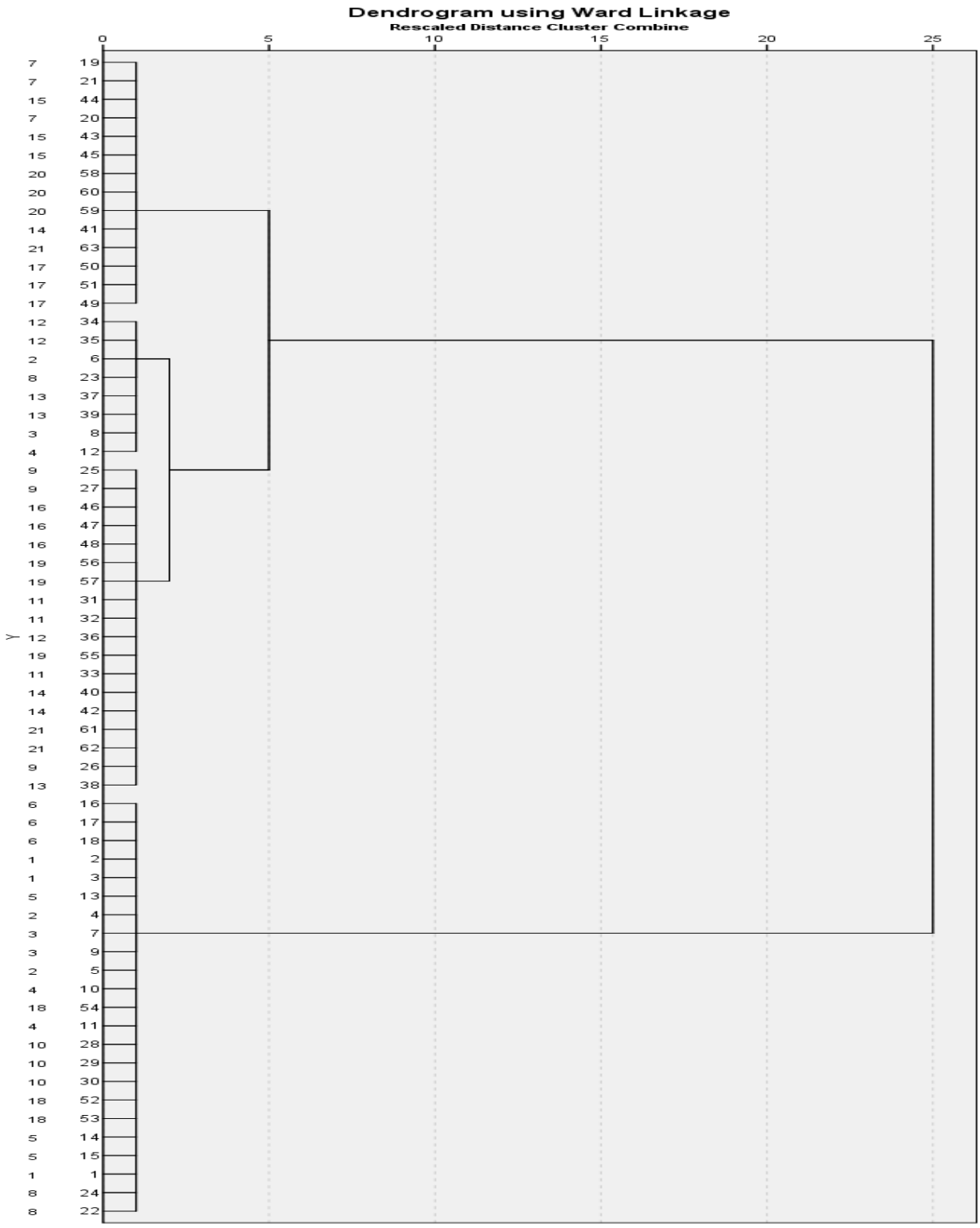

Figure 4.31: Hierarchical Cluster Analysis of the Sampling Points

Similarly, the computations of the HQ (Figure 4.33 and Appendix D) revealed that over 66.0 % of the locations had HQ estimates that were higher than the threshold limit of 1 for infants. Thus the risk of molted teeth and bones in younger people who come in contact with high F^- in water in the affected locations was confirmed (Adeyeye *et al.,* 2021). Similarly, for children, teenagers and adults, the HQ estimates were obtained to be higher than "1" in 71.4, 52.4 and 9.5 % of the study locations respectively.

The estimated daily fluoride intake (EDI) and the hazard quotient (HQ) for children was found to be greater than 1 in most of the studied samples (Figs. 4.32 and 4.33 respectively).The foregoing indicated that children were at the greatest risk of developing fluorosis due to their exposure to fluoride enriched groundwater as compared to the other age categories. Such higher risk established for children even above infants was ascribed to the higher ratio of water intake/body weights obtainable from children. The foregoing is not surprising as children experience extra metabolisms as a result of their more active dispositions (through play and mobility) which entail higher water intakes when likened to the other age groups. Thus in this study, the human health risks potentials were high in children and infants.

Irrespective of the moderate and low risk linked to the exposure of teenagers and adults to fluoride in groundwater, locations P13 and P19 were categorically marked as posing high risk of fluorosis in all age categories. As such, groundwater sourced in locations P13 and P19 must be treated with suitable defluoridation technologies before its consumption for drinking purposes. Such risk levels as reported in the current study have been previously documented by other researchers across the globe (Emenike *et al.,* 2018b; Radfard *et al.,* 2018; Yousefi *et al.,* 2018; Karunanidhi *et al.,* 2019; Nakazawa *et al.,* 2020).

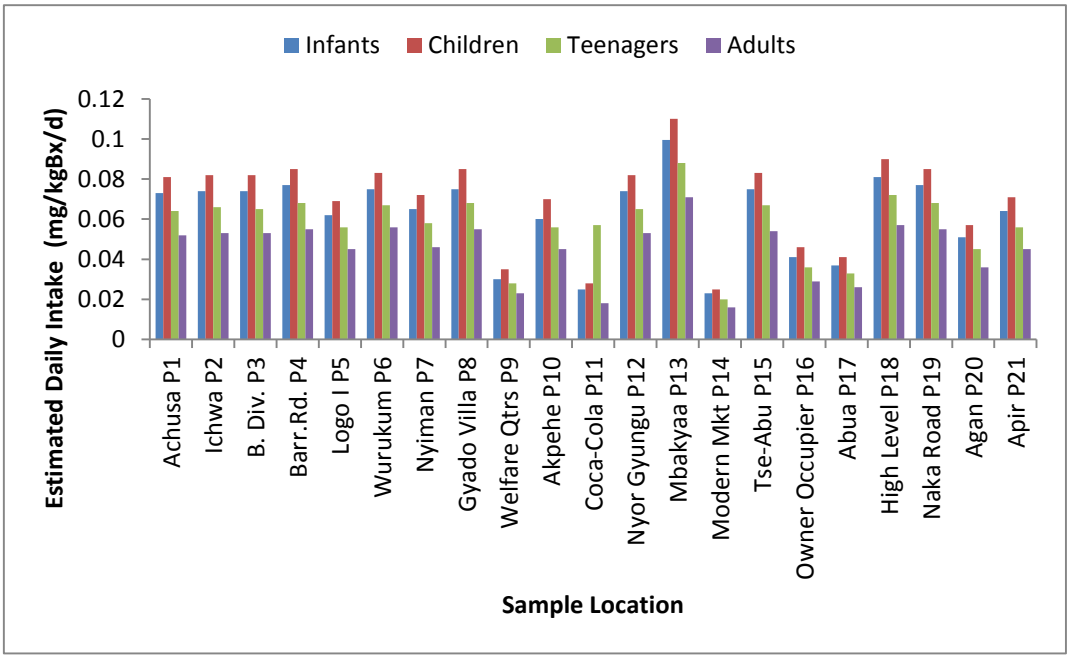

Figure 4.32: Risk Estimations using EDI values for F^- Exposures in the Populations

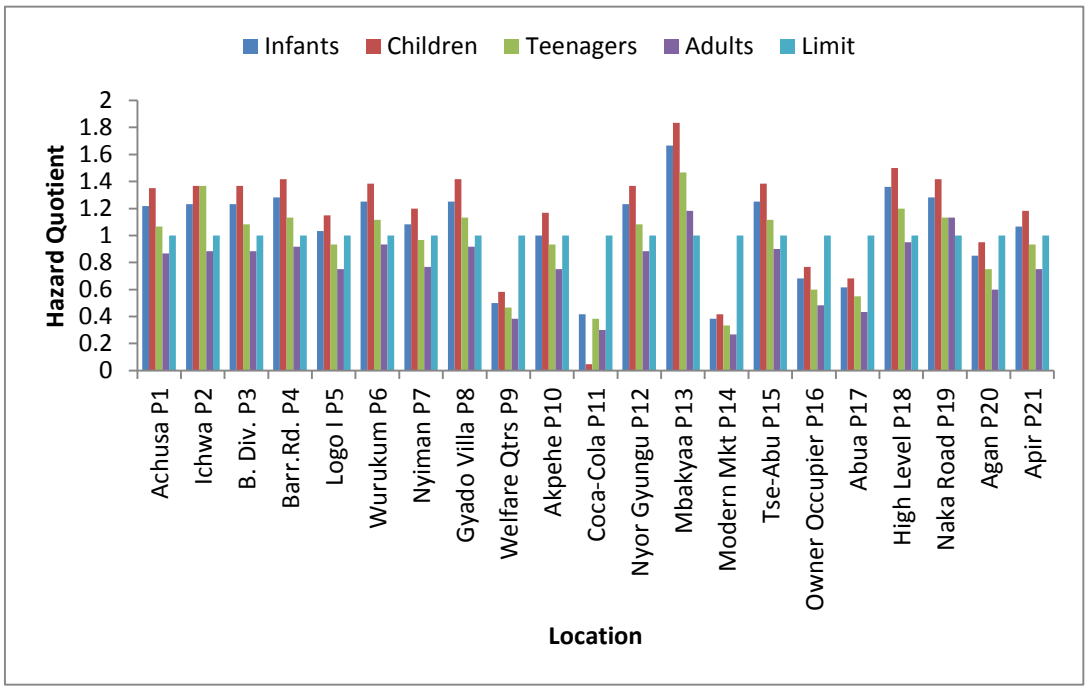

Figure 4.33: Quantification of Human Health Risk of Fluorosis by HQ Values

CHAPTER FIVE

SUMMARY, CONCLUSIONS AND RECOMMENDATIONS

5.1 Summary

This thesis focused on the development and evaluation of raffia palm shell-derived activated carbon and its aluminium oxide composites for batch-mode adsorption of fluoride in groundwater. The performance of the as synthesized adsorbent materials: Raffia Palm Shell Activated Carbon (RPSAC) and Aluminium Oxide Coated Raffia Palm Shell Activated Carbon (ACRPSAC) for fluoride uptake in simulated and actual groundwater samples were compared with a Commercially Available Activated carbon (CAC).

Response Surface Methodology (RSM) was used to optimize the yield and surface area of the RPSAC as a function of activating agent (phosphoric acid) concentration, activation time, and activation temperature and impregnation ratio. The optimally synthesized RPSAC served as a precursor for the synthesis of ACRPSAC by coating its surface with aluminium oxide inorder to further enhance its affinity towards fluoride ions in solution. Standard methods including BET-Surface Area and Porosity Analyses, XRD, SEM, FTIR and EDX were deployed to characterize the novel RPSAC and ACRPSAC. Equilibrium isotherm, kinetics and thermodynamic models were used to study the mechanisms of batch fluoride adsorption by the adsorbents, Again RSM was used to optimize fluoride uptake by ACRPSAC as a function of temperature, adsorbent dosage, initial fluoride concentration and solution pH. The regeneration of spent adsorbent media were tested with sodium hydroxide elusion, recoating with aluminium oxide, re-activation with phosphoric acid and a combination of the processes. Furthermore, water quality index (WQI), multivariate statistics and hazard quotient analysis were used to assess the suitability of

groundwater consumption with regards to fluoride pollution for sources in Makurdi metropolis, North-central Nigeria.

Findings indicate that RSM was a suitable to for optimizing the quality of RPSAC. Similarly, RPSAC was largely mesoporous, amorphous, contained abundant hydroxyl groups on it surface and had enhanced BET surface area of 456.10 $m^{2/}$/g. ACRPSAC on the otherhand had micro-porosities ascribed to it coating with aluminium oxide which favoured the formation of nano-structures such as appatite and hydroxyapatite on it surface. Also ACRPSAC was micro-crystaline and had an enhanced BET surface area of 715.80 m^2/g. Fluoride adsorption on RPSAC and ACRPSAC obeyed the Langmuir and Pseudo second order equilibrium isotherm and inetic models respectively. These indicated the involvement of chemisorption mechanisms in the uptake processes and were both exorthemic, spontaneous and feasible as revealed from thermodynamic modeling. The mechanism of fluoride uptake by the new adsorbents was found to be controlled by one or all of ion exchange, electrostatic attraction, surface complexation and dipole-dipole interaction. Rgeneration of RPSAC was suitable with elution using sodium hydroxide, while that of ACPSAC was economical by recoating the spent samples with aluminium oxide. Again RSM was suitable for optimizing the removal efficiency and adsorption capacity of ACRPSAC. Furthermoremore, 33 % of groundwater samples in Makurdi were found to contain excess levels of fluoride and its contribution to groundwater was largely from both geogenic and anthroponic activities. Infants, children and teenagers were at higher risk of developing fluorosis due to the ingestion fluoride-ladenned groundwater as compared to adults.

It was concluded that the adsorptive capacity of fluoride was in the order of ACRPSAC > RPSAC > CAC. Thus the study recommended the use of ACRPSAC for batch adsorption of fluoride in groundwater meant for drinking in order to avert the risk of fluorosis in yhe vulnerable popolations.

5.2 Conclusions

Raffia palm (*Raphia hookeri*) shells hold great potentials for its conversion into tailored activated carbons for fluoride removal in solution and drinking water sources. This was evidenced from the results of its proximate compositions that revealed high

carbon content (68.83 %), moderate volatile content (22.03 %), low ash and moisture contents (1.37 and 7.7 %) respectively.

RSM is an ideal optimizing the quality of Raffia palm shell-derived activated carbon for drinking water defluoridation. It was elucidated via the RSM that activation temperature was the most significant process variable affecting the qualities of the RPSAC. The models developed for predicting carbon yield and SSA of RPSAC as functions of ATT, IR, AT and AAC were significant (P = 0.05). Optimization studies suggested that the optimum procedural settings for the synthesis of RPSAC are 77.0 %, 4 g/mL (1:4), 524 °C, 104 minutes for AAC, IR, AT, and ATT correspondingly, which gave corresponding carbon yields and specific surface area of 78.0 % and 1762.93 m^2/g respectively. This was confirmed from actual experiments to be true as the carbon yield and specific surface area obtained were 79.4 % and 1815.62 m^2/g respectively, which showed a negligible difference with the predicted values.

ACRPSAC was successfully synthesized using the optimally produced RPSAC as the starting material. Advanced characterization (SEM) revealed that RPSAC had a heterogeneous surface comprising of meso and micro-pores while the ACRPSAC had a homogenous micro-porous surface. ACRPSAC was also observed to have superior qualities for adsorption of pollutants in water when matched with RPSAC and CAC. This was evidenced in the increase of BET surface area and total pore volume from 456.10 – 715.80 m^2/g and 0.25 – 0.47 cc/g respectively. This was attributed to the coating of RPSAC with aluminium oxide to produce ACRPSAC.

Furthermore, FTIR analysis revealed that the surfaces of both RPSAC and ACRPSAC comprised mainly of O-H, C-H, C-N, chloro-compounds and triple and double carbon bonds as main function groups with newer peaks emerging on ACRPSAC. Results of XRD suggest that both RPSAC and ACRPSAC are amorphous with significant traces of microcrystalinity identified on ACRPSAC as a result of the deposition of zeolitic minerals on its surface. The foregoing was also responsible for ACRPSAC's micro-porosity. EDX spectrum revealed that the adsorbents had high carbon, oxygen, phosphorus, nitrogen and silicon contents, with ACPSAC having increased aluminium content as compared to RPSAC, which again demonstrated the successful coating of ACRPSAC with aluminium compounds.

In the comparative batch experiments ,the efficacy of the adsorbent with regards to the fluorideuptake efficiency and capacity at varying conditions of interaction time (30 – 40 minutes), adsorbent dosage (0.5 – 2 g/L), pH (2 – 8), primary F^- concentration (2 – 8 mg/L) and process temperature (303 – 323) was such that ACRPSAC ≥ RPSAC ≥ CAC and significant at P = 0.05, with removal efficiency of RPSAC and ACRPSAC ranging from over 80 to 99 % at all conditions. It was concluded that although both RPSAC and ACRPSAC proved to be suitable adsorbents for fluoride uptake in systems that provide for the range of the studied process conditions, ACRPSAC was found to be the most efficient as compard to RPSAC and CAC.

Isothermal modeling studies showed that fluoride uptake by ACRPSAC, RPSAC and CAC were all chemisorption controlled as fluoride adsorption was best described with the Langmuir model (R^2 = 0.880 – 0.975) for all adsorbents, thus confirming the relative homogenous inclinition of the tested materials. The maximum Langmuir adsorption capacity (q_e) for RPSAC, ACRPSAC and CAC were 2.24, 4.10 and 2.26 mg/g respectively. The separation factor (RL) at the optimum process conditions for RPSAC (0.05), ACRPSAC (0.03) and CAC (0.3) show that fluoride uptake was favourable for all the adsorbent materials tested.

Furthermore, three reaction-based models (PFO, PSO and Elovich) were tested to provide insights on the dynamics of F^- uptake by the three adsorbents. It was observed that the PSO model best represented the kinetics of fluoride uptake by the materials (R^2 = 0.997 – 0.999), with ACRPSAC exhibiting a faster adsorption rate as evidenced from its higher adsorption capacity for fluoride ions. Similarly, two mechanistic models (WMIPD, BPD) were tested on the adsorption data for the three adsorbents and it was observed that particle-particle spread was not the controlling rate factor in the adsorption of fluoride onto the adsorbents' surface.

Fluoride adsorption on ACPSAC and RPSAC involved all of surface (film), pore and intra-particle diffusion mechanisms. Fluoride removal by RPSAC and ACRPSAC also involved surface complexation, precipitation and ion exchange mechanisms as elucidated from the XRD and EDX spectrums of the adsorbents.

Additionally, Fluoride adsorption was found to be endothermic (confirming chemisorption process) and spontaneous for ACRPSAC and RPSAC, while it was

endothermic but non-spontaneous for CAC, which was responsible for its lower fluoride uptake capacity.

For optimization studies, ACRPSAC was selected and further evaluated using RSM to obtain the optimum process conditions and pave way for the testing of ACRPSAC for actual groundwater defluoridation. RSM results showed that maximum fluoride removal abilities (100 % and 2.45 mg/g) of ACRPSAC was possible at initial fluoride content, interaction time, carbon dosage, temperature and pH of 5 mg/L, 30minutes, 0.6g and 35 °C respectively.

Confirmatory studies at the stipulated optimum conditions using actual undergroundwater with initial concentrations of 4.06 mg/L (Kaltungo) and 7.24 mg/L (Langtang) showed that ACRPSAC showed fluoride uptake efficiency of 92.8 and 85.6 % for undergroundwater samples obtained from deep wells in these areas of North-Central Nigeria respectively. The residual fluoride concentrations of the ACRPSAC-treated water also fell lower than the WHO admissible limit of 1.5mg/L in each case.
Regeneration and reuse of RPSAC and ACRPSAC was found to be effective with the use of NaOH and recoating with Al $(OH)_3$ respectively in one cycle.

Furthermore, there was a diverse variability in groundwater features obtained from 21 sampling points in Makurdi metropolis-Nigeria. The concentration of F^- in the water varied greatly across the sampling points and an exceedance of the threshold limit (1.5 mg/L) was found in over 33 % of the samples. Multivariate statistics showed that fluoride enrichment in the water was chiefly caused by natural processes with a little contribution from human activities. 66.7, 71.4, 52.4 and 9.5 % of the samples had hazard quotients (HQ) that were > 1, which suggest the risk of fluorosis in infants, children, teenagers and adults respectively in the study area.

Thus, ACRPSAC was adjudged to be the most efficient adsorbent interms of its high removal efficiency (> 90 %), adsorption capacity (> 4 mg/g) and ease of regeneration for groundwater defluoridation in batch systems as compared to RPSAC and CAC. Furthermore the study concluded that there was a high level of fluoride contamination of groundwater in Makurdi metropolis, Nigeria and recommended the use of ACRPSAC in batch mode for fluoride containment of groundwater at household levels to avert the high risk of fluorosis in the area.

5.3 Recommendations

The following recommendations are made as a fall-out from the current work:

1. ACRPSAC is recommended as the most effective adsorbent for batch fluoride removal in drinking water as compared to RPSAC and CAC and should be deployed under the process conditions of 4.0 mg/L, 120 minutes, 2 g/L and 35^{o}C for initial concentration, contact time, adsorbent dosage and process temperature respectively.
2. It is also recommended that a higher dose of ACRPSAC should be applied to the same quantity of groundwater sourced from regions with fluoride concentrations above the recommended optimum value of 4.0 mg/L as indicated in this study.
3. Competitive batch adsorption studies for fluoride and other common contaminants of groundwater should be carried using ACRPSAC in future research.
4. The model parameters estimated in this study should be used to design a single or two-stage ACRPSAC-based batch adsorber system with reduced contact times to encourage large scale treatment of fluoride contaminated water.
5. Fixed bed studies on the adsorption of fluoride in groundwater using ACRPSAC should be undertaken to provide more design parameters for the deployment of continuous flow Point of Use (PoU) and/or Point of Service (PoS) adsorption systems for fluoride containment in drinking water.
6. Other oxides/hydroxides of metals such as calcium, magnesium, manganese, iron etc should also be explored as potential agents for the functionalization of Raffia palm shells-derived adsorbent for fluoride and other contaminants adsorption from aqueous media.
7. Groundwater quality assessment for fluoride contamination should be encouraged in other parts of Nigeria in order to provide more data for efficient water resources management in the country.

5.4 Contributions to Knowledge

The following contributions have been made to knowledge from this work:

1. A novel and easily reproducible procedure has been developed for the optimal synthesis and characterization of activated carbon from Raffia palm shells for groundwater defluoridation.
2. Procedures and mechanisms for effective fluoride uptake on Raffia palm shells-derived activated carbon have been elucidated in this work. This would pave way for synthesis of similar materials for pollutants removal in drinking water sources.
3. A method for assessment of groundwater water quality with emphasis on fluoride contamination and human health risk in the tropics have been proposed and validated. This would serve as a reference approach for similar studies.

REFERENCES

Abia, A. A. and Asuquo, E. D. 2007. Kinetics of Cd^{2+} and Cr^{3+} sorption from aqueous solution using mercaptaacetic acid modified and unmodified oil palm fibre (*Elaeis guineensis*) adsorbents. *Tsinghua Science and Technology* 12: 485 – 492.

Achary, M. S., Panigrahi, S., Satpathy, K. K., Prabhu, R. K. and Panigrahy, R. C. 2016. Health risk assessment and seasonal distribution of dissolved trace metals in surface waters of Kalpakkam, southwest coast of Bay of Bengal. *Regional Studies in Marine Science* 6: 96–108, https://doi.org/10.1016/j.rsma.2016.03.017.

Adak, M. K., Sen, S. and Dhak, D. 2017. Removal of fluoride from drinking water using highly efficient nano-adsorbent, Al(III)- Fe(III)-La(III) trimetallic oxide prepared by chemical route. *Journal of Alloys and Compounds* 719: 460 - 469, http://dx.doi.org/10.1016/j.jallcom.2017.05.149.

Adel, A. M., Abd El- Wahab, Z. H., Ibrahim, A. A. and Al- Shemy, M. T. 2010. Characterization of microcrystalline cellulose prepared from lignocellulosic materials. Part I. Acid catalysed hydrolysis. *Bioresources Technology* 101. 12: 4446 – 4455..

Adeyeye, O. A., Xiao, C., Zhang, Z., Yawe, A. S. and Liang, X. 2021. Groundwater fluoride chemistry and health risk assessment of multi-aquifers in Jilin Qianan, Northeastern China. *Ecotoxicology and Environmental Safety* 211: 111926, https://doi.org/10.1016/j.ecoenv.2021.111926.

Adimalla, N. and Ventogi, S. 2017. Mechanism of fluorideenrichment in groundwater of hard rock aquifers in Medak, Telangana state, india. Environmental Earth Science 76: 45. https://doi.org/10.1007/s12665-016-6362-2.

_____ Li, P. and Venkatayogi, S. 2018. Hydrogeochemical evaluation of groundwater quality for drinking and irrigation purposes and integrated interpretation with water quality index studies. *Environmental Processes* 5: 363–83.

_____ Venkatayogi, S. and Das, S. V. G. 2019. Assessment of fluoride contamination and distribution: A case study from a rural part of Andhra

Pradesh, India. *Applied Water Science* 9: 94, https://doi.org/10.1007/s13201-019-0968-y.

_____ and Li, P. 2019. Occurrence, health risks, and geochemical mechanisms of fluoride and nitrate in groundwater of the rock-dominant semi-arid region, Telangana State, India. *Human and Ecological Risk Assessment: An International Journal* 25. 1-2: 81-103.

Adinata, D., Daud, W.M.A.W. and Aroua, M.K. 2007. Preparation and characterization of activated carbon from palm shell by chemical activation with K_2CO_3. *Bioresources Technology 98:145-149.*.

Aghazadeh, N., Chitsazan, M. and Golestan, Y. 2016. Hydrochemistry and quality assessment of groundwater in the Ardabil area, Iran. *Applied Water Science* 7. 7: 3599– 3616. https://doi.org/10.1007/s13201-016-0498-9.

Ahmad, A. A., Hameed, B. H. and Ahmad, A. L. 2009. Removal of disperse dye from aqueous solution using waste-derived activated carbon: optimization study. *Journal of Hazardous Materials* 170. 2- 3: 612 - 619.

Ahmedna, M., Johns, M. M., Clark, S. J., Marshall, W. E. and Rao, M. M. 1997. Potential of Agricultural By-products Based activated Carbon for Use in Raw Sugar Discoloration. *Journal of Food and Agriculture* 75: 117-124.

_____ Marshall, W. E. and Rao, R. M. 2000. Production of granular activated carbons from select agricultural by-products and evaluation of their physical, chemical and adsorption properties. *Bioresources Technology* 71. 2: 113 - 123.

Ajai, D. M., Arigbede, A. O., Dosumu, O. O. and Ufomata, D. 2012. The prevalence and severity of dental fluorosis among secondary school children in Ibadan-Nigeria. *Niger Postgraduate Medical journal 19. 2: 102-106.*

Akafu, T., Chimdi, A. & Gomoro, K. (2019). Removal of fluoride from drinking water by sorption using diatomite modified with aluminum hydroxide. *Journal of Analytical Methods in Chem*istry 4831926: 1–11, https://doi.org/10.1155/2019/4831926.

Akoteyon, I. S. 2013. Hydro-chemical studies of ground water in parts of Lagos, Southwestern Nigeria. *Bulletin of Geography – Physical Geography Series* 6: 27 – 42.

Akpata, E. S. 2004. Oral health in Nigeria. *International Dental Journal 54. 3: 361 - 366.*

_____Danifillo, I. S., Otoh, E. C. and Mafeni, J. O. 2009. Geographical mapping of fluoride levels in drinking water sources in Nigeria. *African Health Sciences* 9. 4: 227- 233.

Akpen, G. D., Aho, M. I. and Mamwan, M. H. 2018. Equilibrium and kinetics of colour adsorption from textile wastewater by a novel adsorbent. *Global Journal of Pure and Applied Sciences* 24: 61 – 67.

Akuh, T. I. 2014. Hydrogeology and groundwater quality in Makurdi metropolis and its environs, part of Makurdi (sheet 251), North Central Nigeria. M. Sc. Project, Department of Geology, Faculty of Science, Amhadu Bello University, Zaria, Nigeria. xvi + 151pp.

Alagumuthu, G., Veeraputhiran, V. and Venkataraman, R. 2011. Fluoride sorption using *Cynodon dactylon*-based activated carbon. *Hem. Ind. 65. 1: 23–35.*

Alhogbi, B. G., Altayeb, S., Bahaidarah, A. E. and Zawrah, M. F. 2021. Removal of anionic and cationic dyes from wastewater using activated carbon from palm tree fiber waste. *Processes* 9: 416, https://doi.org/10.3390/pr9030416.

Ali, S. A. and Ali, U. 2018. Hydrochemical characteristics and spatial analysis of groundwater quality in parts of Bundelkhand Massif, India. *Applied Water Science* 8:39.

Ali, S., Thakur, S. K., Sarker, A. and Shekhar, S. 2016. Worldwide contamination of water by fluoride. *Environmental Chemistry Letters. DOI: 10.1007/s10311-016-0563-5*.

Alkali, S. A. 2016. Optimization of activated carbon preparation from corncob for wastewater treatment, M. Sc. Project, Department of Chemical Engineering, Faculty of Engineering, Ahmadu Bello University, Zaria, Nigeria. xvii + 158pp.

Al-Omran, A., Al-Barakah, F., Altuquq, A., Aly, A., Nadeem, M. 2015. Drinking water quality assessment and water quality index of Riyadh, Saudi Arabia. *Water Qual. Res. J. Can*. 50. 3:287–296.

Alslaibi, T., Abustan, I., Azmier, M. and foul, A. A. 2013. A review: Production of activated carbon from agricultural byproducts via conventional and microwave heating. *Journal of Chemical Technology and Biotechnology* 88. 7, DOI: 10.1002/jctb.4028.

Alvarez-Puebla, R. A, Valenzuela-Calahorro, C. and Garrido, J. J. 2004. Retention of Co(II), Ni(II) and Cu(II) on a purified brown humic acid: Modeling and characterization of the sorption process. *Langmuir* 20: 3657–3664.

Amalraj, A. and Pius, A. 2017. Removal of fluoride from drinking water using aluminum hydroxide coated activated carbon prepared from bark of *Morinda tinctoria. Applied Water Science* 7:2653–2665, DOI 10.1007/s13201-016-0479-z

Amadi, A, N., Tukur, A., Okunola, I. A., Olasehinde, P. I. and Jimoh, M. O. 2015. Lithologic influence on the hydrogeochemical characteristics of groundwater in Zango, North-west Nigeria. *Natural Resources and Conservation* 3. 1: 11-18.

Amit, B. Eva, K. and Mika, S. 2011. Fluoride removal from water by adsorption: A review. *Chemical Engineering Journal* 171: 811-840

Amor, T. B., Kassem, M., Hajjaji, W., Jamoussi, F., Amor , M. B. and Hafiane, A. 2018. Study of defluoridation of water using natural clay minerals. *Clays and Clay Minerals* 66. 6: 493–499, DOI: https://doi.org/10.1346/CCMN.2018.064117.

Aniogbu, F. N. 2017. Production and Characterization of Charcoal Briquettes from Raffia Palm Shells. B.Eng. Project, Department of Agricultural and Environmental Engineering, Federal University of Agriculture, Makurdi-Nigeria. xviii + 172pp.

Anupam, K., Dutta, S., Bhattacharjee, C. and Datta, S. 2011. Adsorptive removal of chromium (VI) from aqueous solution over powdered activated carbon: Optimization through response surface methodology. *Chemical Engineering Journal* 173. 1: 135– 143.

APHA, 2005. Standard Methods for the Examination of Water and Wastewater, twentieth ed. American Public Health Association, Baltimore, Maryland, USA.

Araga, R., Soni, S. and Sharma, C. S. 2017. Fluoride adsorption from aqueous solution using activated carbon obtained from KOH treated Jamun (*Syzygium cumini*) seed. *Journal of Environmental Chemical Engineering* 5: 5608–5616.

Arami-Niya, A., Daud, W. M. A. W. and Mjalli, F. S. 2011. Comparative study of the textural characteristics of oil palm shell activated carbon produced by

chemical and physical activation for methane adsorption. *Chemical Engineering Research & Design* 89. 6: 657–664.

ASTM Method D2866-94 (2004). Standard test method for total ash content of activated carbon.

_____ D9214 (1996). Potentiometric determination of fluoride in aqueous samples with ion selective electrodes.

Ashley, P. P. and Burley, M. J. 1994. Controls on the Occurrence of Fluoride in Groundwater in the Rift Valley of Ethiopia. In: *Groundwater Quality*. H., Nash, and G. J. McCall, eds. Oxford: Chapman and Hall. 45-54,

Asuma, O. O., Emekeme, R. I., Aweto, K. E., Ofomola, M. V. 2020. Geophysical investigation of resistivity and groundwater quality in Ogbeh-Ijoh coastal area of Western Niger-Delta of Nigeria. *Applied Water Science* 10:70. https://doi.org/10.1007/s13201-020-1144-0.

Auta, M. and Hameed, B. H. 2011. Optimization waste tea Activated Carbon for Adsorption of methylene blue and acid blue 29 dyes using response surface methodology. *Chemical Engineering Journal* 125: 233-243

_____ 2012. Optimization of tea waste activated carbon preparation parameters for removal of cibacron yellow dye from textile waste waters. *International Journal of Advanced Engineering Research Studies 1. 4: 50-56.*

Ayoob, S., Gupta, A.K. and Bhat, V.T. 2008. A conceptual overview on sustainable technologies for the defluoridation of drinking water. *Critical Reviews in Environmental Science and Technology* 38. 6: 401 – 470. https://doi.org/10.1080/10643380701413310..

Azargohar, R. and Dalai, A. K. 2005. Production of activated carbon from Luscar char:Experimental and modeling studies. *Microporous and Mesoporous Materials* 85: 219- 225.

Babaeivelni, K. and Khodadoust, A. P. 2013. Adsorption of fluoride onto crystalline titanium dioxide: Effect of pH, ionic strength, and co-existing ions. *Journal of Colloid Interface Science* 394: 419–427.

Babu, S. S., Kumar, S., Chowdhury, T. R. and Bhowmick, S. 2015. Occurrence and impacts of fluoride in drinking water: A review. *Indian Groundwater* 5: 40-54.

Bacaoui, A., Yaacoubi, A., Dahbi, C., Bennouna, R., Phan, T., Luu, F. J., Maldonado-Hodar, J., Rivera-Utrilla, C. and Moreno, C. 2001. Optimization of conditions

for the preparation of activated carbons from Olive-waste cakes. *Carbon* 39: 425-432.

Barret, E. P., Joyner, P. B. and Hatenda, P. 1951. The determination of pore volume and area distribution in porous substances: computations from nitrogen isotherms. *Journal of Analytical Chemistry* 73: 373-380.

Bello, L. D. 2020. Fluorosis: An ongoing challenge for India. *The Lancet* 4. 3: E93 – E94.

Bello, M. O., Abdus-Salam, N., Adekola, F. A., Pal, U. 2021. Isotherm and kinetic studies of adsorption of methylene blue using activated carbon from ackee apple pods. *Chemical Data Collections 31: 1 – 9, https://doi.org/10.1016/j.cdc.2020.100607*.

Bempah, C. K. 2014. Arsenic Contamination of Groundwater in South Western Part of Ashanti Region of Ghana. PhD Thesis, Faculty of Environmental Sciences and Process Engineering, Brandenburg University of Technology, Cottbus-Senftenberg, Germany. xxi + 256pp.

Bhatia, S. C. 2009. *Environmental pollution and control in chemical process industry.* 2nd ed. Delhi: Khara Publishers.

Boyle, D. R. and Chagnon, M. 1995. An incidence of skeletal fluorosis associated with groundwaters of the maritime Carboniferous basin, Gaspé region, Quebec, Canada. *Environmental Geochemistry and Health* 17: 5 - 12.

Bia, G., De Pauli, C. P. and Borgnino, L. 2012. The role of Fe(III) modified montmorillonite on fluoride mobility: adsorption experiments and competition with phosphate. *Journal of Environmental Management* 100: 1–9.

Biswas, K. Gupta, K. and Ghosh, U. 2009. Adsorption of fluoride by hydrous iron (III)–tin (IV) bimetal mixed oxide from the aqueous solutions. *Chemical Engineering Journal* 149: 196 - 206,

Bura, B. and Goni, I. B. 2012. Tracing the factors influencing the occurrence of fluoride in groundwater of the middle zone aquifer in Borno State, North-Easthern Nigeria. *Journal of Mining and Geology* 48. 2: 177-184.

_____Goni, I. B., Sherrif, B. M. and Gazali, A. K. 2018. Occurrence and distribution of fluoride in groundwater of chad formation aquifers in Borno State, Nigeria. *International Journal of Hydrology* 2. 4: 528-537.

Cai, H., Xu, L., Chen, G., Peng, C., Ke, F., Liu, Z. *et al.*, 2016. Removal of fluoride from drinking water using modified ultrafine tea powder processed using a ball-mill. *Applied Surface Science* 375: 74-84, https://doi.org/10.1016/j.apsusc.2016.03.005

Calvi, C., Martinez, D., Dapena, C., Gutheim, F. 2016. Abundance and distribution of fluoride concentrations in groundwater: La Ballenera catchment, southeast of Buenos Aires Province, Argentina. *Environmental Earth Science* 75: 534. https://doi.org/10.1007/s12665-015- 4972-8.

Chai, L., Wang, Y., Zhao, N., Yang, W. and You, X. 2013. Sulfate-doped Fe_3O_4/Al_2O_3 nanoparticles as a novel adsorbent for fluoride removal from drinking water. *Water Research* 47. 12: 4040–4049.

Chakrapani, C. H., Suresh, C. H. B., Vani, K. N. K. and Somasekhara, R. K. 2010. Adsorption kinetics for the removal of fluoride from aqueous solution by activated carbon adsorbents derived from the peels of selected citrus fruits. *E-Journal of Chemistry* 7. S1**:** S419-S427.

Chan O. S., Cheung W. H. and McKay G. 2006. Preparation and characterization of demineralized tyre derived activated carbon. *Carbon* 49: 4674- 4687.

Chebet, E. B., Kibet, J. K., Mbui, D. 2020. The assessment of water quality in River Molo water basin, Kenya. *Applied Water Science 10: 92*, https://doi.org/10.1007/s13201-020-1173- 8.

Chen, N., Zhang, Z., Feng, C., Zhu, D., Yang, Y. and Sugiura, N. 2011. Preparation and characterization of porous granular ceramic containing dispersed aluminum and iron oxides as adsorbents for fluoride removal from aqueous solution, *Journal of Hazardous Materials* 186. 1: 863–868.

Chabukdhara, M., Gupta, S. K., Kotecha, Y. and Nema, A. K. 2017. Groundwater quality in Ghaziabad district, Uttar Pradesh, India: Multivariate and health risk assessment. *Chemosphere* 17: 167–178.

Chetan, P. S. and Suthar, S. 2019. Assessment of human health risk associated with high groundwater fluoride intake in southern district of Punjab, India. *Exposure and Health* 11. 2: 267-275, https://doi.org/10.1007/s12403-017-0268-4.

Chubaakum, P., Parimal, C. B., Aola, S., Mridushmita, B., Upasana B. S. and Dipak, S. 2018. Adsorption of Fluoride onto activated carbon synthesized from *Manihot esculenta* biomass: Equilibrium, kinetic and thermodynamic studies.

Journal of Environmental Chemical Engineering, https://doi.org/10.1016/j.jece.2018.02.045

Coates, J. 2000. Interpretation of infrared spectra, A practical approach. *Encyclopedia of Analytical Chemistry*. R.A. Meyers Eds. Newtown, John Wiley & Sons. 10815-10837.

Cuhadar, C. 2005. Production and characterization of activated carbon from hazelnut shell and hazelnut husk. M. Sc. Project. Graduate School of Natural and Applied Sciences, Middle East Technical University, Turkey. xvi + 102pp.

Daifullah, A. A. M., Yakout, S. M.and. Elreefy, S. A. 2007. Adsorption of fluoride in aqueous solutions using KMnO4- modified activated carbon derived from steam pyrolysis of rice straw, *Journal of Hazardous Materials* 147: 633–643. doi:10.1016/j.jhazmat.2007.01.062.

Danbature, W. L., Fai, F. Y. and Ayim, P. 2014. Determination of fluoride and some effects on drinking water of Kaltungo Local government Area of Gombe State, Nigeria. *Asian Journal of Science and Technology* 5. 2: 124-128.

Dash, N., Dasb, S., Patnaik, T., Patel, S. B. and Dey, R. K. 2013. Development of a new manganese oxide modified aluminium oxy (hydroxide) for the effective removal of fluoride from drinking water. *Advances in Applied Science Research* 4. 4: 387-399.

Daud, W. M. A. W. and Ali, W. S. W. 2004. Comparison on pore development of activated carbon produced from palm shell and coconut shell. *Bioresources Technology* 93: 63 – 69, doi:10.1016/j.biortech.2003.09.015.

De Lima, L. S., Araujo, M. D. M., Quináia, S. P., Migliorine, D. W. and Garcia, J. R. 2011. Adsorption modeling of Cr, Cd and Cu on activated carbon of different origins by using fractional factorial design. *Chemical Engineering Journal* 166. 3: 881–889.

Deng, Y., Nordstrom, D. K. and McCleskey, R. B. 2011. Fluoride geochemistry of thermal waters in Yellowstone National Park I: Aqueous fluoride speciation. *Geochemica Et Cosmochimica Acta,* 75: 4476 – 4489.

Dessalegna, M., Zewge, F., Mammo, W., Woldetinsae, G. and Diaz, I. 2018. Effective fluoride adsorption by aluminium oxide modified clays: Ethiopian clays vs commercial montmorillonite. Bulletin of the *Chemical Society of Ethiopia* 32. 2: 199–211, DOI: https://dx.doi.org/10.4314/bcse.v32i2.2.

De Souza, C. F. M., Lima Jr., J. F., Adriano, M. S. P. F., de Calvaho, F. G., Forte, F. D. S., Oliveira, R. F. *et al.*, 2013. Assessment of groundwater quality in a region of endemic fluorosis in the North-east of Brazil. *Environmental Monitoring & Assesment* 185**:** 4735–4743. https://doi.org/10.1007/s10661-012-2900-x.

Dey, S., Goswami, S. and Gosh, U. C. 2004. Hydrous ferrix oxide (HFO)-A scavenger for fluoride from contaminated water. *Water Air Soil Pollution* 158: 311-323.

Dhanya, R. and Shaji, I. 2017. Fluoride contamination in groundwater resources of Alleppey, Southern India. *Geoscience Frontier* 8. 1: 117-124.

Diao, Y., Walawender, W. P. and Fan, L. T. 2002. Activated carbons prepared from phosphoric acid activation of grain sorghum. *Bioresources Technology* 81. 1: 45-52.

Dibal, H. U., Schoeneich, K., Garba, I., Lar, U. A. and Bala, E. A. 2012a. Overview of fluoride distribution in major aquifer units inNorthern Nigeria. *Health* 4. 11: 1287-1294.

_____ Schoeneich, K., Garba, I., Lar, U.A. and Bala, E. A. 2012b. Occurrence of fluoride in the drinking waters of Langtang area, north central Nigeria. *Health* 4. 11: 1116-1126, http://dx.doi.org/10.4236/health.2012.411169

_____ Schoeneich, K., Lar, U. A., Garba, I., Lekmang, I. K. and Daspan, R. I. 2016. Hydrogeochemical appraisal of fluoride in groundwater of Langtang area, Plateau State, Nigeria. *Global Journal of Geological Sciences*, 14: 23-39. **DOI:** http://dx.doi.org/10.4314/gjgs.v14i1.3

Dirisu, C. G., Mafiana, M. O., Okwodu, N. E., and Isaac, A. U. 2016. Fluoride content of community Drinking Water: Biological and public health implications. *American Journal of Water Resources* 4. 3: 54-57.

Diaz-Barriga, F., Leyva, R., Quistian, J., Loyola-Rodriguez, J. B., Pozos, A., Grimaldo, M. 1997. Endemic fluorosis in San Luis Potosi, Mexico. *Fluoride* 30: 219-222.

Doke, K. M. and Khan, E. M. 2012. Equilibrium, kinetic and diffusion mechanism of Cr (VI) adsorption onto activated carbon derived from wood apple shell. *Arabian Journal of Chemistry*. 10.1016/j.arabjc.2012.07.031.

Dominguez, E. L., Uttran, A., Loh, S. K., Manero, M., Upperton, R., Taminu, M. I. *et al.,* 2020. Characterization of industrially produced oil palm kernel shell biochar and its potential use as slow release nitrogen-phosphorus fertilizer and carbon sink. *Materials Today Proceedings* 31, 1: 221 – 227.

Dong, C., Wu, X., Gao, Z., Yang, P. and Khan, M.Y.A. 2021. A novel and efficient metal-oxide fluoride absorbent for drinking water safety and sustainable development. *Sustainability* 13: 883, https:// doi.org/10.3390/su13020883.

Edmunds, W. M. and Walton, N. 1983. The Lincolnshire Limestone - hydrogeochemical evolution over a ten-year period. *Journal of Hydrology* 61: 201-211.

Egbueri, J. C. and Mgbenu, C. N. 2020. Chemometric analysis for pollution source identification and human health risk assessment of water resources in Ojoto Province, southeast Nigeria. *Applied Water Science* 10:98, https://doi.org/10.1007/s13201-020- 01180-9.

Elliott, C. G, Colby, T. V, Kelly, T. M, Hicks, H. G. 1989. Charcoal, lung, Bronchiolitis obliterans after aspiration of activated charcoal. *Chest* 96. 3: 673 – 684, doi: 10.1378/chest.96.3.672.

Elizalde-González, M. P., Mattusch, J., Peláez-Cid, A. A. and Wennrich, R. 2007. Characterization of adsorbent materials preparaed from avocado kernel seeds: Natural, activated and carbonized forms. *Journal of Analytical & Applied Pyrolysis* 78. 1: 185 - 193.

El-Nadeaf, M. A. I. and Honkala, E. 1998. Fluorosis in relation to fluoride in water in central Nigeria. *Community Dentistry and Oral Epidemiology,* 26. 1: 26-30.

Emenike, P. C., Nnaji, C. C. and Tenebe, I. T. 2018a. Assessment of geospartial and hydrochemical interactions of groundwater quality, Southern Nigeria. *Environmental Monitoring and Assessments* 2018: 190-440, DOI: doi.org./10.1007/s10661-018-6799-8.

_____Tenebe, I. T. and Jarvis, P. 2018b. Fluoride contamination in groundwater sources in Southwestern Nigeria: Assessment using multivariate statistical approach and human health risk. *Ecotoxicology and Environmental Safety* 156: 391-402.

Eneji, I.S., Sha'Ato, R. and Annune, P. 2011. An assessment of heavy metals loading in River Benue in the Makurdi Metropolitan Area in Central Nigeria.

Environmental Monitoring and Assessment 184. 1: 201 – 207, DOI: 10.1007/s10661-011-1959-0.

Ephraim-Emmanuel, B. C., Dotimi, D. A., Kei, B. O and Joshua, C. 2013. Prevalence of Dental fluorosis: A case study of the Government Secondary School Ogbia, Bayelsa State, Nigeria. *Continental Journal of MedicalResearch* 7. 2: 1 – 8.

Abara, A. A., Ogbomade, R., and Francis, E. 2016. Prevalence of dental fluorosis among secondary school children in Oloibiri Community. *International Journal of Tropical Diseases and Health 11. 1: 1-7.*

Erabee, I. K., Alhsan, A.,, Zularisam, A. W., Idrus, S., Daud, N., Arunkumar, T., Sathyamurthy, R., and Al-Rawajfeh, A. E. 2017. A new activated carbon prepared from sago palm bark through physiochemical activated process with zinc chloride. *Engineering Journal* 21. 5: 1–14.

FAOSTAT, 2014. FAO Statistical Data Base-Agriculture. Retrieved at http://apps.fao.org.on 6th March 2020.

Faraji, S. and Ani, F. N. 2015. Development of supercapacitor from activated carbon by electroless plating – A review. *Renewable and Sustainable Energy Reviews* 42: 823 – 834.

Fawell, J., Bailey, K., Chilton, J., Dahi, E., Fewtrell, L. and Magara, Y. 2006. *Fluoride in Drinking-Water*. Geneva: World Health Organization.

Fuhong, R. and Shuquin, J., 1988. Distribution and formation of high-fluorine groundwater in China. *Environmental Geology and Water Science* 12: 3-10.

Fulata, M. A., Busugumu, U. A., Ngubdo, A. M., Bukama, A. M. and Gadam, A. 2017. Determination of fluoride in some boreholes (A case of Monguno Local government Area). *Chemistry Research Journal* 2. 4: 42-46.

Ganyaglo, S. Y., Gibrilla, A., Teye, E. M., Owusu-Ansah, E. D. J., Tettey, S., Diabene, P. Y. *et al.* 2019. Groundwater fluoride contamination and probabilistic health risk assessment in fluoride endemic areas of the Upper East Region, Ghana. *Chemosphere*, 233: 862– 872,

Gbadebo, A. M. 2012. Groundwater fluoride and dental fluorosis in Southern Nigeria. *Environmental Geochemistry and Health 34. 5: 597 -604.*

Getachew, T., Hussen, A. and Rao, V. M. 2015. Defluoridation of water by activated carbon prepared from banana (*Musa paradisiaca*) peel and coffee (*Coffea*

arabica) husk. *International Journal of Environmental Science &.Technology* 12:1857–1866.

Gevera, P. and mouri, H. 2018. Natural occurrence of potentially harmful fluoride contamination in groundwater: An example from Nakuru County, the Kenyan Rift Valley. *Environmental Earth Sciences* 77: 356.

Ghasemi, M., Ghoreyshi, A. and Younesi, H. 2015. Synthesis of a high characteristics activated carbon from walnut shell for the removal of Cr(VI) and Fe(II) from aqueous solution: single and binary solutes adsorption. *Iran Journal of Chemical. Engineering* 12: 1 – 29.

Ghogomu, J. N., Muluh, S. N., Ajifack, D. L., Alongamo, A. A. B. and Noufame, D. T. 2016. Adsorption of Lead (II) from Aqueous Solution using Activated Carbon Prepared from Raffia Palm (Raphia Hookeri) Fruit Epicarp. *IOSR Journal of Applied Chemistry* 9. 7: 74-85.

Gitari, W. M., Izuagie, A. A. and Gumbo, J. R. 2020. Synthesis, characterization and batch assessment of groundwater fluoride removal capacity of trimetal Mg/Ce/Mn oxide-modified diatomaceous earth. *Arabian Journal of Chemistry* 13. 1: 1–16.

Giwa, A. A., Bello, L. A., Oladipo, M. A. and Adeoye, D. O. 2013. Removal of cadmium from wastewater by adsorption using the husk of melon (*Citrullus lanatus*) seeds. *International Journal of Basic and Applied Science* 2. 1: 110 – 123.

Gomez, K. R., Lopez-Pasquali, C. E., Gonzalez, G. P., Hernando, P. F., Garcinuno-Martinez, R. M. 2020. Statistical evaluation of fluoride contamination in groundwater resources of Santiago del Estero Province, Argentina. *Geoscience Frontiers* 11: 2197– 2205. .

Gomoro, K., Zewgwe, F., Hundhammer, B, and Megersa, N. 2012. Fluoride removal by adsorption on thermally treated laterite soils. *Bulletin of the Chemical Society of Ethiopia* 26. 3: 361–372.

Goyit, M. P., Solomon, O. A. and Kutshuk, R. J. 2018. Distribution of fluoride in surface and ground water: A case study of Langtang North, Plateau State, Nigeria. *Int. J. Biol. Chem. Sci.* 12. 2: 1057-1067,

Gorzin, F. and Abadi, M. M. B. R. 2017. Adsorption of Cr (VI) from aqueous solution by adsorbent prepared from paper mill sludge: kinetics and thermodynamic studies *Adsorption Science and Technology* 12:.1 – 21.

Gwaha, A. M. 2017. Dental fluorosis in a rural Nigerian Community: Is the water to blame? B.Sc. Project , Department of Natural and Environmental Sciences, American University of Nigeria, xiv + 64pp.

Guo, J. and Lua, A. C. 2003. Textural and chemical properties of adsorbent prepared from palm shell by phosphoric acid activation. *Materials Chemistry and Physics* 80. 1: 114–119.

Haimour, N. M. and Emeish, S. 2006. Utilization of date stones for production of activated carbon using phosphoric acid. *Waste Management* 26: 651–660.

Haji, M., Karuppannan , **S.,** Qin, D., Shube, H., Kawo**,** N. S. 2021. Potential human health risks due to groundwater fluoride contamination: A case study using multi-techniques approaches (GWQI, FPI, GIS, HHRA) in Bilate River Basin of Southern main Ethiopian Rift, Ethiopia. *Archives of Environmental Contaminants and Toxicol*ogy 80. 1: 277- 293, https://doi.org/10.1007/s00244-020-00802-2.

Halla, V. L., Esmeralda, V., Luis, F. J., Horacio, F. and Rene, R. J. 2015. Water defluoridation with special emphasis on adsorbents-containing metal oxides and/or hydroxides: a review. *Separation & Purification Technology* 150: 292-307.

Hamilton, M. 1992. Water fluoridation: a risk assessment perspective. *Journal of Environmental Health* 54: 27-32.

Handa, B. K. 1995. Geochemistry and genesis of fluoride-containing groundwater in India. *Groundwater* 13. 3: 275–281.

Hared, I. A., Dirion, J. L., Salvador, S., Lacroix, M. and Rio, S. 2007. Pyrolysis of wood impregnated with phosphoric acid for the production of activated carbon: Kinetics and porosity development studies. *Journal of Analytical and Applied Pyrolysis* 79. 1-2: 101 - 105.

Hassani A., Alidokht L., Khataee A. R., and Karaca S., 2014. Optimization of comparative removal of two structurally different basic dyes using coal as a low-cost and available adsorbent. *Journal of the Taiwan Institute of Chemical Engineers* 45. 4: 1597–1607.

Hem, J. D. 1985. Study and interpretation of the chemical characteristics of natural water. *USGS Water Supply Paper* 2254. Oct. 5: 263-268.

Hilmi, S. S. 2001. Application of the Kozeny-Carman Equation to Permeability Determination for a Glacial Outwash Aquifer, Using Grain-size Analysis, *Energy Sources* 23 .5: 461- 473, DOI: 10.1080/009083101300058480.

Hosseini, H., Shakeri, A., Rezaei, M., Barmaki, M. D. and Mehr, M. R. 2019. Water chemistry and water quality pollution indices of heavy metals: a case study of Chahnimeh Water Reservoirs, Southeast of Iran. *International Journal of Energy and Water Resources* 4. 1: 63-79, https://doi.org/10.1007/s42108-019-00051-7.

Hu, Z. and Srinivasan, M. P. 1999. Preparation of high-surface-area activated carbons from coconut shell. *Microporous Mesopoous Materials.* 27: 11-18.

_____ and _____ 2001. Mesoporous high surface area activated carbon, *Microporous Mesoporous Materials.* 43. 3: 267 - 275.

_____ Srinivasan, M. P., and Ni, Y. 2001. Novel activation process for preparing highly microporous and mesoporous activated carbons. *Carbon* 39: 877 – 886, doi: 10.1016/S0008-6223(00)00198-6.

Hussein,, M., Zainal, Z. and Keong, K. 1995. The preparation of activated carbon from chips of oil palm trunk catalyzed by $ZnCl_2/CO_2$: Surface area and porosity studies. *Journal* of *Chemical Technology & Biotechnology* 64. 3: 35 - 40.

Inaniyan, M. and Raychoudhury, T. 2018. Application of activated carbon–metal composite for fluoride removal from contaminated groundwater in India. *International Journal of Environmental Science & Technology* 15. 11, https://doi.org/10.1007/s13762-018- 2097-9.

Inyinbor, A. A., Adekola, F. A. and Olatunji, G. A. 2016. Kinetics, isotherms and thermodynamic modeling of liquid phase adsorption of Rhodamine B dye onto *Raphia hookerie* fruit epicarp. *Water Resources and Industry* 15:14–27. http://dx.doi.org/10.1016/j.wri.2016.06.001.

_____and _____ 2017. Kinetics and isothermal modeling of liquid phase adsorption of Rhodamine B onto urea modified *Raphia hookeri* epicarp. *Applied Water Science* 7: 3257–3266, DOI : 10.1007/s13201-016-0471-7.

Iorliam, A.Y., Okwu, P. and Ukya, T. J. 2013. Geotechnical properties of Makurdi shale treated with bamboo leaf ash. *AU J.T*, 16. 3: 174 -180.

IRIS U. 2017. Integrated Risk Information System, USEPA, accessed at https://cfpubepagov/ ncea/iris/search/indexcfm?keyword=fluoride.8 on 15 june 2020.

Isikwue, M. O. and Onyilo, A. F. 2010. Influence of land use on the hydraulic response of a loamy sand tropical soil. *Journal of Emerging Trends in Engineering and Applied Sciences* 1. 2: 144 – 149.

_____and Adakole, S. A. 2011. Effect of tillage and soil cover on soil erosion in the Lower Benue River Basin of Nigeria. Proceeding of The Nigerian Branch of International Soil Tillage Research Organisation (ISTRO). 10th Eds., 335-345.

Islam, S. M. and Mostafa, M. G. 2021. Meta-analysis and risk assessment of fluoride contamination in groundwater. *Water Environment Research* 2020: 1194-1216, Doi: https://doi.org/10.1002/wer.1508.

Itodo, A. U., Abdulrahman, F. W., Hassan, L. G., Maigandi, S. A. and Itodo, H. U. 2010a. Application of methylene blue and iodine adsorption in the measurement of specific surface area by four acid and salt treated activated carbons. *New York Science Journal* 3. 5: 25 – 33.

_____ Itodo, H. U. and Gafar, M. K. 2010b. Estimation of specific surface area using Langmuir isotherm method. *Journal of Applied Science & Environmental Management* 14. 4: 141–145.

Iwar, R.T. 2015. Studies on the removal of residual pollutants in pre-treated brewery effluents using local adsorbents. M.Sc. Project, Department of Agricultural and Environmental Engineering. University of Ibadan. Ibadan, Nigeria. xvii + 168pp.

_____Utsev, J. T.and Hassan, M. 2021d. Assessment of heavy metals and physico chemical pollution loadings of River Benue water at Makurdi using water quality index and multivariate statistics. *Applied Water Science* 11. 7: *124*, https://doi.org/10.1007/s13201-021-01456-8.

Jagtoyen, M. and Derbyshire, F. 1998. Activated carbon from yellow poplar and white oak by H_3PO_4 activation. *Carbon*, 36:1085-1097.

Jia, H., Qian, H., Qu, W., Zheng, L., Feng, W. and Ren, W. 2019. Fluoride occurrence and human health risk in drinking water wells from Southern edge of Chinese Loess Plateau. *International Journal of Environmental Research & Public Health* 16: 1683. doi:10.3390/ijerph16101683.

Jiaping, P.C. 2012. Decontamination of heavy metals: Processes, mechanisms and applications. 1st ed. New York: CRC Press.

Jibril, B., Houache, O., Al-Maamari, R. and Al-Rashidi, B. 2008. Effects of H_3PO_4 and KOH in carbonization of lignocellulosic material. *Journal of Analytical & Applied Pyrolysis* 83: 151 - 156.

Kaghazachi, T., Asasian-Kolur, N. and Soleimani, M. 2010. Licorice residue and Pistachionut shell mixture: A promising precursor for activated carbon. *Journal of Industrial & Engineering Chemistry* 16. 3: 368 - 374.

Kang, D., Yu, X., Tong,S., Ge, M., Zuo, J., Cao, C. and Song, W. 2013. Performance and mechanism of Mg/Fe layered double hydroxides for fluoride and arsenate removal from aqueous solution. *Chemical Engineering Journal* 228: 731 – 740.

Kang, J., Li, B., Song, J., Li, D., Yang, J., Zhan, W. and Liu, D. 2011. Defluoridation of water using calcined magnesia/pullulan composite. *Chemical Engineering Journal* 166. 2: 765–771.

Kanaujia, S., Singh, B. and Singh, S. 2015. Comparative study on removal of fluoride from groundwater by natural and modified bagasse carbon of sugarcane *International Research Journal of Pure and Applied Chemistry* 8: 147 – 156.

Karunanidhi, D., Aravinthasamy, P., Subramani, T., Jianhua Wu, J., Srinivasamoorthy, K. 2019. Potential health risk assessment for fluoride and nitrate contamination in hard rock aquifers of Shanmuganadhi River basin, South India. *Human and Ecological Risk Assessment: An International Journal*. https://doi.org/10.1080/10807039.2019.1568859.

Keta-Rokbani, M., Moncef, G. and Bouhlila, R. 2011. Use of geographical information system and water quality index to assess groundwater quality in El Khairat deep aquifer Enfidha,Tunisian Sahel. *Iran Journal of Energy and Environment* 2: 133 – 144.

Khan, S. J., Murchland, D. and Rhodes, M. 2009, Management of concentrated waste streams from high-pressure membrane water treatment systems. *Critical Reviews in Environmental Science and Technology* 39: 367–415.

Khataee, A. R. 2010. Optimization of UV-promoted peroxydisulphate oxidation of C.I Basic Blue-3 dye using response surface methodology. *Environmental Technology* 31. 1: 73–86.

Kilham, P. and Hecky, R. E. 1973. Fluoride: geochemical and ecological significance in East African waters and sediments. *Limnology & Oceanography,* 18: 932-945.

Kim Y. M., Harrad S. and Harrison R. M. 2001. Concentrations and Sources of VOCs in urban and public micro-environments, *Environmental Science & Technology* 35. 6: 997–1004.

Kiurski, J., Ranogajec, J., Vucetic, S., Zoric, D., Adamovic, S., Oros, I. and Krstic, J. 2012. Fired clay with polymer addition as printing developer purifier. *Applied Clay Science 6:* 48–52.

Kiram, S.M., Bhandari, R., Nehra, A., Manohar, C.S. and Belliraj, S.K. 2020. Zirconium- Cerium and Zirconium-Lanthanum complexed polyvinyl alcohol films for efficient fluoride removal from aqueous solution. *Journal of Dispersion Science and Technology* https://doi.org/10.1080/01932691.2020.1774386.

Kofa, G. P., Gomdje, V. H., Telegang, C. and Koungou, S. N. 2017. Removal of Fluoride from Water by Adsorption onto Fired Clay Pots: Kinetics and Equilibrium Studies. *Journal of Applied Chemistry* 6254683: 1–7.

Koilraj, P. and Kannan, S. 2013. Aqueous fluoride removal using Zn-Cr layered double hydroxides and their polymeric composites: Batch and column studies. *Chemical Engineering Journal* 234: 406–415.

Kondom, F. A., Iwar, R. T**.** and Kon, E. T. 2021. A comparison of water quality indexes for an inland river. *Journal of Engineering Research & Reports* 20. 4: 1–14.

Kumar, A., Balouch, A. and Abdullah, A. 2019. Remediation of toxic fluoride from aqueous media by varioustechniques. *International Journal of Environmental Analytical Chemistry*, https://doi.org/1.1080/03067319.2019.1669580.

Kwaghger, A. 2012. Evaluation of Activated Carbon from Mango Kernels for Adsorption Refrigeration Application. PhD. Thesis. Department of

Mechanical Engineering,. Federal University of Agriculture, Makurdi-Nigeria. xxiv + 208pp.

Kwaghger, A. and Ibrahim, J. S. 2013. Optimization of Conditions for the Preparation of Activated Carbon from Mango Nuts using HCl. *American Journal of Engineering Research* 2. 7: 74 - 85.

Laine, J., Calafate, A. and Labady, M. 1989. Preparation and Characterization of Activated Carbon from Coconut Shell Impregnated with Phosphoric Acid. *Carbon* 27. 2: 191-195.

Leco Corporation, Feb. 16, 2010. Carbon, Nitrogen and Sulfur in plant tissues. Organic Application Note. Retrieved on Aug. 30, 2020 at https://www.chromatographyonline.com/view/leco-corporation-2.

Limón-Pacheco, G. H., Jiménez-Córdova, M. J., Cárdenas-González, M., Retana, I. M. S. Gonsebatt, M. E. and Razo, L. M. D. 2018. Potential co-exposure to arsenic and fluoride and bio-monitoring equivalents for Mexican children. *Annals of Global Health* 84. 2: 257 – 273.

Liu, T., Gao, X., Zhang, X., Li, C. 2020. Distribution and assessment of hydrogeochemical processes of F-rich groundwater using PCA model: a case study in the Yuncheng Basin, China. *Acta Geochim.*,39. 2: 216–225. https://doi.org/10.1007/s11631-019-00374-6.

Liu, J., Zhao, P., Xu, Y. and Jia, X. 2019. Mg-Al mixed oxide adsorbent synthesized using FCT template for fluoride removal from drinking water. *Bioinorganic Chemistry and Applications* 5840205: 1-11, https://doi.org/10.1155/2019/5840205.

Loganathan, P., Vigneswaran, S., Kandasamy, J. and Naidu, R. 2013. Defluoridation of drinking water using adsorption processes. *Journal of Hazardous Materials* 248-249C. 1: 1-19. DOI: 10.1016/j.jhazmat.2012.12.043.

Lua A. C. and Yang T. 2004. Effect of activating temperature on the textural and chemical properties of potassium hydroxide activated carbon prepared from pistachio- nut shell. *Journal of Colloid Science* 274: 594- 601.

Magesh, N. S., Chandrasekar, N. and Elango, L. 2017. Trace element concentrations in the groundwater of the Tamiraparani river basin, South India: Insights from human health risk and multivariate statistical

techniques. *Chemosphere* 185: 468–479, doi: 10.1016/j.chemosphere.2017.07.044

Magoling, B. J. A. and Macalalad, A.A. 2017. Optimization and response surface modeling of activated carbon production from mahogany fruit husk for removal of chromium (VI) from aqueous solution, *Bioresources* 12. 2: 3001–3016.

Mahmud, A., Sikder, S., Joardar, J. C. 2020. Assessment of groundwater quality in Khulna city of Bangladesh in terms of water quality index for drinking purpose. *Applied Water Science* 10: 226. https://doi.org/10.1007/s13201-020-01314-z.

Mahamud, H. S. 2012. Pilot column studies on adsorption of fluoride onto coated high aluminium bauxite ore (HABO) and charcoal. M.Sc. Project, Department of Civil Engineering, Kwame Krumah University of Science and Technology. Ghana. Xviii + 100pp.

Maher, M., Hassan, S., Shoueir, K., Yousif, B. and Abo-Elsoud, M. E. A. 2021. Activated carbon electrode with promising specific capacitance based on potassium bromide redox additive electrolyte for supercapacitor application. *Journal of Materials Research and Technology* 11: 1232 – 1244.

Maitya, J. P., Hsuc , C. M., Lina, T. J., Leec , W. C., Bhattacharyad, P., Bundschuhde, J. and Chena, C. Y. 2018. Removal of fluoride from water through bacterial-surfactin mediated novel hydroxyapatite nanoparticle and its efficiency assessment: Adsorption isotherm, adsorption kinetic and adsorption thermodynamics. *Environmental Nanotechnology Monitoring & Management* 9: 18–2.

Malago, J., Makoba, E. and Muzuka, A. N. N. 2017. Fluoride levels in surface and groundwater in Africa: A review. *American journal of Water Science and Engineering* 3. 1: 1-17.

Malum, J. F., Onoja, S. B. and Udochukwu, M. O. 2019. Prevalence of fluoride contamination in ground watersources in Kaltungo, Gombe State, Nigeria. *International Journal of Trends in Research and Development* 6. 1: 2394-2403

Makoba, E. and Mazuka, A. N. N. 2017. Water quality and hydrogeochemical characteristics of groundwater around Mt. Meru, Northern Tanzania. *Applied Water Science,* 9: 120, https://doi.org/10.1007/s13201-019-0955-3.

_____ and _____ 2018. Natural occurrence of potentially harmful fluoride contamination in groundwater: an example from Nakuru County, the Kenyan Rift Valley.*Environmental & Earth Sciences* 77: 365, https://doi.org/10.1007/s12665-018-7466-7.

Mandal, S. and Mayadevi, S. 2009. Defluoridation of water using as-synthesized Zn/Al/Cl anionic clay adsorbent: Equilibrium and regeneration studies. *Journal of Hazardous Materials* 167:873-878.

Manjunatha, C. R., Nagabhushana, B. M.., Narayana, A., Pratibha, S. and Raghu, M. S. 2019. Effective and fast adsorptive removal of fluoride on $CaAl_2O_4$:Ba nanoparticles: isotherm, kinetics and reusability studies. *Materials Research Express* 6. 11: 5089.

Mariappan, R., Vairamuthu, R. and Ganapathy, A. 2015. Use of chemically activated cotton nut shell carbon for the removal of fluoride contaminated drinking water: Kinetics evaluation, *Chinese Journal of Chemical Engineering* 23: 710–721, doi:10.1016/j.cjche.2014.05.019.

Marshall, E. 1990. The fluoride debate: one more time. *Science,* 247: 276 - 277.

Menéndez-Díaz, J. A. and Martín-Gullón, I. 2006. Types of carbon adsorbents and their production. *Interface Science and Technology* 7: 1–48.

Metcalf and Eddy 2003. Wastewater Engineering: Treatment and Reuse. 2nd ed. New York: McGraw Hill.

Mianowski, A., Owczarek, M. and Marecka, A. 2007. Surface area of activated carbon determined by the iodine adsorption number. *Energy Sources, Part A: Recovery, Utilization and Environmental Effects* 29. 9: 839–850.

Miguel, S. G., Fowler, G. D., Dall'Orso, M. and Sollars, C. J. 2001. Porosity and surface area characteristics of activated carbons produced from waste tyre rubber. *Journal of Chemical Technology & Biotechnology* 77: 1–8.

_____ Fowler, G. D., and Sollars, C. J. 2003. A study of the characteristics of activated carbons produced by steam and carbon dioxide activation of waste tyre rubber. *Carbon* 41. 5: 1009 –1016.

Minju, N., Venka, S. K., Haribabu, K., Sivasubramanian, V. and Senthil, K. P. 2015. Removal of fluoride from aqueous media by magnesium oxide-coated Nanoparticles. *Desalination & Water Treatment* 53: 2905–2914.

Mohammad, Y. S., Shaibu-Imodagbe E. M., Igboro S. B., Giwa A., and Okuofu C. A., 2014. Modeling and Optimization for Production of Rice Husk Activated Carbon and Adsorption of Phenol; *Journal of Engineering* 2014: 1-11, https://doi.org/10.1155/2014/278075.

Mohammadi, S.Z., Karimi, M.A, Afzali, D. and Mansouri, F. 2010. Removal of Pb(II) from aqueous solutions using activated carbon from Seabuckthorn stones by chemical activation. *Desalination* 262. 1–3: 86–93.

Mohammed, H. D., Mansoureh, F., Mahmood, A., Mojtaba, A. and Gordon, M. 2018. Adsorptive removal of fluoride from water by activated carbon derived from $CaCl_2$ – modified *Crocus sativus* leaves: Equilibrium adsorption isotherms, optimization and influence of anions. *Chemical Engineering Communications,* DOI: 10.1080/00986445.2018.1423969. .

Mohammed-Ridha, M. J., Ahmed, A. S. and Raoof, N. N. 2017. Investigation of the thermodynamic, kinetic and equilibrium parameters of batch bio-sorption of Pb(II), Cu(II) and Ni(II) from aqueous phase using low cost bio-sorbent. *Al-Nahrain Journal of Engineering Science* 201: 298 – 310.

Mohammed, M. A., Babagana G. and Bitrus K. H. 2015. Production and Characterization of Activated Carbon From Groundnut Shell Sourced in Maiduguri. *Columbia Journal of Life Science* 17. 1: 18-24.

Mohan, D., Sharma, R., Singh, V. K., Steele, P. and Pittman, C. U. Jr. 2012. Fluoride removal from water using bio-char, a green waste, low-cost adsorbent: equilibrium uptake and sorption dynamics modeling. *Industrial Engineering Chemistry Research* 51: 900–914.

Mohapatra, M., Hariprasad, D., Mohapatra, L., Anand, S. and Mishra, B. K. 2012. Mg-doped nano ferrihydrite: A new adsorbent for fluoride removal from aqueous solutions. *Applied Surface Science* 258. 01: 4228–4236.

Mondal, N. K. and Kundu, M. 2016. Bio-sorption of fluoride from aqueous solution using lichen and its Ca-pretreated biomass. *Water Conservation Science &. Engineering* 1: 143–160.

Montgomery, D. C. 2001. Design and analysis of experiments. 5th ed. New York: John Wiley and Sons.

Mopoung, S., Moonsri, P., Palas, W. and Khumpai, S. 2015. Characterization and properties of activated carbon prepared from Tamarind seeds by KOH

activation for Fe(III) adsorption from aqueous solution. *The Scientific World Journal* 2015: 1–9,

Moreno-Castilla, C., Carrasco-Marín, F., López-Ramón, M. V. and Alvarez-Merino, M. A. 2001. Chemical and physical activation of olive-mill waste water to produce activated carbons. *Carbon* 39. 9: 1415 - 1420.

Mosonik, C .B. 2015. Assessment of fluoride levels in different water sources in lower region of Bomet County, Kenya and remediation using Moringa oleifera seed cake. MSc. Project. Department of Chemistry. Jomo Kenyatta University of Agriculture and Technology. xvi + 73pp.

Mozammel, H. M., Ota, M. and Bhattacharya, S. C. 2002. Activated carbon from coconut shell using $ZnCl_2$ activation. *Biomass and Bioenergy* 22. 5: 397–400.

Mphoweh, J. N., Mesmin, T., Awah, D. and Njombissie, P. I. C. 2015. Agricultural expansion and raffia palm destruction: the case of Bamunka, N.W. Cameroon. *E3 Journal of Environmental Research and Management.* 6. 5: 0304-0314.

Mridha, D., Priyadarshni, P., Bhaskar, K., Gaurav, A., De, A., Joarder, M., *et al.*, 2021. Fluoride exposure and its potential health risk assessment in drinking water and staple food in the population from fluoride endemic regions of

Bihar, India. *Groundwater for Sustainable Development* 13: 100558, Doi: https://doi.org/10.1016/j.gsd.2021.100558.

Mudzielwana, R., Gitari, W. M., Akinyemi, S. A. and Msagati. T. A. M. 2017. Synthesis, characterization, and potential application of Mn2+- intercalated bentonite in fluoride removal: adsorption modeling and mechanism evaluation. *Applied Water Science* 7: 4549–4561,

Mukhopadhyay, K., Ghosh, A., Das, S. K., Show, B., Sasikumar, P. and Ghosh, U. C. 2017. Synthesis and characterization of cerium(IV)-incorporated hydrous iron(III) oxide as an adsorbent for fluoride removal from water. *RSC Advances* **7**: 26037-26051.

Murugan, M. and Subramanian, E. 2006. Studies on defluoridation of water by Tamarind seed, an unconventional biosorbent. *Journal of Water and Health* 4. 4:453-461.

Mwampashi, E. S. 2011). Fluoride removal using bauxite and charcoal as low-cost adsorbents, M.Sc. Project, Unesco-IHE, Delft, Netherland, xv + 158pp.

Nabbou, N., Belhachemi, M., Boumelik, M., Merzougui, T., Lahcene, D., Harek, Y. *et al.* 2019. Removal of fluoride from groundwater using natural clay (kaolinite): Optimization of adsorption conditions. *Comptes Rendus Chimie* 22. 2–3: 105-112.

Nandiyanto, A. B. D., Oktiani, R. and Ragadhita, R. 2019. How to read and interpret FTIR spectroscope of organic material. Indonesian Journal of Science and Technology 4, 1: 97 – 118.

Nakazawa, K., Nagafuchi, O., Otede, U., Chen, J., Kanefuji, K. and Shinozuka, K. 2020. Risk assessment of fluoride and arsenic in groundwater and a scenario analysis for reducing exposure in Inner Mongolia. *RSC Advances* 10: 18296 – 18304.

NISDWQ, 2007. Nigerian Standards for Drinking Water Quality. Retrieved on Nov. 18, 2019 at https://www.health.gov.ng/doc/StandardWaterQuality.pdf.

NOAA, 2016.. National Oceanic and Atmospheric Administration Climatic Report. Release 17-006.. Accessed at https://www.nasa.gov on 7th December, 2020.

Nurul'ain, B. J. 2007. The production and characterization of activated carbon using local agricultural waste through chemical activation process. M.Sc. Project. School of Materials and Mineral Engineering. Universiti Sains Malaysia, Penang, Malaysia. xvi + 95pp.

Nwabanne, J. T. 2010. Adsorption and kinetic modelling of heavy metals uptake from wastewater effluents. Ph.D. Thesis, Department of Chemical Engineering, Nnamdi Azikiwe University, Awka-Nigeria. xxii + 236 pp.

Ogwuche, 2016. Production and characteristics of activated carbon from Raffia palm seeds and shells. B.Eng. Project. Department of Agricultural and Environmental Engineering, Federal University of Agriculture, Makurdi-Nigeria. xvii + 135pp.

Okoye, C. C., Onukwuli, O. D.and Okey-Onyesolu, C. F. 2019. Utilization of salt activated *Raphia hookeri* seeds as bio-sorbent for Erythrosine B dye removal: kinetics and thermodynamics studies. *Journal of King Saud University – Science* 31, 4: 849 – 858. https://doi.org/10.1016/j.jksus.2017.11.004.

Okwuchukwu, P. 2017. Column studies on the removal of cadmium in aqueous solution using Raffia Palm (*Raphia hookeri*) seed activated carbon. B.Eng. Project. Department of Agricultural and Environmental Engineering, Federal University of Agriculture, Makurdi-Nigeria. xvi + 124pp.

Oloworise F. J. 2006. Production and Characterization of Activated Carbon from Rice Husk. B.Eng. Project. Department of Chemical Engineering, Federal University of Technology, Minna-Nigeria. xv + 89pp.

Okunola, I. A., Amadi, A. N., Olasehinde, P. I., Maspalma, S. S. and Okoye, N. O. 2016. Quality assessment of groundwater from shallow aquifers in Hong area, Adamawa State, northern Nigeria. *Ife journal of Sciences* 18. 1: 267-283.

Olasehinde, P. I., Amadi, A. N., Dan-Hassan, M. A., Jimoh, M. O. and Okunola, I. A. 2015. Statistical assessment of groundwater quality in Ogbomosho, South-West Nigeria. *American Journal of Mining and Metallurgy* 3. 1: 21-28.

_____ Amadi, A. N., Okunola, I. A., Dan-Hassan, M. A. and Jimoh, M. O. 2016. Occurrence of fluoride and some heavy metals in groundwater from shallow aquifers near Ogbomosho, North-Central Nigeria. *Journal of Natural Sciences Research* 6. 13: 55-60.

Olugbenga, S. B., Bukola, M. L., Olamide, J. A. and Vunian, E. 2017. Scavenging Rhodamine B dye using *Moringa oleifera* seed pod. *Chemical Speciation and Bio- availability*, 29. 1: 120-134.

Onyango, M. S., Kojimia, Y., Aoyi, O., Bernardo, E. C. and Matsuda, H. 2004. Adsorption equilibrium modeling and solution chemistry dependence of fluoride removal from water by trivalent-cation-exchange zeolite F-9. *Journal of Colloids and Interface Science* 279: 341-350.

Ozacar, M. and Sengil, A. 2006. A two stage batch adsorber design for methylene blue removal to minimize contact time. *Journal of Environmental Management* 80, 4: 372 – 379.

Parkhurst, D. L. and Appelo, C. A. J. 1999. User's guide to PHREEQC (Version 2) - A computer program for speciation, batch-reaction, one-dimensional transport, and inverse geochemical calculations. *Water-Resources Investigations Report* 99 - 4259. USGS, Denver.

Phan, N. H., Rio, S., Faur, C., Le Coq, L., Le Cloirec, P. and Nguyen, T. H. 2006. Production of fibrous activated carbons from natural cellulose (jute, coconut) fibers for water treatment applications. *Carbon* 44: 2569–2577.

Prahas, D., Kartika, Y., Indraswati, N. and Ismadji, S., 2008. Activated carbon from jackfruit peel waste by H_3 PO_4 chemical activation: pore structure and surface chemistry characterization, *Chemical Engineering Journal* 140. 1-3: 32-42.

Puziy, A. M., Poddubnaya, O. I., Martínez-Alonso, A., Suárez-García, F. and Tascón, J. 2005. Surface chemistry of phosphorus-containing carbons of lignocellulosic origin. *Carbon* 43: 2857–2868.

Radfard, M., Rahmatinia, M., Akbari, H., Hashemzadeh, B., Akbari, H., Adibzadeh, A. 2018. Data on health risk assessment of fluoride in water distribution network of Iranshahr, Iran. *Data in Brief* 20:1446–1452. https://doi.org/10.1016/j.dib.2018.08.184.

Radovic, L. R. 2001. Chemistry and physics of carbon materials. 27th Ed. New York: Marcel Dekker, Inc.

Rafique, T., Naseem, S., Usmani, T. H., Bashir, E., Khan, F. A. and Bhanger, M. I. 2009. Geochemical factors controlling the occurrence of high fluoride groundwater in the Nagar Parkar area, Sindh, Pakistan. *Journal of Hazardous Materials* 171: 424–430.

_____ Chadhar, K. M., Usmani, T. H., Memon, S. Q., Shirin, K., Kamaluddin, S. and Soomro, F. 2015. Adsorption behavior of fluoride ion on trimetal-oxide adsorbent. *Desalination & Water Treatment* 56: 1669-1680.

Rajkumar, S., Murugesh, S., Sivasankar, V., Darchen, A., Msagati, T. A. M. and Chaaban, T. 2019. Low-cost fluoride adsorbents prepared from a renewable bio-waste: Syntheses, characterization and modeling studies. *Arabian Journal of Chemistry* 12: 3004–3017.

Rahmani, K., Mahvi, A. H., Vaezi, F., Mesdaghinia, A. R., Nabizade, R. and Nazmara, S. 2009. Bio removal of lead by use of waste activated sludge. *International Journal of Environmental Research* 3: 471- 476.

Rango, T., Kravchenko, J., Atlaw , B., Mc Cornick , P. G., Jeuland, M., Merola, B., *et al.*, 2012. Groundwater quality and its health impact: An assessment of dental fluorosis in rural inhabitants of the Main Ethiopian Rift. *Environment International* 43: 37 – 47. doi:10.1016/j.envint.2012.03.002.

Ranasinghe, N., Kruger, E., Tennant, M. 2019. Spatial distribution of groundwater fluoride levels and population at risk for dental caries and dental fluorosis in Sri Lanka. *International Dental Journal* 69: 295–302.

Rashid, A., Guan, D., Farooqi, A., Khan, S., Zahir, S., Jehan, S. 2018. Fluoride prevalence in groundwater around a fluorite mining area in the flood plain of the River Swat, Pakistan. *Science of the Total Environment* 635: 202 – 213. https://doi.org/10.1016/j.scitotenv.2018.04.064

Rasool, A., Xiao, T., Farooqi, A., Shafeeque, M., Masood, S., Ali, S., Fahad, S. and Nasim, W. 2016. Arsenic and heavy metal contaminations in the tube well water of Punjab, Pakistan and risk assessment: a case study. *Ecological Engineering* 95: 90–100.

Ravikumar, P., Somashekar, R. K., 2017. Principal component analysis and hydrochemical facies characterization to evaluate groundwater quality in Varahi river basin, Karnataka state, India. *Appled Water Science* 7: 745–755, http://dx.doi.org/10.1007/ s13201-015-0287-

Reddy, A. G. S., Reddy, D. V., Rao, P. N. and Prasad, K. M. 2010a. Hydrogeochemical characterization of fluoride rich groundwater of Wailpalli watershed, Nalgonda District, Andhra Pradesh, India. *Environmental Monitoring & Assessment* 171: 561–577.

Reddy, D. V., Nagabhushanam, P., Sukhija, B. S., Reddy, A. G. S., Smedley, P. L. 2010b. Fluoride dynamics in the granitic aquifer of the Wailapally watershed, Nalgonda District, India. *Chemical Geology*, 269: 278-289.

Rodriguez-Reinoso F. 2002. Surface composition and structure of active carbon. *Handbook of porous solids, Vol 3*. F., Schuth, K., Sing. and J. Weiltkamp, eds. Wiley-VCH Verlag GmbH, Weinheim, Germany, 1-17.

Roy, P., Mondal, N. K. and Das, K. 2014. Modeling of the adsorptive removal of arsenic: a statistical approach. *Journal of Environmental Chemical Engineering* 2. 1: 585–597.

Sabio, E., Gonzalez, E., Gonzalez, J.F., Gonzalez-Garcia, C.M., Ramiro, A. and Ganan, J. 2004. Thermal regeneration of activated carbon saturated with p-nitrophenol. *Carbon*, 42. 11: 2285–2293.

Saha, I., Ghosh, A., Nandi, D., Gupta, K., Chatterjee, D. and Ghosh, U.C. 2015. β-Cyclodextrin modified hydrous zirconium oxide: Synthesis, characterization and defluoridation performance from aqueous solution. *Chemical Engineering Journal* 263: 220–230.

Sahu, N., Bhan, C., Sigh, J. 2021. Removal of fluoride from an aqueous solution by batch and column process using activated carbon derived from iron infused *Pisum sativum* peel: characterization, isotherm and kinetics study. *Environmental Engineering Research 26. 4: 200241*, https://doi.org/10.4491/eer.2020.241.

Salifu, A., Petrusevski, B., Ghebremichael, K., Buamah, R. and Amy, G., 2012. Multivariate statistical analysis for fluoride occurrence in groundwater in the Northern region of Ghana. *Journal of Contaminant Hydrology* 140–141: 34–44.

_____ Petrusevski, B., Mwampashi, E. S., Pazi, I. A., Ghebremichael, K., Buamah, R., Aubry, C., Amy, G. L. and Kenedy, M. D. 2016. Defluoridation of groundwater using aluminum-coated bauxite: optimization of synthesis process conditions and equilibrium study. *Journal of Environmental Management* 181: 108–117.

_____ 2017. Fluoride removal from groundwater by adsorption technology: The occurrence, adsorbent synthesis, regeneration and disposal. PhD Thesis. UNESCO-IHE Institute for Water education, Delft, Netherlands. xxiv + 276pp.

Salman, J. M. and Hussein, F. 2014. Batch adsorber design for different solution volume/adsorbate mass ratios of bentazon, carbofuran and 2-4-D adsorption onto date seeds activated carbon. *Journal of Environmental Analytical Chemistry* 2, 1: 1 – 5.

Saxena, V. K. and Ahmed, S. 2001. Dissolution of fluoride in groundwater: a water-rock interaction study. *Environmental Geology* 40: 1084–1087.

Sellami, M., Riahi, H., Maatallah, K., Ferjani, H., Bouaziz, M. C., Ladeb, M. F. 2019. Skeletal fluorosis: don't miss the diagnosis! *Skeletal Radiology*, https ://doi.org/10.1007/s0025 6- 019-03302 -0.

Sentorun-Shalaby, C., Ucak- Astarhoglu, M.G., Artok, L. and Sarici, C. 2006. Preparation and characterization of activated carbons by one- step steam pyrolysis/ activation from apricot stones. *Microporous and Mesoporous Materials* 88: 126–134.

Sharaf, M. A. M.. and Subyani, A. M. 2011. Assessing of Groundwater Contamination by Toxic Elements through Multivariate Statistics and Spatial Interpolation, Wadi Fatimah, Western Arabian Shield, Saudi Arabia. *International Journal of Scientific and Engineering Research* 2: 9 – 16.

Shen, J. and Schäfer, A. I. 2015. Factors affecting fluoride and natural organic matter (NOM) removal from natural waters in Tanzania by nano-filtration/reverse osmosis. *Science of the Total Environment* 527–528:520–529.

Singh K. P., Gupta S., Singh A. K., and Sinha S. 2010. Experimental design and response surface modeling for optimization of Rhodamine B removal from water by magnetic nano-composite. *Chemical Engineering Journal* 165. 1: 151–160.

Smedley, P. L., Nicolli, H. B., Macdonald, D. M. J., Barros, A. J., Tullio, J. O. 2002. Hydrogeochemistry of arsenic and other inorganic constituents in groundwaters from La Pampa, Argentina. *Applied Geochemistry* 17: 259-284.

Smisek, M. and Cerny, S. 1970. Active carbon manufacture, properties and applications. New York: Elsevier Pub. Comp.

Soleimani, M. and Kaghazchi, T. 2008. The investigation of the potential of activated hard shell of apricot stones as gold adsorbents. *Journal of Industrial & Engineering Chemistry* 14: 28-37.

Srinivasakannan, C. and Zailani, M. B. 2004. Production of activated carbon from rubber wood sawdust. *Biomass & Bioenergy* 27: 89- 96.

Su, H., Kang, W., Kang, N., Liu, J. and Li, Z. 2021. Hydro-geochemistry and health hazards of fluoride-enriched groundwater in the Tarim Basin, China. *Environmental Research* 200: 111476.

Sundaryanto, Y., Hartono, S. B., Irawaty, W., Hindarso, H. and Ismadji, K. 2006. High surface area activated carbon prepared from cassava peel by chemical activation. *Bioresources Technology* 97: 734- 739.

Suneetha, M., Sundar, B. S. and Ravindhranath, K. 2015. Removal of fluoride from polluted waters using active carbon derived from barks of *Vitex negundo* plant. *Journal of Analytical Science & Technology* 6: 15-24.

Sunkari, E. D., , Zango, M. S., Abu, M. and Lermi, A. 2019. Occurrence, health risks and geochemical mechanisms of fluoride in groundwater of the Northeastern region, Ghana. *1st International Conference on Environment, Technology and Management (ICETEM).* 1456-1466.

Tan, I. A. W., Ahmad, A. L. and Hameed, B. H. 2007. Preparation of Coconut Husk Activated Carbon: Optimization Study on Removal of 2, 4, 6-Trichlorophenol using Response Surface Optimization Method. *Journal of Hazardous Materials* 153: 709-717.

Tangsir, S., Hafshejani, L. D., Lahde, A., Maljanen, M., Hooshmand, A., Naseri, A. A. *et al.* 2016. Water defluoridation using Al_2O_3 nanoparticles synthesized

by flame spray pyrolysis (FSP) method. *Chemical Engineering Journal* 288: 198-206.

Thakur, R. S., Katoch, S. S. and Modi, A. 2020. Assessment of pine cone derived activated carbon as an adsorbent indefluoridation. *SN Applied Sciences*, 2: 1407. https://doi.org/10.1007/s42452-020-03207-x.

The World Gazetteer, 2010. Arch GIS data and map. Retrieved April, 6th 2020 at https://www.arcgis.com/home/item.html?id=346ce13fa2d4468a9049f71bcc250f37.

Thole, B. 2013. Groundwater contamination with fluoride and potential fluoride removal technologies for East and Southern Africa: Perspectives in water pollution. Blantyre: INTECH Open Science. 66-90.

Tirkey, P., Bhattacharya, T., Chakraborty, S., Baraik, S. 2017. Assessment of groundwater quality and associated health risks: a case study of Ranchi city, Jharkhand, India. *Groundwater for Sustainable Development* 5: 85–100. http://dx.doi.org/10.1016/j.gsd.2017.05.002.

Tukur, A., and Amadi, A. N. 2014. Fluoride contamination of shallow groundwater in parts of Zango Local Government area of Kastina State, North-West Nigeria. *Journal of Geosciences and Geomatics* 2. 5: 178-185.

Turner, B. D., Binning, P. and Stipp, S. L. S. 2005. Fluoride removal by calcite: evidence for fluorite precipitation and surface adsorption. *Environmental Science & Technology* 39: 9561-9568.

Umesi-Koleoso, D. C. 2004. Dental fluorosis and other enamel disorders in 12-years old Nigerian children. *Journal of Community Medicine and Primary health Care*, 16. 1: 25-28.

Uriah, L.A., Dibal, H., and Schoeneich, K. 2014. Fluoride in groundwater in Nigeria: Origin and human health impact. *American Journal of Environmental Protection* 3. 6: 66-69.

USEPA, 1975. National service centre for environmental publication, 1st Ed. New York: Mc- Graw Hill.

_____2011. Environmental Protection Agency Exposure Factors Handbook:. Retrieved on Oct. 28 2018 at https://doi.org/EPA/600/R-090/052F.

USNRC, 2006. Lost Crops of Africa: Volume II: Vegetables. Chapter 11. Locust bean. Washington, DC: The National Academies Press.

Utsev, J. T., Iwar, R. T., and Ifyalem, K. J. 2020. Adsorption of methylene blue from aqueous solution onto *Delonix regia* pod activated carbon: Batch equilibrium isotherm, kinetic and thermodynamic studies, *Materials & Environmental Science* 11. 7: 1058-1078.

Vadez-Alegria, C. J., Fuentes-Rivas, R. M., García-Rivas, J. L., Fonseca-Montes de Oca, R. M. G. and García-Gaitán, B. 2019. Presence and distribution of fluoride ions in groundwater for human in a semi-confined volcanic aquifer. *Resources,* 8. 116: 1- 16. doi:10.3390/resources8020116.

Virginia, H. M., Josafat, G. S. and Jose, I. V. B. 2012. Thermal treatments and activation procedures used in the preparation of activated carbons. V.H. Montoya Eds, Blantyre: InTech 302 – 425.

Vithanage, M., Bhattacharya, P. 2015. Fluoride in the environment: sources, distribution and defluoridation. *Environmental Chemistry Letters* 13. 2: 131–147.

Wang, F. Y., Wang, H., Ma, J. W. 2010. Adsorption of cadmium (II) ions from aqueous solution by a new low-cost adsorbent—bamboo charcoal. Journal of Hazardous Materials 117:.300 – 306.

Wang, L., Shi, C., Wang, L., Pan, L., Zhang, X. and Zou, J. 2020. Rational design, synthesis, adsorption principles and application of metal oxide adsorbents: A review. *RSC Nanoscale,* DOI: 10.1039/C9NR09274A.

Welgemoed, T. J. and Schutte, C. F. 2005. Capacitive deionization technology: an alternative desalination solution. *Desalination* 183: 237-240.

WHO. 2004. The World health report: Changing history. World Health Organization, Geneva, Swizerland. https://apps.who.int/iris/handle/10665/42891

_____ 2006. Fluoride in drinking water. In: Bailey, K., Chilton, J., Dahi, E., Lennon, M., Jackson, P. and Fawell, J. editors. WHO drinking water quality series. London, UK, IWA Publishing.

_____ 2008. Guidelines for drinking water quality, 3rd edition Vol. 1, Geneva, Swizerland.

_____ 2017. Guidelines for drinking water quality, 4th edition incorporating the first addendum. Geneva, Swizerland.

Wongdem, J. G., Aderinokun, G. A., Sridhar, M. K. and Selkur, S. 2000. Prevalence and distribution of pattern of enamel fluorosis in Langtang town, Nigeria. *American Journal of Medical Sciences 29. 2-4: 243-246.*

Woyessa, G. W., Srivastava, B. B. L. and Demissie, E. G. 2014. Synthesis of hydrous aluminum (III) -iron (III)- manganese (IV) ternary mixed oxide for fluoride removal, *International Journal of Science Engineering & Research* 5. 3: 885-892.

Xin-hui, D., Srinivasakannan, C., Qu, W. W., Xin, W., Jin-hui, P. and Li-bo, Z. 2012. Regeneration of microwave assisted spent activated carbon: process optimization, adsorption isotherms and kinetics. *Chemical Engineering &Process:Process Intensification* 53: 53 – 62.

Yadav, K. K., Kumar, S., Pham, B., Gupta, N., Rezania, S., Kamyab, H., *et al.,* 2019. Fluoride contamination: health problems and remediation methods in Asian groundwater: A comprehensive review. *Ecotoxicology and Environmental Safety* 182: 109362. https://doi.org/10.1016/ecoenv.2019.06.045.

Yagmur, E., Ozmak, M. and Aktas, Z. 2008. A novel method for production of activated carbon from waste tea by chemical activation with microwave energy. *Fuel* 87. 15 – 16: 3278 - 3285.

Yang T. and Lua A. C. 2003. Characteristics of activated carbons prepared from pistachio nut shells by physical activation. *Journal of Colloid & Interface Science* 267. 2: 408- 417.

Yavuz, R., Akyildiz, H., Karatepe N. and Çetinkaya, E. 2010. Influence of preparation conditions on porous structures of olive stone activated by H_3PO_4. *Fuel Process Technology* 9. 11: 80-87.

Yihunu, E. W., Yu, H., Junhe, W., Kai, Z., Teffera, Z. L., Weldegebrial, B. and Limin, M. 2020. A comparative study on defluoridation capabilities of bio-sorbents: Isotherm, kinetics, thermodynamics, cost estimation and regeneration study. *Environmental Engineering Research* 25. 3: 384-392.

Yousefi, M., Ghoochani, M., Mahvi, A. H. 2018. Health risk assessment to fluoride in drinking water of rural residents living in the Poldasht city, Northwest Iran. *Ecotoxicology and Environmental Safety* 148: 426 – 430.

Yu, Y. and Paul, C. J. 2014. Fabrication and performance of a Mn-La metal composite for remarkable decontamination of fluoride. *Journal of Materials Chemistry A* 2: 8086– 8093.

_____Yu, L. and Chen, J. P. 2015. Adsorption of fluoride by Fe–Mg–La triple-metal composite: Adsorbent preparation, illustration of performance and study of mechanisms. *Chemical Engineering Journal* 262: 839 –846.

Yusuff, A. S., Olateju, I. J. and Ekanem, S. E. 2017. Equilibrium, kinetic and thermodynamic studies of the adsorption of heavy metals from aqueous solution by thermally treated quail eggshell. *Journal of Environmental Science and Technology* 10. 5: 246 – 257.

_____ 2019. Adsorption of hexavalent chromium from aqueous solution by *Leucaena leucocephala* seed pod activated carbon: equilibrium, kinetic and thermodynamic studies. *Arab Journal of Basic and Applied Sciences, https://doi.org/10.1080/25765299.2019.1567656.*

Zhang, W., Mao, Y. and Lu, Y. 2021. Development of a novel *Artemia* eggshell-zirconium nano-composite for efficient fluoride removal. *PLoS ONE* 16. 1: e0244711, https://doi.org/10.1371/journal.pone.0244711.

Zhang, T., Qiurong, L., Zhenyu, M., Haiyan, X., Hongxiao, L. and Zho, Y. 2014. Adsorption of fluoride ions onto non-thermal plasma-modified CeO_2/$Al2O_3$ composites. *Desalination &Water Treatment* 52. 16 -18: 3367-3376.

Zhang, S., Lu, Y., Lin, X., Su, X. and Zhang, Y. 2014. Removal of fluoride from groundwater by adsorption onto La(III)- Al(III) loaded scoria adsorbent. *Applied Surface Science* 303: 1-5.

Zuo, S., Liu, J., Yang, J. and Cai, X. 2009. Effects of the crystallinity of lignocellulosic material on the porosity of phosphoric acid-activated carbon. *Carbon* 97. 15: 3578 – 3580.

APPENDICES

APPENDIX A

SUPPLEMENTARY DETAILS OF COMPUTATIONS FOR SYNTHESIS OF RPSAC

Proximate Analysis of Raffia Palm Shells

1. *Moisture Content (MC)*

Weight of empty can, W_1 = 63.50g
Weight of empty can + sample, W_2 = 66.33g
Weight of empty can + sample after oven drying, W_3 = 66.11g

$$\%\ moiture\ content = \frac{W2 - W3}{W2 - W1} \times 100$$

$$= \frac{66.33 - 66.11}{66.33 - 63.50} \times \frac{100}{1}$$

$$= \frac{0.22}{2.83} \times \frac{100}{1}$$

$$= \frac{22}{2.83}$$

$$= 7.77\%$$

2. *Ash Content (AC)*

Weight of empty crucible, W_1 = 78.89g
Weight of crucible + sample, W_2 = 81.82g
Weight of crucible + ash, W_3 = 78.93g

$$\%\ Ash\ content = \frac{W3 - W1}{W2 - W1} \times 100$$

$$= \frac{78.93 - 78.89}{81.82 - 78.89} \times 100$$

$$= \frac{0.04}{2.93} \times 100$$

$$= \frac{4}{2.93}$$

= 1.37%

3. *Fixed Carbon Content (FCC)*

W_1 = 78.68g
W_2 = 81.92g
W_3 = 79.69g

$$FCC = \frac{W2 - W3}{W2 - W1} \text{ x } 100$$

$$= \frac{81.92 - 79.69}{81.92 - 78.68} \text{ x } 100$$

$$= \frac{2.23}{3.24} \text{ x } 100$$

$$= \frac{2.23}{3.24} \text{ x } 100$$

$$= \frac{223}{3.24}$$

= 68.83%

4. *Volatile Matter (VM)*

FCC = 100- (AC+MC+MV)

68.83= 100- (1.37+7.77+MV)

9.14+MV=100-68.83

MV= 31.17-9.14

MV= 22.03%

Experimental Design for calculation of Carbon Yield

RUN	W_1 (g)	W_2 (g)	W_3 (g)	Carbon Yield (%)
1	56.90	96.60	64.90	67.18
2	60.40	94.50	68.80	72.80
3	59.90	93.50	68.10	72.83
4	77.10	107.10	85.20	79.55
5	61.00	121.00	84.10	69.50
6	51.70	95.30	64.90	68.10
7	51.10	83.50	56.30	67.43
8	65.70	112.50	80.10	71.20
9	56.70	109.70	84.10	76.66
10	58.70	102.50	72.60	70.83
11	68.50	115.50	81.30	70.39
12	50.40	85.00	61.90	72.82
13	65.20	112.10	81.50	72.70
14	58.00	93.00	72.20	77.55
15	58.00	108.60	79.90	73.57
16	60.50	96.40	76.10	78.94
17	58.00	109.40	75.00	68.56
18	52.10	92.60	64.00	69.11
19	69.10	98.10	78.30	79.82
20	68.80	118.50	86.80	73.25
21	61.30	119.00	90.80	76.30
22	53.60	79.50	61.40	77.23
23	69.50	112.80	80.10	71.01
24	55.40	84.80	64.50	76.06

25	50.60	94.70	60.20	63.57
26	62.00	108.10	71.40	66.05
27	68.60	98.80	78.10	79.05
28	51.30	84.00	62.40	74.29
29	52.20	81.80	57.30	70.05
30	51.60	91.30	68.90	75.47

KEYWORDS: W_1: Weight of empty crucible; W_2: Weight of crucible + sample**;** W_3: Weight of crucible + carbonized product

$$\% \text{ Carbon yield } = \frac{W_c}{W_r} \times 100$$

Where:

W_c is weight of carbonized product

W_r is weight of raw material.

Experimental Design for calculation of Surface Area (M^2/g)

RUN	Volume (M^3)	Surface Area (M^2/g)
1	56.66	1788
2	56.91	1796
3	57.59	1818
4	56.41	1780
5	56.28	1776
6	56.88	1795
7	58.66	1852
8	56.00	1764
9	52.88	1667
10	56.06	1769
11	55.56	1753

12	53.41	1684
13	53.28	1680
14	44.34	1394
15	55.56	1753
16	55.13	1739
17	55.75	1759
18	57.34	1810
19	56.66	1788
20	54.69	1725
21	55.22	1742
22	55.47	1750
23	57.06	1801
24	56.59	1786
25	56.88	1795
26	58.13	1835
27	55.97	1766
28	54.34	1714
29	55.47	1750
30	55.34	1746

KEYWORDS: Sears equation (1979) S= 32V-25

Where S= Surface area (m^2/g)

V= the volume of Sodium hydroxide (NaOH) required to raise the pH of the sample from 4-9

Model Analysis for Carbon Yield

Response 1 **Carbon Yield** **Transform:** **None**

Summary (detailed tables shown below)

Source	Sequential p-value	Lack of Fit p-value	Adjusted R-Squared	Predicted R-Squared	
Linear	0.0015	0.7459	0.4112	0.3197	
2FI	0.2712	0.8043	0.4609	0.4006	
Quadratic	0.0341	0.9886	0.6448	0.5216	Suggested
Cubic	0.9462	0.9410	0.4304	0.3310	Aliased

Sequential Model Sum of Squares [Type I]

Source	Sum of Squares	df	Mean Square	F Value	p-value Prob> F	
Mean vs Total	1.587E+005	1	1.587E+005			
Linear vs Mean	266.14	4	66.54	6.06	0.0015	
2FI vs Linear	83.47	6	13.91	1.38	0.2712	
Quadratic vs 2FI	91.62	4	22.90	3.46	0.0341	Suggested
Cubic vs Quadratic	24.97	8	3.12	0.29	0.9462	Aliased
Residual	74.32	7	10.62			
Total	1.592E+005	30	5307.62			

Lack of Fit Tests

Source	Sum of Squares	Df	Mean Square	F Value	p-value Prob> F	
Linear	201.84	20	10.09	0.70	0.7459	
2FI	118.38	14	8.46	0.58	0.8043	
Quadratic	26.76	10	2.68	0.18	0.9886	Suggested
Cubic	1.79	2	0.89	0.062	0.9410	Aliased
Pure Error	72.53	5	14.51			

Model summary statistics

Source	Std. Dev.	R-Squared	Adjusted R-Squared	Predicted R-Squared	PRESS	
Linear	3.31	0.4924	0.4112	0.3197	367.69	
2FI	3.17	0.6468	0.4609	0.4006	324.00	
Quadratic	2.57	0.8163	0.6448	0.5216	258.58	Suggested
Cubic	3.26	0.8625	0.4304	0.3310	361.60	Aliased

Std. Dev.	2.57	R-Squared	0.8163
Mean	72.73	Adj R-Squared	0.6448
C.V. %	3.54	Pred R-Squared	0.5216
PRESS	258.58	Adeq Precision	8.284
-2 Log Likelihood	121.04	BIC	172.06
		AICc	185.33

Descriptive

Factor	Coefficient Estimate	df	Standard Error	95% CI Low	95% CI High	VIF
Intercept	75.66	1	1.05	73.42	77.90	
A-Concentration	0.18	1	0.53	-0.94	1.30	1.00
B-Impregnation Ratio	1.59	1	0.53	0.48	2.71	1.00
C-Activation Temperature	-2.92	1	0.53	-4.04	-1.80	1.00
D-Activation Time	-0.022	1	0.53	-1.14	1.10	1.00
AB	0.028	1	0.64	-1.34	1.40	1.00
AC	-1.96	1	0.64	-3.33	-0.59	1.00
AD	0.47	1	0.64	-0.90	1.84	1.00
BC	0.78	1	0.64	-0.59	2.15	1.00
BD	0.64	1	0.64	-0.73	2.01	1.00
CD	-0.40	1	0.64	-1.77	0.97	1.00
A^2	-0.99	1	0.49	-2.04	0.058	1.05
B^2	-0.28	1	0.49	-1.32	0.77	1.05
C^2	-0.82	1	0.49	-1.87	0.23	1.05
D^2	-1.57	1	0.49	-2.62	-0.53	1.05

Graphical Model of Carbon Yield

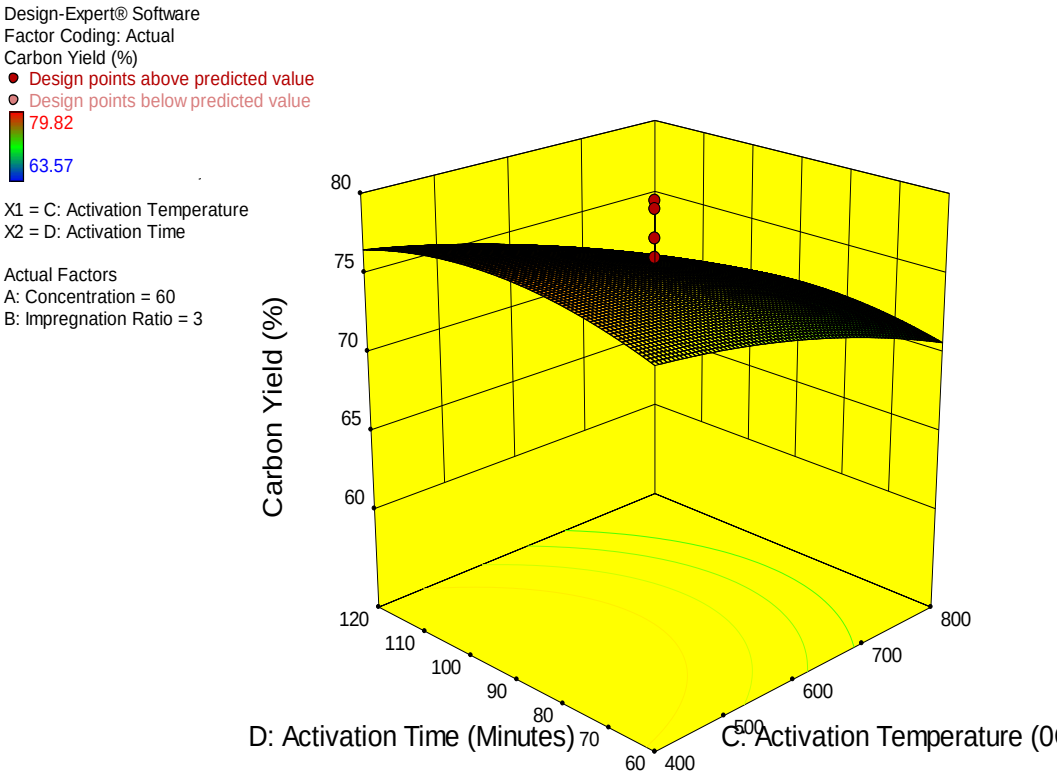

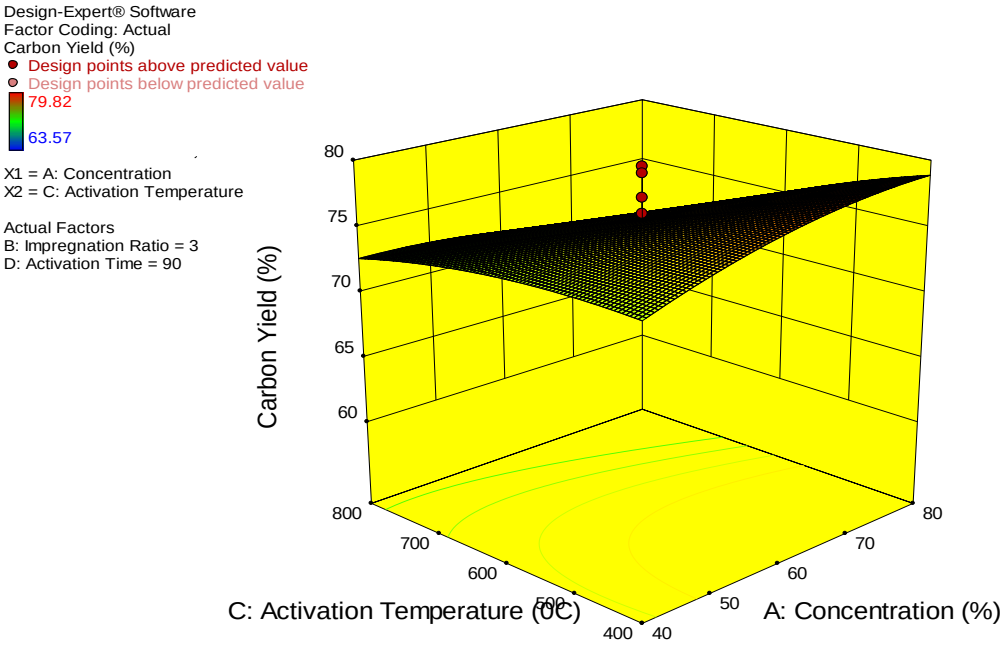

Model Analysis for Specific Surface Area

Factor	Coefficient Estimate		Standard Error	95% CI Low	95% CI High	VIF
Intercept	1769.67	1	20.26	1726.48	1812.85	
A-Concentration	5.08	1	10.13	-16.51	26.68	1.00
B-Impregnation Ratio	3.58	1	10.13	-18.01	25.18	1.00
C-Activation Temperature	68.75	1	10.13	47.16	90.34	1.00
D-Activation Time	-1.17	1	10.13	-22.76	20.43	1.00
AB	2.50	1	12.41	-23.95	28.95	1.00
AC	-3.25	1	12.41	-29.70	23.20	1.00
AD	6.38	1	12.41	-20.07	32.82	1.00
BC	-3.87	1	12.41	-30.32	22.57	1.00
BD	1.00	1	12.41	-25.45	27.45	1.00
CD	-1.00	1	12.41	-27.45	25.45	1.00
A^2	0.58	1	9.48	-19.61	20.78	1.05
B^2	8.21	1	9.48	-11.99	28.41	1.05
C^2	-31.54	1	9.48	-51.74	-11.34	1.05
D^2	1.71	1	9.48	-18.49	21.91	1.05

Graphical Model of Specific Surface Area

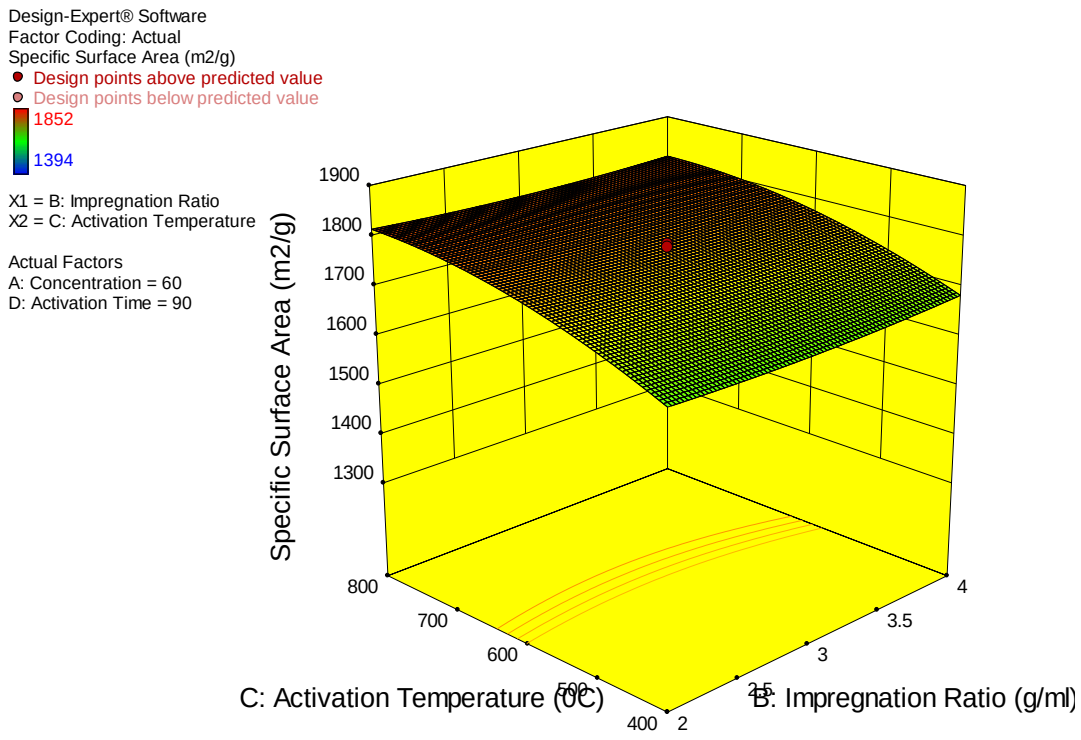

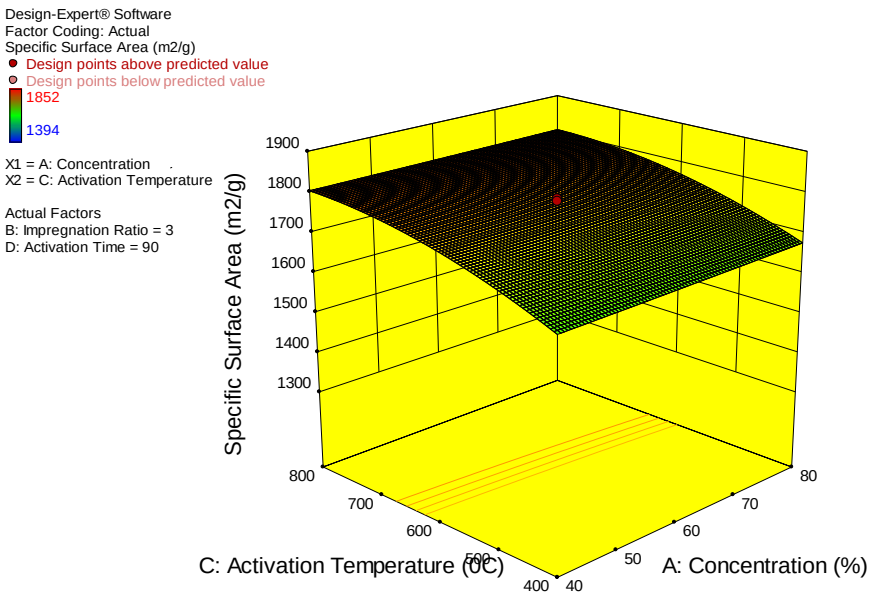

Graphical Model for Optimization of the Responses

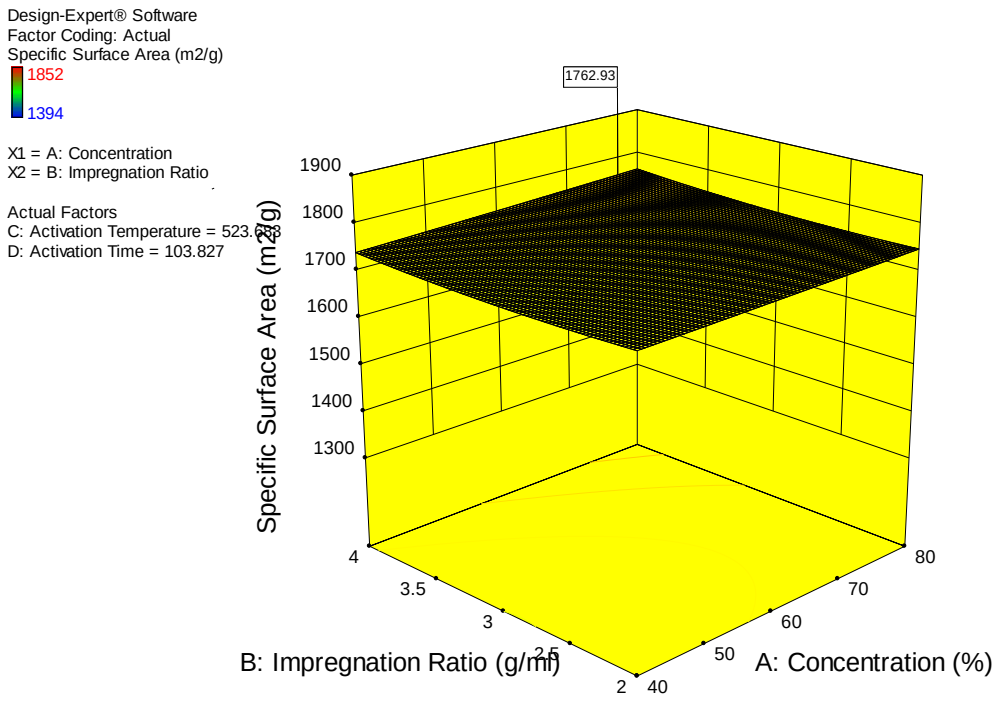

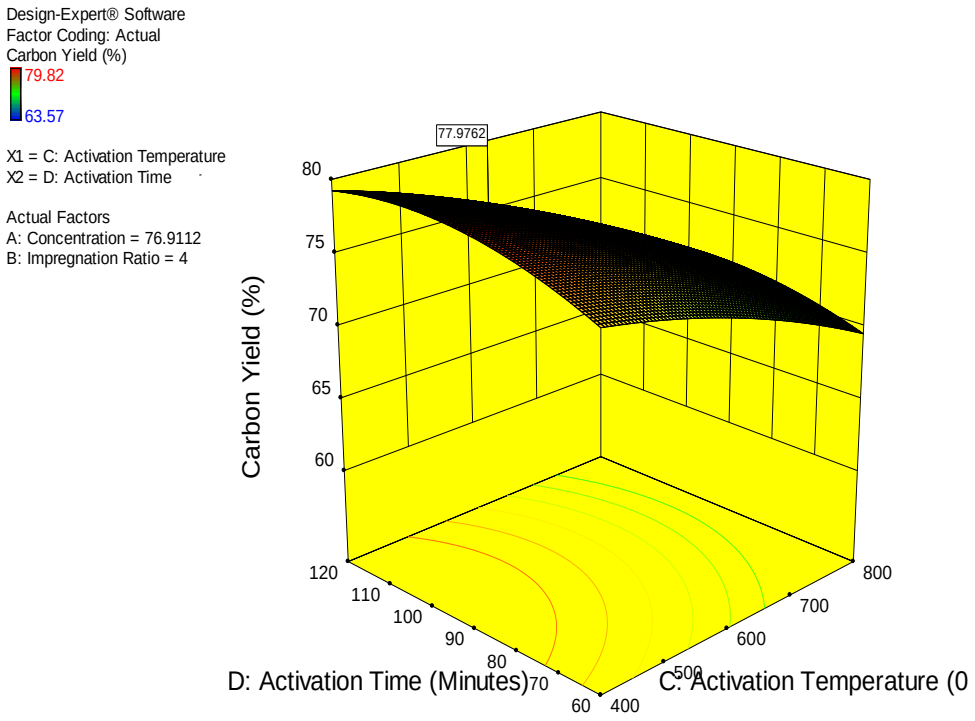

APPENDIX B

SUPPLEMENTARY DATA FOR CHARACTERIZATION OF ACTIVATED CARBON SAMPLES

Measurement Conditions: (Bookmark 1)

Dataset Name	RPSAC_20200821_144016_G01_S01_M01
File name	C:\RPSAC_20200821_144016_G01_S01_M01.rw
Raw Data Origin	Rigaku-binary (.RAW)
Scan Axis	Gonio
Start Position [°2Th.]	2.0000
End Position [°2Th.]	70.0000
Step Size [°2Th.]	0.0200
Scan Step Time [s]	1.0000
Scan Type	Pre-set time
Offset [°2Th.]	0.0000
Divergence Slit Type	Fixed
Divergence Slit Size [°]	1.0000
Specimen Length [mm]	10.00
Receiving Slit Size [mm]	0.1000
Measurement Temperature [°C]	25.00
Anode Material	Cu
K-Alpha1 [Å]	1.54060
K-Alpha2 [Å]	1.54443
K-Beta [Å]	1.39225
K-A2 / K-A1 Ratio	0.50000
Generator Settings	0 mA, 0 kV
Diffractometer Number	0
Goniometer Radius [mm]	240.00
Dist. Focus-Diverg. Slit [mm]	91.00
Incident Beam Monochromator	No
Spinning	No

Main Graphics, Analyze View: (Bookmark 2)

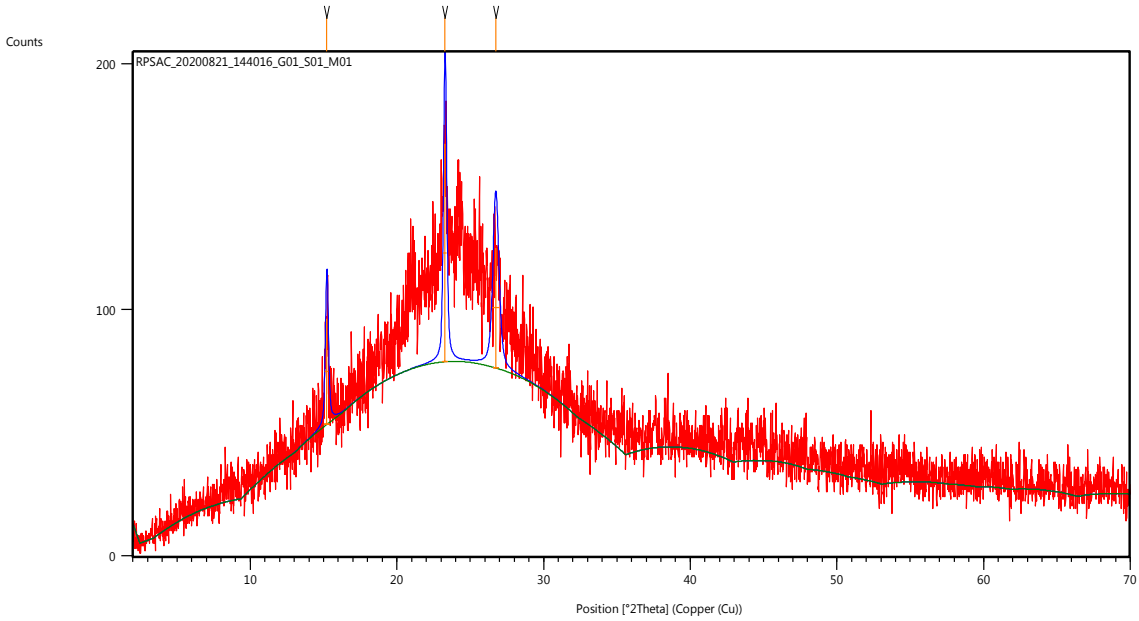

Peak List: (Bookmark 3)

Pos. [°2Th.]	Height [cts]	FWHM Left [°2Th.]	d-spacing [Å]	Rel. Int. [%]
15.2218	42.97	0.2362	5.82079	48.42
23.2737	88.75	0.2362	3.82205	100.00
26.7303	48.90	0.4723	3.33514	55.10

Pattern List: (Bookmark 4)

Document History: (Bookmark 5)

Insert Measurement:

- File name = RPSAC_20200821_144016_G01_S01_M01.raw
- Modification time = "8/21/2020 7:48:53 PM"
- Modification editor = "USER"

Determine Background:

- Add to net scan = "Nothing"
- User defined intensity = "-5"
- Correction method = "Automatic"
- Bending factor = "5"
- Minimum significance = "0.7"
- Minimum tip width = "0"
- Maximum tip width = "1"
- Peak base width = "2"
- Use smoothed input data = "Yes"
- Granularity = "20"
- Modification time = "2/22/2001 10:17:43 AM"
- Modification editor = "PANalytical"

Search Peaks:

- Minimum significance = "2"
- Minimum tip width = "0.01"
- Maximum tip width = "1"
- Peak base width = "2"
- Method = "Minimum 2nd derivative"
- Modification time = "2/20/2001 11:55:18 AM"
- Modification editor = "PANalytical"

Search & Match:

- Allow pattern shift = "No"
- Auto residue = "Yes"

- Data source = "Profile and peak list"
- Demote unmatched strong = "Yes"
- Multi phase = "Yes"
- Restriction set = "Minerals"
- Restriction = "Restriction set"
- Subset name = ""
- Match intensity = "Yes"
- Two theta shift = "0"
- Identify = "Yes"
- Max. no. of accepted patterns = "5"
- Minimum score = "27"
- Min. new lines / total lines = "40"
- Search depth = "6"
- Minimum new lines = "3"
- Minimum scale factor = "0.06"
- Intensity threshold = "0"
- Use line clustering = "Yes"
- Line cluster range = "1.5"
- Search sensitivity = "1.8"
- Use adaptive smoothing = "Yes"
- Smoothing range = "1.5"
- Threshold factor = "3"
- Modification time = "2/5/2001 11:17:06 AM"
- Modification editor = "PANalytical"

Quantachrome NovaWin - Data Acquisition and Reduction
for NOVA instruments
©1994-2013, Quantachrome Instruments
version 11.03

Analysis

Operator:	Abdulrahman AbdulkareemDate:2007/05/14		
Sample ID:	Sample RPSAC	**Filename:**	Sample RPSAC.qps
Sample Desc:		**Comment:**	
Sample weight:	0.12 g	**Sample Volume:**	1 cc
Outgas Time:	3.0 hrs	**OutgasTemp:**	250.0 C
Analysis gas:	Nitrogen	**Bath Temp:**	273.0 K
Press. Tolerance:	0.100/0.100 (ads/des)	**Equil time:**	60/60 sec (ads/des)
Analysis Time:	64.1 min	**End of run:**	2007/05/14 0:05:21
Cell ID:	2		

Report

Operator:	quantachrome	**Date:**	2020/08/24
Equil timeout:	240/240 sec (ads/des)		
Instrument:	Nova Station B		

Multi-Point BET Plot

Data Reduction Parameters

Adsorbate	Nitrogen	Temperature	77.350K		
	Molec. Wt.: 28.013	**Cross Section:**	16.200 Å²	**Liquid Density:**	0.808 g/cc

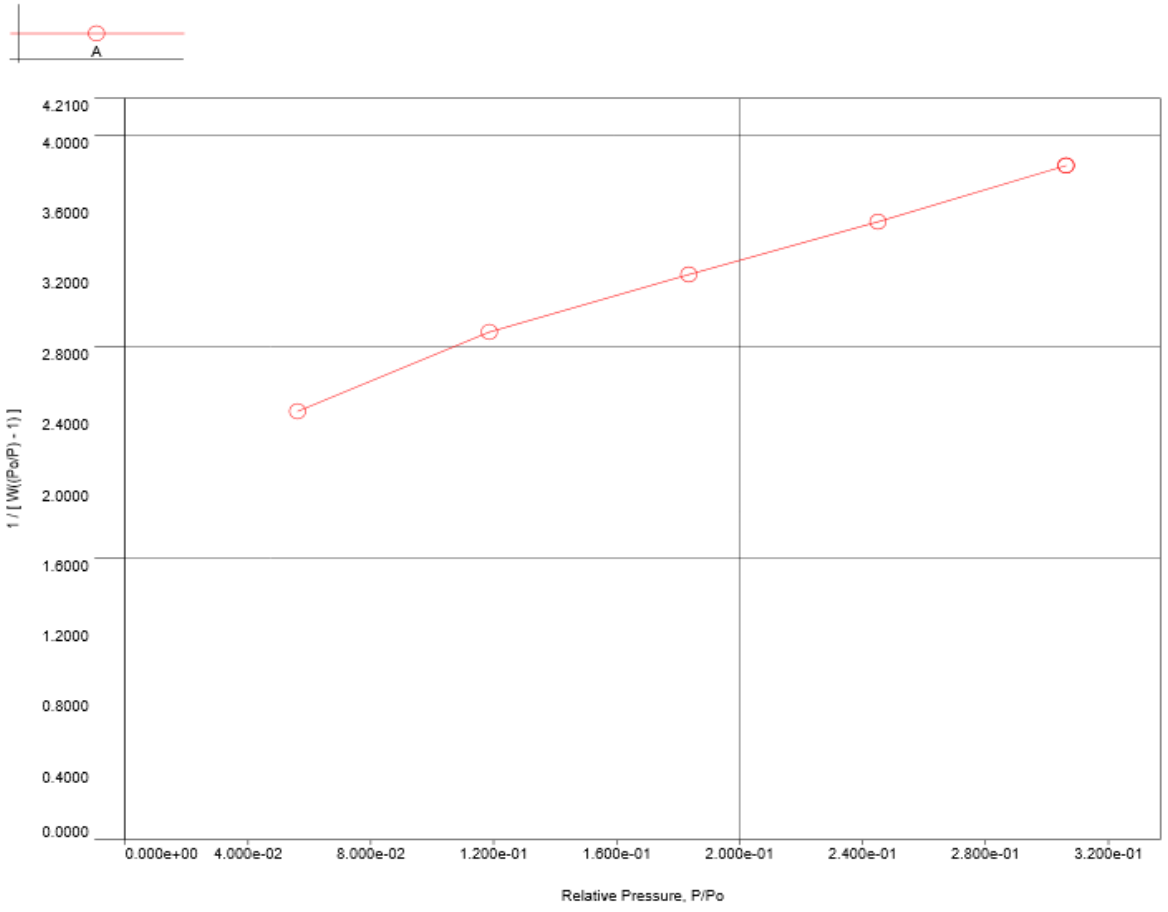

BET summary

Slope =	5.455
Intercept =	2.180e+00
Correlation coefficient, r =	0.996820
C constant=	3.503
Surface Area =	456.143 m²/g

Quantachrome NovaWin - Data Acquisition and Reduction
for NOVA instruments
©1994-2013, Quantachrome Instruments
version 11.03

Analysis				Report			
Operator:	Abdulrahman Abdulkareem	Date:2007/05/14		Operator:	quantachrome	Date:2020/08/24	
Sample ID:	Sample RPSAC	Filename:		Sample RPSAC.qps			
Sample Desc:		Comment:					
Sample weight:	0.12 g	Sample Volume:		1 cc			
Outgas Time:	3.0 hrs	OutgasTemp:		250.0 C			
Analysis gas:	Nitrogen	Bath Temp:		273.0 K			
Press. Tolerance:	0.100/0.100 (ads/des)	Equil time:		60/60 sec (ads/des)	Equil timeout:	240/240 sec (ads/des)	
Analysis Time:	64.1 min	End of run:		2007/05/14 0:05:21	Instrument:	Nova Station B	
Cell ID:	2						

DA Plot

Data Reduction Parameters

DA Method	Incr. E:	500.000	Incr. n:	0.100	Interact. Const. (K):	2.960nm³ x kJ / mol	
Adsorbate	Nitrogen		Temperature	77.350K			
	Molec. Wt.:	28.013	Cross Section:	16.200 Å²	Liquid Density:	0.808 g/cc	

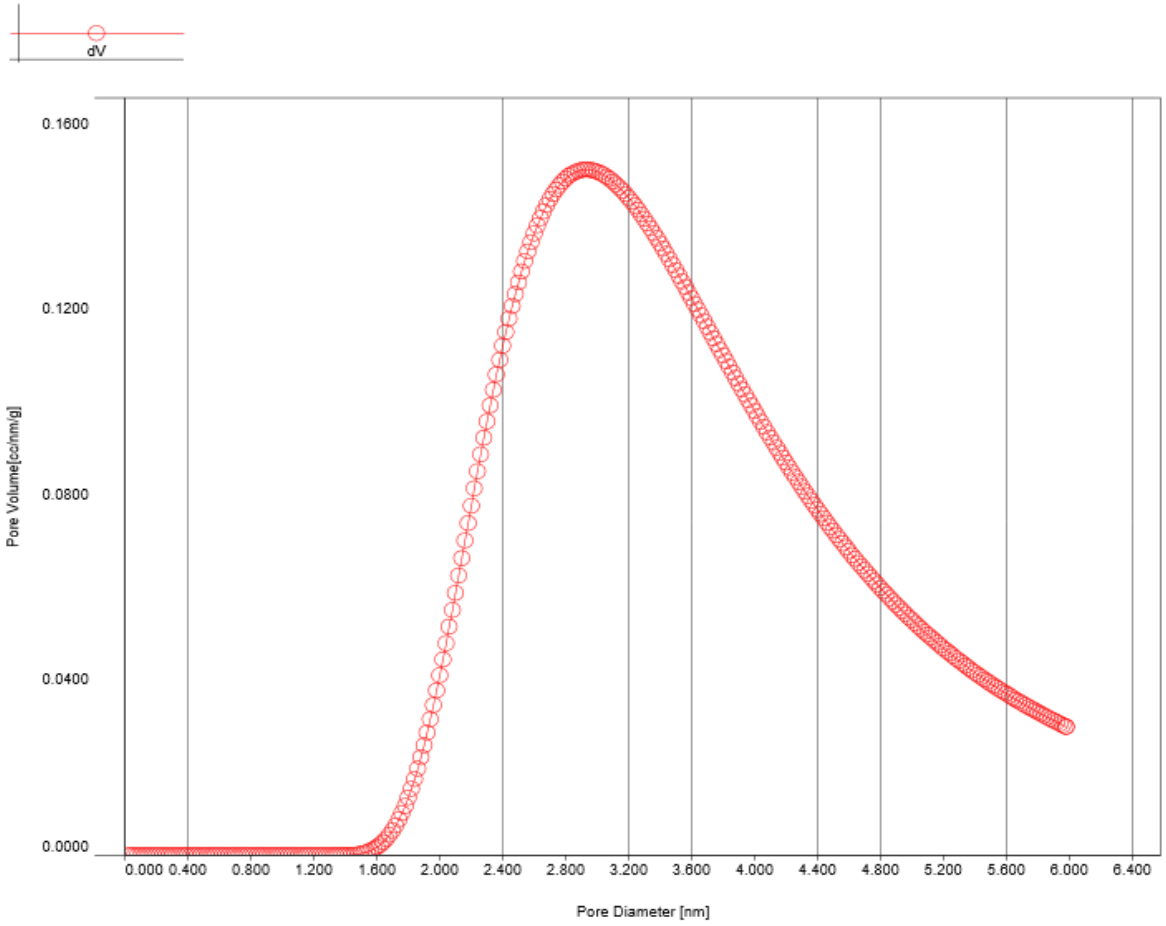

DA method summary

Best E =	0.705 kJ/mol
Best n =	1.000
DA Micropore Volume =	0.413 cc/g
Pore Diameter (mode)=	2.940e+00 nm

Quantachrome NovaWin - Data Acquisition and Reduction
for NOVA instruments
©1994-2013, Quantachrome Instruments
version 11.03

Analysis				Report			
Operator:	Abdulrahman Abdulkareem	Date:2007/05/14		Operator:	quantachrome	Date:2020/08/24	
Sample ID:	Sample RPSAC	Filename:		Sample RPSAC.qps			
Sample Desc:		Comment:					
Sample weight:	0.12 g	Sample Volume:		1 cc			
Outgas Time:	3.0 hrs	OutgasTemp:		250.0 C			
Analysis gas:	Nitrogen	Bath Temp:		273.0 K			
Press. Tolerance:	0.100/0.100 (ads/des)	Equil time:		60/60 sec (ads/des)		Equil timeout:	240/240 sec (ads/des)
Analysis Time:	64.1 min	End of run:		2007/05/14 0:05:21		Instrument:	Nova Station B
Cell ID:	2						

Multi-Point BET

Data Reduction Parameters Data

Adsorbate	Nitrogen		Temperature	77.350K		
	Molec. Wt.:	28.013	Cross Section:	16.200 Å²	Liquid Density:	0.808 g/cc

Multi-Point BET Data

Relative Pressure [P/Po]	Volume @ STP [cc/g]	1 / [W((Po/P) - 1)]	Relative Pressure [P/Po]	Volume @ STP [cc/g]	1 / [W((Po/P) - 1)]
5.61640e-02	19.5780	2.4319e+00	2.45000e-01	74.0090	3.5082e+00
1.18544e-01	37.3335	2.8822e+00	3.06167e-01	92.2510	3.8272e+00
1.83441e-01	56.0103	3.2092e+00			

BET summary

Slope =	5.455
Intercept =	2.180e+00
Correlation coefficient, r =	0.996820
C constant=	3.503
Surface Area =	456.143 m²/g

Quantachrome NovaWin - Data Acquisition and Reduction
for NOVA instruments
©1994-2013, Quantachrome Instruments
version 11.03

Analysis				Report			
Operator:	Abdulrahman Abdulkareem	Date:2007/05/14		Operator:	quantachrome	Date:2020/08/24	
Sample ID:	Sample RPSAC	Filename:		Sample RPSAC.qps			
Sample Desc:		Comment:					
Sample weight:	0.12 g	Sample Volume:		1 cc			
Outgas Time:	3.0 hrs	OutgasTemp:		250.0 C			
Analysis gas:	Nitrogen	Bath Temp:		273.0 K			
Press. Tolerance:	0.100/0.100 (ads/des)	Equil time:		60/60 sec (ads/des)		Equil timeout:	240/240 sec (ads/des)
Analysis Time:	64.1 min	End of run:		2007/05/14 0:05:21		Instrument:	Nova Station B
Cell ID:	2						

Langmuir

Data Reduction Parameters Data

Adsorbate	Nitrogen		Temperature	77.350K		
	Molec. Wt.:	28.013	Cross Section:	16.200 Å²	Liquid Density:	0.808 g/cc

Langmuir Data

P/Po	P/Po/W [(g/g)]	P/Po	P/Po/W [(g/g)]
5.61640e-02	2.2953e+00	2.45000e-01	2.6487e+00
1.18544e-01	2.5406e+00	3.06167e-01	2.6554e+00
1.83441e-01	2.6205e+00		

Langmuir summary

Slope =	1.32641
Intercept =	2.31087
Correlation coefficient, r =	0.872
Surface Area =	2625.517 m²/g

Quantachrome NovaWin - Data Acquisition and Reduction
for NOVA instruments
©1994-2013, Quantachrome Instruments
version 11.03

Analysis				Report			
Operator:	Abdulrahman Abdulkareem	**Date:**	2007/05/14	**Operator:**	quantachrome	**Date:**	2020/08/24
Sample ID:	Sample RPSAC	**Filename:**		Sample RPSAC.qps			
Sample Desc:		**Comment:**					
Sample weight:	0.12 g	**Sample Volume:**		1 cc			
Outgas Time:	3.0 hrs	**OutgasTemp:**		250.0 C			
Analysis gas:	Nitrogen	**Bath Temp:**		273.0 K			
Press. Tolerance:	0.100/0.100 (ads/des)	**Equil time:**		60/60 sec (ads/des)	**Equil timeout:**		240/240 sec (ads/des)
Analysis Time:	64.1 min	**End of run:**		2007/05/14 0:05:21	**Instrument:**		Nova Station B
Cell ID:	2						

Isotherm

Data Reduction Parameters Data

Adsorbate	Nitrogen				
	Molec. Wt.:	28.013	**Temperature**	77.350K	
			Cross Section:	16.200 Å²	**Liquid Density:** 0.808 g/cc

Isotherm Data

Relative Pressure	Volume @ STP [cc/g]	Relative Pressure	Volume @ STP [cc/g]	Relative Pressure	Volume @ STP [cc/g]
5.61640e-02	19.5780	1.83441e-01	56.0103	3.06167e-01	92.2510
1.18544e-01	37.3335	2.45000e-01	74.0090		

Quantachrome NovaWin - Data Acquisition and Reduction
for NOVA instruments
©1994-2013, Quantachrome Instruments
version 11.03

Analysis				Report			
Operator:	Abdulrahman Abdulkareem	Date:2007/05/14		Operator:	quantachrome	Date:2020/08/24	
Sample ID:	Sample RPSAC	Filename:		Sample RPSAC.qps			
Sample Desc:		Comment:					
Sample weight:	0.12 g	Sample Volume:		1 cc			
Outgas Time:	3.0 hrs	OutgasTemp:		250.0 C			
Analysis gas:	Nitrogen	Bath Temp:		273.0 K			
Press. Tolerance:	0.100/0.100 (ads/des)	Equil time:		60/60 sec (ads/des)	Equil timeout:	240/240 sec (ads/des)	
Analysis Time:	64.1 min	End of run:		2007/05/14 0:05:21	Instrument:	Nova Station B	
Cell ID:	2						

DR method

Data Reduction Parameters Data

DR method	Affinity coefficient (ß): 0.3300				
Adsorbate	Nitrogen	Temperature	77.350K		
	Molec. Wt.: 28.013	Cross Section:	16.200 Å²	Liquid Density:	0.808 g/cc
	Critical Temp.: 126.200 K	Critical Press.:	33.500 atm	SuperCritic. K.:	1.000
Adsorbent	Carbon				
	DR. Exp (n): 2.000				

DR method Data

Log2(P/Po)	Weight Adsorbed [(g)]	Log2(P/Po)	Weight Adsorbed [(g)]
1.563855e+00	2.9363e-03	3.731181e-01	1.1100e-02
8.576990e-01	5.5993e-03	2.642388e-01	1.3836e-02
5.424375e-01	8.4004e-03		

DR method summary

Slope =	-5.044e-01
Intercept =	1.693e-02
Correlation Coefficient =	0.9891
Average Pore width =	6.243nm
Adsorption energy =	4.165 kJ/mol
Micropore volume =	0.175 cc/g
Micropore surface area =	491.299 m²/g

Analysis
Operator: Abdulrahman Abdulkareem **Date:** 2007/05/14
Sample ID: Sample RPSAC **Filename:**

Report
Operator: quantachrome **Date:** 2020/08/24
Sample RPSAC.qps

DA Method Micropore Analysis Data continued

Diameter [nm]	dV(d) [cc/nm/g]	Diameter [nm]	dV(d) [cc/nm/g]
4.66000e+00	6.33337e-02	5.34000e+00	4.10577e-02
4.68000e+00	6.25225e-02	5.36000e+00	4.05480e-02
4.70000e+00	6.17218e-02	5.38000e+00	4.00454e-02
4.72000e+00	6.09314e-02	5.40000e+00	3.95498e-02
4.74000e+00	6.01514e-02	5.42000e+00	3.90611e-02
4.76000e+00	5.93815e-02	5.44000e+00	3.85792e-02
4.78000e+00	5.86218e-02	5.46000e+00	3.81041e-02
4.80000e+00	5.78721e-02	5.48000e+00	3.76355e-02
4.82000e+00	5.71324e-02	5.50000e+00	3.71735e-02
4.84000e+00	5.64025e-02	5.52000e+00	3.67179e-02
4.86000e+00	5.56823e-02	5.54000e+00	3.62687e-02
4.88000e+00	5.49718e-02	5.56000e+00	3.58257e-02
4.90000e+00	5.42708e-02	5.58000e+00	3.53889e-02
4.92000e+00	5.35793e-02	5.60000e+00	3.49581e-02
4.94000e+00	5.28971e-02	5.62000e+00	3.45334e-02
4.96000e+00	5.22242e-02	5.64000e+00	3.41146e-02
4.98000e+00	5.15604e-02	5.66000e+00	3.37015e-02
5.00000e+00	5.09057e-02	5.68000e+00	3.32943e-02
5.02000e+00	5.02599e-02	5.70000e+00	3.28927e-02
5.04000e+00	4.96229e-02	5.72000e+00	3.24966e-02
5.06000e+00	4.89947e-02	5.74000e+00	3.21061e-02
5.08000e+00	4.83751e-02	5.76000e+00	3.17209e-02
5.10000e+00	4.77640e-02	5.78000e+00	3.13411e-02
5.12000e+00	4.71613e-02	5.80000e+00	3.09666e-02
5.14000e+00	4.65669e-02	5.82000e+00	3.05972e-02
5.16000e+00	4.59808e-02	5.84000e+00	3.02329e-02
5.18000e+00	4.54027e-02	5.86000e+00	2.98737e-02
5.20000e+00	4.48326e-02	5.88000e+00	2.95194e-02
5.22000e+00	4.42705e-02	5.90000e+00	2.91700e-02
5.24000e+00	4.37161e-02	5.92000e+00	2.88254e-02
5.26000e+00	4.31695e-02	5.94000e+00	2.84856e-02
5.28000e+00	4.26304e-02	5.96000e+00	2.81504e-02
5.30000e+00	4.20988e-02	5.98000e+00	2.78198e-02
5.32000e+00	4.15746e-02		

DA method summary

Best E =	0.705 kJ/mol
Best n =	1.000
DA Micropore Volume =	0.413 cc/g
Pore Diameter (mode)=	2.940e+00 nm

Quantachrome NovaWin - Data Acquisition and Reduction
for NOVA instruments
©1994-2013, Quantachrome Instruments
version 11.03

Analysis				Report			
Operator:	Abdulrahman Abdulkareem	Date:2007/05/14		Operator:	quantachrome	Date:2020/08/24	
Sample ID:	Sample RPSAC	Filename:		Sample RPSAC.qps			
Sample Desc:		Comment:					
Sample weight:	0.12 g	Sample Volume:		1 cc			
Outgas Time:	3.0 hrs	OutgasTemp:		250.0 C			
Analysis gas:	Nitrogen	Bath Temp:		273.0 K			
Press. Tolerance:	0.100/0.100 (ads/des)	Equil time:		60/60 sec (ads/des)	Equil timeout:	240/240 sec (ads/des)	
Analysis Time:	64.1 min	End of run:		2007/05/14 0:05:21	Instrument:	Nova Station B	
Cell ID:	2						

DFT method Pore Size Distribution

Data Reduction Parameters Data

DFT method	Calc. Model: N2 at 77 K on carbon (slit pore, NLDFT equilibrium model)			Moving pt. avg:	off
	Rel. press. range: 0.0000 - 1.0000				
Adsorbate	Nitrogen	Temperature	77.350K		
	Molec. Wt.: 28.013	Cross Section:	16.200 Å²	Liquid Density:	0.808 g/cc

DFT method Pore Size Distribution Data

Pore width [nm]	Cumulative Pore Volume [cc/g]	Cumulative Surface Area [m²/g]	dV(d) [cc/nm/g]	dS(d) [m²/nm/g]
1.7656	0.0000e+00	0.0000e+00	0.0000e+00	0.0000e+00
1.8469	2.5019e-03	2.7093e+00	3.0786e-02	3.3338e+01
1.9319	1.0949e-02	1.1454e+01	9.9362e-02	1.0286e+02
2.0208	1.8521e-02	1.8948e+01	8.5155e-02	8.4277e+01
2.1138	1.9023e-02	1.9423e+01	5.4004e-03	5.1096e+00
2.2111	2.8447e-02	2.7947e+01	9.6863e-02	8.7613e+01
2.3129	4.6528e-02	4.3582e+01	1.7765e-01	1.5362e+02
2.4194	6.3058e-02	5.7247e+01	1.5527e-01	1.2836e+02
2.5307	8.3539e-02	7.3432e+01	1.8392e-01	1.4535e+02
2.6472	1.0856e-01	9.2336e+01	2.1480e-01	1.6228e+02
2.7691	1.3215e-01	1.0938e+02	1.9363e-01	1.3985e+02

DFT method summary

Pore volume =	0.132 cc/g
Surface area =	109.376 m²/g
Lower confidence limit =	1.766 nm
Fitting error =	3.061 %
Pore width (Mode) =	2.647 nm
Moving point average :	off

Quantachrome NovaWin - Data Acquisition and Reduction
for NOVA instruments
©1994-2013, Quantachrome Instruments
version 11.03

Analysis				Report			
Operator:	Abdulrahman Abdulkareem	Date:2007/05/14		Operator:	quantachrome	Date:2020/08/24	
Sample ID:	Sample RPSAC	Filename:		Sample RPSAC.qps			
Sample Desc:		Comment:					
Sample weight:	0.12 g	Sample Volume:		1 cc			
Outgas Time:	3.0 hrs	OutgasTemp:		250.0 C			
Analysis gas:	Nitrogen	Bath Temp:		273.0 K			
Press. Tolerance:	0.100/0.100 (ads/des)	Equil time:		60/60 sec (ads/des)		Equil timeout:	240/240 sec (ads/des)
Analysis Time:	64.1 min	End of run:		2007/05/14 0:05:21		Instrument:	Nova Station B
Cell ID:	2						

Area-Volume Summary

Data Reduction Parameters Data

	Thermal Transpiration: on	Eff. mol. diameter (D): 3.54 Å		Eff. cell stem diam. (d): 4.0000 mm
t-Method	Calc. method: de Boer			
BJH/DH method	Moving pt. avg.: off			
DR method	Affinity coefficient (ß): 0.3300			
HK method	Tabulated data interval: 1			
SF method	Tabulated data interval: 1			
DFT method	Calc. Model: N2 at 77 K on carbon (slit pore, NLDFT equilibrium model)			
	Rel. press. range: 0.0000 - 1.0000			Moving pt. avg: off
Adsorbate	Nitrogen	Temperature	77.350K	
	Molec. Wt.: 28.013	Cross Section:	16.200 Å²	Liquid Density: 0.808 g/cc
	Critical Temp.: 126.200 K	Critical Press.:	33.500 atm	SuperCritic. K.: 1.000
Adsorbent	Carbon			
	DR. Exp (n): 2.000			

Surface Area Data

SinglePoint BET	2.786e+02 m²/g
MultiPoint BET	4.561e+02 m²/g
Langmuir surface area	2.626e+03 m²/g
BJH method cumulative adsorption surface area	5.132e+02 m²/g
DH method cumulative adsorption surface area	5.459e+02 m²/g
t-method external surface area	4.561e+02 m²/g
DR method micropore area	4.913e+02 m²/g
DFT cumulative surface area	1.094e+02 m²/g

Pore Volume Data

BJH method cumulative adsorption pore volume	2.524e-01 cc/g
DH method cumulative adsorption pore volume	2.581e-01 cc/g
DR method micropore volume	1.746e-01 cc/g
HK method micropore volume	7.282e-02 cc/g
SF method micropore volume	1.534e-02 cc/g
DFT method cumulative pore volume	1.322e-01 cc/g

Pore Size Data

BJH method adsorption pore Diameter (Mode Dv(d))	2.133e+00 nm
DH method adsorption pore Diameter (Mode Dv(d))	2.133e+00 nm
DR method micropore Pore width	6.243e+00 nm
DA method pore Diameter (Mode)	2.940e+00 nm
HK method pore Diameter (Mode)	1.847e+00 nm
SF method pore Diameter (Mode)	3.506e+00 nm
DFT pore Diameter (Mode)	2.647e+00 nm

Measurement Conditions: (Bookmark 1)

Dataset Name ACRRPSAC_20200821_121152_G02_S02_M02

File nameC:\ACRRPSAC_20200821_121152_G02_S02_M02.raw

Raw Data Origin	Rigaku-binary (.RAW)
Scan Axis	Gonio
Start Position [°2Th.]	2.0000
End Position [°2Th.]	70.0000
Step Size [°2Th.]	0.0200
Scan Step Time [s]	1.0000
Scan Type	Pre-set time
Offset [°2Th.]	0.0000
Divergence Slit Type	Fixed
Divergence Slit Size [°]	1.0000
Specimen Length [mm]	10.00
Receiving Slit Size [mm]	0.1000
Measurement Temperature [°C]	25.00
Anode Material	Cu
K-Alpha1 [Å]	1.54060
K-Alpha2 [Å]	1.54443
K-Beta [Å]	1.39225
K-A2 / K-A1 Ratio	0.50000
Generator Settings	0 mA, 0 kV
Diffractometer Number	0
Goniometer Radius [mm]	240.00
Dist. Focus-Diverg. Slit [mm]	91.00
Incident Beam Monochromator	No
Spinning	No

Main Graphics, Analyze View: (Bookmark 2)

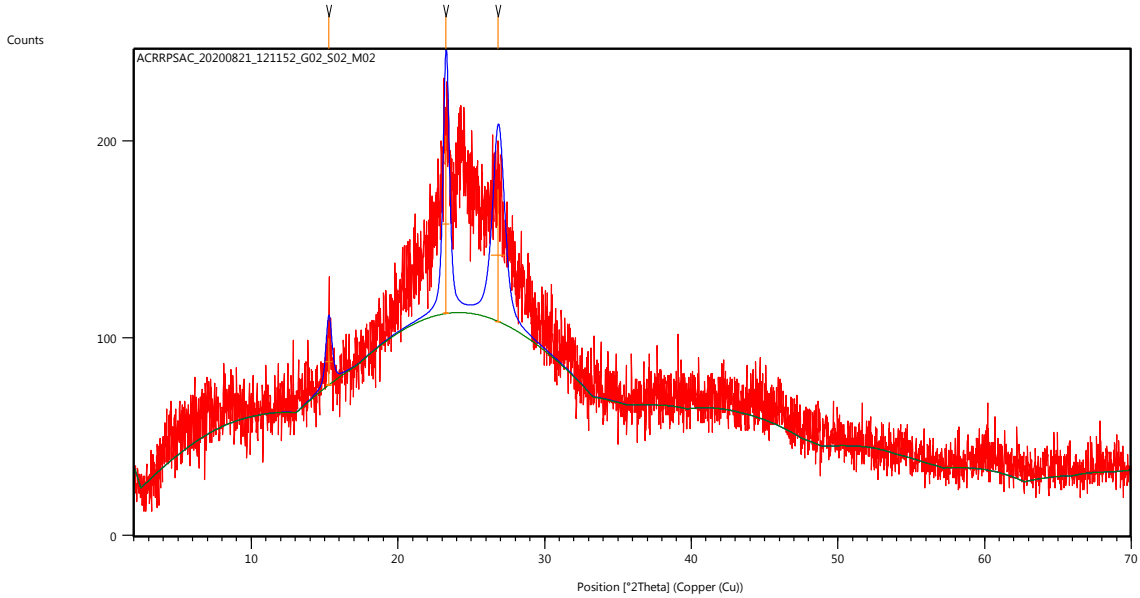

Peak List: (Bookmark 3)

Pos. [°2Th.]	Height [cts]	FWHM Left [°2Th.]	d-spacing [Å]	Rel. Int. [%]
15.2878	23.70	0.4723	5.79582	26.19
23.2792	90.48	0.4723	3.82116	100.00
26.8433	66.96	0.9446	3.32135	74.01

Pattern List: (Bookmark 4)

Document History: (Bookmark 5)

Insert Measurement:

- File name ACRRPSAC_20200821_121152_G02_S02_M02.raw
- Modification time = "8/21/2020 7:45:14 PM"
- Modification editor = "USER"

Determine Background:

- Add to net scan = "Nothing"
- User defined intensity = "-5"
- Correction method = "Automatic"
- Bending factor = "5"
- Minimum significance = "0.7"
- Minimum tip width = "0"
- Maximum tip width = "1"
- Peak base width = "2"
- Use smoothed input data = "Yes"
- Granularity = "20"
- Modification time = "2/22/2001 10:17:43 AM"
- Modification editor = "PANalytical"

Search Peaks:

- Minimum significance = "2"
- Minimum tip width = "0.01"
- Maximum tip width = "1"
- Peak base width = "2"
- Method = "Minimum 2nd derivative"
- Modification time = "2/20/2001 11:55:18 AM"
- Modification editor = "PANalytical"

Search & Match:

- Allow pattern shift = "No"

- Auto residue = "Yes"
- Data source = "Profile and peak list"
- Demote unmatched strong = "Yes"
- Multi phase = "Yes"
- Restriction set = "Minerals"
- Restriction = "Restriction set"
- Subset name = ""
- Match intensity = "Yes"
- Two theta shift = "0"
- Identify = "Yes"
- Max. no. of accepted patterns = "5"
- Minimum score = "27"
- Min. new lines / total lines = "40"
- Search depth = "6"
- Minimum new lines = "3"
- Minimum scale factor = "0.06"
- Intensity threshold = "0"
- Use line clustering = "Yes"
- Line cluster range = "1.5"
- Search sensitivity = "1.8"
- Use adaptive smoothing = "Yes"
- Smoothing range = "1.5"
- Threshold factor = "3"
- Modification time = "2/5/2001 11:17:06 AM"
- Modification editor = "PANalytical"

Quantachrome NovaWin - Data Acquisition and Reduction
for NOVA instruments
©1994-2013, Quantachrome Instruments
version 11.03

Analysis

Operator:	Abdulrahman Abdulkareem	**Date:**	2007/05/14
Sample ID:	Sample ACRPSAC	**Filename:**	Sample ACRPSAC.qps
Sample Desc:		**Comment:**	
Sample weight:	0.08 g	**Sample Volume:**	1 cc
Outgas Time:	3.0 hrs	**OutgasTemp:**	250.0 C
Analysis gas:	Nitrogen	**Bath Temp:**	273.0 K
Press. Tolerance:	0.100/0.100 (ads/des)	**Equil time:**	60/60 sec (ads/des)
Analysis Time:	68.7 min	**End of run:**	2007/05/14 17:48:54
Cell ID:	3		

Report

Operator:	quantachrome	**Date:**	2020/08/24
Equil timeout:	240/240 sec (ads/des)		
Instrument:	Nova Station C		

Multi-Point BET Plot

Data Reduction Parameters

Adsorbate	Nitrogen	Temperature	77.350K		
	Molec. Wt.: 28.013	**Cross Section:**	16.200 Å²	**Liquid Density:**	0.808 g/cc

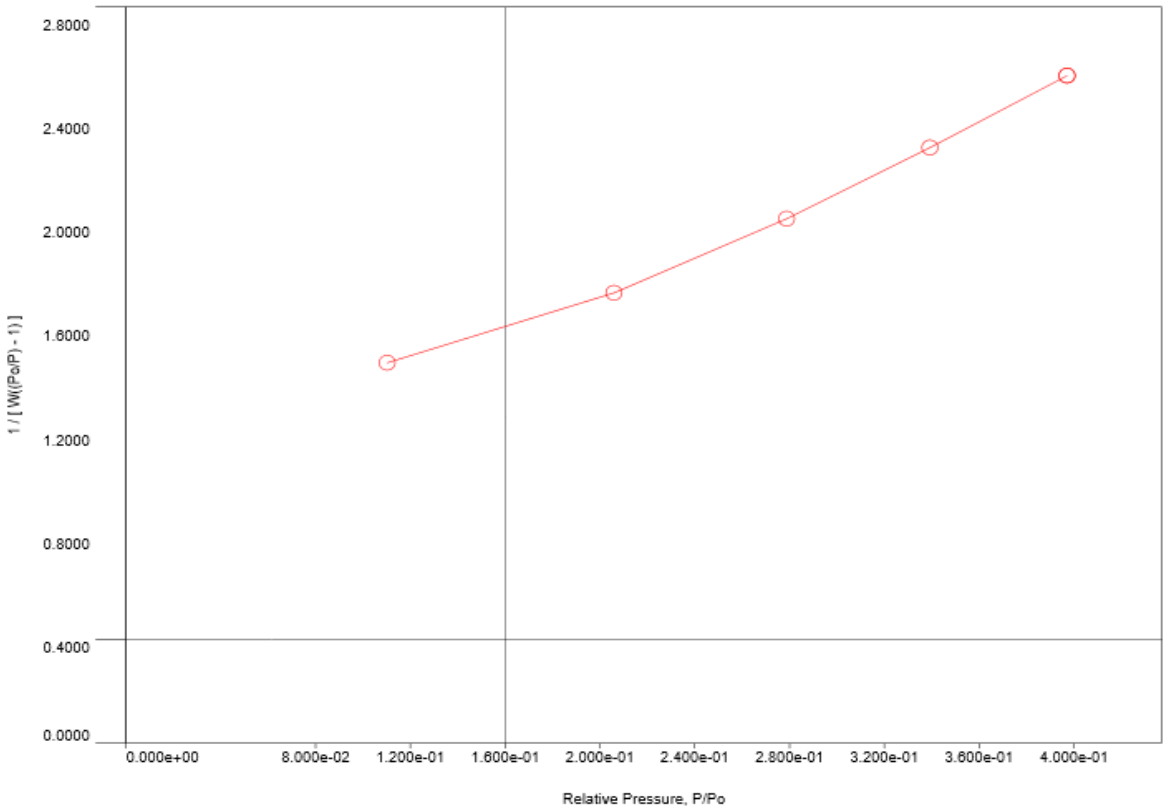

BET summary

Slope =	3.878
Intercept =	9.870e-01
Correlation coefficient, r =	0.993751
C constant=	4.929
Surface Area =	715.804 m²/g

Quantachrome NovaWin - Data Acquisition and Reduction
for NOVA instruments
©1994-2013, Quantachrome Instruments
version 11.03

Analysis				Report			
Operator:	Abdulrahman Abdulkareem	Date:2007/05/14		Operator:	quantachrome	Date:2020/08/24	
Sample ID:	Sample ACRPSAC	Filename:		Sample ACRPSAC.qps			
Sample Desc:		Comment:					
Sample weight:	0.08 g	Sample Volume:		1 cc			
Outgas Time:	3.0 hrs	OutgasTemp:		250.0 C			
Analysis gas:	Nitrogen	Bath Temp:		273.0 K			
Press. Tolerance:	0.100/0.100 (ads/des)	Equil time:		60/60 sec (ads/des)	Equil timeout:	240/240 sec (ads/des)	
Analysis Time:	68.7 min	End of run:		2007/05/14 17:48:54	Instrument:	Nova Station C	
Cell ID:	3						

DA Plot

Data Reduction Parameters

DA Method	Incr. E:	500.000	Incr. n:	0.100	Interact. Const. (K):	2.960nm³ x kJ / mol
Adsorbate	Nitrogen		Temperature	77.350K		
	Molec. Wt.:	28.013	Cross Section:	16.200 Å²	Liquid Density:	0.808 g/cc

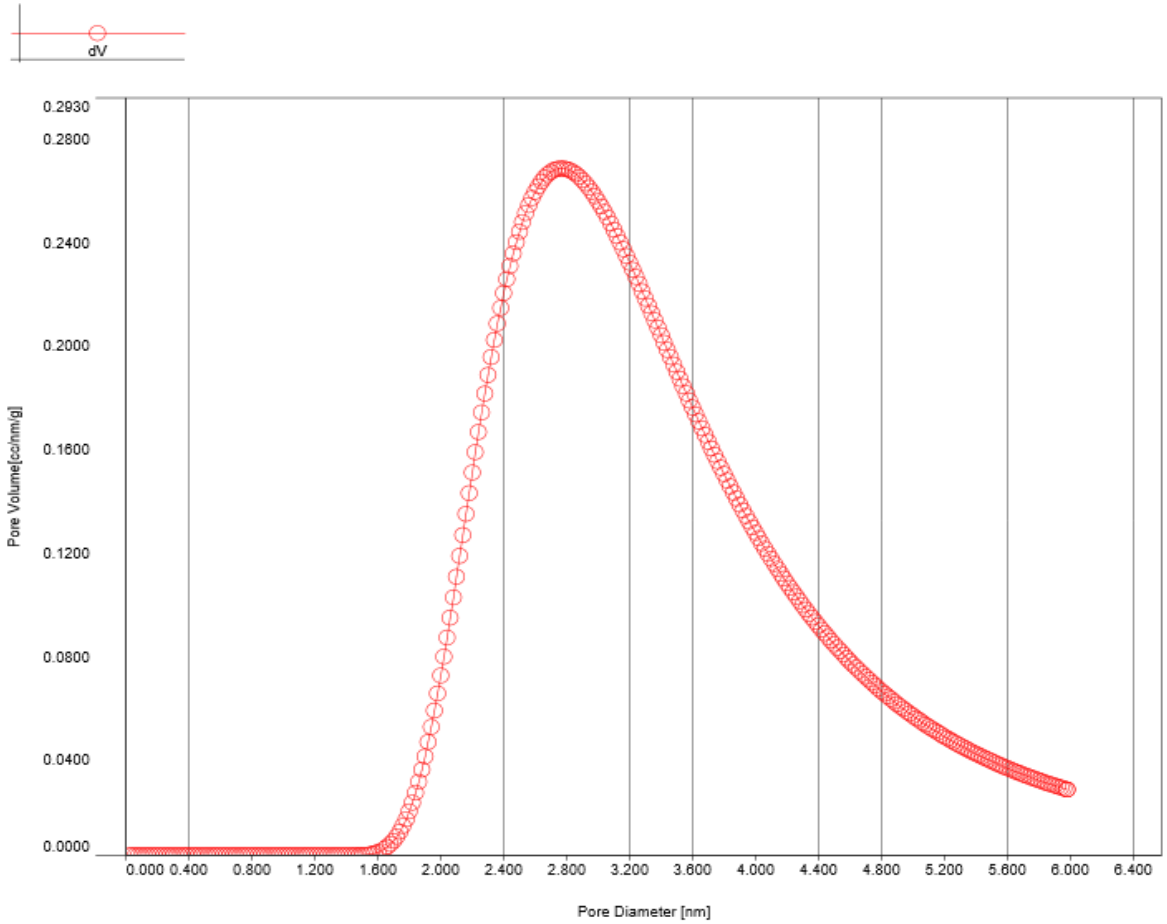

DA method summary

Best E =	0.911 kJ/mol
Best n =	1.200
DA Micropore Volume =	0.574 cc/g
Pore Diameter (mode)=	2.760e+00 nm

Quantachrome NovaWin - Data Acquisition and Reduction
for NOVA instruments
©1994-2013, Quantachrome Instruments
version 11.03

Analysis				Report			
Operator:	Abdulrahman Abdulkareem	Date:2007/05/14		Operator:	quantachrome	Date:2020/08/24	
Sample ID:	Sample ACRPSAC	Filename:		Sample ACRPSAC.qps			
Sample Desc:		Comment:					
Sample weight:	0.08 g	Sample Volume:		1 cc			
Outgas Time:	3.0 hrs	OutgasTemp:		250.0 C			
Analysis gas:	Nitrogen	Bath Temp:		273.0 K			
Press. Tolerance:	0.100/0.100 (ads/des)	Equil time:		60/60 sec (ads/des)	Equil timeout:	240/240 sec (ads/des)	
Analysis Time:	68.7 min	End of run:		2007/05/14 17:48:54	Instrument:	Nova Station C	
Cell ID:	3						

Multi-Point BET

Data Reduction Parameters Data

Adsorbate	Nitrogen		Temperature	77.350K		
	Molec. Wt.:	28.013	Cross Section:	16.200 Å²	Liquid Density:	0.808 g/cc

Multi-Point BET Data

Relative Pressure [P/Po]	Volume @ STP [cc/g]	1 / [W((Po/P) - 1)]	Relative Pressure [P/Po]	Volume @ STP [cc/g]	1 / [W((Po/P) - 1)]
1.10281e-01	67.5831	1.4674e+00	3.39213e-01	178.7745	2.2975e+00
2.05990e-01	119.5314	1.7366e+00	3.97060e-01	204.6807	2.5743e+00
2.78838e-01	152.9617	2.0225e+00			

BET summary

Slope =	3.878
Intercept =	9.870e-01
Correlation coefficient, r =	0.993751
C constant=	4.929
Surface Area =	715.804 m²/g

Quantachrome NovaWin - Data Acquisition and Reduction
for NOVA instruments
©1994-2013, Quantachrome Instruments
version 11.03

Analysis				Report			
Operator:	Abdulrahman Abdulkareem	Date:2007/05/14		Operator:	quantachrome	Date:2020/08/24	
Sample ID:	Sample ACRPSAC	Filename:		Sample ACRPSAC.qps			
Sample Desc:		Comment:					
Sample weight:	0.08 g	Sample Volume:		1 cc			
Outgas Time:	3.0 hrs	OutgasTemp:		250.0 C			
Analysis gas:	Nitrogen	Bath Temp:		273.0 K			
Press. Tolerance:	0.100/0.100 (ads/des)	Equil time:		60/60 sec (ads/des)	Equil timeout:	240/240 sec (ads/des)	
Analysis Time:	68.7 min	End of run:		2007/05/14 17:48:54	Instrument:	Nova Station C	
Cell ID:	3						

Langmuir

Data Reduction Parameters Data

Adsorbate	Nitrogen		Temperature	77.350K		
	Molec. Wt.:	28.013	Cross Section:	16.200 Å²	Liquid Density:	0.808 g/cc

Langmuir Data

P/Po	P/Po/W [(g/g)]	P/Po	P/Po/W [(g/g)]
1.10281e-01	1.3056e+00	3.39213e-01	1.5182e+00
2.05990e-01	1.3788e+00	3.97060e-01	1.5521e+00
2.78838e-01	1.4585e+00		

Langmuir summary

Slope =	0.89515
Intercept =	1.20430
Correlation coefficient, r =	0.996
Surface Area =	3890.431 m²/g

Quantachrome NovaWin - Data Acquisition and Reduction
for NOVA instruments
©1994-2013, Quantachrome Instruments
version 11.03

Analysis				Report			
Operator:	Abdulrahman Abdulkareem	**Date:**	2007/05/14	**Operator:**	quantachrome	**Date:**	2020/08/24
Sample ID:	Sample ACRPSAC	**Filename:**		Sample ACRPSAC.qps			
Sample Desc:		**Comment:**					
Sample weight:	0.08 g	**Sample Volume:**		1 cc			
Outgas Time:	3.0 hrs	**OutgasTemp:**		250.0 C			
Analysis gas:	Nitrogen	**Bath Temp:**		273.0 K			
Press. Tolerance:	0.100/0.100 (ads/des)	**Equil time:**		60/60 sec (ads/des)	**Equil timeout:**		240/240 sec (ads/des)
Analysis Time:	68.7 min	**End of run:**		2007/05/14 17:48:54	**Instrument:**		Nova Station C
Cell ID:	3						

Isotherm

Data Reduction Parameters Data

Adsorbate	Nitrogen				
	Molec. Wt.:	28.013	**Temperature**	77.350K	
			Cross Section:	16.200 A^2	**Liquid Density:** 0.808 g/cc

Isotherm Data

Relative Pressure	Volume @ STP [cc/g]	Relative Pressure	Volume @ STP [cc/g]	Relative Pressure	Volume @ STP [cc/g]
1.10281e-01	67.5831	2.78838e-01	152.9617	3.97060e-01	204.6807
2.05990e-01	119.5314	3.39213e-01	178.7745		

Analysis				Report			
Operator:	Abdulrahman Abdulkareem	Date:2007/05/14		Operator:	quantachrome	Date:2020/08/24	
Sample ID:	Sample ACRPSAC	Filename:		Sample ACRPSAC.qps			
Sample Desc:		Comment:					
Sample weight:	0.08 g	Sample Volume:		1 cc			
Outgas Time:	3.0 hrs	OutgasTemp:		250.0 C			
Analysis gas:	Nitrogen	Bath Temp:		273.0 K			
Press. Tolerance:	0.100/0.100 (ads/des)	Equil time:		60/60 sec (ads/des)	Equil timeout:	240/240 sec (ads/des)	
Analysis Time:	68.7 min	End of run:		2007/05/14 17:48:54	Instrument:	Nova Station C	
Cell ID:	3						

DR method

Data Reduction Parameters Data

DR method	Affinity coefficient (ß): 0.3300				
Adsorbate	Nitrogen	Temperature	77.350K		
	Molec. Wt.: 28.013	Cross Section:	16.200 Å²	Liquid Density:	0.808 g/cc
	Critical Temp.: 126.200 K	Critical Press.:	33.500 atm	SuperCritic. K.:	1.000
Adsorbent	Carbon				
	DR. Exp (n): 2.000				

DR method Data

Log2(P/Po)	Weight Adsorbed [(g)]	Log2(P/Po)	Weight Adsorbed [(g)]
9.168049e-01	6.7574e-03	2.204561e-01	1.7875e-02
4.708071e-01	1.1951e-02	1.609164e-01	2.0465e-02
3.076344e-01	1.5294e-02		

DR method summary

Slope =	-6.214e-01
Intercept =	2.450e-02
Correlation Coefficient =	0.9960
Average Pore width =	6.929nm
Adsorption energy =	3.752 kJ/mol
Micropore volume =	0.379 cc/g
Micropore surface area =	1066.338 m²/g

Analysis
Operator: Abdulrahman Abdulkareem **Date:** 2007/05/14
Sample ID: Sample ACRPSAC **Filename:** Sample ACRPSAC.qps

Report
Operator: quantachrome **Date:** 2020/08/24

DA Method Micropore Analysis Data continued

Diameter [nm]	dV(d) [cc/nm/g]	Diameter [nm]	dV(d) [cc/nm/g]
4.66000e+00	7.13194e-02	5.34000e+00	4.11184e-02
4.68000e+00	7.01378e-02	5.36000e+00	4.04822e-02
4.70000e+00	6.89776e-02	5.38000e+00	3.98573e-02
4.72000e+00	6.78384e-02	5.40000e+00	3.92434e-02
4.74000e+00	6.67197e-02	5.42000e+00	3.86405e-02
4.76000e+00	6.56214e-02	5.44000e+00	3.80482e-02
4.78000e+00	6.45429e-02	5.46000e+00	3.74664e-02
4.80000e+00	6.34840e-02	5.48000e+00	3.68949e-02
4.82000e+00	6.24443e-02	5.50000e+00	3.63334e-02
4.84000e+00	6.14235e-02	5.52000e+00	3.57818e-02
4.86000e+00	6.04211e-02	5.54000e+00	3.52399e-02
4.88000e+00	5.94370e-02	5.56000e+00	3.47075e-02
4.90000e+00	5.84707e-02	5.58000e+00	3.41844e-02
4.92000e+00	5.75219e-02	5.60000e+00	3.36705e-02
4.94000e+00	5.65903e-02	5.62000e+00	3.31655e-02
4.96000e+00	5.56757e-02	5.64000e+00	3.26693e-02
4.98000e+00	5.47776e-02	5.66000e+00	3.21817e-02
5.00000e+00	5.38957e-02	5.68000e+00	3.17026e-02
5.02000e+00	5.30298e-02	5.70000e+00	3.12318e-02
5.04000e+00	5.21796e-02	5.72000e+00	3.07692e-02
5.06000e+00	5.13448e-02	5.74000e+00	3.03145e-02
5.08000e+00	5.05251e-02	5.76000e+00	2.98677e-02
5.10000e+00	4.97201e-02	5.78000e+00	2.94285e-02
5.12000e+00	4.89297e-02	5.80000e+00	2.89969e-02
5.14000e+00	4.81535e-02	5.82000e+00	2.85726e-02
5.16000e+00	4.73913e-02	5.84000e+00	2.81556e-02
5.18000e+00	4.66429e-02	5.86000e+00	2.77458e-02
5.20000e+00	4.59078e-02	5.88000e+00	2.73429e-02
5.22000e+00	4.51860e-02	5.90000e+00	2.69468e-02
5.24000e+00	4.44771e-02	5.92000e+00	2.65575e-02
5.26000e+00	4.37809e-02	5.94000e+00	2.61748e-02
5.28000e+00	4.30972e-02	5.96000e+00	2.57985e-02
5.30000e+00	4.24257e-02	5.98000e+00	2.54286e-02
5.32000e+00	4.17662e-02		

DA method summary

Best E =	0.911 kJ/mol
Best n =	1.200
DA Micropore Volume =	0.574 cc/g
Pore Diameter (mode)=	2.760e+00 nm

Analysis

Operator:	Abdulrahman AbdulkareemDate:2007/05/14		
Sample ID:	Sample ACRPSAC	**Filename:**	Sample ACRPSAC.qps
Sample Desc:		**Comment:**	
Sample weight:	0.08 g	**Sample Volume:**	1 cc
Outgas Time:	3.0 hrs	**OutgasTemp:**	250.0 C
Analysis gas:	Nitrogen	**Bath Temp:**	273.0 K
Press. Tolerance:	0.100/0.100 (ads/des)	**Equil time:**	60/60 sec (ads/des)
Analysis Time:	68.7 min	**End of run:**	2007/05/14 17:48:54
Cell ID:	3		

Report

Operator:	quantachrome	**Date:**	2020/08/24
Equil timeout:	240/240 sec (ads/des)		
Instrument:	Nova Station C		

DFT method Pore Size Distribution

Data Reduction Parameters Data

DFT method	**Calc. Model:** N2 at 77 K on carbon (slit pore, NLDFT equilibrium model)				
	Rel. press. range: 0.0000 - 1.0000			**Moving pt. avg:** off	
Adsorbate	Nitrogen	Temperature	77.350K		
	Molec. Wt.: 28.013	**Cross Section:**	16.200 Å²	**Liquid Density:**	0.808 g/cc

DFT method Pore Size Distribution Data

Pore width [nm]	Cumulative Pore Volume [cc/g]	Cumulative Surface Area [m²/g]	dV(d) [cc/nm/g]	dS(d) [m²/nm/g]
2.0208	2.4663e-02	3.1321e+01	4.9821e-02	4.9307e+01
2.1138	2.4663e-02	3.1321e+01	0.0000e+00	0.0000e+00
2.2111	3.3984e-02	3.9752e+01	9.5800e-02	8.6652e+01
2.3129	6.4884e-02	6.6471e+01	3.0361e-01	2.6254e+02
2.4194	9.3510e-02	9.0136e+01	2.6890e-01	2.2229e+02
2.5307	1.2452e-01	1.1464e+02	2.7848e-01	2.2008e+02
2.6472	1.6120e-01	1.4236e+02	3.1492e-01	2.3793e+02
2.7691	1.9651e-01	1.6786e+02	2.8974e-01	2.0927e+02
2.8965	2.2996e-01	1.9096e+02	2.6249e-01	1.8125e+02
3.0298	2.5848e-01	2.0978e+02	2.1389e-01	1.4119e+02
3.1693	2.9242e-01	2.3120e+02	2.4338e-01	1.5359e+02

DFT method summary

Pore volume =	0.292 cc/g
Surface area =	231.199 m²/g
Lower confidence limit =	2.021 nm
Fitting error =	2.090 %
Pore width (Mode) =	2.647 nm
Moving point average :	off

Analysis				Report			
Operator:	Abdulrahman Abdulkareem	**Date:**	2007/05/14	**Operator:**	quantachrome	**Date:**	2020/08/24
Sample ID:	Sample ACRPSAC	**Filename:**		Sample ACRPSAC.qps			
Sample Desc:		**Comment:**					
Sample weight:	0.08 g	**Sample Volume:**		1 cc			
Outgas Time:	3.0 hrs	**OutgasTemp:**		250.0 C			
Analysis gas:	Nitrogen	**Bath Temp:**		273.0 K			
Press. Tolerance:	0.100/0.100 (ads/des)	**Equil time:**		60/60 sec (ads/des)	**Equil timeout:**		240/240 sec (ads/des)
Analysis Time:	68.7 min	**End of run:**		2007/05/14 17:48:54	**Instrument:**		Nova Station C
Cell ID:	3						

Area-Volume Summary

Data Reduction Parameters Data

	Thermal Transpiration: on	**Eff. mol. diameter (D):** 3.54 Å		**Eff. cell stem diam. (d):** 4.0000 mm
t-Method	**Calc. method:** de Boer			
BJH/DH method	**Moving pt. avg.:** off			
DR method	**Affinity coefficient (ß):** 0.3300			
HK method	**Tabulated data interval:** 1			
SF method	**Tabulated data interval:** 1			
DFT method	**Calc. Model:** N2 at 77 K on carbon (slit pore, NLDFT equilibrium model)			
	Rel. press. range: 0.0000 - 1.0000			**Moving pt. avg:** off
Adsorbate	Nitrogen	**Temperature**	77.350K	
	Molec. Wt.: 28.013	**Cross Section:**	16.200 Å²	**Liquid Density:** 0.808 g/cc
	Critical Temp.: 126.200 K	**Critical Press.:**	33.500 atm	**SuperCritic. K.:** 1.000
Adsorbent	Carbon			
	DR. Exp (n): 2.000			

Surface Area Data

SinglePoint BET	5.371e+02 m²/g
MultiPoint BET	7.158e+02 m²/g
Langmuir surface area	3.890e+03 m²/g
BJH method cumulative adsorption surface area	8.319e+02 m²/g
DH method cumulative adsorption surface area	8.958e+02 m²/g
t-method external surface area	7.158e+02 m²/g
DR method micropore area	1.066e+03 m²/g
DFT cumulative surface area	2.312e+02 m²/g

Pore Volume Data

BJH method cumulative adsorption pore volume	4.709e-01 cc/g
DH method cumulative adsorption pore volume	4.858e-01 cc/g
DR method micropore volume	3.790e-01 cc/g
HK method micropore volume	1.399e-01 cc/g
SF method micropore volume	3.007e-02 cc/g
DFT method cumulative pore volume	2.924e-01 cc/g

Pore Size Data

BJH method adsorption pore Diameter (Mode Dv(d))	1.853e+00 nm
DH method adsorption pore Diameter (Mode Dv(d))	1.853e+00 nm
DR method micropore Pore width	6.929e+00 nm
DA method pore Diameter (Mode)	2.760e+00 nm
HK method pore Diameter (Mode)	1.847e+00 nm
SF method pore Diameter (Mode)	3.340e+00 nm
DFT pore Diameter (Mode)	2.647e+00 nm

APPENDIX C

SUPPLEMENTARY BATCH ADSORPTION DATA

Equilibrium Isotherm Modeling Data for RPSAC

RPSAC Freudlich

Co	Ce	qe	lnCe	lnqe
2	0.08	0.96	-2.53	-0.04
4	0.21	1.9	-1.56	0.64
6	0.36	2.82	-1.02	1.04
8	1.39	3.32	0.33	1.2
10	1.44	4.28	0.36	1.45
12	1.49	5.26	0.4	1.66
14	1.53	6.24	0.43	1.83
16	1.72	7.14	0.54	1.97

RPSAC Langmuir					**RPSAC Temkin**			
Co	**Ce**	**qe**	**1/Ce**	**1/qe**	**Co**	**Ce**	**lnCe**	**qe**
2	0.08	0.96	12.5	1.04	2	0.08	-2.53	0.96
4	0.21	1.9	4.76	0.53	4	0.21	-1.56	1.9
6	0.36	2.82	2.78	0.35	6	0.36	-1.02	2.82
8	1.39	3.32	0.72	0.3	8	1.39	0.33	3.32
10	1.44	4.28	0.69	0.23	10	1.44	0.36	4.28
12	1.49	5.26	0.67	0.19	12	1.49	0.4	5.26
14	1.53	6.24	0.65	0.16	14	1.53	0.43	6.24
16	1.72	7.14	0.58	0.14	16	1.72	0.54	7.14

Equilibrium Isotherm Modeling Data for ACRPSAC

ACRPSAC Freudlich				
Co	**Ce**	**qe**	**lnCe**	**lnqe**
2	0.06	0.97	-2.81	-0.03
4	0.09	1.96	-2.41	0.67
6	0.82	2.59	-0.2	0.95
8	0.9	3.55	-0.11	1.27
10	1.24	4.38	0.22	1.48
12	1.36	5.32	0.31	1.67
14	1.49	6.26	0.4	1.83
16	1.53	7.24	0.42	1.98

ACRPSAC Langmuir					ACRPSAC Temkin			
Co	**Ce**	**qe**	**1/Ce**	**1/qe**	**Co**	**Ce**	**lnCe**	**qe**
2	0.06	0.97	16.67	1.03	2	0.06	-2.81	0.97
4	0.09	1.96	11.11	0.51	4	0.09	-2.41	1.96
6	0.82	2.59	1.22	0.39	6	0.82	-0.2	2.59
8	0.9	3.55	1.11	0.28	8	0.9	-0.11	3.55
10	1.24	4.38	0.81	0.23	10	1.24	0.22	4.38
12	1.36	5.32	0.74	0.19	12	1.36	0.31	5.32
14	1.49	6.26	0.67	0.16	14	1.49	0.4	6.26
16	1.53	7.24	0.65	0.14	16	1.53	0.42	7.24

Equilibrium Isotherm Modeling Data for CAC

CAC Freudlich				
Co	**Ce**	**qe**	**lnCe**	**lnqe**
2	0.46	0.77	-0.78	-0.26
4	1.02	1.49	0.02	0.4
6	2.18	1.91	0.78	0.65
8	2.98	2.51	1.09	0.92
10	3.19	3.41	1.16	1.23
12	3.86	4.07	1.35	1.4
14	4.25	4.88	1.45	1.59
16	4.94	5.53	1.6	1.71

CAC Langmuir				
Co	**Ce**	**qe**	**1/Ce**	**1/qe**
2	0.46	0.77	2.17	1.3
4	1.02	1.49	0.98	0.67
6	2.18	1.91	0.46	0.52
8	2.98	2.51	0.34	0.4
10	3.19	3.41	0.31	0.29
12	3.86	4.07	0.26	0.25
14	4.25	4.88	0.24	0.2
16	4.94	5.53	0.2	0.18

CAC Temkin			
Co	**Ce**	**lnCe**	**qe**
2	0.46	-0.78	0.77
4	1.02	0.02	1.49
6	2.18	0.78	1.91
8	2.98	1.09	2.51
10	3.19	1.16	3.41
12	3.86	1.35	4.07
14	4.25	1.45	4.88
16	4.94	1.6	5.53

Kinetics Data for RPSAC

RPSAC Pseudo First Order					
t	**Ce**	**qe**	**qt**	**t**	**Log(qe - qt)**
15	0.91	2.99	2.54	15	-0.347
30	0.74	2.99	2.63	30	-0.444
45	0.26	2.99	2.87	45	-0.921
60	0.04	2.99	2.98	60	-2
75	0.03	2.99	2.985	75	-2.301
90	0.02	2.99	2.99	90	0
105	0.02	2.99	2.99	105	0
120	0.02	2.99	2.99	120	0

RPSAC Pseudo 2nd Order			
t	**qt**	**t**	**t/qt**
15	2.54	15	5.91
30	2.63	30	11.41
45	2.87	45	15.68
60	2.98	60	20.13
75	2.985	75	25.13
90	2.99	90	30.1
105	2.99	105	35.11
120	2.99	120	40.13

RPSAC Webber-Moris Intra-particle Diffusion		
t	**$t^{1/2}$**	**qt**
15	3.87	2.54
30	5.48	2.63
45	6.71	2.87
60	7.75	2.98
75	8.66	2.985
90	9.49	2.99
105	10.25	2.99
120	10.95	2.99

RPSAC Bangham's Pore Diffusion				
t	**qt**	**ci/(ci - qt)m**	**Logt**	**LogLog [ci/(ci - qi)m]**
15	2.54	8.67	1.18	-0.028
30	2.63	8.9	1.48	-0.022
45	2.87	9.58	1.65	-0.008
60	2.98	9.93	1.78	-0.001
75	2.985	9.95	1.88	-0.0009
90	2.99	9.97	1.95	-0.0006
105	2.99	9.97	2.02	-0.0006
120	2.99	9.97	2.08	-0.0006

RPSAC Elovich		
t	**lnt**	**qt**
15	2.71	2.54
30	3.4	2.63
45	3.81	2.87
60	4.09	2.98
75	4.32	2.985
90	4.5	2.99
105	4.65	2.99
120	4.79	2.99

Kinetics Data for ACRPSAC

ACRPSAC Pseudo First Order					
t	**Ce**	**qe**	**qt**	**t**	**Log(qe - qt)**
15	0.49	3	2.76	15	-0.62
30	0.25	3	2.88	30	-0.921
45	0.2	3	2.9	45	-1
60	0.09	3	2.96	60	-1.4
75	0.04	3	2.98	75	-1.7
90	0.01	3	3	90	0
105	0.01	3	3	105	0
120	0.01	3	3	120	0

ACRPSAC Pseudo 2nd Order			
t	**qt**	**t**	**t/qt**
15	2.76	15	5.43
30	2.88	30	10.42
45	2.9	45	15.52
60	2.96	60	20.27
75	2.98	75	25.18
90	3	90	30
105	3	105	35
120	3	120	40

ACRPSAC Weber-Morris Intra-Particle Diffusion		
t	$t^{1/2}$	qt
15	3.87	2.76
30	5.48	2.88
45	6.71	2.9
60	7.75	2.96
75	8.66	2.98
90	9.49	3
105	10.25	3
120	10.95	3

ACRPSAC Bangham's Pore Diffusion				
t	**qt**	**ci/(ci - qt)m**	**Logt**	**LogLog [ci/(ci - qi)m]**
15	2.76	9.26	1.18	-0.015
30	2.88	9.62	1.48	-0.007
45	2.9	9.68	1.65	-0.006
60	2.96	9.87	1.78	-0.003
75	2.98	9.93	1.88	-0.001
90	3	10	1.95	0
105	3	10	2.02	0
120	3	10	2.08	0

ACRPSAC Elovich		
t	**lnt**	**qt**
15	2.71	2.76
30	3.4	2.88
45	3.81	2.9
60	4.09	2.96
75	4.32	2.98
90	4.5	3
105	4.65	3
120	4.79	3

Kinetics Data for CAC

CAC Pseudo first Order					
t	**Ce**	**qe**	**qt**	**t**	**Log(qe - qt)**
15		2.68	2.14	15	-0.268
30		2.68	2.21	30	-0.328
45		2.68	2.42	45	-0.585
60		2.68	2.51	60	-0.77
75		2.68	2.59	75	-1.046
90		2.68	2.68	90	0
105		2.68	2.75	105	0
120		2.68	2.75	120	0

CAC Pseudo 2nd Order			
t	**qt**	**t**	**t/qt**
15	2.14	15	7.01
30	2.21	30	13.57
45	2.42	45	18.6
60	2.51	60	23.9
75	2.59	75	28.96
90	2.68	90	33.58
105	2.75	105	38.18
120	2.75	120	43.64

CAC WeberMorris Intra-Particle Diffusion		
t	**$t^{1/2}$**	**qt**
15	3.87	2.14
30	5.48	2.21
45	6.71	2.42
60	7.75	2.51
75	8.66	2.59
90	9.49	2.68
105	10.25	2.75
120	10.95	2.75

CAC Bangham's Pore Diffusion				
t	**qt**	**ci/(ci - qt)m**	**Logt**	**LogLog [ci/(ci - qi)m]**
15	2.14	7.77	1.18	-0.05
30	2.21	7.92	1.48	-0.046
45	2.42	8.38	1.65	-0.035
60	2.51	8.6	1.78	-0.03
75	2.59	8.8	1.88	-0.025
90	2.68	9.04	1.95	-0.02
105	2.75	9.04	2.02	-0.02
120	2.75	9.04	2.08	-0.02

CAC Elovich		
t	**lnt**	**qt**
15	2.71	2.14
30	3.4	2.21
45	3.81	2.42
60	4.09	2.51
75	4.32	2.59
90	4.5	2.68
105	4.65	2.75
120	4.79	2.75

Appendix C Contd;

ANOVA Results for Statistical Comparisons of the Adsorbents

Between-Subjects Factors

		Value Label	N
Adsorbent Type	1	ACRPSAC	3
	2	RPSAC	3
	3	CAC	3

Descriptive Statistics

	Adsorbent Type	Mean	Std. Deviation	N
Removal Efficiency (%)	ACRPSAC	99.1333	.30551	3
	RPSAC	94.5667	1.05987	3
	CAC	80.3667	.70946	3
	Total	91.3556	8.50090	9
Adsorption Capacity (mg/g)	ACRPSAC	3.3533	.22368	3
	RPSAC	2.9300	.06083	3
	CAC	2.2667	.22502	3
	Total	2.8500	.50110	9

Multivariate Tests[a]

Effect		Value	F	Hypothesis df	Error df	Sig.
Intercept	Pillai's Trace	1.000	69843.486[b]	2.000	5.000	.000
	Wilks' Lambda	.000	69843.486[b]	2.000	5.000	.000
	Hotelling's Trace	27937.394	69843.486[b]	2.000	5.000	.000
	Roy's Largest Root	27937.394	69843.486[b]	2.000	5.000	.000
Adsorbent	Pillai's Trace	1.151	4.063	4.000	12.000	.026
	Wilks' Lambda	.004	39.202[b]	4.000	10.000	.000
	Hotelling's Trace	234.363	234.363	4.000	8.000	.000
	Roy's Largest Root	234.180	702.539[c]	2.000	6.000	.000

a. Design: Intercept + Adsorbent

b. Exact statistic

c. The statistic is an upper bound on F that yields a lower bound on the significance level.

Tests of Between-Subjects Effects

Source	Dependent Variable	Type III Sum of Squares	df	Mean Square	F	Sig.
Corrected Model	Removal Efficiency (%)	574.682[a]	2	287.341	501.176	.000
	Adsorption Capacity (mg/g)	1.800[b]	2	.900	25.871	.001
Intercept	Removal Efficiency (%)	75112.538	1	75112.538	131010.240	.000
	Adsorption Capacity (mg/g)	73.103	1	73.103	2101.317	.000
Adsorbent	Removal Efficiency (%)	574.682	2	287.341	501.176	.000
	Adsorption Capacity (mg/g)	1.800	2	.900	25.871	.001
Error	Removal Efficiency (%)	3.440	6	.573		
	Adsorption Capacity (mg/g)	.209	6	.035		
Total	Removal Efficiency (%)	75690.660	9			
	Adsorption Capacity (mg/g)	75.111	9			
Corrected Total	Removal Efficiency (%)	578.122	8			
	Adsorption Capacity (mg/g)	2.009	8			

a. R Squared = .994 (Adjusted R Squared = .992)

b. R Squared = .896 (Adjusted R Squared = .861)

Estimated Marginal Means

1. Grand Mean

Dependent Variable	Mean	Std. Error	95% Confidence Interval	
			Lower Bound	Upper Bound
Removal Efficiency (%)	91.356	.252	90.738	91.973
Adsorption Capacity (mg/g)	2.850	.062	2.698	3.002

2. Adsorbent Type

Dependent Variable	Adsorbent Type	Mean	Std. Error	95% Confidence Interval	
				Lower Bound	Upper Bound
Removal Efficiency (%)	ACRPSAC	99.133	.437	98.064	100.203
	RPSAC	94.567	.437	93.497	95.636
	CAC	80.367	.437	79.297	81.436
Adsorption Capacity (mg/g)	ACRPSAC	3.353	.108	3.090	3.617
	RPSAC	2.930	.108	2.667	3.193
	CAC	2.267	.108	2.003	2.530

Post Hoc Tests

Removal Efficiency (%)

Duncan[a,b,c]

Adsorbent Type	N	Subset		
		1	2	3
CAC	3	80.3667		
RPSAC	3		94.5667	
ACRPSAC	3			99.1333
Sig.		1.000	1.000	1.000

c. Alpha = .05.

Adsorption Capacity (mg/g)

Duncan[a,b,c]

Adsorbent Type	N	Subset		
		1	2	3
CAC	3	2.2667		
RPSAC	3		2.9300	
ACRPSAC	3			3.3533
Sig.		1.000	1.000	1.000

c. Alpha = .05.

APPENDIX D

RAW AND OTHER STATISTICAL DATA FOR GROUNDWATER QUALITY ASSESSMENT

Table SI: Raw Water Quality Data with Replications

Sample	Replications	pH	TDS (mg/l)	EC (µS/cm)	Cl^- (mg/l)	CO_3^{2-} (mg/l)	HCO_3^- (mg/l)	SO_4^{2-} (mg/l)	NO_3^- (mg/l)	F^- (mg/l)	Na^+ (mg/l)	K^+ (mg/l)	Ca^{2+} (mg/l)	Mg^{2+} (mg/l)
Achusa P1	**1**	6.82	1187.4	2139.5	136.3	8.7	431.4	**383.2**	6.91	1.44	289.3	5.72	78.9	183.2
	2	6.74	1268.1	2383.4	188.9	8,1	389.2	432.0	7.14	1.39	217.7	6.06	69.0	202.3
	3	6.81	1278.2	2393.6	178.7	7.6	382.4	384.5	6.83	1.53	237.9	6.32	72.3	216.7
Ichwa P2	**1**	**6.73**	1136.0	2218.9	231.2	12.6	317.2	**469.0**	10.51	1.56	372.5	6.91	134.8	82.4
	2	**6.70**	905.1	1893.7	218.0	12.3	368.0	**462.3**	10.43	1.51	403.1	4.83	156.7	93.8
	3	6.75	899.6	1384.5	186.4	11.0	304.5	487.3	9.29	1.37	387.6	7.39	132.4	80.4
B Div. P3	**1**	6.48	921.2	1812.7	**167.3**	14.0	293.7	**326.7**	5.80	1.35	229.1	7.31	174.6	65.6
	2	6.43	856.5	1520.4	**209.5**	15.3	236.8	**290.0**	6.32	1.62	234.5	9.02	149.0	43.9
	3	6.47	992.7	1722.6	159.1	14.8	244.9	314.2	6.41	1.44	302.3	8.11	189.3	54.8
Barr. Rd. P4	**1**	6.43	998.3	1749.5	**358.6**	27.1	521.9	249.1	2.93	1.56	158.2	4.82	72.3	162.7
	2	6.21	1048.0	1836.0	**482.4**	19,6	408.3	286.0	2.91	1.55	179.3	4.80	68.3	128.6
	3	6.39	793.7	1307.9	532.6	25.1	513.7	301.6	2.88	1.48	153.2	3.76	84.2	237.7
Logo I P5	**1**	6.80	1232.4	2487.4	93.7	17.9	448.7	**283.4**	8.32	1.23	244.9	5.44	83.6	113.4

	2	6.68	1056.2	1896.3	127.4	18.3	482.3	**232.8**	7.90	1.30	246.8	6.34	76.5	146.3
	3	6.77	1107.4	2032.6	96.1	13.5	483.6	298.4	8,92	1.22	274.4	5.92	70.2	149.0
Wurukum P6	**1**	6.74	1358.7	2019.1	**174.9**	33.6	216.0	369.2	4.75	1.52	262.8	8.19	125.7	36.9
	2	6.80	1382.5	2086.7	**177.3**	29.9	164.9	372.2	3.75	1.58	289.0	6.39	146.6	52.1
	3	6.71	1471.5	2249.5	186.0	21.6	198.4	340.4	4.31	1.57	322.2	8.00	128.2	28.6
Nyiman P7	**1**	**6.83**	209.3	411.8	211.4	9.8	184.5	263.4	8.93	1.35	212.7	3.08	69.2	54.6
	2	**6.45**	306.9	474.0	307.8	4.5	206.2	198.3	9.00	1.21	189.3	4.19	57.3	65.7
	3	6.34	200.5	397.4	199.2	6.7	173.4	243.1	9.02	1.33	193.4	3.85	74.1	48.3
Gyado Villa P8	**1**	6.67	**1136.1**	**1982.3**	38.1	20.3	601.6	**412.6**	2.69	1.47	338.5	9.21	143.8	96.1
	2	6.28	**811.8**	**1489.1**	38.5	16.4	532.2	**483.5**	2.61	1.58	379.1	9.38	134.5	82.1
	3	6.53	1129.7	**2110.2**	44.7	24.7	468.5	492.1	2.39	1.53	344.2	11.49	126.9	103.2
Welfare Qtrs P9	**1**	6.48	**697.6**	**937.3**	228.1	11.6	338.5	428.5	1.48	0.43	314.7	7.65	127.4	154.5
	2	6.36	**424.5**	**733.5**	206.7	9.1	300.8	387.4	0.58	0.81	275.4	7.83	163.2	209.1
	3	6.41	602.9	1092.4	208.1	12.5	334.5	403.7	1.14	0.65	320.3	6.95	148.7	182.6
Akpehe P10	**1**	6.69	**1215.0**	**1974.8**	47.4	19.7	273.8	**89.5**	4.67	1.18	79.4	2.64	72.1	58.3
	2	6.52	**1328.3**	**2134.8**	69.5	21.6	179.0	**108.3**	6.39	1.29	115.6	2.04	69.5	43.5
	3	6.49	984.6	1843.9	58.2	16.8	236.4	83.4	4.85	1.31	123.7	1.85	78.6	74.8
Coca Cola P11	**1**	6.71	**447.5**	**732.9**	190.3	28.4	373.4	**134.7**	3.72	0.49	86.8	2.30	112.7	66.0
	2	6.69	**467.8**	**881.1**	147.6	27.0	334.1	**123.2**	6.22	0.61	74.5	3.52	124.4	51.0
	3	6.44	301.4	629.5	144.2	28.1	377.0	130.4	6.36	0.44	68.9	2.76	113.8	63.7
Nyor Gyungu P12	**1**	6.37	887.6	**1321.2**	126.5	12.7	119.3	39.6	5.30	1.33	34.3	2.15	65.9	69.8
	2	6.51	803.4	**1235.6**	89.1	14.9	95.0	48.3	4.71	1.62	69.0	1.47	78.3	81.4
	3	6.38	528.6	927.4	119.2	11.1	112.3	53.9	4.03	1.47	46.2	2.03	79.9	72.1
Mbaky	**1**	6.30	704.5	1372.0	331.4	6.04	214.0	374.9	14.15	2.06	245.6	6.24	90.2	127.1

aa P13	**2**	6.33	458.1	748.5	402.3	5.06	226.7	232.1	16.39	1.92	184.5	7.40	106.4	95.7
	3	6.41	766.2	1432.5	384.8	8.29	273.2	342.4	15.60	2.00	259.2	7.03	121.5	116.4
Modern Mkt P14	**1**	6.50	347.4	629.4	58.9	10.9	389.7	158.3	2.78	0.43	69.9	1.96	74.5	60.2
	2	6.37	177.3	368.9	52.7	7.3	402.2	177.4	3.99	0.32	112.3	1.74	53.6	62.3
	3	6.48	394.0	521.4	49.0	11.9	378.6	163.0	4.03	0.61	87.4	2.32	58.3	75.8
Tse Abu P15	**1**	6.66	**157.6**	**293.5**	**176.6**	14.5	149.8	**281.5**	3.21	1.51	173.2	3.29	62.6	61.7
	2	6.73	**201.5**	**374.0**	**238.3**	10.3	116.3	**309.7**	3.19	1.50	138.5	2.78	76.4	83.1
	3	6.82	121.3	248.5	183.1	13.7	137.5	318.3	2.86	1.51	109.4	2.38	78.1	65.9
Owner Occ Qtrs P16	**1**	6.20	**571.5**	**896.7**	**49.5**	18.9	460.2	**314.7**	2.83	0.83	285.6	4.85	65.3	70.3
	2	6.25	**610.3**	**1025.3**	**41.5**	18.7	502.0	**299.0**	3.02	0.88	327.6	5.09	59.0	68.3
	3	6.34	394.7	821.4	47.2	17.4	504.2	307.7	3.00	0.75	341.4	4.65	57.4	74.2
Abua P17	**1**	6.82	**98.3**	**176.6**	**68.0**	0.0	232.4	392.2	9.36	0.61	270.1	4.03	135.3	62.2
	2	6.73	**89.8**	**158.4**	**90.3**	0.0	198.8	422.2	8.73	0.53	230.2	3.37	179.4	83.6
	3	6.60	106.4	183.9	75.2	0.0	186.3	438.4	8.97	1.07	248.3	5.64	213.7	77.4
High Level P18	**1**	**6.38**	1292.5	**2154.2**	268.2	25.6	570.5	274.6	0.89	1.59	116.5	3.14	81.4	83.9
	2	**6.49**	1182.0	**1932.2**	301.4	26.4	562.7	277.1	2.15	1.55	148.0	4.50	58.3	59.3
	3	6.33	957.1	1732.5	296.7	25.0	539.1	223.8	1.74	1.72	157.6	3.74	72.3	66.9
Naka Rd P19	**1**	**6.76**	721.7	1098.1	139.3	21.8	419.6	87.4	6.40	1.53	83.8	2.53	77.6	34.5
	2	**6.42**	574.2	972.1	111.5	19.8	438.9	88.0	5.20	1.57	80.2	1.90	68.5	47.3
	3	6.31	520.4	892.6	138.6	14.6	426.3	83.6	5.68	1.50	76.4	2.15	70.9	48.1
Agan P20	**1**	**6.47**	**273.7**	439.2	**72.1**	0.00	294.5	321.7	7.22	1.03	292.3	6.09	169.3	136.7
	2	**6.49**	**202.3**	388.7	**62.1**	0.00	345.6	344.7	7.05	0.92	305.6	7.11	203.8	89.3
	3	6.35	285.5	479.2	74.4	0.00	307.1	348.2	8.18	1.10	314.2	6.29	221.0	109.6
Apir P21	**1**	6.32	433.4	785.7	103.6	13.2	324.7	291.1	8.17	1.27	225.7	5.30	58.7	65.1
	2	6.20	379.2	643.0	89.8	15.1	326.9	306.6	8.06	1.22	198.6	5.00	45.8	53.0
	3	6.38	207.6	495.8	115.8	17.3	314.2	299.4	7.49	1.31	199.3	4.86	63.2	38.2

Table SIII: Relative Weights of Water Quality Parameters in accordance with the WHO (2011) Guidelines for Drinking Water Quality

S/No	Chemical Parameter	WHO Standard	Weight (w_i)	Relative Weight (W_i)
1	pH	6.5 - 8.5	5	0.1
2	TDS (mg/L)	1000	5	0.1
3	EC (µs/cm)	1500	5	0.1
4	Chloride (mg/L)	200	5	0.1
5	Fluoride (mg/L)	1.5	5	0.1
6	Nitrate (mg/L)	50	5	0.1
7	Sulphate (mg/L)	250	4	0.08
8	Potassium (mg/L)	50	4	0.08
9	Bicarbonate (mg/L)	500	3	0.06
10	Sodium (mg/L)	200	3	0.06
11	Calcium (mg/L)	75	3	0.06
12	Magnesium (mg/L)	150	3	0.06

Table SIV: Computation of WQI for All Locations

Sample Location	S/No	Parameter	C_i	W_i	S_i	$q_i = C_i/S_i \times 100$	$Sl_i = W_i \times q_i$
P1 (Achusa)							
	1	pH	6.79	0.1	8.50	79.88	7.99
	2	TDS	1244.57	0.1	1000	124.46	12.45
	3	EC	2305.50	0.1	1500	153.7	15.37
	4	Chloride	167.97	0.1	200	83.99	8.40
	5	Fluoride	1.45	0.1	1.5	96.67	9.67
	6	Nitrate	6.96	0.1	50	13.92	1.39
	7	Sulphate	399.90	0.08	250	159.96	12.80
	8	Potassium	6.03	0.08	50	12.06	0.96
	9	Bicarbonate	401.00	0.06	500	80.2	4.81
	10	Sodium	248.30	0.06	200	124.15	7.45
	11	Calcium	73.40	0.06	75	97.87	5.87
	12	Magnesium	200.73	0.06	150	133.82	8.03
		$WQI = \sum_{i=1}^{n} SI_i$					**95.19**

Sample Location	S/No	Parameter	C_i	W_i	S_i	$q_i = C_i/S_i \times 100$	$Sl_i = W_i \times q_i$
P2 (Ichwa)	1	pH	6.72	0.1	8.50	79.06	7.91
	2	TDS	980.00	0.1	1000	98.00	9.80
	3	EC	1832.87	0.1	1500	122.19	12.22
	4	Chloride	211.87	0.1	200	105.94	10.59
	5	Fluoride	1.48	0.1	1.5	98.67	9.87
	6	Nitrate	10.08	0.1	50	20.16	2.02
	7	Sulphate	472.87	0.08	250	189.15	15.13

	8	Potassium	6.38	0.08	50	12.76	1.02
	9	Bicarbonate	329.90	0.06	500	65.98	3.96
	10	Sodium	387.73	0.06	200	193.87	11.63
	11	Calcium	141.30	0.06	75	188.40	11.30
	12	Magnesium	85.53	0.06	150	57.02	3.42
		$WQI = \sum_{i=1}^{n} SI_i$					**98.87**
Sample Location	**S/No**	**Parameter**	**C_i**	**W_i**	**S_i**	**$q_i = C_i/S_i \times 100$**	**$Sl_i = W_i \times q_i$**
P3 (B. Div.)							
	1	pH	6.46	0.1	8.50	76.00	7.60
	2	TDS	923.47	0.1	1000	92.35	9.24
	3	EC	1685.23	0.1	1500	112.35	11.24
	4	Chloride	178.63	0.1	200	89.32	8.93
	5	Fluoride	1.47	0.1	1.5	98.00	9.80
	6	Nitrate	6.18	0.1	50	12.36	1.24
	7	Sulphate	310.30	0.08	250	124.12	9.93
	8	Potassium	8.15	0.08	50	16.30	1.30
	9	Bicarbonate	258.47	0.06	500	51.69	3.10
	10	Sodium	255.30	0.06	200	127.65	7.66
	11	Calcium	170.97	0.06	75	227.96	13.68
	12	Magnesium	54.77	0.06	150	36.51	2.19
		$WQI = \sum_{i=1}^{n} SI_i$					**85.91**

Sample Location	S/No	Parameter	C_i	W_i	S_i	$q_i = C_i/S_i \times 100$	$Sl_i = W_i \times q_i$
P4 (Barr. Rd.)							
	1	pH	6.34	0.1	8.50	74.59	7.46
	2	TDS	946.67	0.1	1000	94.67	9.47
	3	EC	1631.13	0.1	1500	108.74	10.87
	4	Chloride	457.87	0.1	200	228.93	22.89
	5	Fluoride	1.53	0.1	1.5	102.00	10.2
	6	Nitrate	2.91	0.1	50	5.82	0.58
	7	Sulphate	278.90	0.08	250	111.56	8.92
	8	Potassium	4.46	0.08	50	8.92	0.71
	9	Bicarbonate	481.30	0.06	500	96.26	5.78
	10	Sodium	163.57	0.06	200	81.79	4.91
	11	Calcium	74.93	0.06	75	99.91	5.99
	12	Magnesium	176.33	0.06	150	117.55	7.05
		$WQI = \sum_{i=1}^{n} SI_i$					**94.83**

Table SV: Computation of Fluoride Risk Parameters

Location	F^- Conc. (C_i in mg/L)	Rfd (mg/kg/d)	Mean Water intake (C_y in L/d)				Average Body Weight (B_x in kg)				Estimated Daily Intake (EDI in mg/kgB_x/d)				Hazard Quotient (HQ = EDI/RfD)			
			Infants	Children	Teenagers	Adults	Infants	Children	Teenagers	Adults	Infants	Children	Teenagers	Adults	Infants	Children	Teenagers	Adults
P1	1.45	0.06	0.50	1.00	2.00	2.5	10.0	18.0	45.00	70.0	0.073	0.081	0.064	0.052	1.217	1.350	1.067	0.867
P2	1.48	0.06	0.50	1.00	2.00	2.5	10.0	18.0	45.00	70.0	0.074	0.082	0.066	0.053	1.233	1.367	1.067	0.883
P3	1.47	0.06	0.50	1.00	2.00	2.5	10.0	18.0	45.00	70.0	0.074	0.082	0.065	0.053	1.233	1.367	1.083	0.883
P4	1.53	0.06	0.50	1.00	2.00	2.5	10.0	18.0	45.00	70.0	0.077	0.085	0.068	0.055	1.283	1.417	1.133	0.917
P5	1.25	0.06	0.50	1.00	2.00	2.5	10.0	18.0	45.00	70.0	0.062	0.069	0.056	0.045	1.033	1.15	0.933	0.75
P6	1.56	0.06	0.50	1.00	2.00	2.5	10.0	18.0	45.00	70.0	0.075	0.083	0.067	0.056	1.250	1.383	1.117	0.933
P7	1.30	0.06	0.50	1.00	2.00	2.5	10.0	18.0	45.00	70.0	0.065	0.072	0.058	0.046	1.083	1.200	0.967	0.767
P8	1.53	0.06	0.50	1.00	2.00	2.5	10.0	18.0	45.00	70.0	0.075	0.085	0.068	0.055	1.250	1.417	1.133	0.917
P9	0.63	0.06	0.50	1.00	2.00	2.5	10.0	18.0	45.00	70.0	0.030	0.035	0.028	0.023	0.500	0.583	0.467	0.383
P10	1.26	0.06	0.50	1.00	2.00	2.5	10.0	18.0	45.00	70.0	0.060	0.070	0.056	0.045	1.000	1.167	0.933	0.750
P11	0.51	0.06	0.50	1.00	2.00	2.5	10.0	18.0	45.00	70.0	0.025	0.028	0.023	0.018	0.417	0.467	0.383	0.300

P12	1.47	0.06	0.50	1.00	2.00	2.5	10.0	18.0	45.00	70.0	0.074	0.082	0.065	0.053	1.233	1.367	1.083	0.883
P13	1.99	0.06	0.50	1.00	2.00	2.5	10.0	18.0	45.00	70.0	0.100	0.110	0.088	0.071	1.667	1.833	1.467	1.183
P14	0.45	0.06	0.50	1.00	2.00	2.5	10.0	18.0	45.00	70.0	0.023	0.025	0.020	0.016	0.383	0.417	0.333	0.267
P15	1.51	0.06	0.50	1.00	2.00	2.5	10.0	18.0	45.00	70.0	0.075	0.083	0.067	0.054	1.250	1.383	1.117	0.900
P16	0.82	0.06	0.50	1.00	2.00	2.5	10.0	18.0	45.00	70.0	0.041	0.046	0.036	0.029	0.683	0.767	0.600	0.483
P17	0.74	0.06	0.50	1.00	2.00	2.5	10.0	18.0	45.00	70.0	0.037	0.041	0.033	0.026	0.617	0.683	0.550	0.433
P18	1.62	0.06	0.50	1.00	2.00	2.5	10.0	18.0	45.00	70.0	0.081	0.090	0.072	0.057	1.360	1.500	1.200	0.950
P19	1.53	0.06	0.50	1.00	2.00	2.5	10.0	18.0	45.00	70.0	0.077	0.085	0.068	0.055	1.283	1.417	1.133	1.133
P20	1.02	0.06	0.50	1.00	2.00	2.5	10.0	18.0	45.00	70.0	0.051	0.057	0.045	0.036	0.850	0.95	0.750	0.600
P21	1.27	0.06	0.50	1.00	2.00	2.5	10.0	18.0	45.00	70.0	0.064	0.071	0.056	0.045	1.067	1.183	0.933	0.750

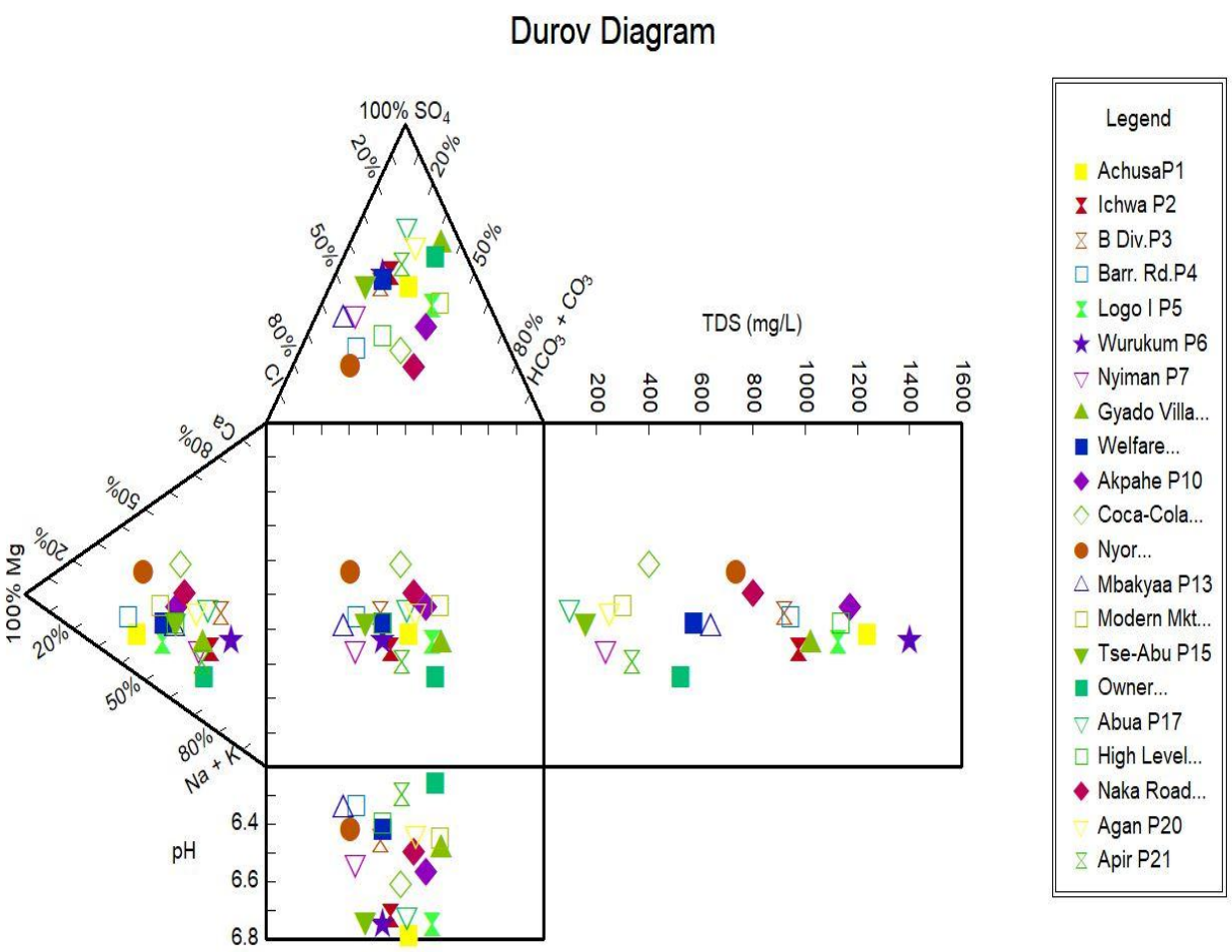
Durov Diagram
100% SO4
20%
20%
50%
50%
80%
Cl
80%
HCO3 + CO3
Ca
80%
50%
20%
100% Mg
20%
50%
80%
Na + K
TDS (mg/L)
200
400
600
800
1000
1200
1400
1600
pH
6.4
6.6
6.8
Legend
AchusaP1
Ichwa P2
B Div.P3
Barr. Rd.P4
Logo I P5
Wurukum P6
Nyiman P7
Gyado Villa...
Welfare...
Akpahe P10
Coca-Cola...
Nyor...
Mbakyaa P13
Modern Mkt...
Tse-Abu P15
Owner...
Abua P17
High Level...
Naka Road...
Agan P20
Apir P21

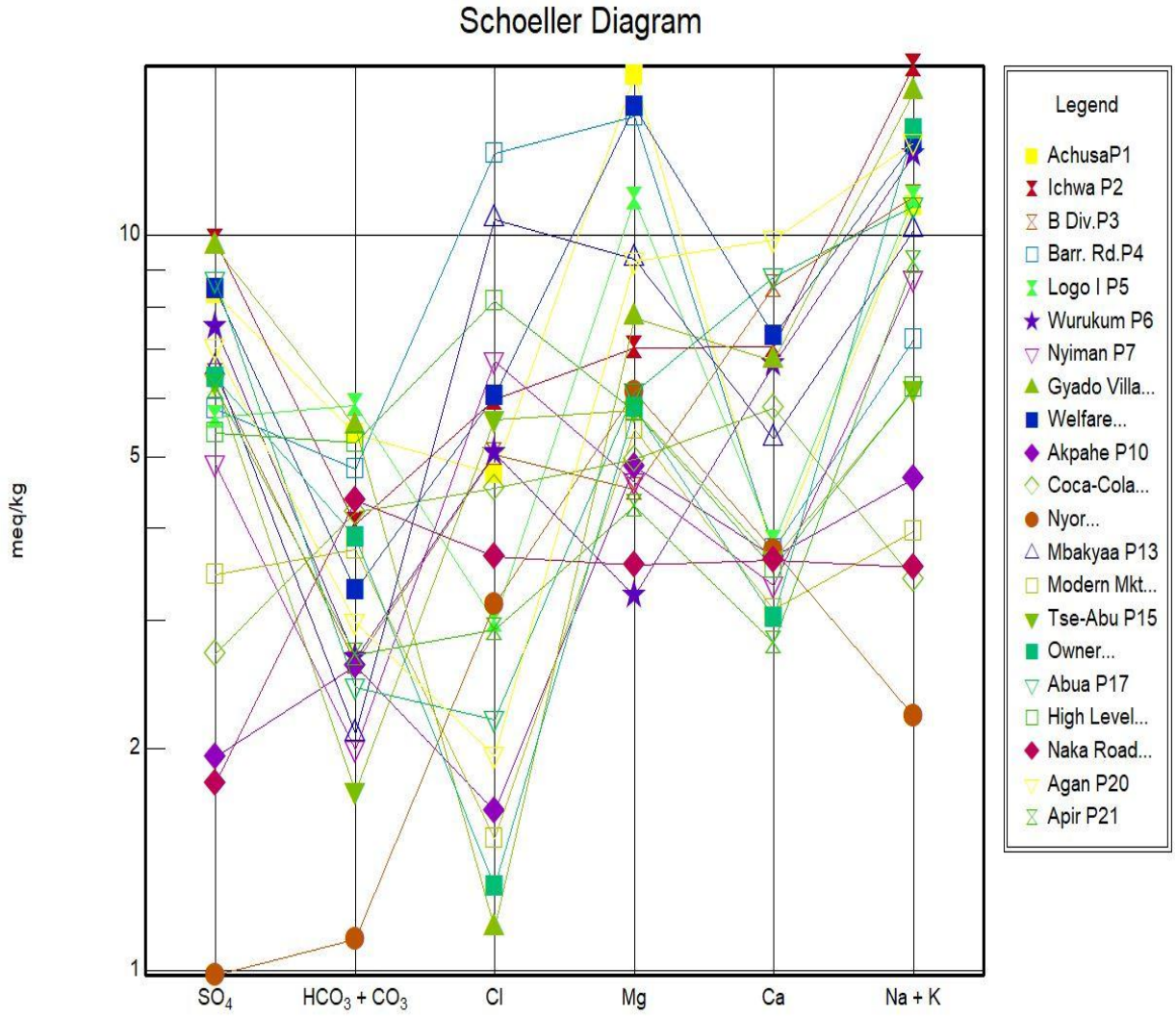
Schoeller Diagram
meq/kg
10
5
2
1
SO4
HCO3 + CO3
Cl
Mg
Ca
Na + K
Legend
AchusaP1
Ichwa P2
B Div.P3
Barr. Rd.P4
Logo I P5
Wurukum P6
Nyiman P7
Gyado Villa...
Welfare...
Akpahe P10
Coca-Cola...
Nyor...
Mbakyaa P13
Modern Mkt...
Tse-Abu P15
Owner...
Abua P17
High Level...
Naka Road...
Agan P20
Apir P21

APPENDIX E

LIST OF PUBLICATIONS FROM THE THESIS

This work has produced the following journal articles:

1. **Iwar, R.T.,** Ogedengbe, K. and Ugwudike, B.O. (2022). Groundwater fluoride removal by novel activated carbon/aluminium oxide composite derived from raffia palm shells: Optimization of batch operations and and field scale point of use system evaluation. *Results in Engineering*, 14: 100407. https://doi.org/10.1016/j.rineng.2022.100407 (Elsevier).
2. **Iwar, R.T.,** Iorhemen, O.T., Ogedengbe, K. and Katibi, K.K. (2021). Novel aluminium (hydr) oxide-functionalized activated carbon derived from Raffia palm (Raphia hookeri) shells: Augmentation of its adsorptive potentials for fluoride uptake in aqueous media. *Environmental Chemistry and Ecotoxicology*, 3: 142 – 154. https://doi.org/10.1016/j.enceco.2021.03.003. (Elsevier).
3. **Iwar, R.T.,** Ogedengbe, K., Katibi, K.K. and Oshido, L.E. (2021). Meso-micro porous activated carbon derived from Raffia palm shells: Optimization of synthesis conditions using response surface methodology. *Heliyon*, 7(6): e07301. https://doi.org/10.1016/j.heliyon.2021.e07301, (Elsevier).
4. **Iwar, R.T.,** Ogedengbe, K., Katibi, K.K. and Jabbo, J.N. (2021). Fluoride levels in deep aquifers of Makurdi, North-central, Nigeria: An appraisal based on multivariate statistics and human health risk analysis. *Environmental Monitoring and Assessment*, 193(8): 477. https://doi.org/10.1007/s10661-021-09230-8 (Springer).

And the following conference paper:

1. **Iwar, R.T.,** Ogedengbe, K. and Katibi, K.K. (2022). Fluoride in Groundwater: An Overview of its occurrence, human health risk potentials and removal by adsorption technologies. *In Proceedings of the 5th International Water Conference of the Nigerian Institution of Water Engineers (NIWE), held on 12th – 15th September, 2022 at the National Engineering Centre, Central Business District, Garki, Abuja***.**

APPENDIX F

Dept. of Agric. & Environmental Engineering
Faculty of Technology,
University of Ibadan, Ibadan-Nigeria
12th October 2020.

To Every Prospective Respondent,

Dear Sir/Ma,

SOLICITATION FOR SUPPORT TOWARDS MY STUDY

The writer is a postgraduate student of the above mentioned department and institution pursuing a PhD in Agricultural Engineering. Presently, I am carryin-out a study on the assessment of groundwater quality in Makurdi, Benue state and human health risk quantification with reference to fluoride content in the water.

It may interest you to know that the water intake rate and body weights of the populations in the study area (infants, children, teenagers and adults) are very essential variables needed to complete my research.

Thus, it is my pleasure to let you know that you would be a participant in this study as a respondent. Therefore I would be pleased if you avail tour self and also give true and consise answers to the questions raised in the questionnaire delivered. Your body weight would be taken in the field using my instruments. I plead that you give a response to each question raised and also promise not to disclose your personal details ot opinions to the public or any third party. Your answers and particulars would be solely used for the actualization of the set research objectives.

Thank you.

Yours Dependably,

Engr. Raphael T. Iwar
07030920174

A MINI-QUESTIONNAIRE TO ASCERTAIN GROUNDWATER CONSUMPTION IN THE POPULATIONS OF MAKURDI AND ITS ENVIRONS

SECTION I: LOCATION

State: _____ LGA.: _____Village: _____

Questionnaire No. _____ Name of Enumerator: _____ Date of interview:_____

Dear respondent,

The information required from you is for research purpose and would be strictly used for the intended purpose. Thank you.

SECTION II: DEMOGRAPHICS OF THE RESPONDENT

1. Sex: Male ( ) Female ( ) (*tick as appropriate*)
2. Age _____ years
3. Main Occupation _____ Secondary Occupation _____
4. Marital Status: Single ( ) Married ( ) Divorce ( ) Widowed ( )
5. Highest Level of Education: No Formal Education ( ) Islamiyyah ( ) Adult Education ( ) Primary ( ) Secondary ( ) Tertiary ( ) (*tick as appropriate*)
6. What is your household size? ___
7. How many adults are in your household _____
8. How many teenagers are in your household _____
9. How many children are in your household _____
10. How many infants are in your household _____

SECTION III: WATER CONSUMPTION RATE AND BODY WEIGHT

11. Please provide the quantity of water that each category of people in your household consume per person per day in litres

    Adult_____

    Teenager._____

    Child_____

    Infant _____
12. Would you permit me to take the body weights of each population category in your household (a) Yes (b) No *please tick as appropriate*.

Once again, thank you for your time.

METHOD OF QUESTIONAIRE ADMINISTRATION AND RETRIEVAL

Only households with the four population categories were selected. Thus a total of 50 houses were systematically selected for the study and one questionnaire each was administered to each population category in the selected household. Thus a total of 200 questionnaires were administered and retrieved from the respondents. A 100 % recovery was possible because the questionnaire were administered and collected right on the field. The researcher and field workers ensured the quality and suitability of the responses at all times.

The mini-questionnaire was administered to literate adults in the households who also answered for the infants and children in the household. The teens were administered with the questionnaire, just like with the adults. The field works were done on Saturdays such that most members of the households were found on ground. The body weights of each respondent were taken using the appropriate digital weighing balance, just after the questionnaires were retrieved from the respondents.